Calculations in perturbative QCD and analyses involving scalar mesons

Done, Philip J.

CALCULATIONS IN PERTURBATIVE QCD AND ANALYSES INVOLVING SCALAR MESONS

CALCULATIONS IN PERTURBATIVE QCD AND ANALYSES INVOLVING SCALAR MESONS

A Thesis submitted to

The University of Durham

by

Philip J. Done, B.Sc. (Durham)

For the Degree of M.Sc.

Department of Physics
University of Durham

January 1983

CONTENTS

PART II

ANALYSES INVOLVING THE S* AND

RELATED SCALAR MESONS

ABSTRACT.

The thesis is split into two independent parts.

In part I we discuss the phenomenology of jets in e^+e^- annihilation at small relative transverse momentum, with a view to testing higher order perturbative QCD (viz. the quark form factor). We phenomenologically extrapolate the quark form factor to cover the whole range in transverse momentum by using the exact $O(\alpha_s)$ cross section in the Parisi-Petronzio prescription (PPP). This then enables us to calculate the transverse momentum distribution of charged hadrons at small transverse momentum; we show that this is a poor way of testing the quark form factor, due to problems in fragmentation. Energy-energy correllations at small angles are found to be a much easier cross section to deal with. However, although the quark form factor is compatible with the data in energy-energy correllations, intrinsic transverse momentum dependence was incorporated in a very naive way, using the smearing function $\rho(b)$ borrowed from Drell-Yan (where it describes hadronic structure).

Fragmentation and intrinsic transverse momentum can be incorporated in a more physically meaningful way using the appropriate evolution equations. Erroneous approximations stemming from incorrect kinematic limits and misleading leading logarithms are discussed and corrected. This then allows a calculation of the energy weighted acollinearity of jets using a numerical solution of the evolution equations. Results are obtained in both singlet and non-singlet sectors and shown to be compatible with data at Q=30 Gev. The non-singlet sector is shown to be the dominant one at both Q=30 and at 100 Gev, where predictions are also made for the acollinearity. The effect of intrinsic transverse momentum is found to be much more significant in the evolution equation approach than when using the PPP, although at Q=100 Gev this effect is much lessened. Calculations

using two-loop Altarelli-Parisi probabilities are discussed and it is demonstrated that these cannot be relied upon to give an unambiguous description of the data, due to gauge and renormalization scheme dependence. Various forms of the running coupling α_s are used, but the data as yet does not show a strong preference for one or another.

In part II we are concerned with analyses involving the S* and related scalar mesons. We investigate resonant effects in the isoscalar S wave scattering near the $K\bar{K}$ threshold using data on $\pi\pi$ and $K\bar{K}$ production. Various coupled channel parametrizations are considered, and using information from below and above $K\bar{K}$ threshold, the parameters of the S* and ε resonance effects are determined. The ε (1400) is found to be in agreement with an ANL analysis, and the S* is compatible with a $K\bar{K}$ bound state picture.

We also study interference effects between the (P wave) ϕ meson and the underlying (K^-K^+) S wave in the reaction $K^-p \to (K^-K^+)\Lambda$ at 4.2 Gev/c. A model independent amplitude analysis of the double multipole moments is performed and we investigate the implications for the $K\bar{K} \to K\bar{K}$ S wave amplitude.

ACKNOWLEDGEMENTS.

It is my pleasure to thank Alan Martin and Mike Pennington for their invaluable support and guidance throughout the course of this work. My thanks to them also for many stimulating discussions, along with my fellow colleagues of the Graduate Workshop, Tony Rimmer, Tim Spiller, Anthony Worral and James Webb. To these and the remaining members of the group, Fred Gault and Peter Collins, I offer my gratitude for creating the convivial atmosphere in which this work was performed.

I also thank Joan Scott for a speedy and painstaking typing of the manuscript.

Finally I thank the Science and Engineering Research Council for providing financial support.

PART I

Measuring Higher Order QCD

In e^+e^- Annihilation

INTRODUCTION

Much hope nowadays is pinned on gauge theories [1] to explain the forces of nature, especially since the success of Quantum Electrodynamics (Q.E.D.). It is therefore of utmost importance to test experimentally the non-abelian gauge theories of the unified electroweak interaction and the strong interaction (Quantum Chromodynamics Q.C.D. [2]); in view of the fact that QCD is now widely believed to be the theory of strong interactions, it is a confrontation of QCD with experiment which will be discussed in this part of the thesis.

Quantum Chromodynamics is a non-abelian gauge theory which describes the interactions of a triplet of coloured quarks by the exchange of an octet of vector gluons. The spin = $\frac{1}{2}$, fractionally charged quarks are described by spinors $\psi_i^\alpha(x)$ with the colour index, α = 1,2,3 (red, green, blue), and the flavour index i = u,d,s,c,b,... transform as the fundamental representation of $SU(3)_c$, which is assumed to be an exact symmetry. The gluon fields $A^a_\mu(x)$ with space-time (μ) and $SU(3)_c$ indices, a=1, ...8 transform according to the adjoint representation, with one gluon associated with each generator of $SU(3)_c$. Gluons do not couple to flavour. The Lagrangian density for QCD with $SU(3)_c$ gauge symmetry is written:

$$\mathcal{L}(x) = -\frac{1}{4} F^a_{\mu\nu}(x) F_a^{\mu\nu}(x) + i \sum_{i=1}^{n_f} \bar{\psi}_i^\alpha(x) \gamma_\mu D^\mu_{\alpha\beta} \psi_i^\beta(x) - \sum_{i=1}^{n_f} m_i \bar{\psi}_i^\alpha(x) \psi_\alpha^i(x) \qquad (I1)$$

where:

$F^a_{\mu\nu}(x)$, a=1,....8 are the Yang-Mills field strength tensors:

$$F^a_{\mu\nu}(x) = \partial_\mu A^a_\nu(x) - \partial_\nu A^a_\mu(x) + g f_{abc} A^b_\mu(x) A^c_\nu(x) \qquad (I2)$$

with f_{abc} the $SU(3)_c$ structure constants satisfying

$$\left[\frac{\lambda^a}{2}, \frac{\lambda^b}{2}\right] = i f_{abc} \frac{\lambda^c}{2} \qquad (I3)$$

g is the QCD coupling constant and $\lambda^a/2$ are the generators of the $SU(3)_c$ algebra.

$D^{\mu}_{\alpha\beta}$ is the Yang-Mills covariant derivative:

$$D^{\mu}_{\alpha\beta} = \delta_{\alpha\beta}\partial^{\mu} - ig\sum_{a}\frac{1}{2}\lambda^{a}_{\alpha\beta}A^{\mu}_{a}(x) \qquad (I4)$$

and Mi are the quark masses.

In order to covariantly quantize the theory it is necessary to add a gauge fixing term to the Lagrangian of eq.(I1); and in order to maintain unitarity it is also necessary to add in unphysical scalar fields (Fadeev-Popov Ghosts) in a covariant gauge which remove the extra degrees of freedom present in the gluon field, [4,5]. The question of choice of gauge will be discussed in a little more detail in Chapter 2. However, for the simple points considered here, it is merely necessary to be aware of the existance of such terms. It is the other terms which provide the main interactions of the theory.

The non-abelian nature is evident from eq.(I2), with f_{abc} being non-zero. This third term is therefore responsible for the triple and quartic gluon self interactions shown in fig (I1) which originate from the first term in eq (I1). The second term describes the quark—gluon interaction as shown in fig (I2).

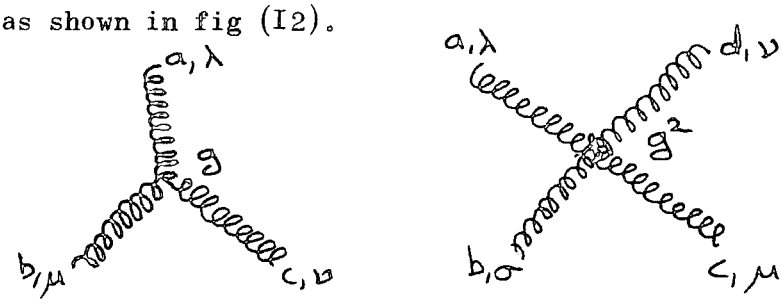

Fig (I1)
Gluon-gluon interactions.

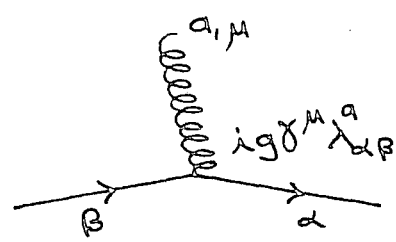

Fig (I2)
quark-gluon interaction.

Using the Renormalization Group Equation, it can be shown [1] that as a consequence of the gluon self interaction, the coupling constant g is found to be "asymptotically free" and can be written in terms of a momentum scale Q as:

$$\alpha_s(Q^2) \equiv \frac{g^2(Q^2)}{4\pi} = \frac{4\pi}{\beta_0 \ln(Q^2/\Lambda^2)} \qquad (I5)$$

where, $\beta_0 = 11 - \frac{2}{3} n_f$

with n_f = the number of quark flavours, and where the momentum scale Λ^2 is introduced by renormalization.

As a consequence, at momentum scales large with respect to Λ, the coupling constant $\alpha_s(Q^2)$ is small and it therefore makes sense to make a perturbative expansion in terms of the strong coupling α_s. Indeed as $Q^2 \to \infty$, $\alpha_s(Q^2) \to 0$ and the theory becomes (asymptotically) free. However, in the other kinematic regime of large separation, or small momentum scales, the theory is expected to lead to confinement of the (coloured) constitutents within the hadron, which it must at present energies since free quarks and gluons are not observed. The observable hadrons are colour singlets. While the non-perturbative part of the theory is not yet fully understood, it is still possible to test the theory perturbatively, which in itself must be successful for the whole theory to be so.

QCD therefore modifies the simple predictions of the parton model [3] and it is these deviations which must be looked for in the first instance (e.g. scaling violations). The subsequent chapters concentrate on those tests of QCD which involve the observation of the effects of transverse momentum of jets of hadrons [6], which originates from the emission of one or more gluons. Particular attention will be paid to the energy weighted acollinearity distribution [12], which has the virtue of being fairly easy to measure, since the collection of data does not require a detailed event-by-event analysis; and also the effects looked for are a result of the underlying dynamics, which means it is quite a direct way to measure QCD. The main body of the next three chapters will be concerned with those events which occur at small values of transverse momentum.

Chapter 1 explains the general ideas and reviews first order

calculations. Chapter 2 concentrates on the regime of soft gluons and, after giving a brief description of the quark from factor, goes on to examine the phenomenology of the Parisi-Petronzio Prescription [24] for obtaining the form factor, viz. the transverse momentum distribution of hadrons and the energy weighted acollinearity distribution. Problems encountered with this method are hopefully overcome in Chapter 3, where the effects of fragmentation are included in a more physically meaningful and more manageable way, by using the evolution equations of Bassetto et al. [40].

CHAPTER 1.

General Ideas and $O(\alpha_s)$ Calculations.

Two jet hadronic final states in e^+e^- annihilation are believed to be the evolution products of a primary quark-antiquark pair created from the virtual photon, as shown in fig (1.1).

Fig (1.1)

Production of two hadronic jets.

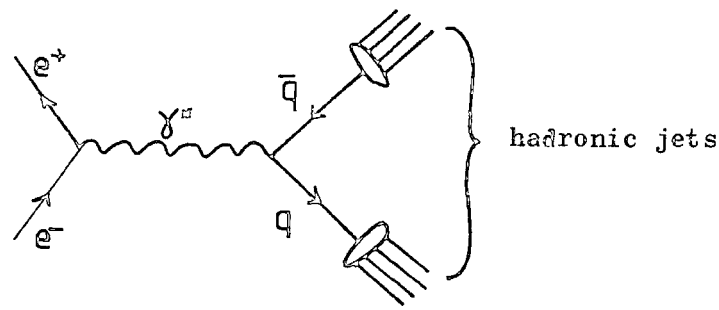

This view is now backed up by much experimental evidence; for example, the ratio:

$$R = \frac{\sigma_{tot}(e^+e^- \to had)}{\sigma_{tot}(e^+e^- \to \mu^+\mu^-)} \qquad (1.1)$$

(where σ_{tot} is the appropriate total cross section) can be shown to be equal to:

$$3 \sum_{flav.i} e_i^2 \left[1 + \frac{\alpha_s}{\pi} + O(\alpha_s^2) + \dots \right] \qquad (1.2)$$

where terms beyond the first one are QCD corrections, and where it is assumed the quarks fragment with unit probability. This result is quite well verified by high energy PETRA, PEP data (above bottom quark threshold) [7].

If just zeroth order $q\bar{q}$ pair production is considered then one expects them to be produced primarily in a back-to-back orientation in the e^+e^- centre of mass frame, followed by fragmentation into hadrons. The transverse momentum, P_T, of the hadrons with respect to this jet axis (to be defined more clearly later) will then be small with $\langle P_T \rangle \lesssim 300-400$ MeV. This small transverse momentum originates from the intrinsic transverse

momentum, k_T, of the quarks inside the hadron after fragmentation. At higher energies (presently up to about 30 GeV) noticeable jet broadening is seen to occur, corresponding to a definite increase in the average transverse momentum. This phenomenon is thought to be due to the process $e^+e^- \longrightarrow q\,\bar{q}\,g$, where one of the quarks emits a gluon [8]. It has been predicted that due to the hard sub processes like those of figure (1.2),

$$\langle p_T \rangle \sim \text{constant}.\alpha_s.\sqrt{s} \qquad (1.3)$$

where $\sqrt{s}$ is the centre of mass (c.m.) energy [9]. So although QCD processes like those in fig (1.2) decrease in frequency with respect to $e^+e^- \longrightarrow q\,\bar{q}$ in accordance with asymptotic freedom, the average P_T gets larger, while at the same time producing a more jet-like structure, since the ratio $\langle p_T \rangle/\sqrt{s}$ is decreasing with $\sqrt{s}$.

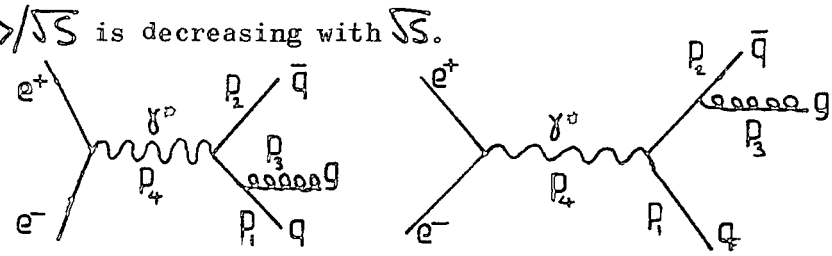

Fig (1.2)
$e^+e^- \longrightarrow q\,\bar{q}\,g$ to lowest order in QCD

So the quark and antiquark become more acollinear, and the emerging hadrons therefore have more transverse momentum themselves. Data from PETRA and elsewhere have confirmed this. It is hoped that one can compare the results of perturbative QCD calculations with the data at the highest available energies. The observable quantities should of course make manifest the non-zero angle between the unperturbed quark and that which emitted the gluon. The quantities to be discussed here are the hadron transverse momentum distributions and energy-weighted acollinearity distributions of jets. However, before going on to do that it is necessary to obtain the $O(\alpha_s)$ cross section in $e^+e^- \longrightarrow$ hadrons and to briefly discuss some of its salient features.

1.1 A Quick Look at the $O(\alpha_s)$ Cross Section.

The diagrams which provide the $O(\alpha_s)$ cross section are shown in fig (1.2) with momenta labelled. The quarks are considered as massless

for simplicity, and the gluon will be given a mass λ to exhibit the infra red features of the cross section. Using the Feynman rules for QCD, the modulus squared of the amplitude corresponding to the graphs of fig (1.2) (excluding the trivial lepton vertex) can be written [2(f)];

$$|A(s',t)|^2 = C_F \alpha_s \left[\frac{s'}{t} + \frac{t}{s'} - \frac{2Q^2}{s't}(s'+t-Q^2) - \frac{2\lambda^2}{s't}(s'+t+\lambda^2) - Q^2\lambda^2\left(\frac{1}{s'^2}+\frac{1}{t^2}-\frac{4}{s't}\right)\right] \qquad (1.3)$$

where these particular Mandelstam invariants are given by :

$$s' = (P_4 - P_1)^2 = Q^2(1-x_1)\,; \quad t = (P_4 - P_2)^2 = Q^2(1-x_2)\,;$$
$$u = (P_4 - P_3)^2 = Q^2(1 - x_3 + \lambda^2/Q^2),$$

and where $Q \equiv \sqrt{s}$ is the virtual photon mass.

The cross section will be obtained in the c.m. system in terms of the fractional momenta of the partons defined as : $x_i = \frac{2P_i}{Q}$ where P_i, i=1,2,3 are the 3-momenta of the q,$\bar{q}$ and g respectively. These variables are particularly useful when discussing jet production.

The differential cross-section is fivefold differential since it depends on two independent final state momenta (or two of the X_i) and three angles defining the q $\bar{q}$ g plane relative to the incoming e^+e^- axis [8]. Integration over the angular variables of the three body phase space yields :

$$\frac{1}{\sigma_0}\frac{d\sigma'}{dx_1 dx_2} = \frac{C_F \alpha_s}{2\pi}\left[\frac{x_1^2+x_2^2}{(1-x_1)(1-x_2)} + \frac{2\lambda^2(x_1+x_2-\lambda)}{Q^2(1-x_1)(1-x_2)} - \frac{\lambda^2}{Q^2(1-x_1)^2} - \frac{\lambda^2}{Q^2(1-x_2)^2}\right] \qquad (1.4)$$

where

$$\sigma_0 \equiv \sigma(e^+e^- \to q\bar{q}) = \frac{4\pi\alpha^2}{Q^2}\sum_f e_f^2$$

and where α is the QED coupling constant.

The first term of eq. (1.4), originally derived by Ellis et al. [8], is the only term relevant for massless quarks and is the source of all

$O(\alpha_s)$ predictions concerning jets discussed here:

$$\frac{1}{\sigma_0}\frac{d\sigma}{dx_1 dx_2} = \frac{C_F \alpha_s}{2\pi}\frac{x_1^2 + x_2^2}{(1-x_1)(1-x_2)} \tag{1.5}$$

However, to look at the infra-red structure of the theory, it will be necessary to keep the other terms in eq. (1.4).

Integration over X_1 and X_2 yields:

$$\frac{1}{\sigma_0}\sigma' = \frac{C_F \alpha_s}{2\pi}\left[\ln^2\frac{Q^2}{\lambda^2} - 3\ln\frac{Q^2}{\lambda^2} + 5 - \pi^2/3\right] \tag{1.6}$$

which is obviously singular when $\lambda \longrightarrow 0$. (The terms which vanish when $\lambda \longrightarrow 0$ have been thrown away). However, the virtual diagrams have not been considered at $O(\alpha_s)$, i.e. those of fig.(1.3b). They introduce more singularities since the loop integrals diverge for

Fig.(1.3)

$e^+e^- \longrightarrow q\,\bar{q}$

(a) zeroth order

(b) $O(\alpha_s)$ virtual corrections.

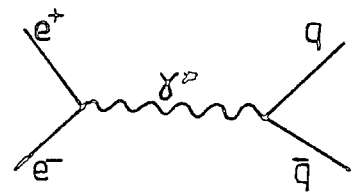

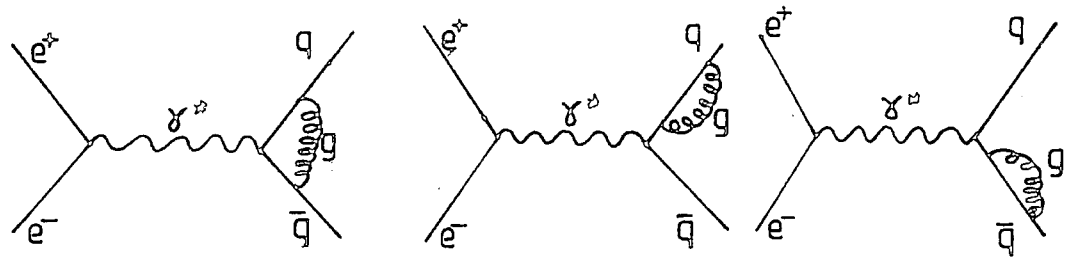

massless gluons. Including these diagrams the total cross section to $O(\alpha_s)$ for $e^+e^- \longrightarrow q\,\bar{q}$ is:

$$\frac{1}{\sigma_0}\sigma(e^+e^- \to q\bar{q}) = 1 + \frac{C_F \alpha_s}{2\pi}\left[-\ln^2\frac{Q^2}{\lambda^2} + 3\ln\frac{Q^2}{\lambda^2} - \frac{7}{2} + \frac{\pi^2}{3}\right] \tag{1.7}$$

from which it can be seen that upon adding eqs.(1.6) and (1.7) together to obtain the total cross section to $O(\alpha_s)$, the singularities exactly cancel between the real and virtual diagrams, rendering the observable

cross section finite and leading to the result of eq.(1.2). This is an example of the Kinoshita-Lee-Nauenberg (KLN) theorem, which states that any transition probability in a theory involving massless particles is finite to all orders provided a sum is performed over all degenerate states [14]. This is particularly important since it also applies to energy weighted distributions (to be discussed later).

The infra red singularities discussed above result from poles in the quark propagator. Denoting the q or $\bar{q}$ momentum by p and that of the gluon by k, these divergencies will occur when $(p+k)^2 = p^2$ or $2p.k + k^2 = 0$. For massless quarks the gluons this can happen when either $k = 0$ or $k \propto p$, the former occurring with the emission of soft gluons and the latter resulting from collinear gluons emitted parallel to the quark. Both cases correspond to the situation of being unable to resolve the quark from the gluon. These poles are manifest in the cross section of eq.(1.5) as x_1, $x_2 \longrightarrow 1$. The singularities arise in an analogous way in QED. A simple calculation shows how.

Consider the scatter of an electron off a charged source, and which emits a photon of momentum k, as shown in fig. (1.4).

Fig. (1.4)
Photon bremsstrahlung in QED.

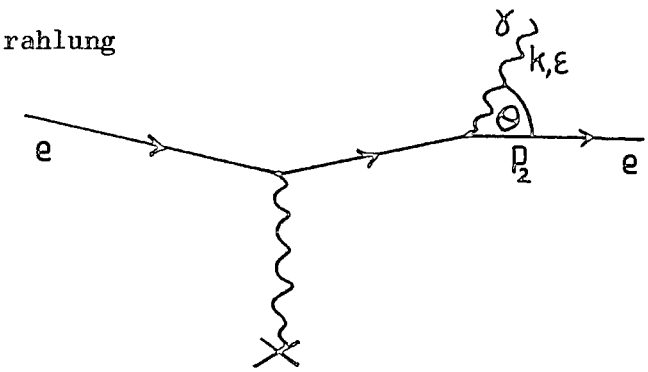

The amplitude can be written:

$$M \sim 2\varepsilon.P_2/((k+P_2)^2 - M_e^2) \qquad (1.8)$$

where ε is the emitted photon polarisation 4- vector and P_2 the 4-momentum of the scattered electron. M_e is the electron mass. And one can write,

$$k=(|\vec{k}|,\vec{k})$$

$$P_2=((P_2^2+m_e^2)^{1/2},\vec{P_2})=(P_2(1+\frac{m_e^2}{2P_2^2}),\vec{P_2}) \quad \text{for} \quad m_e^2 \ll P_2^2$$

And so:

$$M \sim \frac{-\vec{\varepsilon}.\vec{P_2}}{|\vec{k}||\vec{P_2}|(1+\frac{m_e^2}{2|\vec{P_2}|^2})-\vec{k}.\vec{P_2}}$$

$$= \frac{\vec{\varepsilon}.\vec{P_2}}{|\vec{k}||\vec{P_2}|(1-\cos\theta+\frac{m_e^2}{2|\vec{P_2}|^2})} \quad \text{for} \quad m_e^2 \ll P_2^2 \qquad (1.9)$$

The collinear singularity for $\theta=0$ is in fact regulated by a finite M_e. The factor $1/|\vec{k}|$ is responsible for the soft divergence. In order to reproduce the situation of massless quarks in QCD as closely as possible, neglect M_e. Then the two divergences appear together. The denominator in eq. (1.9) thus behaves as θ^2 for small θ. Since a polarization vector $\vec{\varepsilon}$ of a real photon is perpendicular to $\vec{k}$, then $\vec{\varepsilon}.\vec{P_2}=|\vec{P_2}|\cos(90-\theta)\simeq|\vec{P_2}|\theta$. Therefore in the infra red ($k\sim 0$) and collinear limit ($\theta\sim 0$):

$$M \sim 1/k\theta \qquad (1.10)$$

The cross section for single photon bremsstrahlung is thus proportional to:

$$\int\frac{d^3k}{2k_0}|M|^2 \simeq \int\frac{k^2dk}{k}\frac{d(\cos\theta)}{k^2\theta^2} \simeq \int_{M_\gamma}^{|\vec{P_2}|}\frac{dk}{k}\int_{\theta_{min}}^{\theta_{max}}\frac{d\theta}{\theta} \qquad (1.11)$$

where M_γ is some ficticious photon mass. And so infra red singularities appear from both integrals in eq.(1.11), which give $\ln(|\vec{P_2}|/M_\gamma)\cdot\ln(\frac{\theta_{max}}{\theta_{min}})$. An analogous situation occurs in QCD for gluon bremsstrahlung, and so the origins of the divergencies in eq.(1.5) become clear. We can now use eq.(1.5) as the basis of $O(\alpha_s)$ QCD predictions.

1.2 Transverse Momentum Distributions of Charged Hadrons.

When working in the e^+e^- centre of mass, where the virtual photon

is created at rest, the three body final state can be drawn as in fig. (1.5), which defines the energy fractions X_i and momenta P_i of the appropriate particles. Transverse momentum Q_T is measured with respect to a thrust axis T, which is defined by:

Fig.(1.5)
3 body kinematics relative to a thrust axis.

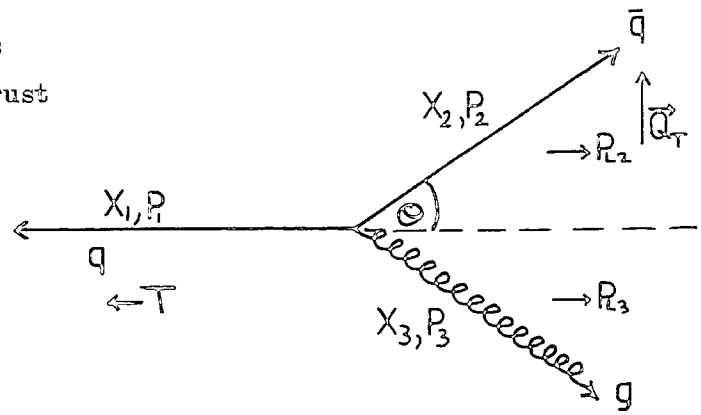

$$T = \max \sum_i |P_{Li}| \Big/ \sum_i |P_i| \tag{1.12}$$

where the P_{Li} are components of the momenta P_i along some axis. This then reduces to T=max (x_1, x_2, x_3) corresponding to the direction of the unperturbed quark as drawn in fig.(1.5).

Energy conservation gives:

$$\sum_i E_i = Q \tag{1.13}$$

so that:

$$x_1 + x_2 + x_3 = 2 \tag{1.14}$$

Now,
$$Q_T = \frac{Q}{2} x_2 \sin\Theta \tag{1.15}$$

and momentum conservation along the thrust axis gives $P_1 = P_{L2} + P_{L3}$ giving:
$$Q_T^2 = \frac{(1-x_1)(1-x_2)(1-x_3)Q^2}{x_1^2} \tag{1.16}$$

in the case where the quark defines the thrust axis. Equations (1.15) and (1.16) give:

$$x_2 = 2(1-x_1)/(2-x_1 \mp x_1 \cos\Theta) \tag{1.17}$$

where Θ is the angle between q and $\bar{q}$ as shown in fig (1.5).

We now wish to transform eq.(1.5) first into a distribution in

Q_T^2 of partons, and then into a distribution in hadron transverse momentum P_T^2. The integration of eq.(1.5) to obtain the parton cross section $\frac{1}{\sigma_0}\frac{d\sigma}{dQ_T^2}$ with respect to Q_T^2 is done in Appendix A and is utilized again in Chapter 2. Using $z = P_T/Q_T$, the hadron distribution can be written:

$$\frac{1}{\sigma_0}\frac{d\sigma^h}{dP_T^2} = \sum_h \int_{\sqrt{12}P_T/Q}^{1} \frac{dz}{z}\left[\frac{1}{\sigma_0}\frac{d\sigma^q}{dQ_T^2}\left\{G_q^h(z) + G_{\bar{q}}^h(z) + 2G_g^h(z)\right\} + \frac{1}{\sigma_0}\frac{d\sigma^g}{dQ_T^2}\left\{G_q^h(z) + G_{\bar{q}}^h(z)\right\}\right] \qquad (1.18)$$

where $d\sigma^q$ and $d\sigma^g$ are the distributions with the quark (or antiquark) and gluon respectively as thrust axis, and the G's are functions representing the fragmentation of partons into hadrons. Since all expressions are symmetrical with respect to quark and antiquark, then that explains the appropriate weightings of the cross sections with the G functions. From now on a universal set of $G(z)$ functions will be used, viz. $G_q(z) \equiv \sum_h G_q^h(z)$. To find their correspondence to the usual fragmentation functions $D(z)$, one can use the multiplicity of charged hadrons $\langle n\rangle_c = \sigma/\sigma_0$. For simplicity write:

$$\left[\frac{1}{\sigma_0}\frac{d\sigma^q}{dQ_T^2}\cdots\cdots\right] \equiv \frac{1}{\sigma_0}\frac{d\sigma}{dQ_T^2}G(z)$$

$$\therefore \langle n\rangle_c = \int_0^{Q^2/12} dP_T^2 \frac{d\sigma^h}{dP_T^2}\frac{1}{\sigma_0}$$

$$= \int_0^{Q^2/12} dP_T^2 \int_{\sqrt{12}P_T/Q}^{} \frac{dz}{z} G(z)\frac{1}{\sigma_0}\frac{d\sigma}{dQ_T^2}$$

$$= \int_0^{Q^2/12} dP_T^2 \int_{P_T}^{Q/\sqrt{12}} \frac{dQ_T}{Q_T} G\left(\frac{P_T}{Q_T}\right)\frac{1}{\sigma_0}\frac{d\sigma}{dQ_T^2}$$

$$= \frac{1}{\sigma_0}\int_0^{\sqrt{5/12}} \frac{dQ_T}{Q_T}\frac{d\sigma}{dQ_T^2}\int_{Q_T^2}^{\sqrt{5/12}} dP_T^2\, G\left(P_T/Q_T\right)$$

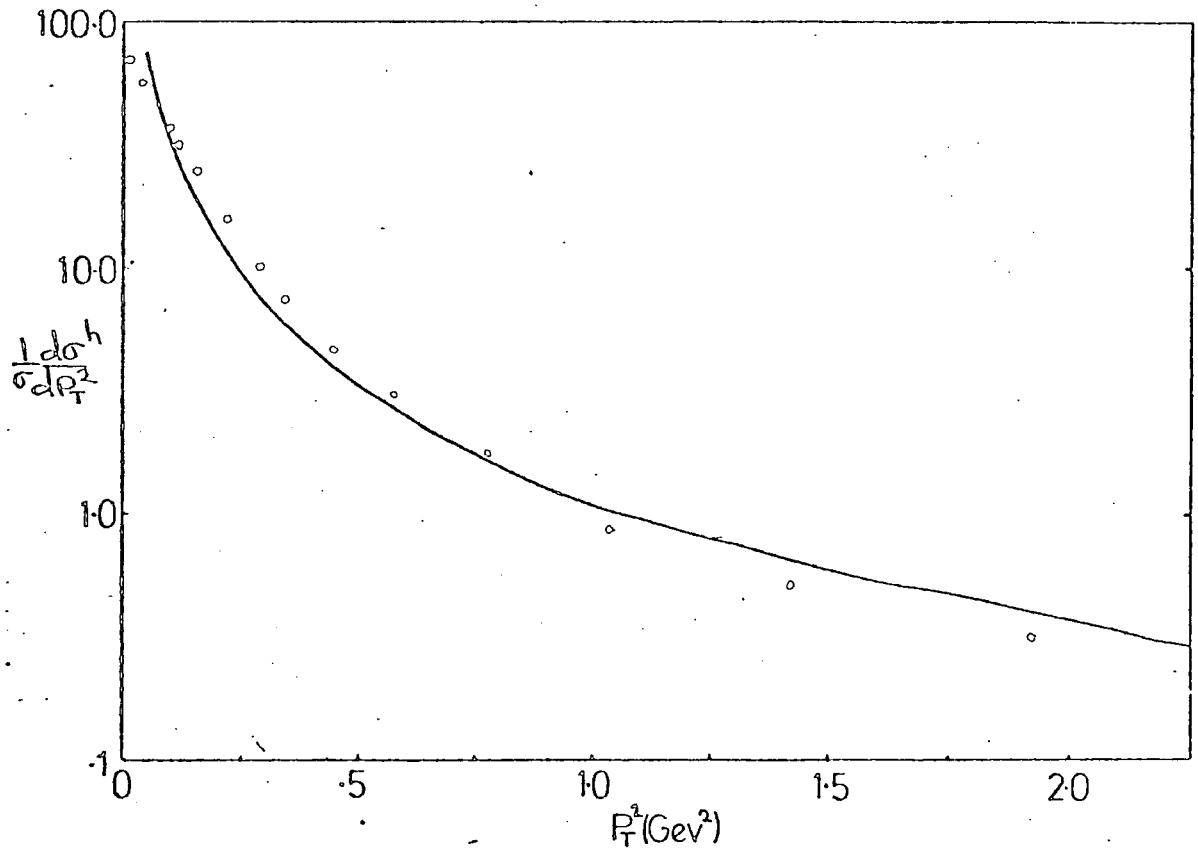

Fig.(1.6). The transverse momentum distribution of charged hadrons $\frac{1}{\sigma} d\sigma^h/dP_T^2$, eq.(1.19) to $O(\alpha_s)$. $Q=31.6$ Gev, $\Lambda = 0.5$ Gev, $\alpha_s=0.184$. Data (approx. taken) from Ref [17].

$$= \int_0^{\sqrt{s/2}} dQ_T^2 \frac{1}{\sigma_0}\frac{d\sigma}{dQ_T^2} \int_{Q/\sqrt{2}Q_T}^1 d\xi \; \xi \, G(\xi)$$

where $\xi = P_T/Q_T$

The fragmentation functions are usually normalized according to $\int dz\, D(z) = \langle n \rangle$, so one can redefine the fragmentation functions to be: $D(z) = zG(z)$ and one can re-write eq (1.18) as:

$$\frac{1}{\sigma_0}\frac{d\sigma^h}{dP_T^2} = \int_{P_T\sqrt{12/s}}^1 \frac{dz}{z^2} D(z) \frac{1}{\sigma_0}\frac{d\sigma}{dQ_T^2}$$

i.e.

$$\frac{1}{\sigma_0}\frac{d\sigma^h}{dP_T^2} = \frac{1}{2}\int_{P_T^2}^{Q^2/12} \frac{dQ_T^2}{Q_T P_T}\left[\frac{1}{\sigma_0}\frac{d\sigma^q}{dQ_T^2}\left\{D_q\left(\frac{P_T}{Q_T}\right) + D_{\bar{q}}\left(\frac{P_T}{Q_T}\right) + 2D_g\left(\frac{P_T}{Q_T}\right)\right\}\right.$$

$$\left. + \frac{1}{\sigma_0}\frac{d\sigma^g}{dQ_T^2}\left\{D_q\left(\frac{P_T}{Q_T}\right) + D_{\bar{q}}\left(\frac{P_T}{Q_T}\right)\right\}\right] \qquad (1.19)$$

The result of an $O(\alpha_s)$ calculation with the simple form for the fragmentation functions :

$$D_q(z) = D_{\bar{q}}(z) = D_g(z) = 3(1-z)^2/z$$

(x 2/3 for charged hadrons)

is shown in Fig (1.6) [10,11], and compared with the data of reference [17], from which it can be seen that the QCD result fits the data closely. This will be discussed in more detail in chapter 2, but at this point it can be seen that one must introduce the phenomenological quantities $D(z)$ which leaves the calculation not wholly dependent on QCD, but also on predicted forms for $D(z)$ at Q = 30 GeV. This problem can be overcome at $O(\alpha_s)$ by discussing observable cross sections in the form of energy weighted distributions.

1.3 Energy Flow

The Washington group S. Ellis et al.[12] proposed the study of

a hierarchy of energy-weighted cross sections in e^+e^- annihilation, in order to test predictions of QCD in as far as possible an unambiguous way; these quantities become increasingly finely tuned to the process considered. The first member is the total cross section in e^+e^-, $\sigma_{tot}^{e^+e^-}$, which was discussed above. The other two members are the "antenna" energy pattern $d\Sigma/d\Omega$ and the energy-energy correllation cross section (energy weighted acollinearity) $d^2\Sigma/d\Omega\, d\Omega'$ in e^+e^-. These partial cross sections involve energy weightings and this should ensure that they are free of infra red singularities due to the emission of massless soft or collinear gluons.

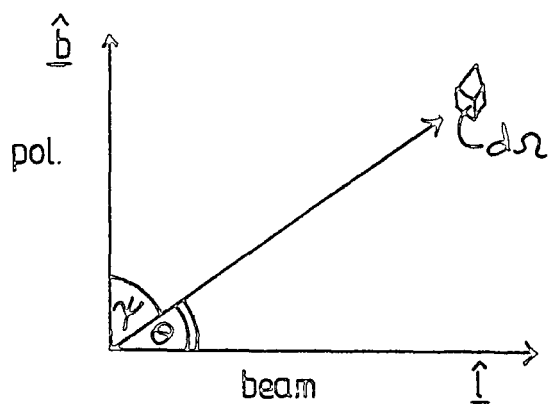

Fig.(1.7). Set up to measure energy flow.

The set up for measuring energy flow is shown in Fig (1.7). $d\Sigma/d\Omega$ is simply the power radiated into solid angle $d\Omega$ divided by the energy flux of the incident e^+e^- colliding beam. So experimentally a calorimeter is placed at various orientations with respect to the beam axis, and it measures the energy flowing through the solid angle, without the need to look for specific hadrons which carry the energy. So at the hadronic level one measures:

$$\frac{d\Sigma^h}{d\Theta} = \sum_h \int dz_h\, z_h \frac{d\sigma}{dz_h\, d\Theta} \qquad (1.20)$$

and one can calculate the energy flow of partons in perturbative QCD:

$$\frac{d\Sigma^{p}}{d\Theta} = \sum_{q} \int dz_q \, z_q \frac{d\sigma}{dz_q \, d\Theta} \tag{1.21}$$

where $z_i = 2P_i/Q$. Both of the above expressions will be seen to be the same (as one might naively expect from energy conservation), which renders this particular quantity particularly easy to test to $O(\alpha_s)$.

Energy flow in lowest order $e^+e^- \longrightarrow \gamma^* \longrightarrow q\,\bar{q}$ is particularly simple since the differential cross section $d\Sigma/d\Omega$ is the same as the ordinary differential cross section since the quark or antiquark carries away exactly half of the total incident energy $\sqrt{s} \equiv Q$.

$$\therefore \frac{d\Sigma^{o}}{d\Omega} = \frac{d\sigma^{e^+e^- \to q\bar{q}}}{d\Omega} = \frac{\alpha^2}{4Q^2} \sum_{q} 3e_q^2 (1+\cos^2\Theta)$$

for unpolarized beams

or

$$= \frac{\alpha^2}{2Q^2} 3\sin^2\chi \sum_{q} e_q^2 \tag{1.22}$$

for perfectly polarized beams.

In the subsequent discussion it is irrelevant whether one considers polarized or unpolarized beams, so we will just look at the former for simplicity.

Again we require the result of the calculation to be infra-red safe. In lepto-production, Drell-Yan or semi-inclusive hadron production in e^+e^- annihilation, these infra-red complications can be adsorbed into the parton densities $D(z)$ or $F(x)$. But in the case of energy flow in jets all predictable quantities must be free of infra-red singularities, as was the total cross section σ^{tot} . These singularities can be removed by using Sterman-Weinberg cuts [13] .

However, energy weighted distributions will be seen to be finite in accord with the KLN theorem by adding real and virtual emission graphs as in the case for σ^{tot}. Again introducing a gluon mass λ, the virtual graphs of fig (1.3b) give to $O(\alpha_s)$ [12]:

$$\frac{d\Sigma_q[\text{virtual}]}{d\Omega} = \frac{\alpha^2 \sin^2\chi}{Q^2} \sum_q \frac{e_q^2 \alpha_s}{\pi} \left[\ln^2 \frac{Q^2}{\lambda^2} + 3 \ln \frac{Q^2}{\lambda^2} + \frac{\pi^2}{3} - \frac{7}{2} \right] \tag{1.23}$$

for the contribution of virtual gluon emission to the energy flow of quarks (c.f. eq. (1.7)).

Similarly:

$$\frac{d\Sigma_q[\text{real}]}{d\Omega} = \frac{\alpha^2}{Q^2} \sum_q \frac{e_q^2 \alpha_s}{\pi} \left[\frac{1}{2}(3\cos^2\chi - 1) + \sin^2\chi \left(\ln^2 \frac{Q^2}{\lambda^2} - \frac{13}{3} \ln \frac{Q^2}{\lambda^2} - \frac{\pi^2}{3} + \frac{80}{9} \right) \right] \tag{1.24}$$

for the real contribution to the energy flow of quarks from the graphs of fig (1.2). The same singularities appear as in σ^{tot}.

The leading $\ln^2 Q^2/\lambda^2$ mass singularities now cancel upon addition of eqs (1.23), (1.24), but there still remains the $\ln Q^2/\lambda^2$ divergence. As one might have expected, this is a consequence of the fact that perturbative QCD cannot give flavour dependent properties, which are a non-perturbative problem. However, to complete the calculation one must also add in the contribution of the gluon energy:

$$\frac{d\Sigma_g}{d\Omega} = \frac{\alpha^2}{Q^2} \sum_q \frac{e_q^2 \alpha_s}{\pi} \left[(3\cos^2\chi - 1) + \sin^2\chi \left(\frac{4}{3} \ln \frac{Q^2}{\lambda^2} - \frac{35}{9} \right) \right] \tag{1.25}$$

Adding this to the above two equations now removes all mass singularities [12] and so rendering energy flow infra-red safe.

1.4 Energy-Energy Correllations.

The energy weighted acllinearity distribution is a more interesting quantity since it emphasises more the underlying dynamics. The experimental set up is similar to that of fig.(1.7), but the energies of two jets are measured simultaneously at a particular angle with respect to each other. Thus there is no need to invoke the use of a thrust axis, since there is no need to use one experimentally, as there was when measuring transverse momentum distributions.

Although slightly more complicated to evaluate, this quantity is again free of mass singularities [12]. One can define the energy-energy correlation cross section as:

$$\frac{dA}{d\Theta} = \sum_{\substack{\text{configurations} \\ i,j\, i\neq j}} \int_{x_{i\min}}^{x_{i\max}} dx_i\, x_i x_j \frac{1}{\sigma_0} \frac{d\sigma}{dx_i d\Theta} \qquad (1.26)$$

[10,12,15] where one adds the distributions in angle between q $\bar{q}$ and q g, with $x_{i\min} \simeq 0$, $x_{i\max} \simeq 1$, i.e. the configurations of fig.(1.8).

Fig.(1.8)
Configurations for energy-energy correllations.

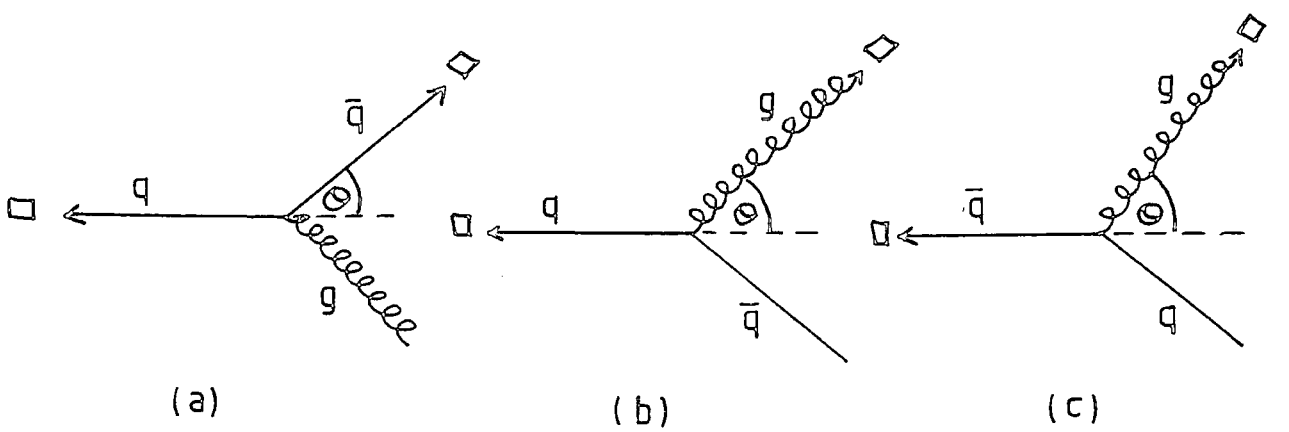

It is straightforward to show that $dA/d\Theta$ for partons is the same as that for hadrons (which is true for energy flow in general). Let the hadrons a,b have energy fractions $x_H = 2p_H/Q$ and similarly for partons A,B. So the energy fraction of hadron H with respect to parton P is $\xi_H = x_H/x_P$. The cross section for hadron production a,b is:

$$\frac{1}{\sigma_0}\frac{d\sigma}{dx_a dx_b d\Theta} = \sum_{A,B}\iint d\xi_a d\xi_b dx_A dx_B \frac{1}{\sigma_0}\frac{d\sigma}{dx_A dx_B d\Theta} \cdot$$

$$\cdot D_A^a(\xi_a) D_B^b(\xi_b)\delta(x_a - \xi_a x_A)\delta(x_b - \xi_b x_B) .$$

Using $\delta(x_H - \xi_H x_P) = \frac{1}{x_P}\delta(\xi_H - x_H/x_P)$ and integrating over the ξ's gives:

$$\sum_{A,B}\int \frac{dx_A}{x_A}\frac{dx_B}{x_B} D_A^a\left(\frac{x_a}{x_A}\right) D_B^b\left(\frac{x_b}{x_B}\right)\frac{1}{\sigma_0}\frac{d\sigma}{dx_a dx_b d\Theta}$$

Now the energy weighted acollinearity for hadrons is:

$$\sum_{a,b}\iint dx_a dx_b x_a x_b \frac{1}{\sigma_0}\frac{d\sigma}{dx_a dx_b d\Theta}$$

$$= \sum_{A,B}\sum_a \int \frac{dx_a}{x_A}\frac{x_a}{x_A} D_A^a\left(\frac{x_a}{x_A}\right)\sum_b \int \frac{dx_b}{x_B}\frac{x_b}{x_B} D_B^b\left(\frac{x_b}{x_B}\right).$$

$$\cdot \iint x_A x_B \frac{1}{\sigma_0}\frac{d\sigma}{dx_A dx_B d\Theta} dx_A dx_B .$$

And using momentum conservation, $\sum_a \int_0^1 dz\, z\, D^a(z) = 1$, the above equation reduces to

$$\sum_{A,B}\iint dx_A dx_B x_A x_B \frac{1}{\sigma_0}\frac{d\sigma}{dx_A dx_B d\Theta}$$

which is the energy-energy correllation cross section for partons and can be written in the form of eq. (1.26) since,

$$\frac{1}{\sigma_0}\frac{d\sigma}{dx_A dx_B d\Theta} = \frac{1}{\sigma_0}\frac{d\sigma}{dx_A d\Theta}\delta(x_B - x_B(x_A,\Theta))$$

where $x_3(x_A,\Theta)$ is given by eq. (1.17).

So one can make a measurement of the energy flow of hadrons and make a direct prediction by calculating it for partons using perturbative QCD. The phenomenological fragmentation functions have been removed, and the strong coupling constant α_s appears as normalization, so one should be able to predict both shape and normalization of the distributions.

One can only expect the $O(\alpha_s)$ calculations to hold good for $60^\circ \lesssim \Theta \lesssim 120^\circ$, since single hard gluon bremsstrahlung is unlikely to be the dominant effect at small and large Θ which will be discussed in the next chapter.

Using equations (1.5) and (1.17) one can find $\frac{1}{\sigma_0} d\sigma/dx_1 d\Theta$ and then using equations (1.17) and (1.26) one has $dA/d\Theta$ to $O(\alpha_s)$. The contributions from configurations (1.8) a,b,c are:

$$(1.8)a \quad \frac{dA}{d\Theta} = \frac{8\alpha_s}{3\pi} \frac{1}{\tan\Theta/2} \int_0^1 \frac{dx_1\, x_1(1-x_1)(x_1^2 + x_2^2(x_1,\Theta))}{D^2}$$

$$(1.8)b,c \quad \frac{dA}{d\Theta} = \frac{8\alpha_s}{3\pi} \tan\Theta/2 \int_0^1 \frac{dx_1\, x_1 (x_1^2 + (2-x_1-x_2(x_1,\Theta))^2)}{D^2}$$

where $D = 2 - x_1 - x_1\cos\Theta$.

To do the above integrals numerically one encounters severe problems of precision at small Θ, near $x_1=1$ (see fig. (1.9)). If you integrate all the way to $x_1=1$, then $|dx_2/dx_1|$ becomes very large

Fig. (1.9)
X_1X_2 phase space.

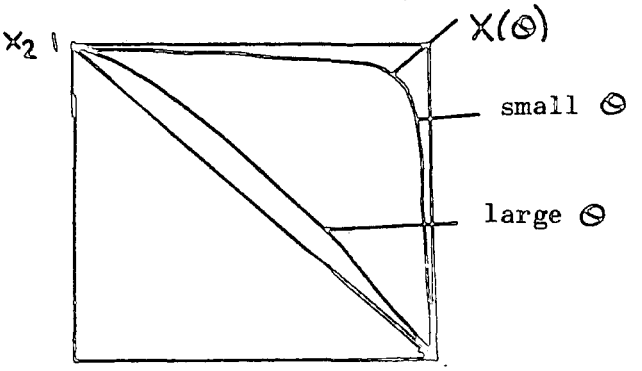

towards $X_1=1$. Thus the $1/Q^2$ factor in the integrand gives a very large contribution at $X_1=1$. In order not to have to use an incredible number of intervals, it is much easier to divide the integrations up and integrate from 0 to the point $X(\theta)$, where $X_1 = X_2$, first in X_1 and then in X_2. From equation (1.17), $X(\theta) = (1-\sin\frac{\theta}{2})/\cos^2\frac{\theta}{2}$. Then using $\frac{dx_2}{dx_1} = -\frac{2(1-\cos\theta)}{Q^2}$ the troublesome half of the integration becomes:

$$\int_{X(\theta)}^{1} dx_1 \ldots\ldots = \int_{X(\theta)}^{0} dx_2 \frac{dx_1}{dx_2} \ldots\ldots\ldots = \int_{0}^{X(\theta)} dx_2 \frac{Q^2}{2(1-\cos\theta)} \ldots\ldots$$

The result of such an $O(\alpha_s)$ calculation is shown in fig (1.10), with $\Lambda = 0.5$, $Q = 31.6$ Gev and $\alpha_s(Q^2)$. (For data see ref. [18]). This shows the simple $O(\alpha_s)$ result overshoots the data drastically below θ about 30°.

The non-perturbative effects, (i.e. the intrinsic transverse momentum of partons inside a hadron, the parton "Fermi motion"), can be estimated to fall off as $1/Q$ [12] if they are put in phenomenologically in a simple way by assuming a Gaussian distribution in k_T^2 with $\langle k_T^2 \rangle \simeq 350$ Mev. The perturbative contribution only falls off as $1/\ln Q$ so eventually one might hope to completely forget about intrinsic k_T. However, at present energies it must be included, particularly at small angles. In a simple model, where non-perturbative effects are put in additively, they are symmetrical about $\theta \leftrightarrow \pi - \theta$, whereas the perturbative term in asymmetric since for $\theta \sim 0^\circ$ both collinear and soft gluon emission contribute, while at $\theta \sim 180^\circ$ only collinear emission contributes. This is shown

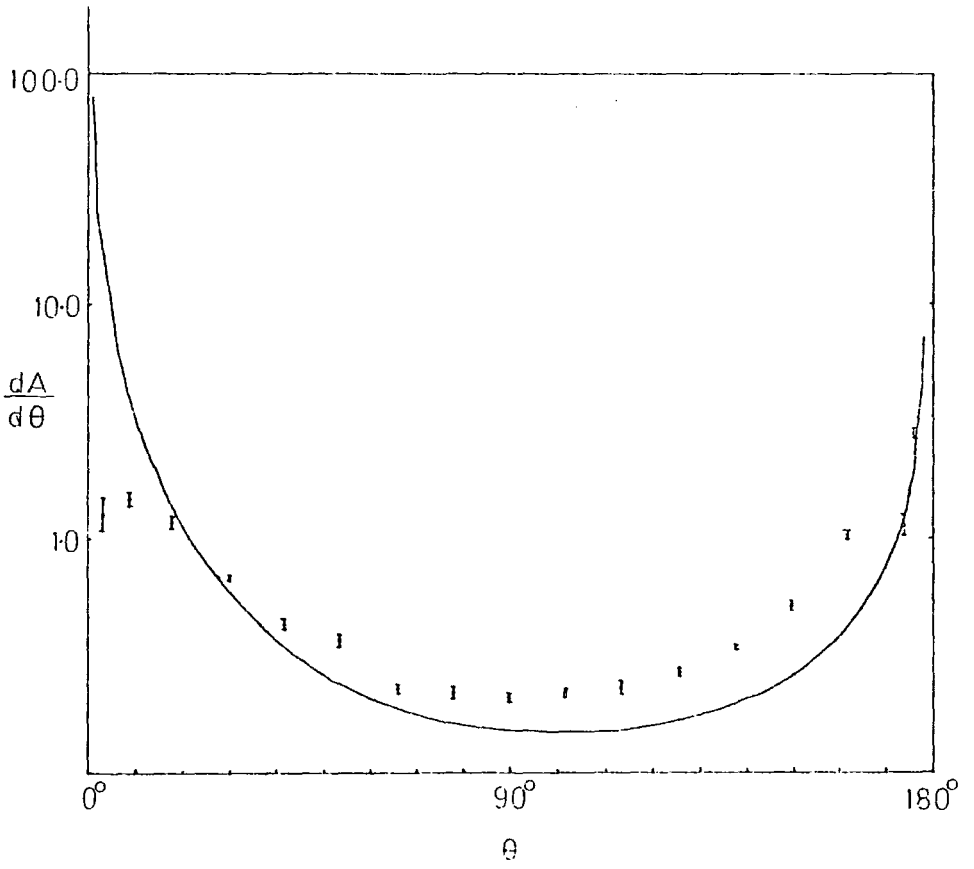

Fig.(1.10). The energy-energy correllation cross section $dA/d\Omega$ to $O(\alpha_s)$ using $\alpha_s(Q^2)$, $Q=31.6$ Gev and $\Lambda=0.5$ Gev, compared with PLUTO data from ref [18].

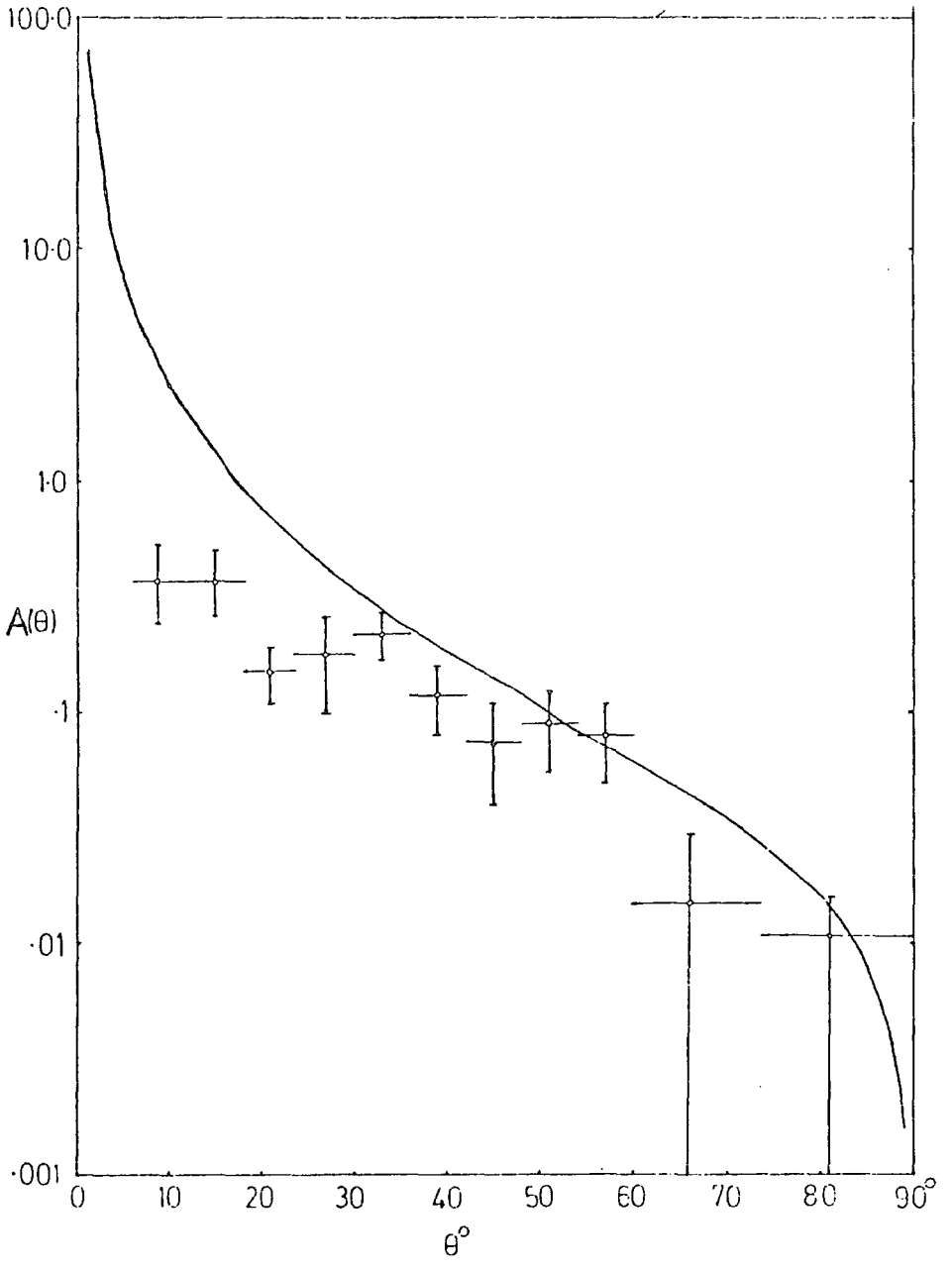

Fig.(1.11) The asymmetry A(θ) in the energy-energy correllation cross section to O(αs) obtained from fig (1.10) and compared with PLUTO data [18].

in fig (1.10) where $dA/d\Theta$ is plotted. So assuming that non-perturbative effects can be put in in an additive way, one might hope that the forward-backward asymmetry,

$$A(\Theta) = \left\{ \frac{dA}{d\Theta}(\Theta) - \frac{dA}{d\Theta}(\pi - \Theta) \right\} \tag{1.27}$$

is relatively free from non-perturbative ambiguities. This does in fact give quite good agreement with data [18] , as shown in fig (1.11), in the central region $45^\circ \lesssim \Theta \lesssim 90^\circ$.

This can be taken as a genuine manifestation of gluon bremsstrahlung within the limits imposed by the following corrections [7] :

(i) detector imperfections, e.g. confusion between electrons, photons and hadrons in jets, escaping neutral particles, or other experimental difficulties.

(ii) radiative corrections. Photon radiation in an initial e^+e^- state causes changes in the cross section and boosts the event into a moving frame, thereby altering the angular correllations[16] .

(iii) hadronization effects, as discussed briefly above.

All of the above effects occur together, so that they can only really be taken into account correctly using Monte Carlo techniques. The PLUTO group have done this and found that $A(\Theta)$ is in fact dominated by the perturbative QCD contribution at Q = 30 GeV for $45^\circ < \Theta < 90^\circ$, corrections being $\sim 10\text{-}20\%$. So the agreement of $A(\Theta)$ with data is indeed significant.

One could repeat the above procedure using a model of scalar gluons [8] to find agreement with data for a strong scalar coupling of ~ 2.0 [10,15] , which makes no sense perturbatively.

Having discussed the general approach of this method of measuring QCD, one must now see what happens at small transverse momentum, which contains the main body of data and which is a

particularly interesting regime since single gluon effects can no longer be expected to dominate.

CHAPTER 2

The Region of Small Transverse Momentum.

2.1 Introduction

Up to this point it has been assumed that hard parton scattering is the dominant mechanism, which is a good approximation for $Q_T^2 \sim Q^2$. However, when $Q_T^2 \ll Q^2$, the perturbative expansion breaks down due to the emergence of double logarithmic terms of the form $\alpha_s^n \left[\ln Q^2/Q_T^2\right]^{2n}$ which obviously diverge for small Q_T; these double leading logarithms (DLL) can be resummed in order to control these soft emissions (as done by Block-Nordsiek in QED). This results in a quark form factor. The assumption that a quark radiates just a single gluon is unrealistic in the regime where $\Lambda^2 \ll Q_T^2 \ll Q^2$, and so one must take into account multiple soft gluon emission, which means summing all orders in α_s if possible. This was originally done by DDT[19], and has since been the source of much interest [19-27,30,33,34].

The problem was originally encountered in order to derive the transverse momentum distribution of lepton pairs produced in Drell-Yan ; the parton diagrams are simply related to those of e^+e^- by crossing symmetry, and the resulting quark from factor is the same in both cases. Consider lowest order corrections to Drell-Yan, as shown in fig. (2.1), where the virtual photon γ^* recoils against the single gluon with transverse momentum Q_T. Consider just the $2\to2$ subprocesses ($q\bar{q}\to\gamma^* g$) depicted in fig (2.1) (b) and let us define the usual Mandelstam variables $\hat{s}, \hat{t}, \hat{u}$, where $\hat{t} = (p_1 - Q)^2$, $\hat{s} = (p_1 + p_2)^2$ etc. and $C_F = 4/3$ is the $SU(3)_c$ Casimir operator. Then the modulus squared of the amplitude corresponding to the diagrams in fig.(2.1) (b) is proportional to

$$C_F \alpha_s \left[\frac{(\hat{s}+\hat{t})^2 + (\hat{s}+\hat{u})^2}{\hat{t}\,\hat{u}}\right] \qquad (2.1)$$

fig.(2.1)

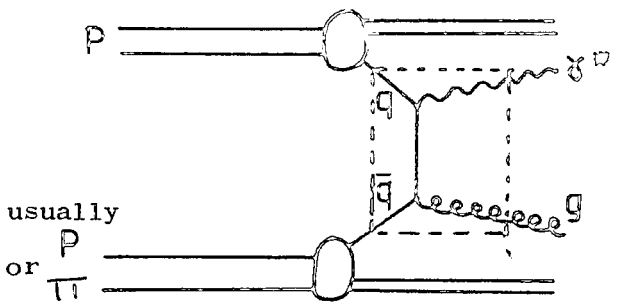

(a) An $O(\alpha_s)$ correction to Drell-Yan.

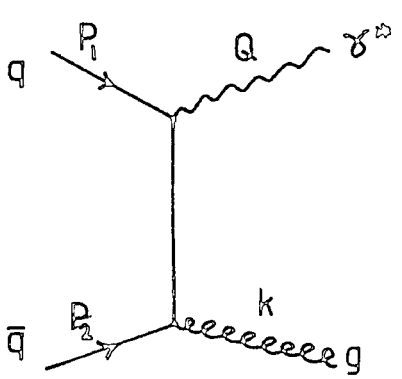

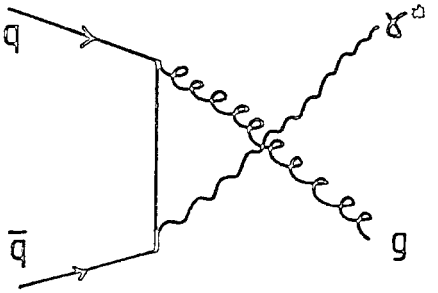

(b) $O(\alpha_s)$ subprocess real diagrams for production of a virtual photon with non zero transverse momentum.

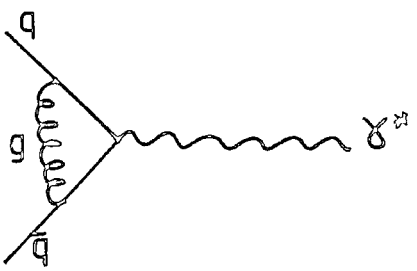

(c) An $O(\alpha_s)$ virtual correction.

[20], which is gauge independent. Integrating this quantity over the gluon phase space now produces logarithms of $\hat{s}/Q_T^2$. These are the source of the singularities which spoil lowest-order perturbation theory. To see how this happens, it proves convenient to make a Sudakov decomposition of the gluon momentum, viz.

$$k^\mu = \alpha P_1^\mu + \beta P_2^\mu + \vec{k}_T \qquad (2.2)$$

Where $\vec{k}_T \cdot P_1 = \vec{k}_T \cdot P_2 = 0$, and one can write

$$\frac{d^3k}{2k_0} = (P_1 \cdot P_2)\, d\theta\, d\mu\, d^2\vec{k}_T\, \delta(\theta\mu - k_T^2/2P_1\cdot P_2)$$

$$= \frac{\hat{s}}{2}\, d\theta\, d\mu\, d^2\vec{k}_T\, \delta(\theta\mu - k_T^2/\hat{s}) \tag{2.3}$$

where we are again considering massless quarks and gluons, and the δ function comes from the fact that $k_T^2 = -\theta\mu 2(P_1\cdot P_2) \equiv -\theta\mu\hat{s}$ from eq. (2.2). Also, forming the 4-vector products $k\cdot P_1$, and $k\cdot P_2$ from eq. (2.2), we find:

$$\mu = \frac{k\cdot P_1}{P_1\cdot P_2} \equiv -\frac{\hat{u}}{\hat{s}}\ ;\quad \theta = \frac{k\cdot P_2}{P_1\cdot P_2} = -\frac{\hat{t}}{\hat{s}} \tag{2.4}$$

so that $\delta(\hat{s}+\hat{u}+\hat{t}-Q^2) \equiv \delta(\hat{s}(1-\theta-\mu) - Q^2)$. One can therfore write the cross section in the form:

$$\frac{1}{\sigma_{0\gamma}}\frac{d\hat{\sigma}}{dQ_T^2} = \frac{\alpha_s C_F}{2\pi}\int d\mu\, d\theta\, d^2\vec{k}_T\, \delta^2(\vec{k}_T+\vec{Q}_T)\,\delta(\theta\mu - k_T^2/\hat{s}).$$

$$\cdot\frac{dQ^2}{Q^2}\,\delta(\hat{s}(1-\theta-\mu)-Q^2)\,\frac{[(1-\theta)^2+(1-\mu)^2]}{\theta\mu} \tag{2.5}$$

where $\sigma_{0\gamma}$ is the zeroth order cross section, $\sigma_{0\gamma} = 4\pi\alpha^2/9\hat{s}$.

Utilizing the appropriate δ functions to do the Q^2 and θ integrations yeilds:

$$\frac{1}{\sigma_{0\gamma}}\frac{d\hat{\sigma}}{dQ_T^2} = \frac{\alpha_s C_F}{2\pi}\int\frac{d^2\vec{k}_T}{k_T^2}\int_{\mu_{min}}^{\mu_{max}} d\mu\,\delta^2(\vec{k}_T+\vec{Q}_T).$$

$$\cdot\,\frac{\left[\left(1-k_T^2/\hat{s}\mu\right)^2+(1-\mu)^2\right]}{\mu\left(1-k_T^2/\hat{s}\mu-\mu\right)} \tag{2.6}$$

In order to obtain the soft gluon cross section, one can make the approximation $k_T^2/\hat{s} \ll 1$, and so neglect all terms of this form in the integrand of eq. (2.6), where the leading logarithmic contribution also comes from the region of small μ. Thus one can also neglect terms which depend on powers of μ. Thus the μ dependent part of the integrand in eq. (2.6)can be written,

$$\frac{2(1-\mu)+\mu^2}{\mu(1-\mu)}$$

$$= \frac{2}{\mu} \text{ in leading log.} \tag{2.7}$$

The next step in the soft gluon approximation is to overestimate the μ (orΘ) phase space by setting the upper limit to 1, which corresponds to $k_T^2 = 0$. Also from eq. (2.4) $\mu_{min} \sim k_T^2/\hat{s}$ so that one is left with :

$$\frac{1}{\sigma_{0\gamma}}\frac{d\hat{\sigma}}{dQ_T^2} = \frac{\alpha_s C_F}{2\pi}\int \frac{d^2\vec{k}_T}{k_T^2}\,\delta^2(\vec{k}_T+\vec{Q}_T)\int_{k_T^2/\hat{s}}^{1}\frac{d\mu}{\mu}$$

$$= \frac{\alpha_s C_F}{2\pi}\int \frac{d^2\vec{k}_T}{k_T^2}\,\ln\frac{\hat{s}}{k_T^2}\,\delta^2(\vec{k}_T+\vec{Q}_T) \tag{2.8}$$

$$\therefore \frac{1}{\sigma_{0\gamma}}\frac{d\hat{\sigma}'}{dQ_T^2} = \frac{\alpha_s C_F}{\pi Q_T^2}\ln\frac{\hat{s}}{Q_T^2} \tag{2.9}$$

To exhibit the double logarithmic character of the above first order result ($d\hat{\sigma}'$), consider the integrated quantity,

$$\sum_{real}{}'(p_T^2/\hat{s}) = \int_{\lambda^2}^{p_T^2} dQ_T^2\,\frac{1}{\sigma_{0\gamma}}\frac{d\hat{\sigma}'}{dQ_T^2} \tag{2.10}$$

where λ is again a ficticious gluon mass. This leads to,

$$\sum_{\text{real}}{}'(p_T^2/\hat{s}) = -\frac{\alpha_s C_F}{2\pi}\left[\ln^2\frac{\hat{s}}{p_T^2} - \ln^2\frac{\hat{s}}{\lambda^2}\right] \tag{2.11}$$

Similarly, a calculation of the lowest order virtual diagram of Fig. (2.7)(c) leads to

$$\sum_{\text{virtual}}{}'(p_T^2/\hat{s}) = -\frac{\alpha_s C_F}{2\pi}\ln^2\frac{\hat{s}}{\lambda^2} \tag{2.12}$$

And so, although the mass divergence cancels between real and virtual graphs, this is not enough, and the double logs in eq. (2.11) emerge to spoil the perturbative expansion. Note, that in the hard scattering regime, where $p_T^2 \sim \hat{s}$, these double log terms are negligible; it is the terms which we have thrown away here which become important.

Since the virtual graphs only contribute at $Q_T=0$, one can define a regularized cross section, order-by-order, as,

$$\left.\frac{1}{\sigma}\frac{d\sigma}{dQ_T^2}\right|_{reg} = \frac{1}{\sigma}\frac{d\sigma}{dQ_T^2} - \delta(Q_T^2)\int dk_T^2\,\frac{1}{\sigma}\frac{d\sigma}{dk_T^2} \tag{2.13}$$

which will take care of the mass singularities (as shown above to $O(\alpha_s)$ and explicitly to $O(\alpha_s^3)$ by Lo and Sullivan [23] working in the Feynman gauge).

The way to proceed is now to calculate second order diagrams and so on, and hope that a way to sum up all soft emissions emerges. Before doing that, it is worthwhile to mention a couple of points which have made practical calculations easier, viz, the choice of gauge sec(2.2) and the factorization of soft emissions sec(2.3) which are basically the main ingredients used by the original workers in the field [19,20-25, 34]. This will then enable us to understand how the quark

form factor emerges, after which we turn to phenomenology at small Q_T.

2.2 The Choice Gauge.

Consider again e^+e^- annihilation. The cross section for single gluon emission in $e^+e^- \rightarrow q\bar{q}g$ is given by eq. (1.5). This includes both leading log contributions (like that of eq (2.9) with $\hat{s}=Q^2$) and others, and is gauge independent. It was obtained [8] by summing the amplitudes of fig. (1.2) and taking the square modulus. Diagramatically this then gives three separate contributions to the overall cross section of the form $|M_1|^2$, $|M_2|^2$ and $2M_1M_2^*$, if M_1, and M_2 are the amplitudes of fig. (1.2). These are shown diagramatically in Table I, along with the partial cross sections derived from each with the various choices of gauge for the gluon propagator (from [21]).

The gluon propagator in an axial gauge is given by:

$$D_{\mu\nu}(k) = \frac{K_{\mu\nu}(k)}{k^2} = \frac{1}{k^2}\left(-g_{\mu\nu} + \frac{n_\mu k_\nu + n_\nu k_\mu}{(n.k)} - \frac{n^2 k_\mu k_\nu}{(n.k)^2}\right) \tag{2.14}$$

where the gauge is specified by the vector n, such that $n.\varepsilon=0$, where ε is the gluon polarization vector and k the gluon momentum.

TABLE I: Contributions to the total cross section from ladder and interference diagrams, in various gauges.

diagram \ gauge	Feynman	Axial n=q	Axial n=P_1
M_1 : 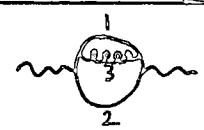	$\frac{2(1-X_1)}{(1-X_2)}$	$\frac{2(1+X_1^2)}{(1-X_1)(1-X_2)} - 4/(1-X_1)X_3$	$\frac{2(1-X_1)}{(1-X_2)}$
M_2 : 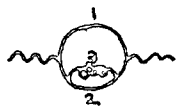	$\frac{2(1-X_2)}{(1-X_1)}$	$\frac{2(1+X_2^2)}{(1-X_1)(1-X_2)} - 4/(1-X_2)X_3$	$\frac{2(X_1+(1-X_3)^2)}{(1-X_1)(1-X_2)}$
M_1M_2 : 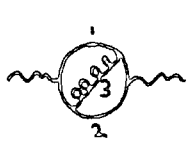	$\frac{4(1-X_3)}{(1-X_1)(1-X_2)}$	0	$\frac{4(1-X_3)}{(1-X_2)}$

Note that $k^\mu K_{\mu\nu} = 0$, $n^\mu K_{\mu\nu} = 0$ when $k^2 = 0$, so that when the gluon is on-shell it can only be polarized in directions orthogonal to the plane defined by its momentum k_μ and the gauge vector n_μ. The third term in the propagator does not contribute in leading log; in fact in most cases n_μ is chosen to be a null vector, and so the term will be neglected. With the gluon only having physical degrees of freedom, i.e. only transverse polarizations, there is no need to introduce an unphysical ghost contribution to cancel the scalar component.

Even though the overall cross section is always the same gauge independent result, the gauge does affect the diagramatic interpretation. For example, in an axial gauge specified by $n = P_1$, the gluon can be pictured, in the leading log approximation, as being emitted solely from one of the quarks, whereas when $n=q$, it may be viewed as being emitted with equal probability from either; this can be seen in table I where the leading log behaviour comes from the regions of phase space where X_1, $X_2 \Rightarrow$ maximum. (as shown for example in Appendix A, where physical predictions are made by integrating eq. (1.5)). On the other hand in the Feynman gauge it is the interference diagram which dominates in leading log, and we cannot determine from which quark leg the gluon was emitted. So if one chooses to work in an axial gauge, then this permits a probabilistic interpretation of the process, as originally suggested by DDT [19].

In performing leading log calculations in an axial gauge, one therefore only need consider ladder diagrams, such as that in fig (2.2).

Fig. (2.2): Ladder diagram in e^+e^-.

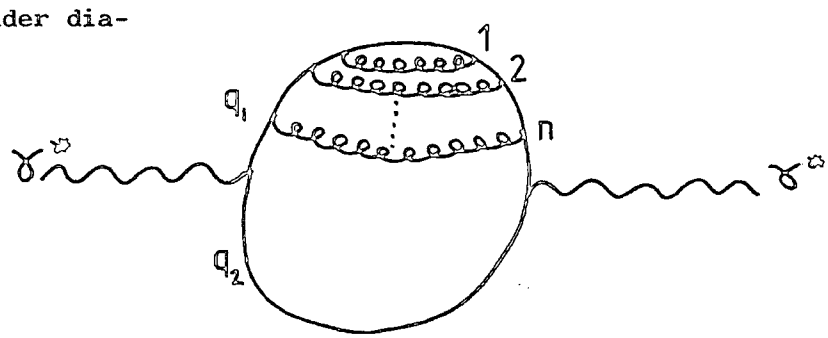

The dominant region of phase space is that in which the transverse momentum of the gluons is strongly ordered i.e.

$$k_{T1}^2 \ll k_{T2}^2 \ll \ldots\ldots \ll k_{Tn}^2 \ll Q^2 \tag{2.15}$$

(see below sec.(2.4)). This enables an n-rung graph to be wirtten as a product of single rung diagrams, so that their sum leads to simple exponentiation [19].

2.3 Independent Emissions.

Also in the region of small transverse momentum Q_T, the calculation of multigluon amplitudes is greatly simplified because the emission of gluons becomes independent. Consider for example just two gluon emission as depicted in fig. (2.3), (corresponding as drawn to an axial gauge $n=P_1$). The amplitude is proportional to,

$$\frac{\not p - \not k_1}{(p-k_1)^2}\cdot\frac{\not p - \not k_1 - \not k_2}{(p-k_1-k_2)^2} + \frac{\not p - \not k_2}{(p-k_2)^2}\cdot\frac{\not p - \not k_2 - \not k_1}{(p-k_2-k_1)^2} \tag{2.16}$$

which for massless quarks and gluons, with $k_1, k_2 \ll P$ becomes,

$$\frac{\not p}{2p.k_1}\cdot\frac{\not p}{2p.(k_1+k_2)} + \frac{\not p}{2p.k_2}\cdot\frac{\not p}{2p.(k_1+k_2)}$$

$$= \frac{\not p}{2p.k_1}\cdot\frac{\not p}{2p.k_2} \tag{2.17}$$

on combining terms.

Fig.(2.3): 2 contributions to the amplitude for 2 gluon emission. Emissions from the other quark leg and from both may or may not contribute, depending on the gauge.

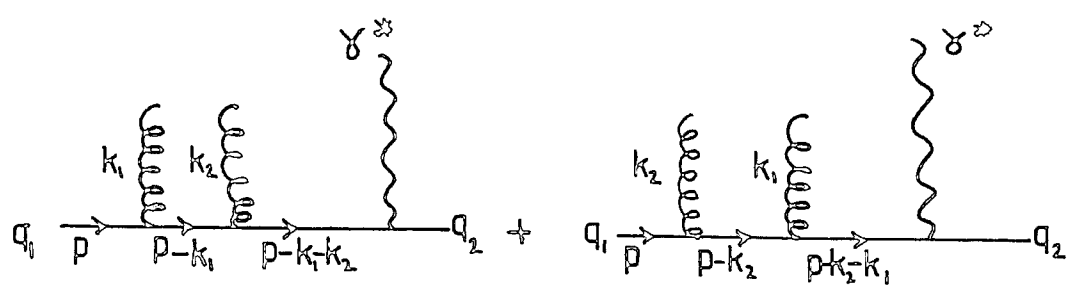

Thus, the emission has factorized, and this can easily be seen to generalize to an arbitrary number of soft gluons.

2.4 The Quark Form Factor.

In terms of the Sudakov variables, the above factorization property can be seen to come from the region of phase space where $\theta_i, \mu_i \ll 1$ and $\vec{k}_{Ti}$ are small, along with the constraint that the μ_i are ordered [20,22]. So the denominators in eq.(2.16) can be written,

$$(p-k_1)^2 = -\hat{s}\mu_1 \tag{2.18a}$$

$$(p-k_1-k_2)^2 = -\hat{s}\left[\mu_1(1-\theta_2)+\mu_2(1-\theta_1)-\frac{\vec{k}_{T1}\cdot\vec{k}_{T2}}{\hat{s}}\right]$$

$$= -\hat{s}\mu_2 \quad \text{if} \quad \mu_2 \gg \mu_1 \tag{2.18b}$$

If one also ignores the constraint of energy conservation, (which hopefully will not be too bad if the gluons are very soft), then the integrals for each gluon can be treated independently, with an identical factor coming from each gluon. So the extension of the single gluon cross section eq(2.8) to 2 gluons (or any number for that matter) is simple, and can be written as [20,22,25],

$$\frac{1}{\sigma_0}\frac{d\sigma^2}{dQ_T^2} = \left[\frac{C_F\alpha_s}{\pi}\right]^2 \frac{1}{2\pi}\int_{\lambda^2}^{Q_T^2} \frac{d^2\vec{k}_{T1}}{k_{T1}^2}\frac{d^2\vec{k}_{T2}}{k_{T2}^2}\ln\frac{Q^2}{k_{T1}^2}\ln\frac{Q^2}{k_{T2}^2} \cdot \delta^2(\vec{k}_{T1}+\vec{k}_{T2}+\vec{Q}_T) \tag{2.19}$$

for e^+e^- annihilation, where λ is again a ficticious gluon mass and where α_s is considered fixed for the moment for simplicity. All necessary diagrams have been included in leading log to obtain eq.(2.19), and so the gauge dependence, (which explicitly occurs in factors $\sim 1/2n\cdot k_i = 1/\hat{s}(\theta_i+\mu_i)$ with $n=P_1+P_2$), has dropped out. Eq.(2.19) is therefore the leading logarithmic (soft) cross section for producing a $q\bar{q}$ pair in e^+e^- annihilation with relative

transverse momentum $Q_{\perp}$, due to the emission of 2 independent gluons. Eq.(2.19) is the starting point, or master formula, from which the expressions for the quark from factor are derived.

The simplest approach from this point is to recognise that the dominant range of integration in eq.(2.19) comes from the region of strong ordering,

$$k_{T1,2}^2 \ll k_{T2,1}^2 \simeq Q_T^2 \tag{2.20}$$

so that eq(2.19) becomes:

$$\frac{1}{\sigma_0}\frac{d\sigma^2}{dQ_T^2} = \left[\frac{C_F \alpha_s}{2\pi}\right]^2 \frac{1}{Q_T^2} \ln\left[\frac{Q^2}{Q_T^2}\right] \int_{\lambda^2}^{Q_T^2} \frac{dk_T^2}{k_T^2} \ln\left[\frac{Q^2}{k_T^2}\right] \tag{2.21}$$

$$= \frac{1}{2}\left[\frac{C_F \alpha_s}{\pi}\right]^2 \frac{1}{Q_T^2} \ln\left[\frac{Q^2}{Q_T^2}\right] \left\{ \ln^2 \frac{Q^2}{\lambda^2} - \ln^2 \frac{Q^2}{Q_T^2} \right\} \tag{2.22}$$

Regularizing the cross section of eq.(2.22) by adding in the same order virtual graphs, according to the prescription of eq.(2.13) removes the $\ln^2 Q^2/\lambda^2$ term above. So that eq.(2.22) can be written in terms of the 1 gluon cross section as,

$$\frac{1}{\sigma_0}\frac{d\sigma^2}{dQ_T^2} = -\left[\frac{1}{\sigma_0}\frac{d\sigma^1}{dQ_T^2}\right] \frac{C_F \alpha_s}{2\pi} \ln^2\left[\frac{Q^2}{Q_T^2}\right] \tag{2.23}$$

where the single gluon cross section in e^+e^- annihilation is (c.f.eq. (2.9) with $\hat{s} \equiv Q^2$ in e^+e^-),

$$\frac{1}{\sigma_0}\frac{d\sigma^1}{dQ_T^2} = \frac{4\alpha_s}{3\pi Q_T^2} \ln\left[\frac{Q^2}{Q_T^2}\right] \tag{2.24}$$

Notice that the $O(\alpha_s^2)$ cross section is negative, which cancels

against that of $O(\alpha_s)$. This gives an indication that leading logs do in fact tend to cancel against each other in successive orders, in the regime $Q_T^2 \ll Q^2$.

It can be seen that eqns.(2.24), (2.23) form the first two terms of an exponential, (with $\frac{1}{\sigma_0} d\sigma'/dQ_T^2$ a common factor). In fact eq.(2.19) can be trivially extended to any number of gluons and the exponentiation can be seen to occur to all orders, with the result that,

$$\left.\frac{1}{\sigma_0}\frac{d\sigma}{dQ_T^2}\right|_{\substack{\text{All}\\ \text{Orders}}} = \frac{1}{\sigma_0}\frac{d\sigma'}{dQ_T^2} \operatorname{Exp}\left[-\frac{C_F \alpha_s}{2\pi} \ln^2 Q^2/Q_T^2\right] \qquad (2.25)$$

This has exactly the same form as the form factor derived for QED [23], and so eq.(2.25) will be called the Sudakov type quark form factor [20-26]. The physical process it describes is outlined in fig. (2.4), where e^+e^- is compared with Drell-Yan.

Fig.(2.4) The Perturbative Quark form factor
(A) $e^+e^- \longrightarrow q\,\bar{q} + ng$
(B) $(p\bar{p} \rightarrow) q\,\bar{q} \rightarrow l\bar{l} + ng$

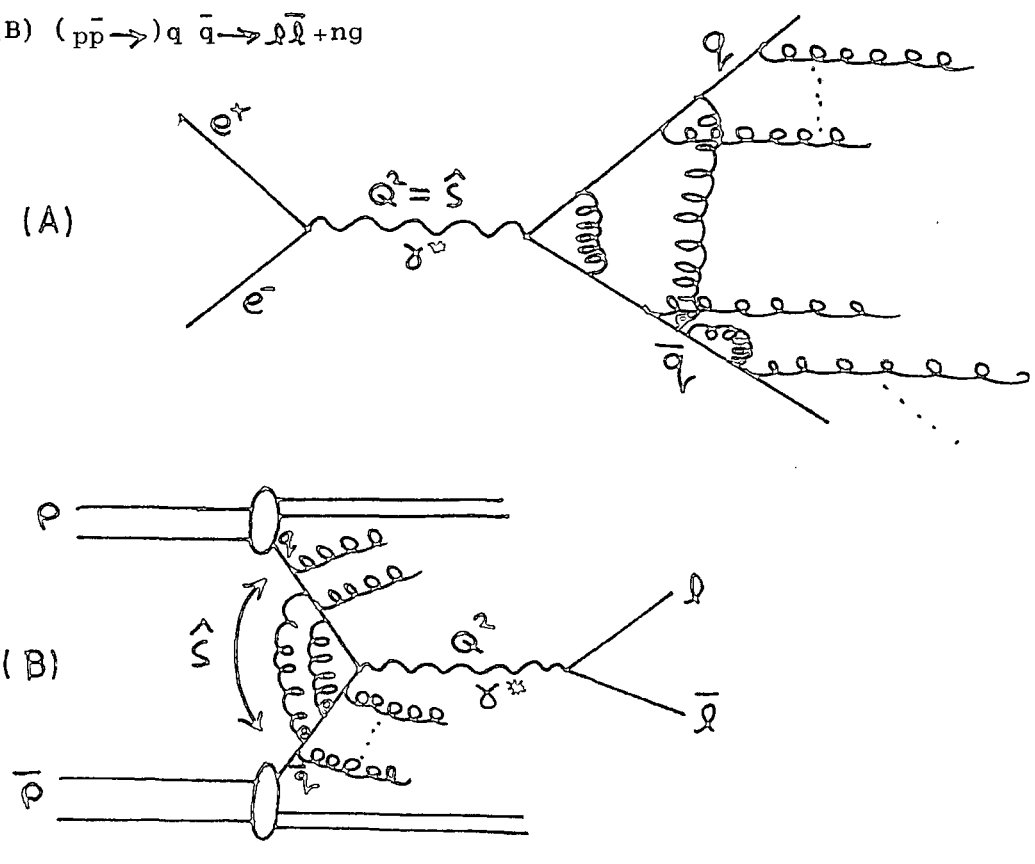

In e^+e^-, therefore, the quarks recoil against many soft gluons, and it is this which we eventually want to measure. Moreover, eq.(2.25) predicts a suppression in the cross section when $Q_T^2 \ll Q^2$, and this point has been the source of some investigation [22,24,25]. The case of a running coupling constant is discussed in Appendix B, where it is shown that log logs appear which soften the suppression. If this were a correct prediction, then one might hope to look for it experimentally to support the approximations used, (ie. those of multiple, soft independent emissions), and the theory. However, in the next section this will be seen to be in some doubt, when momentum conservation in eq. (2.19) is considered accurately.

2.5 Relaxing The Approximation of Strong Ordering.

The approximation of strong ordering (eqn .(2.15), (2.20)) is obviously a doubtful one, particularly when $Q_T \longrightarrow 0$, where it is clearly incorrect. Strong ordering envisages the situation where effectively a single gluon balances the transverse momentum of the quarks, and it picks out purely leading log behaviour from eq.(2.19). This very limited physical regime can be improved upon by taking into account transverse momentum conservation more accurately, and this will shortly be seen to have significant consequences [24]. This can be done by writing the δ function of eq. (2.19) as an integral in a two dimensional (impact parameter) space $\vec{b}$; i.e. generalizing to n gluons,

$$\delta^2\left(\vec{k}_{T1}+\vec{k}_{T2}+\ldots+\vec{k}_{Tn}+\vec{Q}_T\right)$$

$$=\frac{1}{(2\pi)^2}\int d^2\vec{b}\; e^{i\left(\vec{k}_{T1}+\vec{k}_{T2}+\ldots+\vec{k}_{Tn}+\vec{Q}_T\right).\vec{b}} \qquad (2.26)$$

and substituting this result into the n-gluon equivalent of eq.(2.19), and changing the order of the $\vec{b}$ and $\vec{k}_{T\lambda}$ integrations results in the $\vec{k}_{T\lambda}$ integrals factorizing, so that one obtains a product of the

b-space transforms of the probability of emitting a single independent gluon. This then simply gives exponentiation in b-space of the 1 gluon cross section, as shown by Parisi and Petronzio [24] (see also [34]). So defining the b space transform as,

$$\Delta(b) = \int_{}^{k_{T\,max}^2} dk_T^2 \, \frac{1}{\sigma_0} \frac{d\sigma'}{dk_T^2}\Big|_{reg} J_0(bk_T) \tag{2.27}$$

where '$|_{reg}$' is defined in eq.(2.13).

(Where the angular integration has been performed using,

$$\int \frac{d^2k_T}{\pi} \frac{1}{\sigma_0} \frac{d\sigma'}{dk_T^2}\Big|_{reg} e^{i\vec{k}_T.\vec{b}} = \int dk_T^2 \frac{1}{\sigma_0} \frac{d\sigma'}{dk_T^2}\Big|_{reg} J_0(k_T b) \quad)$$

And using eq.(2.13), this becomes

$$\Delta(b) = \frac{4}{3\pi} \int_{M^2}^{k_{T\,max}^2} \frac{dk_T^2}{k_T^2} \alpha_s(k_T^2) \ln\left[\frac{k_T^2}{Q^2}\right] \left[J_0(k_T b) - 1\right] \tag{2.28}$$

and one can then write the cross section for multigluon emission as,

$$\frac{1}{\sigma_0} \frac{d\sigma}{dQ_T^2} = \frac{1}{4} \int db^2 \, Exp[\Delta(b)] J_0(bQ_T) \tag{2.29}$$

and so we have another expression for the quark from factor. Eq.(2.13) has provided a neat way to take care of the virtual graphs order-by-order.

The strong coupling constant α_s is now allowed to run with k_T^2 and so is taken under the integral in eq. (2.28). (For a more detailed discussion of the argument of the running coupling see chapter 3). This then introduces the problem that $\alpha_s(k_T^2)$ diverges when $k_T^2 = \Lambda^2$, and so a regulator M^2 is used on the bottom limit. The regulator M^2 is, however, not needed if an appropriate form for $\alpha_s(k_T^2)$ is used. Since this is the first time a running coupling is introduced, it is worthwhile at this point to discuss its form , before examining eqs.

(2.28), (2.29).

e^+e^- annihilation or Drell-Yan is a timelike process, so when using a running coupling, the coupling constant has to be analytically continued from that used in leptoproduction i.e. the $\ln(Q^2/\Lambda^2)$ in leptoproduction goes to $\ln(-Q^2/\Lambda^2)$ in e^+e^- annihilation, so that $\alpha_s(Q^2) \sim 1/(\ln Q^2/\Lambda^2 - i\pi)$. For processes (such as the one under consideration) involving small transverse momentum k_T, then the leading logarithmic contribution to the running coupling comes from the k_T dependence, so α_s is chosen to run with k_T. One is now left with a choice of the best expansion parameter α_s to use [28], i.e. for instance $\alpha_s(|k_T^2|)$ or $|\alpha_s(k_T^2)|$. Because of the π's which occur in the spacelike to timelike continuation of the $\ln k^2$, there are large higher order corrections if one chooses to expand in $\alpha_s(|k^2|)$ [28]. These terms are of $O(\alpha^2(|k^2|)\pi^2)$ with respect to leading QCD corrections and will not be small until $\ln^2(|k^2|/\Lambda^2) \lesssim 3\pi^2$ i.e. $k^2/\Lambda^2 \gtrsim 200$. So $\alpha_s(|k^2|)$ is not a good expansion parameter for present purposes. The so called "frozen coupling" $|\alpha_s(k^2)|$ is a better choice, and has been shown to be so explicitly, by calculating the ratio R in e^+e^- [28]. This choice has not got the rapidly varying form of $\alpha_s(|k^2|)$, and is a more natural parameter which can be used in both space-like and time-like regions. It can then be written as,

$$|\alpha_s(k_T^2)| = \left|\frac{12\pi}{(33-2n_f)\ln(k_T^2/\Lambda^2)}\right| = \frac{12\pi}{(33-2n_f)\left[\ln^2\left(\frac{k_T^2}{\Lambda^2}\right)+\pi^2\right]^{1/2}} \qquad (2.30)$$

which "freezes" out to a fixed value as $k_T^2 \to 0$. This therefore automatically takes care of the singularity arising from the lower limit of integration in eq.(2.28), and so makes the regulator M^2 redundant. Having taken care of this point, we can now mention some

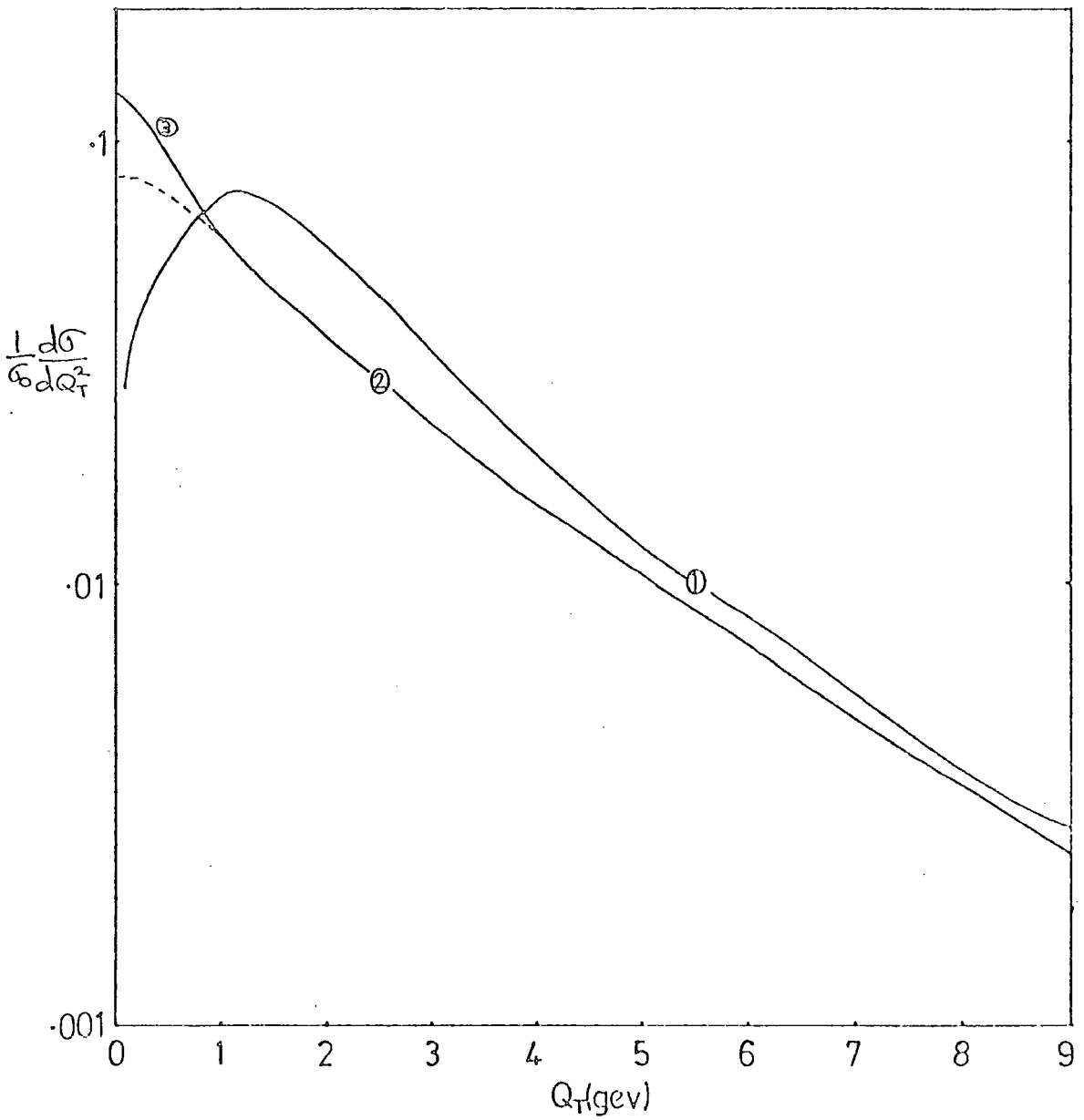

Fig.(2.5) The quark form factor $\frac{1}{\sigma_0} d\sigma/dQ_T^2$ using a running coupling $\alpha_s(k_T^2)$ and $\Lambda = 0.5$, $Q = 31.6$ Gev. Curve 1 is the Sudakov type form factor and curves 2 and 3 are the Parisi-Petronzio prescription, eqs.(2.28), (2.29). Curve 3 contains the smearing function $\rho(b)$ of eqs. (2.45), (2.46), with $\langle k_T \rangle$ =400 Mev. We use four flavours of quarks.

points connected with eqs. (2.28), (2.29).

Eqns. (2.28), (2.29) give extra terms, order-by-order, which are powers of logarithms of (Q^2/Q_T^2) down from the leading term. For example, in the two gluon case, the cross section is modified by a positive constant, compared with a leading $\ln^3(Q^2/Q_T^2)$ (see [25] for instance). These non-leading terms however, turn out to be very important since they fill in the dip as $Q_T \to 0$ when summed to all orders, with the leading log terms cancelling against each other (as was seen to second order in eqs. (2.23), (2.24)). This can be seen in Fig. (2.5) , where both the Sudakov-type form factor of eq. (2.25) and the Parisi-Petronzio form factor of eq. (2.29) are plotted for Q=30 Gev and Λ =0.5 Gev. Since the very small transverse momentum contribution in the multigluon sum of eqs. (2.28), (2.29) has completely cancelled out, then very small Q_T can only be obtained by the cancellation of two or more much harder gluons, and so perturbative QCD can be applied there. Therefore, as suggested by Parisi and Petronzio [24], the effects of intrinsic transverse momentum (in Drell-Yan anyway) might be expected to be washed out against those of the much harder gluons.

Whilst on the point of non-perturbative effects and so called "intrinsic" transverse momentum, it must be noted that Drell-Yan and e^+e^- cannot be looked upon in the same way in this respect. The intrinsic transverse momentum $k_{T\,int}$ in Drell-Yan is intrinsic in the correct sense of the word, in that it originates from the hadronic structure, whereas that $k_{T\,int}$ in e^+e^- results from fragmentation which is entirely a different process, although both are non-perturbative. A parametrization of the $k_{T\,int}$ distribution to represent "hadronic wobble" must therefore be put in at the start of any calculation of an observable quantity in Drell-Yan, but in e^+e^- this only comes at the end when the quarks fragment, up to which point the form factor might be expected to give an adequate description. This point will be

considered in more detail in chapter 3, where this distinction is more correctly considered.

To summarize this section, there can be considered three distinct physical regions in b: $0 \leq b \leq 1/Q$ where lowest order perturbation theory may be expected to dominate; $1/Q \leq b \leq 1/\Lambda$ where resummed perturbation theory can be used; and $b \gtrsim 1/\Lambda$ which is sensitive to hadronic size and therefore the non-perturbative regime. However, in view of the above discussion, one can now hope to do feasible perturbative calculations in the latter regime, where the major contribution comes from two or more hard gluons cancelling vectorially against each other.

So even though large b is the dominant region, order-by-order, the massive cancellations which occur ensure that small b is the relevant and dominant region of integration in eq. (2.29) (i.e. $b \lesssim 1/\Lambda$).

We now have all the ingredients necessary to do phenomenology. However, it might be worthwhile taking a digression for a moment to look at large b behaviour and asymptotic results using eqs. (2.28) (2.29), since much interest has been focused on them in the literature [22,25,26], and it is necessary to try and estimate their importance to phenomenological questions.

2.6 Large b and Asymptotic Results.

Eqns. (2.28), (2.29) (which will be referred to as the Parisi-Petronzio prescription (PPP)) cannot be precisely evaluated analytically, especially since $k_{T\,max}^2$ is proportional to Q^2. However, analytic approximations can be useful in order to see how the cross section behaves as $Q^2 \to \infty$ or for large b. For instance, it is useful to rewrite eqn. (2.28) in terms of the variables $Z=b^2Q^2$, $X= k_T^2/Q^2$ and $\lambda = \alpha_s C_F/\pi$ as done by S.Ellis et al [22] to give,

$$\Delta(b) \to \Delta(z) = \lambda \int_0^1 \frac{dx}{x} \ln \frac{1}{x} \left[J_0(\sqrt{xz}) - 1 \right]$$

where for simplicity α_s is assumed fixed. Then writing $y = \sqrt{xz} \equiv bk_T$ one obtains,

$$\Delta(z) = -2\lambda \int_0^{\sqrt{z}} dy\, J_1(y) \ln^2 \left(\frac{y}{\sqrt{z}} \right) \tag{2.31}$$

after performing integration by parts. $\Delta(z)$ is now in a form convenient for investigating its asymptotic behaviour and can be written,

$$\Delta(z) = -\frac{\lambda}{2} a_0(\sqrt{z}) \ln^2 z + 2\lambda a_1(\sqrt{z}) \ln z - 2\lambda a_2(\sqrt{z}) \tag{2.32}$$

where the coefficients $a_r(\sqrt{z})$ are given by :

$$a_r(\sqrt{z}) = \int_0^{\sqrt{z}} dy\, J_1(y) \ln^r(y) \tag{2.33}$$

In particular, the asymptotic limits $a_r(\infty)$ are given by,

$$a_r(\infty) = \int_0^{\infty} dy\, J_1(y) \ln^r(y) \tag{2.34}$$

so one can write the contribution to the integrals from the phase space between $\sqrt{z}$ and ∞ as,

$$\delta a_r \equiv a_r(\infty) - a_r(\sqrt{z}) = \int_{\sqrt{z}}^{\infty} dy\, J_1(y) \ln^r(y)$$

$$= \ln^r(\sqrt{z}) J_0(\sqrt{z}) + r \int_{\sqrt{z}}^{\infty} \frac{J_0(y) \ln^{r-1}(y)}{y}\, dy \tag{2.35}$$

after integration by parts. For large Z the second term gives a negligible contribution and the first term goes to zero as $Z \to \infty$, as expected, and can be written as $\Delta\left(\frac{2}{\pi\sqrt{Z}}\right)^{1/2} \ln\sqrt{Z}\, \cos\left(\sqrt{Z} - \pi/4\right)$. Using just the first term of eq.(2.35), the relative contribution of δa_r to $\Delta(Z)$ in eq. (2.32) can be estimated. The large b result is obviously less affected by overestimating the range of integration. However, as discussed earlier, it is small b which is the dominant region in eq.(2.29) and so it's crucial to get this correct in $\Delta(b)$.

Returning to the asymptotic form for $\Delta(Z)$, all one needs in eq. (2.32) are the coefficients $a_r(\infty)$. These have a generating function given by [22,29],

$$\sum_{r=0}^{\infty} \frac{1}{r!} t^r a_r(\infty) = \int_0^{\infty} dy\, J_1(y) \sum_{r=0}^{\infty} \frac{1}{r!} \ln^r(yt) = \int_0^{\infty} dy\, J_1(y)\, y^t$$

$$= 2^t\, \Gamma(1+t/2)/\Gamma(1-t/2)$$

$$= 2^t \exp\left\{ -\ln(1+t/2) + \frac{t}{2}(1-\gamma) + \sum_{n=2}^{\infty} (-1)^n \left(\zeta(n)-1\right) \frac{t^n}{2^n n} \right\} \cdot$$

$$\cdot \exp\left\{ \ln(1-t/2) + t/2\,(1-\gamma) - \sum_{m=2}^{\infty} (-1)^{2m} \left(\zeta(m)-1\right) t^m / 2^m m \right\}.$$

which after combining terms becomes,

$$\exp\left\{ t(\ln 2 - \gamma) - 2 \sum_{m=1}^{\infty} \frac{\zeta(2m+1)}{(2m+1)} \left(\frac{t}{2}\right)^{2m+1} \right\} \tag{2.36}$$

The second term above does not contribute until t^3, so the first three coefficients are easily obtained to be,

$$a_0(\infty) = 1\,, \quad a_1(\infty) = \ln 2 - \gamma\,, \quad a_2(\infty) = (\ln 2 - \gamma)^2$$

where γ is Euler's constant. So one can now write,

$$\Delta(z)\Big|_{z\to\infty} \simeq -\frac{\lambda}{2}\left[\ln^2 z - 4(\ln 2-\gamma)\ln z + 4(\ln 2-\gamma)^2\right]$$

or writing

$$z_0 \equiv \exp(2a_1(\infty)),$$

$$\Delta(z)\Big|_{z\to\infty} \simeq -\frac{\lambda}{2}\ln^2 z/z_0$$

which is,

$$\Delta(b)\Big|_{bQ\to\infty} \simeq -\frac{a_s C_F}{\pi}\left[\ln\frac{bQ}{2}+\gamma\right]^2 \qquad (2.37)$$

If one now substitutes eq(2.37) into eq.(2.19) using eq. (2.26), one obtains [25],

$$\frac{1}{\sigma_0}\frac{d\sigma^2}{dQ_T^2} = 2\left(\frac{2a_s}{3\pi}\right)^2\int_0^\infty db^2\left\{\ln\frac{bQ}{2}+\gamma\right\}^4 J_0(bQ_T)$$

$$= -2\left(\frac{2a_s}{3\pi}\right)\frac{1}{Q_T^2}\left[\ln^3\frac{Q^2}{Q_T^2} - 4\zeta(3)\right]$$

which is the asymptotic result for two gluon emission, and one can see explicitly the correction term picked up by exact use of transverse momentum conservation, which is three powers of logarithms down from the leading term [22,25].

Summing soft gluons, in b space merely results in exponentiating eq. (2.37), or in general eq.(2.32). From the form of the latter, one can easily see that $\exp(\Delta(b))$ decreases to zero faster than any inverse powers of Q as $Q\to\infty$, and since the b integral in eq. (2.29) will be depressed by this factor, then the probability of no emission of gluons with transverse momentum less than a fixed value decreases in the same way, and so events at $Q_T \geq 0$ can only be obtained asymptotically by the emission of two or more much harder gluons.

For large b, $\Delta(b)$ can be easily found by approximating $[J_0(k_T b)-1]$ in eq. (2.28) by $-\Theta(k_T b-1)$, resulting in,

$$\Delta(b) \lesssim -\frac{4\alpha_s}{3\pi}\int_{1/b^2}^{Q^2}\frac{dk_T^2}{k_T^2}\ln\left(\frac{k_T^2}{Q^2}\right)$$

or

$$\Delta(b)\Big|_{b\to\infty} \lesssim -\frac{2\alpha_s}{3\pi}\ln^2(b^2Q^2) \qquad (2.38)$$

When α_s runs with k_T^2 one has to evaluate,

$$\Delta(b) = \frac{16}{3\beta_0}\int_{}^{Q^2}\frac{dk_T^2}{k_T^2}\,\frac{\ln[k_T^2/Q^2]}{\ln[k_T^2/\Lambda^2]}\left[J_0(k_Tb)-1\right]$$

Using the same heuristic Θ function approximation as above and integrating by parts yields,

$$\Delta(b)\Big|_{b\to\infty} \lesssim \frac{16}{25}\left[\ln\left(\frac{Q^2}{\Lambda^2}\right)\ln\left[\frac{\ln(1/b^2\Lambda^2)}{\ln(Q^2/\Lambda^2)}\right]+\ln b^2Q^2\right] \qquad (2.39)$$

Equations (2.38),(2.39) are the leading forms of the single gluon b space transform [24,26,30], which demonstrate that large b might be dominant order-by-order, but exponentiation in b space then forces cancellations, resulting in small b dominating the multigluon cross section.

One can utilize b space to discuss the various levels of approximation if desired. [This is in analogy with discussing the double leading log approximation as terms like $[\alpha_s\ln^2 Q^2/Q_T^2\ ]^n$ and next to leading as $[\alpha_s\ln Q^2/Q_T^2\ ]^n$ etc... in k_T space]. With this in mind, one can write eq. (2.28) as,

$$\Delta(b) \underset{b\to\infty}{=} \frac{C_F}{\pi\beta_0}\sum_{N=1}^{\infty}\sum_{M=0}^{N+1} d_N^M\,\frac{(\ln b^2Q^2)^M}{(\ln Q^2/\Lambda^2)^N} \qquad (2.40)$$

(see for example [30]) where the leading terms in b space arise for

M = N+1, and next to leading for M = N etc... One can rewrite eq. (2.40) to explicitly show this structure,

$$\Delta(b) = \ln Q^2 b^2 \sum_N d_N^{N+1} \left[\frac{\ln Q^2 b^2}{\ln Q^2/\Lambda^2}\right]^N + \sum_N d_N^N \left[\frac{\ln Q^2 b^2}{\ln Q^2/\Lambda^2}\right]^N$$

$$+ \text{lower orders} \sim \frac{1}{\ln Q^2 b^2} \sum_N d_N^{N-1} \left[\frac{\ln Q^2 b^2}{\ln Q^2/\Lambda^2}\right]^N + \ldots$$

$$\equiv \Delta_1(b) + \Delta_2(b) + \ldots \qquad (2.41)$$

where $\Delta_1(b)$ correspondes to the leading result written down in eq. (2.39). One can then speculate whether all possible contributions to a given level of approximation have been included, (more of which in chapter 3).

However, discussing leading or non-leading terms, order-by-order, in b space can be misleading since the dominant contribution to the cross section comes from small b. So in order to confront the cross section with experiment at finite values of Q^2, it will be necessary to integrate eqns. (2.28)(2.29) numerically, and this then forms the basis of the subsequent phenomenology.

2.7. A First Attempt at Phenomenology

The quark cross section of eqns.(2.28),(2.29) is not directly confrontable with data, since the partons fragment into hadrons before they are observed. One must first turn it into a transverse momentum distribution of secondary hadrons or find their energy weighted acollinearity distribution. These results will be the main ones of this chapter and hopefully help to point the way to a better physical description.

This is an appropriate place at which to mention how the effects of intrinsic transverse momentum were put in. As was mentioned in Chapter 1, one could hope to parametrize the distribution of intrinsic

hadronic wobble as a Gaussian [24],

$$f(k_T^2) = A\exp(-Ak_T^2) \tag{2.42}$$

with,

$$\int_0^\infty f(k_T^2)\, dk_T^2 = 1$$

then,

$$\langle k_T\rangle_{int} = A\int_0^\infty dk_T^2\, k_T e^{-Ak_T^2} = \sqrt{\frac{\pi}{4A}} \tag{2.43}$$

and,

$$\langle k_T^2\rangle_{int} = 1/A \tag{2.44}$$

So, to correspond to a measured $\langle k_T^2\rangle \simeq 400$ MeV, A=2.5. Then this distribution can be incorporated into the calculation by smearing eq.(2.29) with it in b space. So one needs the b space transform,

$$\rho(b) \equiv \frac{1}{\pi}\int d^2\vec{k_T}\, e^{-i\vec{k_T}\cdot\vec{b}} f(k_T)$$

$$= 2A\int_0^\infty dk_T\, k_T e^{-Ak_T^2} J_0(k_T b) = e^{-b^2/4A} \tag{2.45}$$

(using eq.11.4.29 of ref.(29))

And then this simply modifies eq.(2.29) to,

$$\frac{1}{\sigma_0}\frac{d\sigma}{dQ_T^2} = \frac{1}{4}\int db^2\, \rho(b)\, e^{\Delta(b)} J_0(Q_T b) \tag{2.46}$$

The effect of this factor can be seen in fig. (2.5), where it

merely causes the cross section to increase slightly for $Q_T \lesssim 1$ Gev. This procedure is essentially borrowed from Drell-Yan [24], where it was used to incorporate the effects from hadronic structure, and so it must not be taken too seriously when discussing fragmentation. It is merely a first attempt to incorporate the latter, in order to test the parton distribution with experiment.

Bearing in mind the rather naive approach of using the smearing function $\rho(b)$, at least, so far, it sets up the calculation to give both the shape and normalization of the observed cross section. This seems a better approach than another prescription which was proposed by Altarelli , Parisi and Petronzio [32], again to account for transverse momentum distributions of high mass lepton pairs in Drell-Yan. Using this method [10,11] the P_T distribution of hadrons in the $P_T \simeq 0$ region is given by,

$$\frac{1}{\sigma}\frac{d\sigma}{dP_T^2} = \langle n \rangle f(P_T)$$

where $f(P_T)$ describes the intrinsic transverse momentum distribution of quark fragmentation into hadrons and is identical to the one used above (eq.(2.42)), and $\langle n \rangle$ is the average multiplicity. The above equation is used to describe two jet events, and so $f(P_T)$ can be fitted to data. This is then added to the $O(\alpha_s)$ result by,

$$\frac{1}{\sigma}\frac{d\sigma}{dP_T^2} = \langle n \rangle f(P_T) + \frac{1}{\pi}\int d^2\vec{k}_T \frac{1}{\sigma}\frac{d\sigma'}{dk_T^2}\left[f(\vec{P}_T - \vec{k}_T) - f(\vec{P}_T)\right]$$

where $d\sigma'$ is the $O(\alpha_s)$ hadronic result derived from eq.(1.19).

The above prescription is finite at $P_T \simeq 0$ and it also posseses the following desirable properties,

(i) $$\int \frac{1}{\sigma}\frac{d\sigma}{dP_T^2} dP_T^2 = \langle n \rangle$$

(ii) $\frac{1}{\sigma}\frac{d\sigma}{dP_T^2} \simeq \frac{1}{\sigma}\frac{d\sigma}{dP_T^2}'$ for large P_T^2

However, the prescription appears somewhat artificial. For instance, at small P_T the first term dominates and by virtue of its parametrization the cross section acquires the correct normalization, since $\langle n \rangle$ is taken from experiment, where it is observed to have a $\ln Q^2$ rise (which means the fragmentation functions $D(z)$ must be $\sim 1/z$ for small z). So there is no dependence on any underlying dynamics when $P_T \sim 0$, and over the remaining range in P_T, the prescription is difficult to understand physically. The PPP using eq.(2.46) at least merits a clear physical picture and provides a simple procedure to incorporate non-perturbative effects, which can also be applied simply in energy-energy correllations.

2.7.1. Transverse Momentum Distribution of Hadrons.

In this section, what we try to do is improve upon the first order result [10,11] used in eq. (1.19). From the form of eq.(1.19), it is clear that for small hadron transverse momentum P_T, the hadron distribution will have a large contribution from the parton cross section at small Q_T. This is just the region where the $O(\alpha_s)$ result diverges, and so in order to achieve a meaningful comparison with data, the cross section from multigluon emission must be used. However, eq.(1.19) must still be integrated to the edge of phase space, i.e., $Q^2/12$ since we must invoke the use of a thrust axis in this section (see Appendix A). And towards the edge of phase space the $O(\alpha_s)$ cross section can be expected to dominate, so it would be nice if one could incorporate multigluon emission at small Q_T, and single hard gluon emission at large Q_T, with a smooth transition between the two, at least phenomenologically. This forms the subject of the next subsection.

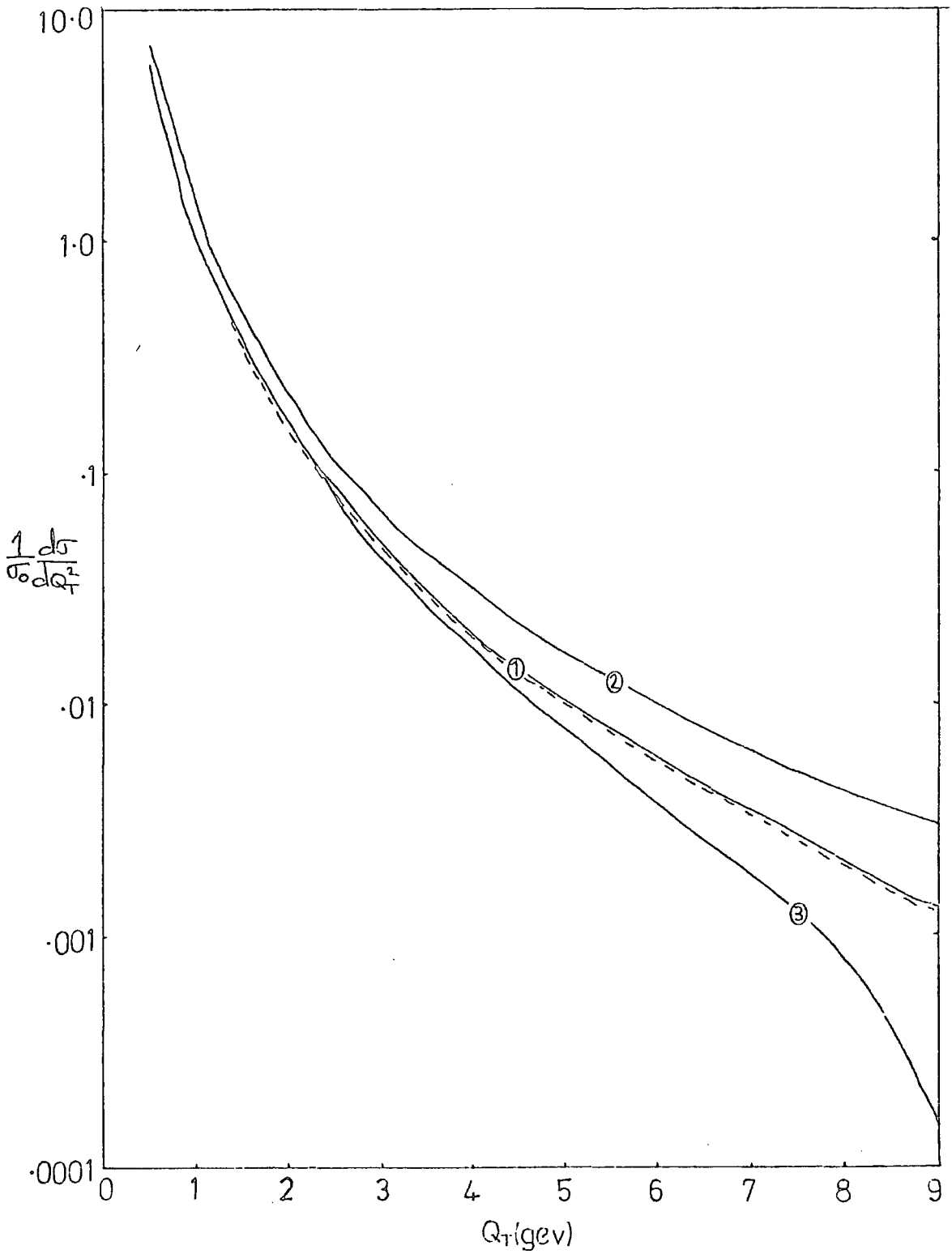

Fig.(2.6) Comparison of different forms of $\frac{1}{\sigma_0} d\sigma/dQ_T^2$ to $O(\alpha_s)$ using a running coupling $\alpha_s(Q_T^2)$ and $\Lambda = 0.5$ Gev, $Q = 31.6$ Gev. Curve 1 (Solid line) is the LLA using $\ln(1/x_T^2)$ and curve 2 is the LLA using $\ln(Q^2/Q_T^2)$. Curve 1 (dotted line) is the full $O(\alpha_s)$ result correctly integrated for the case of no preferential thrust direction. Curve 3 is the full $O(\alpha_s)$ result obtained when using a thrust axis (c.f. eqn(A2)).

2.7.1(a) Describing The Whole Range In Q_T

The $O(\alpha_s)$ leading log approximation (LLA), eq. (2.24), used in eq. (2.28), does not vanish at the edge of phase space (which is clearly defined in this case when a thrust axis is used); this it should do to give a meaningful physical cross section. The full $O(\alpha_s)$ result (obtained from eq. (1.5) in Appendix A) will have this property, and will automatically merge into the LLA for small Q_T. The whole region of phase space is integrated over to obtain $\Delta(b)$, and especially since the very small Q_T region is physically obtained by the vectorial addition of two or more large k_T gluons (in the PPP), then it would be sensible to get this region correct. A form of the LLA frequently seen in the literature is $\frac{C_F \alpha_s}{\pi k_T^2} \ln\left[1/x_T^2\right]$ where $X_T = \frac{2k_T}{Q}$. The extra factor of 4 in the argument of the logarithm does in fact cause this form of the LLA (solid curve 1 in fig. (2.6)) to resemble the correctly integrated $O(\alpha_s)$ result (curve 3 of fig(2.6)) more closely than eq.(2.24) (curve 2). Fig.(2.6) also shows that this form of the LLA mimics almost exactly the integrated $O(\alpha_s)$ result where no thrust axis is defined (dotted curve 1). The factor of 4 has almost the same effect as adding in the non-leading, non-logarithmic pieces to obtain the full $O(\alpha_s)$ result, and so provides a convenient parametrization.

With the above point in mind, one can then write eq.(2.28) as,

$$\Delta(b) = \int_{}^{k_{T\max}^2} dk_T^2 \frac{1}{\sigma_0} \frac{d\sigma'}{dk_T^2} \left[J_0(k_T b) - 1\right] \qquad (2.47)$$

where $\frac{1}{\sigma_0}\frac{d\sigma'}{dk_T^2}$ represents the full $O(\alpha_s)$ result, curve 3 in fig. (2.6) in this case.

As mentioned already, in order to use eq. (2.47), it is necessary to integrate eq (1.5), and to use eq. (1.19) this must be done with each parton in turn as thrust axis. This is carried out in

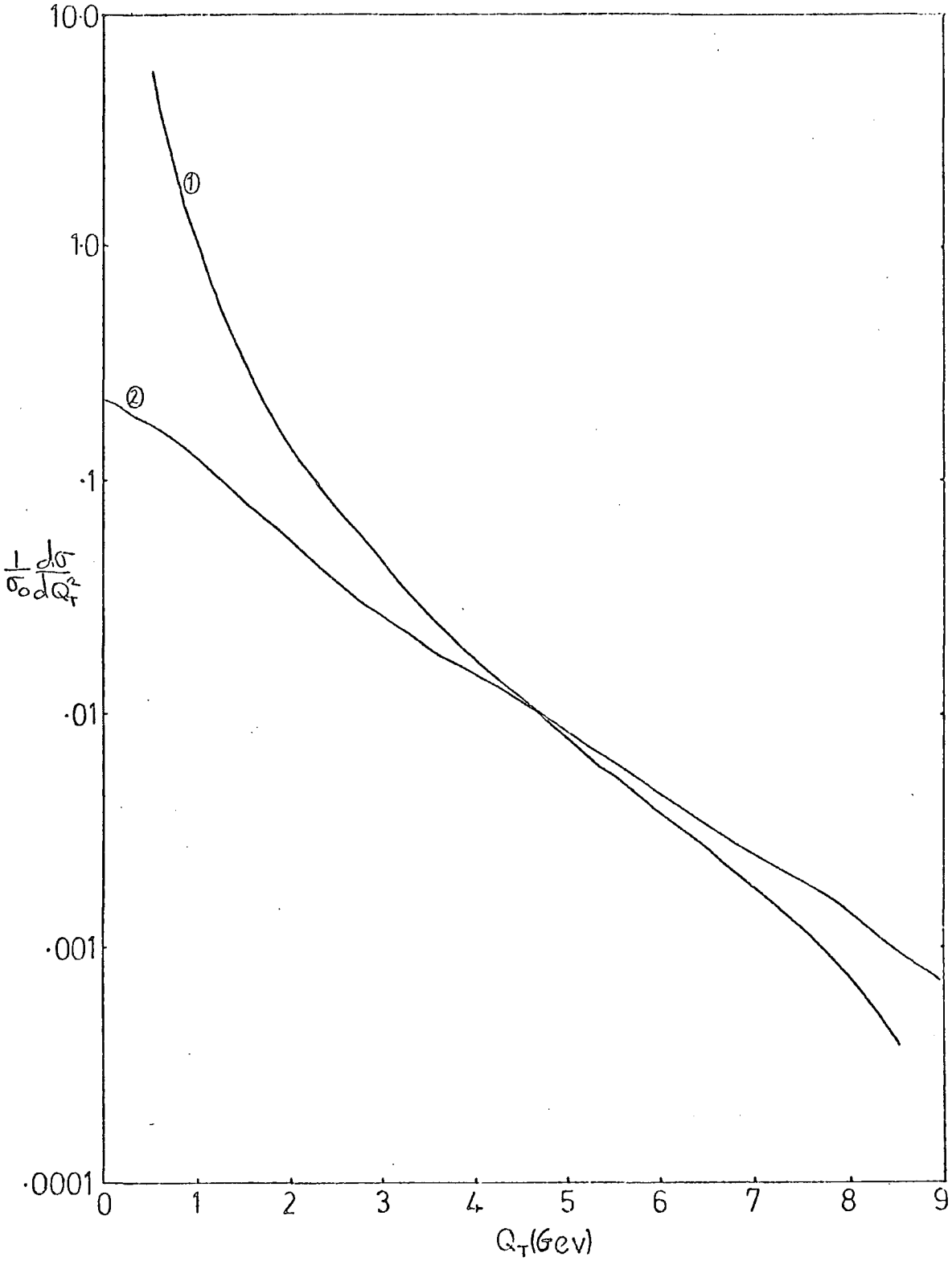

Fig. (2.7) The full $O(\alpha_s)$ input ($\Lambda = 0.5$ Gev, $Q = 31.6$ Gev, with a running coupling of $\alpha_s(k_T^2)$) to the Parisi-Petronzio prescription (PPP) of eqs. (2.47), (2.46) (Curve 1) and the resulting multigluon cross section (curve 2).

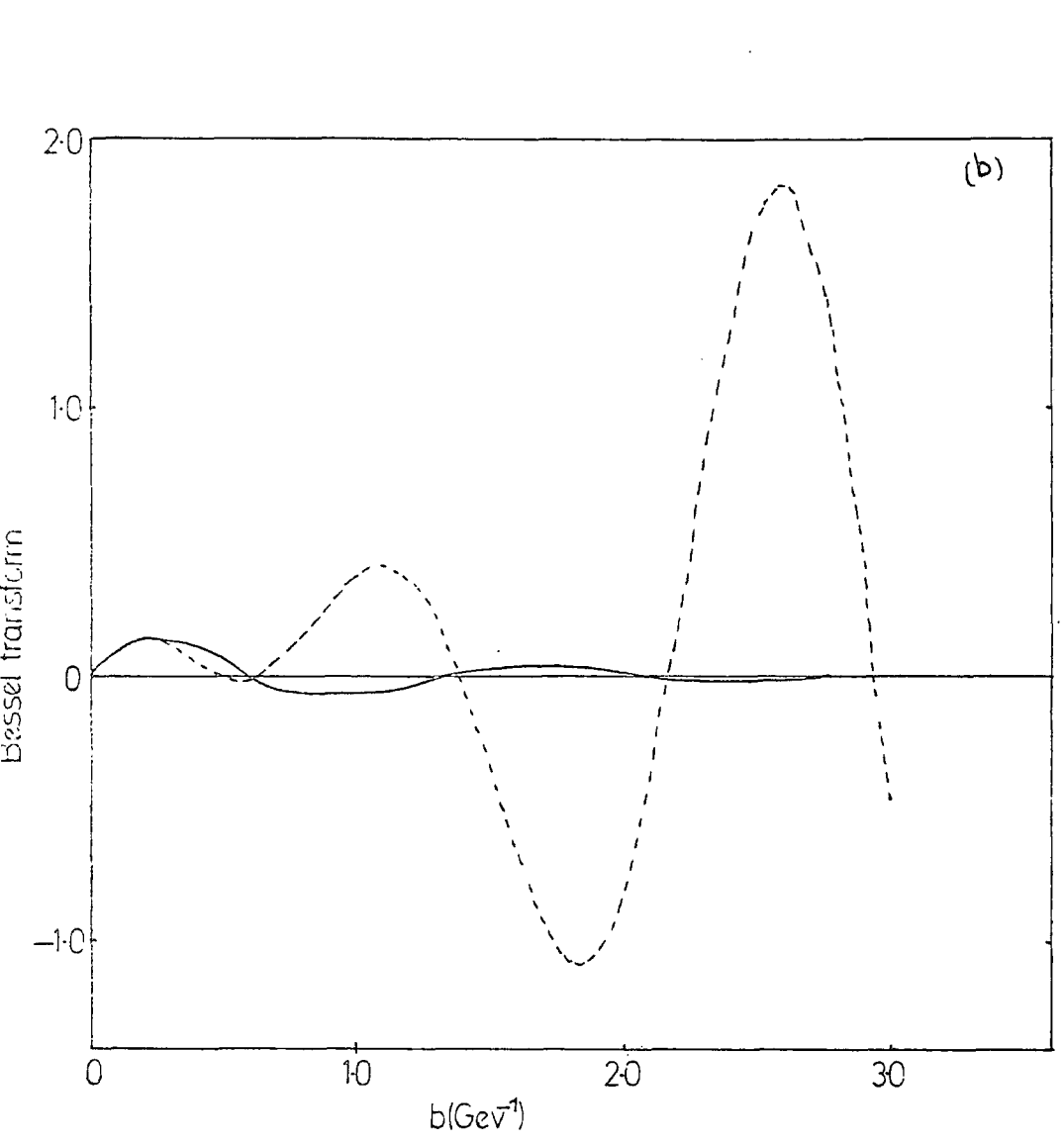

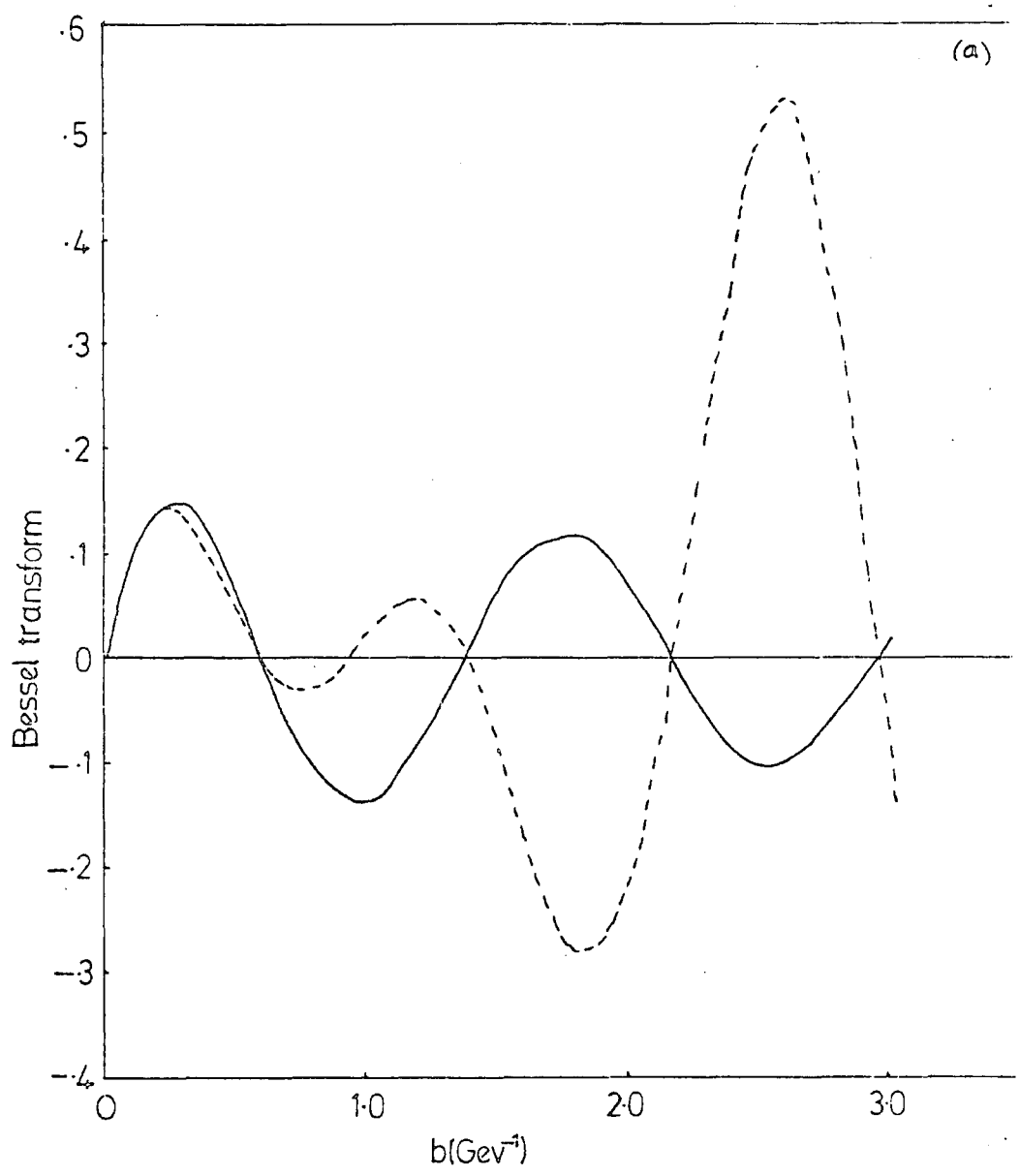

Fig.(2.8) The integrand of eq. (2.29) for multigluon emission (full line) and (0+1) gluon emission (dotted line) for $Q=31.6$ Gev, $\Lambda=0.5$ Gev, $Q_T=4.0$ Gev, and (a) α_s fixed at 0.184, (b) $\alpha_s(R_T^2)$.

Appendix A where the kinematics are discussed in a little more detail. Having done this, the $O(\alpha_s)$ configurations, where the q and $\bar{q}$ define the thrust axis, can be added together. One can then use eqns. (2.46), (2.47) to obtain the parton cross section $\frac{1}{\sigma_0} d\sigma/dQ_T^2$ for multi-gluon emission. The term with the gluon defining the thrust axis cannot be treated in this way, since for the gluon to define the thrust axis, it must be hard ($Q_T^2 \sim Q^2$) and the PPP only applies to independent emissions. One can use the Sudakov-type form factor on this term, but as shown in fig. (A3), this term is much smaller than the other one over most of the range in Q_T, and so will have little bearing on the final result. This merely reflects the fact, pointed out by Floratos et al [37], that the probability for a quark or antiquark to carry the thrust, for large thrust, tends to unity.

Eqns. (2.46), (2.47) can now be used to obtain the multigluon cross section, with in this case $k_{T max}^2 = Q^2/12$ in accord with the use of a thrust axis; the result is shown in fig.(2.7) along with the $O(\alpha_s)$ cross section from which it was calculated. It is this multigluon cross section which we now discuss.

What we have attempted to do is simply extrapolate the quark form factor of eqns. (2.28),(2.29) to include the whole region of Q_T, by inserting the full $O(\alpha_s)$ result into it. One might hope that the non logarithmic terms in $\frac{1}{\sigma_0} d\sigma'/dk_T^2$ would be enough to make the PPP mimic single hard gluon behaviour at larger Q_T, and then in that case smoothly merge the two regimes together.

That this is actually the case seems unlikely when comparing the integrands (i.e. the integral transforms) in eq.(2.29) for the two cases; i.e. multigluon where the integrand is effectively $b \exp[\Delta(b)]$ $J_0(bQ_T)$, and non plus one gluon where the integrand is $b(1+\Delta(b))$ $J_0(bQ_T)$, where in both cases $\Delta(b)$ is given by eq. (2.47). An example is shown in fig. (2.8), where it can be seen that the curve

corresponding to the gluon sum dies away as b increases, whereas that for (0+1) gluons develops massive oscillations. Notice that the case of a running coupling damps out the multigluon sum much faster than in the fixed coupling case, which makes it easier to handle numerically. One might expect the integration of the two functions to give something quite different at large Q_T, which is not what is required. However, because of the property of the Bessel function that the oscillations cancel upon integration beyond an argument of about 2.0, it is only the region $b \lesssim 2/Q_T$ which gives a significant contribution to the transform; and as shown in fig(2.8) the two integrands are very similar in that region, even for modest Q_T. Clearly for larger Q_T the situation gets better. This forces the multigluon cross section to merge with that for a single gluon at large values of Q_T. The multigluon cross section is smaller for a large part of the allowed region in Q_T, as expected from cancellations between neighbouring orders of perturbation theory.

The resulting cross sections in fig.(2.7) show that the two curves are reasonably close together over a reasonable range in Q_T, which indicates that the $O(\alpha_s)$ cross section dominates even at moderate Q_T. This situation gets better asymptotically, as shown by M.R. Pennington [27] for Q=100 GeV where the single and approximate multigluon cross sections are equal to within 25% for $12 \leq Q_T \leq 32$ Gev. So this suggests that the quark from factor does in fact provide a simple phenomenological interpolation formula from the small to large Q_T regimes.

Moreover, taking the inverse Fourier transform of eqn.(2.29) one obtains,

$$\exp[\Delta(b)] = \int d^2Q_T \left(\frac{1}{\sigma_0}\frac{d\sigma}{d^2Q_T}\right) e^{-i\vec{b}.\vec{Q}_T}$$

(2.48)

and since $\vec{b}$ is a two dimensional vector,

$$-\frac{\partial^2\left[e^{\Delta(b)}\right]}{\partial b_\alpha \partial b_\alpha}\Bigg|_{b=0} = \int d^2Q_T \left(\frac{1}{\sigma_0}\frac{d\sigma}{d^2Q_T}\right) Q_T^2 \, e^{-i\vec{b}\cdot\vec{Q}_T}\Bigg|_{b=0} = \langle Q_T^2 \rangle$$

where $\langle Q_T^2 \rangle$ is the average multigluon transverse momentum. So

$$\langle Q_T^2 \rangle = \left\{-\left(\frac{1}{b}\frac{\partial}{\partial b} + \frac{\partial^2}{\partial b^2}\right) e^{\Delta(b)}\right\}\Bigg|_{b=0} \tag{2.49}$$

and using the fact that,

$$\frac{\partial}{\partial b}\Delta(b) = -\int d^2k_T \left(\frac{1}{\sigma_0}\frac{d\sigma'}{d^2k_T}\right) k_T J_1(k_T b)$$

$$\frac{\partial^2}{\partial b^2}\Delta(b) = -\int d^2k_T \left(\frac{1}{\sigma_0}\frac{d\sigma'}{d^2k_T}\right) k_T^2 \left\{J_0(k_T b) - \frac{1}{k_T b} J_1(k_T b)\right\}$$

from eq.(2.28), one finds, substituting in eq. (2.49) that,

$$\langle Q_T^2 \rangle = \langle k_T^2 \rangle \tag{2.50}$$

So the Q_T^2 moments of the input and output distributions in the PPP must be the same i.e. $O(\alpha_s)$ and multigluon. This forces the two curves to cross at some point, as shown in fig.(2.7), with the cross section from the multigluon sum being the larger at large Q_T. In the light of recent exact $O(\alpha_s^2)$ calculations of energy-energy correllations [37,38], one might look upon this as rather fortunate phenomenologically, since the $O(\alpha_s^2)$ calculations predict about a 35% increase over a wide range of angles.

One can now put the extrapolated form factor of figure (2.7) and eqns. (2.46), (2.47) into eqn.(1.19) to obtain the hadron distribution.

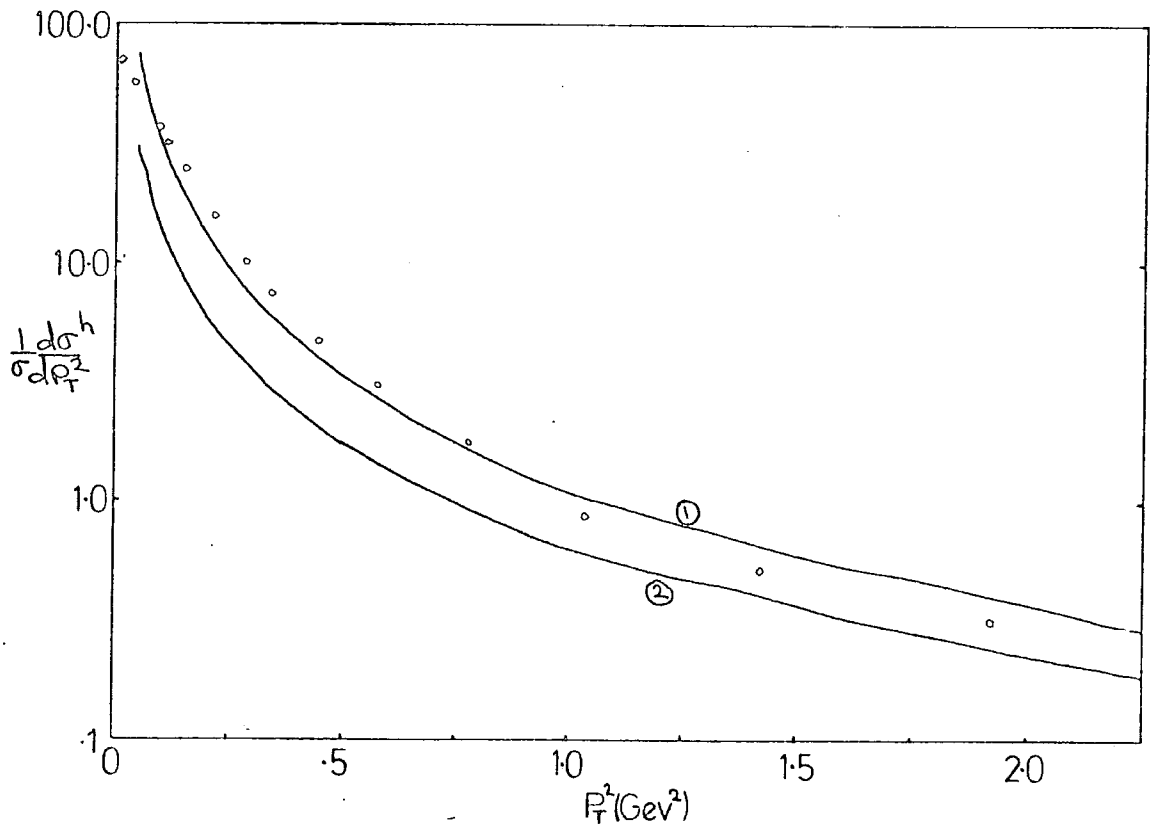

Fig. (2.9) The transverse momentum distribution of hadrons $\frac{1}{\sigma}d\sigma^h/dP_T^2$ eq(1.19) to O(α_s) (curve 1) and with multigluon emission (curve2) using the PPP of eqs (2.46), (2.47). Both curves are for Q=31.6 Gev, Λ =0.5 and a running couplingα_s, and are derived from those of Fig. (2.7) using eq (1.19) and the fragmentation functions of eq (2.51) Data (black dots) are from reference [17].

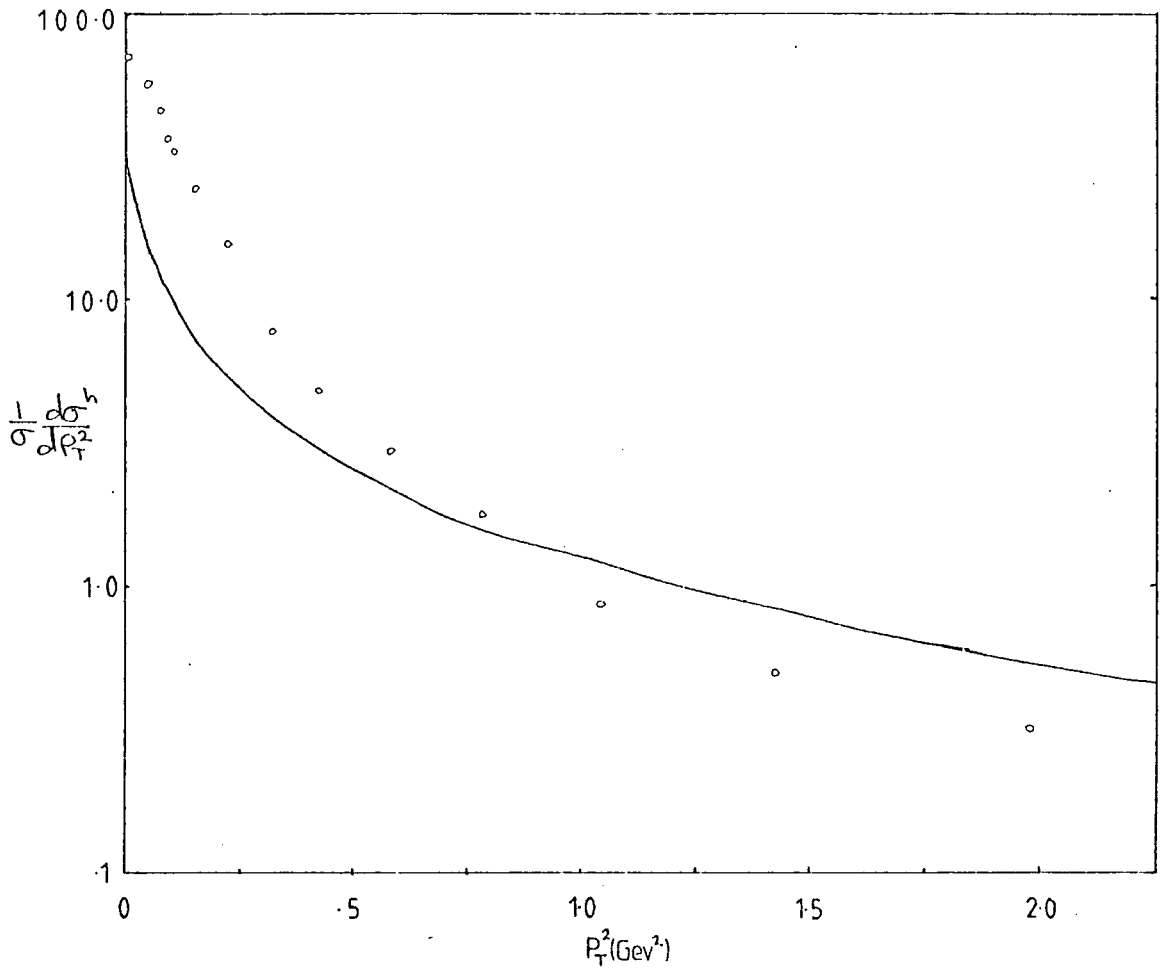

Fig. (2.10). The transverse momentum distribution of charged hadrons derived from multigluon emission (as in fig.(2.9)) with fragmentation functions of the form $D(z) \sim z^{\alpha}(1-z)^{\beta}$, with $\alpha=1.1$, $\beta=4.0$. Data are from ref [17].

2.7.1(b) Results.

A simple form was chosen for the fragmentation functions, as in chapter 1, allowing no distinction for fragmentation from gluons,

$$D_q(z) = D_{\bar{q}}(z) = D_g(z) = 3(1-z)^2/z \tag{2.51}$$

times 2/3 for charged hadrons. The transverse momentum distributions of secondary hadrons is not particularly sensitive to the details of the fragmentation functions (see for example [11]), and changing the above parametrization for the gluon fragmentation functions does not significantly affect results.

The resulting hadron transverse momentum distribution is shown in fig.(2.9) for Q=31.6 GeV, Λ =0.5, along with the $O(\alpha_s)$ result obtained using the integrated parton cross sections of Appendix A. Clearly the $O(\alpha_s)$ result has the singularity at small P_T, arising from that of the parton cross section. The hadron cross section obtained from multigluon emission is noticeably smaller than that using the $O(\alpha_s)$ result, due to the finite multigluon cross section as $Q_T \to 0$. The experimental hadronic cross section is finite at $P_T^2 = 0$ (as can be seen from the data of ref [17] in fig. (2.9)), so using a finite parton cross section one might at first sight expect to produce a finite hadronic one. However, as can be seen from eq.(1.19) (and approximating $\frac{1}{\sigma_0} d\sigma/dQ_T^2$ by a constant for simplicity), if $D(z) \sim 1/z$ at small z(as in the forms used above), then one obtains a factor $1/P_T^2$ irrespective of whether the parton cross section is finite or not, and so the hadronic cross section will always diverge at $P_T^2 = 0$. This is rather annoying, since one expects $D(z) \sim 1/z$ for small z to give the logarithmic rise in multiplicity with Q^2. The shape of the curves at least does appear to be correct over most of the range in P_T, but although the moments of P_T are finite [11], it is impossible

to check the multiplicity of $\frac{1}{\sigma} d\sigma^h/dP_T^2$ due to the singularity, which is not present in the data.

To remove this singularity, one could try various other forms of fragmentation function, especially since the form for soft fragmentation is not known and this might have a significant affect on the result. For instance one could try,

$$D(z) \sim z^\alpha (1-z)^\beta \tag{2.52}$$

appropriately normalized in accord with momentum conservation $\int_0^1 dz\, z D(z) = 1$. Inserting this form into eq. (1.19) and again assuming a constant parton cross section for simplicity, results in a hadronic cross section,

$$\frac{1}{\sigma}\frac{d\sigma^h}{dP_T^2} \sim 2\left(\frac{1}{\sigma_0}\frac{d\sigma}{dQ_T^2}\right)\left\{\frac{(Q/\sqrt{12})^{1-\alpha}}{1-\alpha} P_T^{\alpha-1} + \frac{\beta}{\alpha} P_T^\alpha (Q/\sqrt{12}) - \frac{1}{1-\alpha} - \frac{\beta}{\alpha}\right\} \tag{2.53}$$

So if we choose $\alpha > 1$, this will remove the spurious singularity. The result of using this form is shown in fig. (2.10) with $\alpha = 1 \cdot 1, \beta = 4.0$, and normalization $\frac{\Gamma(8.1)}{\Gamma(3.1)\Gamma(5.1)} z^{1.1}(1-z)^{4.0}$. From this it can be seen that although the overall normalization is approximately correct, the shape is not.

That the results in figs. (2.9), (2.10) are reasonably close to the data may be viewed as encouraging, however, it is clear that fragmentation must be included in a better way (see chapter 3). It is partly for this reason that energy-energy correllations will from now on be considered. This will only partly overcome the problem, since the role of fragmentation is only naively included in the function $P(b)$. However, this will hopefully be improved upon in chapter 3. Before

proceeding, it is worthwhile mentioning a few limitations of the PPP which have been pointed out by Pennington [27].

2.7.2 Limitations of the PPP.

More careful analysis of the PPP, using eqs. (2.28), (2.29) for instance, does indicate some shortcomings of the scheme [27]. These equations were obtained by interchanging the order of the $\vec{b}$ and $\vec{R}_{T\lambda}$ integrations. If the integrations were done in the order in which they appear, then for $n \geq 3$ independent gluons other singularities appear. Using the PPP, the integrals are regularized by the addition of the appropriate soft virtual graphs; this removes the soft singularities, but a more detailed study of momentum conservation reveals that the cross section is singular due to the incorrect treatment of collinear configurations which occur when no momenta are soft. The correct result is only obtained if the interchange of the $\vec{b}$ and $\vec{R}_{T\lambda}$ integrations is valid (as it is in the double leading log approximation (DLLA) where these extra collinear singularities do not occur). The result of this is that when trying to extend the quark from factor beyond the DLLA, considering independent emissions and exact momentum conservation does not provide the whole result. Physically this means that one only considers graphs of the type in fig. (2.11a), ignoring those of fig. (2.11b).

Fig. (2.11)

a) Independent and
b) dependent gluon emission.

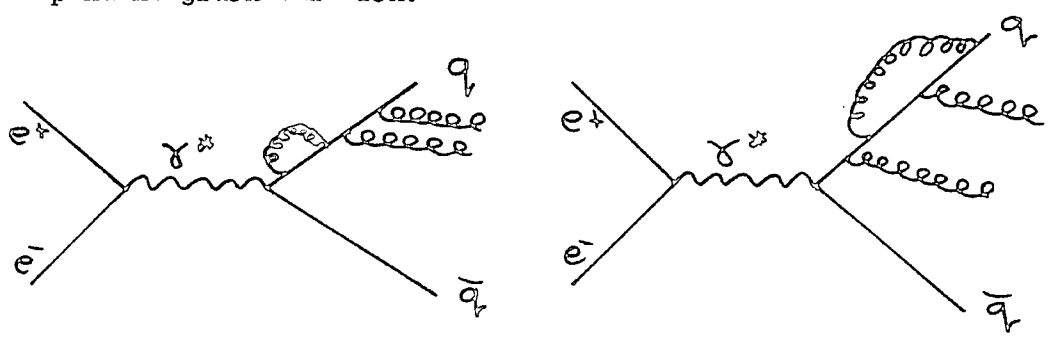

(a) (b)

Also it is important to remember that at small Q_T, the leading logarithm terms cancel , leaving the non leading terms three powers of logarithms down from those to fill in the dip as $Q_T \rightarrow 0$. It would also therefore be useful to see the effect of adding in the interference terms (in an axial gauge) and triple gluon interactions, which order-by-order are themselves only down by two powers of logarithms from the leading logs. These non leading terms however, are also not gauge invariant which in principle suggests the need for an exact all orders calculation!

So an accurate calculation of the small Q_T cross section and an extrapolation to high Q_T will have to await an exact calculation, outlined by Collins and Soper [39], which will unfortunately have to be performed in order to make detailed, unambiguous predictions in the small Q_T regime, and to gain an understanding of how a large number of soft gluons became one or two hard ones at large Q_T. The PPP does however, indicate the importance of non-leading terms in summing the perturbation expansion, and must be regarded as a step in the right direction, but in looking at phenomenological consequences it is necessary to bear in mind its limitations as mentioned above.

2.7.3 Energy-Energy Correllations.

In order to bypass the problems encountered using fragmentation functions in transverse momentum distributions, it is simple to test the predictions of the quark form factor by looking at energy-energy correllations in the small angle regime, where one can make the approximation, $Q_T = \frac{\Theta}{2} Q$, where if χ is the angle between two emergent jets, $\Theta = \pi - \chi$. So Θ measures the angle by which the jets are away from the back-to-back orientation. And, as mentioned earlier, the complications due to the use of a thrust axis are no longer there, and experimentally it is a comparatively simple quantity

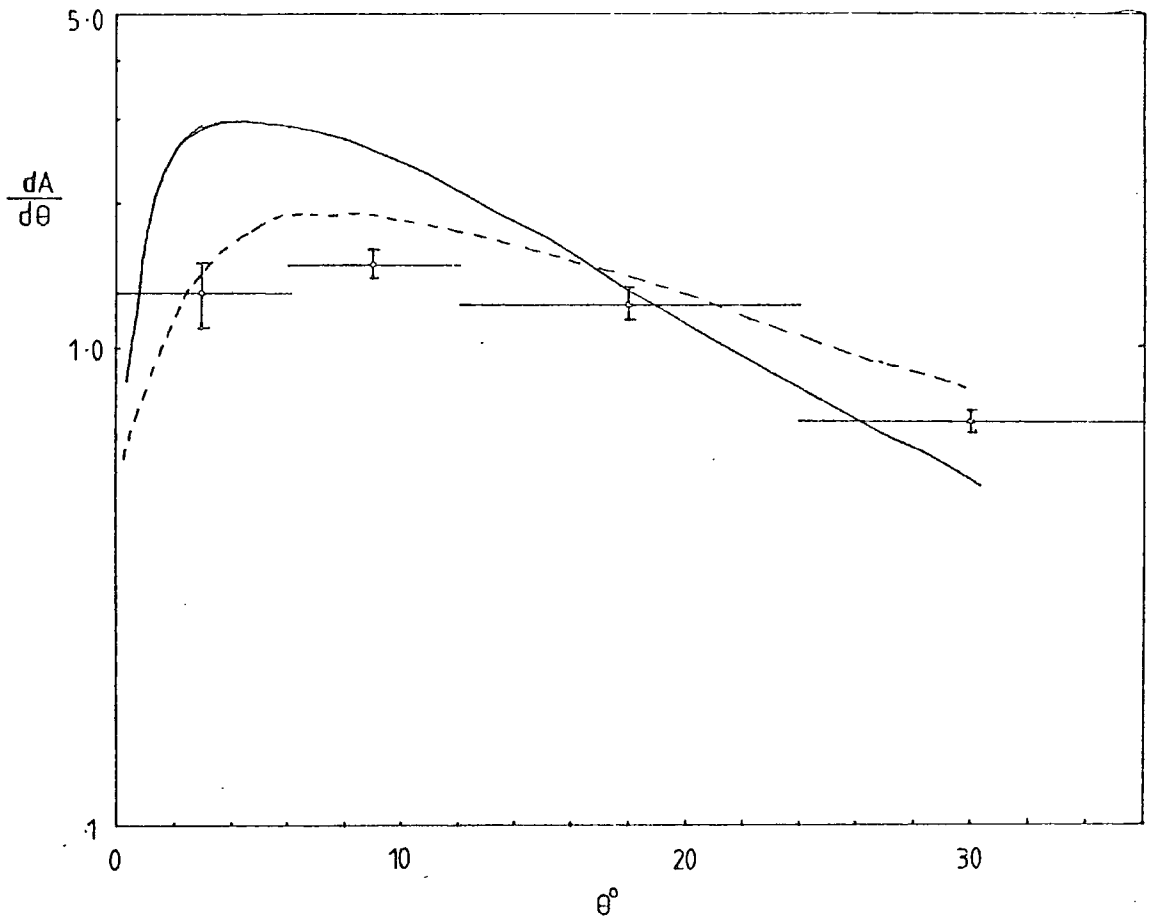

Fig. (2.12) Energy-energy correllations obtained from multigluon emission using the PPP (eqs(2.46),(2.47)) with full $O(\alpha_s)$ input (curve 1) and LLA input of eq.(2.24) (curve 2). $Q=30$ Gev, $\Lambda=0.5$ Gev and $\alpha_s(R_T^2)$. Data are from reference [18].

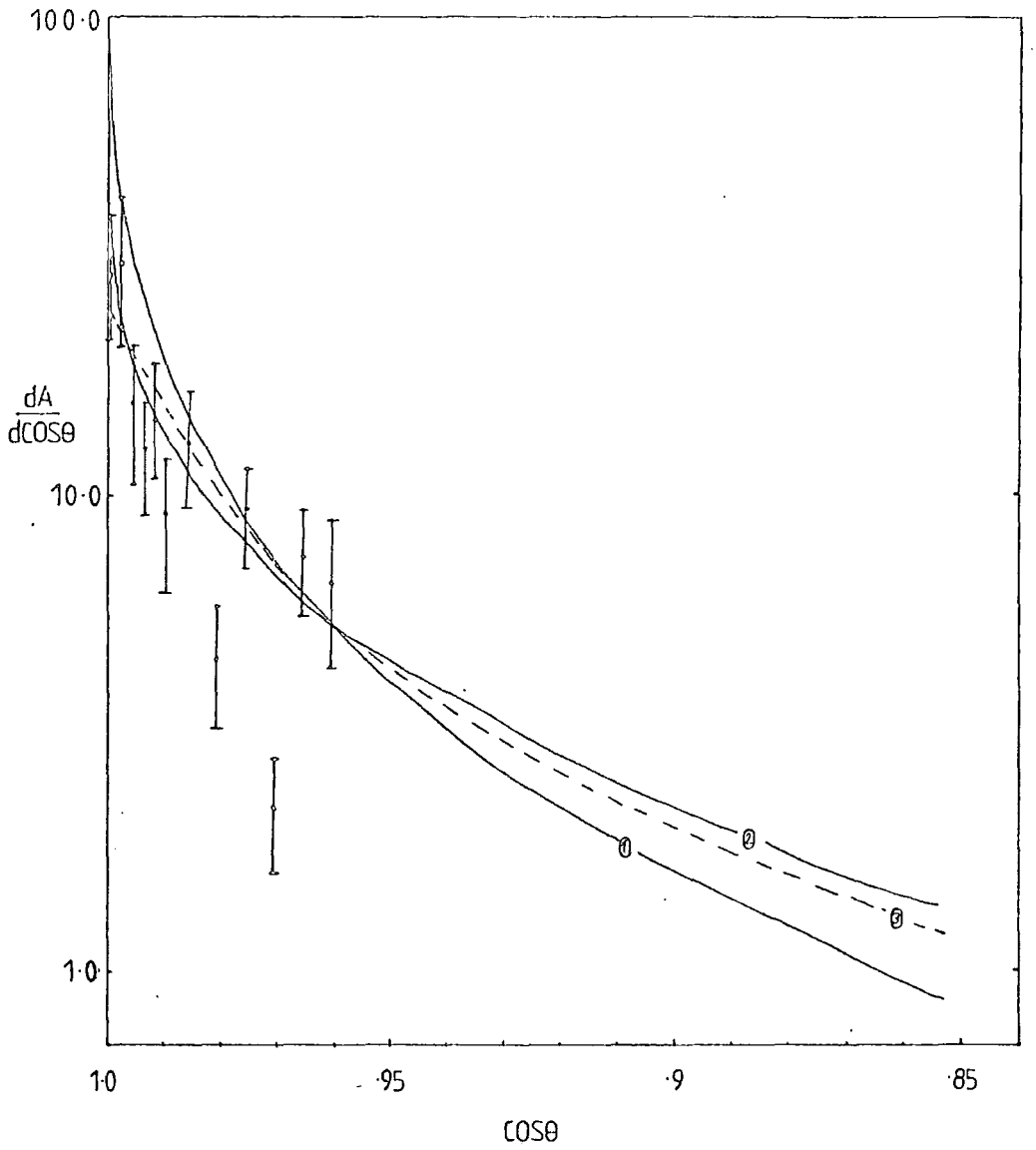

Fig. (2.13) Energy-energy correllations as a function of $\cos\Theta$ for Q=30 Gev, Λ =0.5 Gev, $\alpha_s(R_T^2)$. Curves 1 and 2 correspond to those of fig (2.12), and curve 3 uses the PPP with R_T^2 max = Q^2 and LLA input (eq (2.28), (2.29)). Data are from [18].

to measure. Also in using eq.(1.26) to evaluate $dA/d\Theta$, in the small angle regime one might hope to be able to write $x_i \simeq x_j \simeq$ | (which may be a rather harsh approximation in the light of subsequent discussion in chapter 3), so that the energy weighted acollinearity distribution can simply be written as,

$$\frac{dA}{d\Theta} = \frac{\Theta}{2} Q^2 \frac{1}{\sigma_0} \frac{d\sigma}{dQ_T^2} \tag{2.54}$$

in terms of the multigluon cross section. Eqns. (2.46), (2.47) were again used, but in this case, since a thrust axis is not used, $k_{Tmax}^2 = Q^2/4$. And eq.(2.28) was used to compare with a purely leading log result.

The results are shown in fig. (2.12) with Q=30 GeV, $\Lambda = 0.5$ and PLUTO data from ref.[18] (c.f.[35], [36]). Since the correllations as a function of angle contain the trivial kinematic zero at $\Theta = 0$, when discussing small angle results in detail it is more sensible to use the distribution $dA/d\cos\Theta$, which is finite at $\Theta = 0$. Also the experiment was performed in finer bins to obtain the latter, giving more data at small angles. These results are shown in fig.(2.13). Both figures show reasonable agreement with data.

The main difference between using the full $O(\alpha_s)$ result or the LLA in the PPP seems to be that the LLA gives a smaller cross section (in Θ) at small angles (or Q_T) than does the full $O(\alpha_s)$ and vice-versa at large Θ . A representative sample of PLUTO data [18] is shown in fig.(2.13), from which it can be seen that it is not possible to say which curve fits the data best, although the overall agreement is encouraging. Curve 1 does peak very sharply as $\Theta \to 0$, which is because it has the smallest value of $|\Delta(b)|$. Curve 3 corresponds to taking $k_{Tmax}^2 = Q^2$ (c.f.[25]) which at moderate Q^2 is clearly an overestimate of available phase space, and provides a less peaked cross

section at $\Theta = 0^{\circ}$.

Due to the necessity of having to change variables from Q_T to Θ (or $\cos\Theta$), it is not possible to use a simple extrapolation of the quark from factor to describe the whole range in Θ, since Q_T is in general a double valued function of X_i and Θ and so it's not possible to use eqn.(1.26) to evaluate the correllations. However, Collins and Soper have provided a neat way to do this by separating out the leading behaviour of the exact $O(\alpha_s)$ result from the other terms, which are left as they are, with the leading part providing the multigluon sum [39] (see Chapter 3). The correllations from the two parts are then added together, with each part dominating in its own angular regime, and the two merging smoothly in the middle.

So far the effects of intrinsic transverse momentum originating in fragmentation have been included in a rather ad-hoc manner, blindly bringing over the smearing function $\rho(b)$ from Drell-Yan, where it parametrizes the effects of hadron structure. It is now hoped in chapter three to address this problem more correctly and to include soft fragmentation which was overlooked in this section, particularly when discussing the hadron transverse momentum distributions, which was not adequately described in the small P_T region, $P_T \lesssim 0$.

Chapter 3

Soft Gluon Emission Based on the Evolution Equations for the Fragmentation Functions

3.1 Introduction

It is the purpose of this chapter to evaluate a cross section for the acollinearity distribution of hadrons in e^+e^- annihilation using the evolution equations of Bassetto et al. [40] for the fragmentation functions $D_q^h(x,\vec{k}_T,Q^2)$ of a quark q into a hadron h (with energy fraction x, and transverse momentum $\vec{k}_T$). Solving these equations provides one with the k_T dependence in the soft limit, by summing the emission of gluons to all orders in perturbation theory.

Consider first just the Q^2 evolution of the fragmentation functions, which is given by the standard Altarelli-Parisi equations [41] and can be simply written for the non-singlet partas,

$$\frac{\partial D_q^h(x,Q^2)}{\partial \ln Q^2} = \frac{\alpha_s(Q^2)}{2\pi}\int_x^1 \frac{dy}{y} D_q^h(y,Q^2)\left[P_{qq}\left(\frac{x}{y}\right)\right]_+ \qquad (3.1)$$

where $P_{qq}(z)$ is the appropriate Altarelli-Parisi splitting function, which gives the probability that a quark with momentum fraction x decays into a quark with momentum fraction y by the emission of a gluon, as shown in fig (3.1), and is given by,

Fig (3.1)

Altarelli-Parisi Splitting function $P_{qq}(\frac{x}{y})$

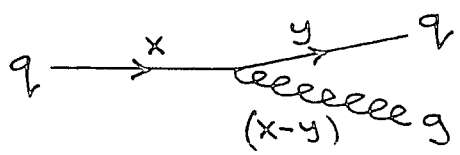

$$P_{qq}(z) = C_F\left(\frac{1+z^2}{1-z}\right) \qquad (3.2)$$

All momentum fractions y must be integrated over for a given x, to give the Q^2 dependence of the fragmentation functions arising from multiple single gluon emission.

There is clearly an infra red singularity in eq (3.2) as $z \to 1$ which must be taken care of by the addition of the appropriate virtual

graphs, as in chapter 2. This is the origin of the '+' prescription used in eq (3.1), which is defined by

$$\int_0^1 dz\, f(z)\left[h(z)\right]_+ \equiv \int_0^1 dz\, h(z)\left[f(z)-f(1)\right] \tag{3.3}$$

where $f(z)$ and $h(z)$ are any test functions. This regularizes the behaviour at the upper limit by adding in the virtual graphs as in eq (2.13), and renders the integral finite. This simple method of regularizing is clearly very useful when discussing the evolution equations, and one can equivalently write $P_{qq}(z)$ in the form,

$$P_{qq}(z) = C_F\left[\frac{1+z^2}{(1-z)_+} + \frac{3}{2}\delta(z-1)\right] \tag{3.4}$$

which explicitly shows the $\delta(z-1)$ which is that part corresponding to no emission of gluons.

However, when considering the emission of many soft gluons eq (3.1) is not enough, since one also needs information about the other mass scale in the system, i.e. the transverse momentum carried away by the gluons. Using the appropriate evolution equations [40], one can include the details of the transverse momentum dependence into the fragmentation functions $D_q^h(x,\vec{k}_T,Q^2)$. This approach does place more emphasis on how the soft gluons fragment into hadrons. The evolution equations as derived in ref [40] in the LLA by summing dressed ladder diagrams [19] using the Bethe-Salpeter equation and are written (again in the non-singlet sector for the moment),

$$\frac{\partial D_q^h(Q^2,\vec{P}_T,x)}{\partial \ln Q^2} = \int_x^1 \frac{dz}{z}\left[\frac{\alpha_s(Q^2)}{2\pi} P_{qq}(z)\right]_+ \cdot$$

$$\cdot \int \frac{d^2\vec{k}_T}{\pi}\,\delta\left(z(1-z)Q^2-k_T^2\right) D_q^h\left(Q^2,\vec{P}_T-\frac{x}{z}\vec{k}_T,\frac{x}{z}\right), \tag{3.5}$$

where the transverse momentum dependence has been explicitly folded in. (More attention will be paid to the argument of the strong coupling constant α_s later). The δ function indicates the (z, Q^2)

Fig (3.2) Schematic Physical Picture (showing just a single q for simplicity)

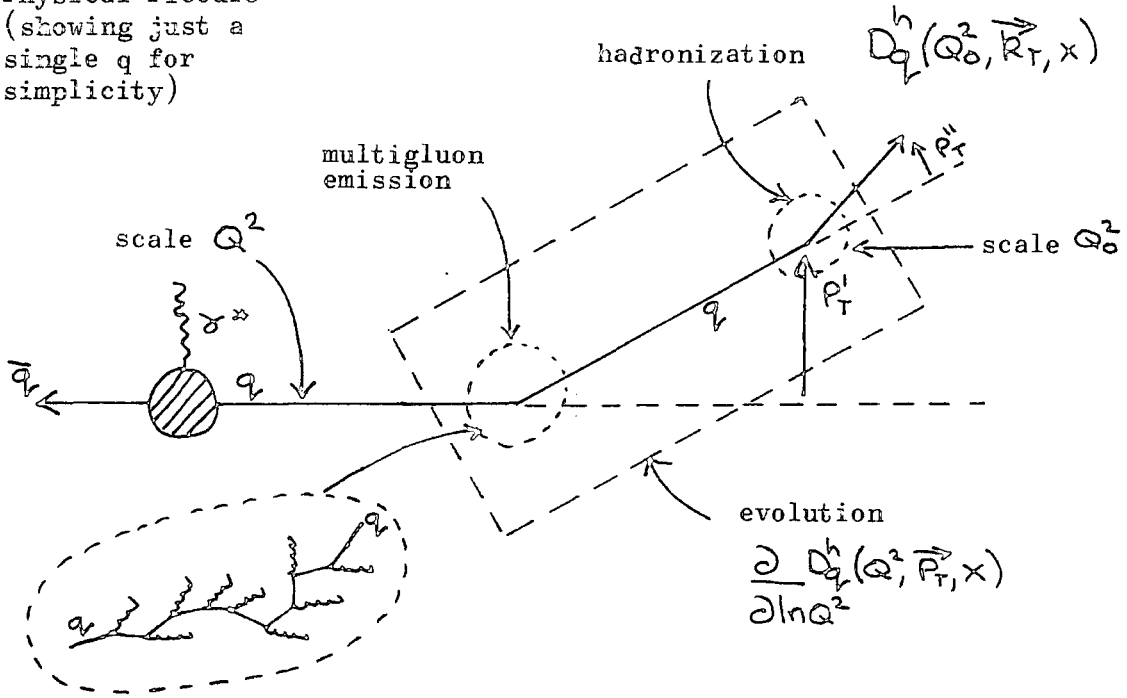

dependence of the transverse momentum (c.f. eq(1.16)), whose maximum value is clearly given by the virtualness of the internal quark line (ζ' in eq(1.3)), i.e. $Q^2(1-z)$. In general k_T^2 will be a fraction, z of this.

The physical picture is drawn schematically in fig (3.2), which shows the two contributions to the transverse momentum of the quarks arising from multigluon emission (p_T') and hadronization (p_T''). The $q\bar{q}$ pair are created at a momentum scale Q^2 with zero transverse momentum; the subsequent evolution in Q^2 and $\vec{p}_T$ is given by eq (3.5), after which the quark fragments in a known way, (i.e. the experimentally well defined two jet region) at momentum scale Q_0^2.

Since the (infra red safe) energy weighted acollinearity distribution is relatively easy to measure (with good data from PLUTO [18] and CELLO [36]), this is the quantity which will be discussed,

especially since it lends itself particularly easily to the use of the evolution equations.

3.2 The Energy Weighted Acollinearity Distribution

Consider the cross section for hadron production again; it can be written in terms of the fragmentation functions $D_q^h(x,\vec{R}_T,Q^2)$ as [42],

$$\frac{1}{\sigma}\frac{d\sigma}{dx_a dx_b d^2\vec{P}_T} = \frac{1}{\sum_q e_q^2}\int d^2\vec{R}_{Ta}\, d^2\vec{R}_{Tb}\,\delta^{(2)}\left(\vec{P}_T - \frac{\vec{R}_{Ta}}{x_a} - \frac{\vec{R}_{Tb}}{x_b}\right)\cdot$$

$$\cdot\left\{\sum_q e_q^2\, D_q^{h_a}(x_a,\vec{R}_{Ta},Q^2)\, D_{\bar{q}}^{h_b}(x_b,\vec{R}_{Tb},Q^2) + (q\leftrightarrow\bar{q})\right\}. \qquad (3.6)$$

where the sums over the quark charges give the appropriate weightings to the cross section for electromagnetically creating a $q\,\bar{q}$ pair with charges $\pm e_q$. P_T is the scaled relative transverse momentum of hadrons a and b, which are created with energy fractions x_a and x_b, and so originate from quarks with transverse momenta $\vec{R}_{Ta}/x_a$ and $\vec{R}_{Tb}/x_b$ respectively. Hence the particular form of the δ function in eq (3.6).

Eq (3.6) must now be converted into the acollinearity distribution defined by,

$$\frac{dA}{d\Theta} \equiv \frac{1}{2}\sum_{h_a h_b}\int_0^1 dx_a\, dx_b\, x_a x_b\, \frac{1}{\sigma}\frac{d\sigma}{dx_a dx_b d\Theta} \qquad (3.7)$$

where the factor of $\frac{1}{2}$ originates in order to avoid double counting in going from P_T to Θ, since P_T is a double valued function of Θ, the acollinearity angle. In the small angle limit the relation is simply $P_T^2 = \frac{Q^2\Theta^2}{4}$.

It is convenient, in order to use eq(3.7), to take moments of the functions $D_q^h(x,\vec{R}_T,Q^2)$ (to obtain the energy weightings), and to go into impact parameter space (which will pick up the next to double leading logarithm corrections, as discussed in chapter 2). This is

one by taking the Fourier-Mellin transform, (which also facilitates a straightforward approximate solution to the evolution equations); so one can define,

$$d_q^h(n,b,Q^2) = \int_0^1 dx\, x^{n-1} \int_{\text{All } \vec{k}_T} d^2\vec{k}_T \exp\left[-i\vec{k}_T.\vec{b}/x\right] D_q^h(x,\vec{k}_T,Q^2) \tag{3.8}$$

where the $1/x$ in the exponential can be traced back to the kinematics described by the δ function in eq (3.6). One can now write the acollinearity distribution as,

$$\frac{dA}{d\theta} = \frac{1}{4}\frac{Q^2}{\sum_q e_q^2}\int_0^\infty db\, b\, J_0\left(b\frac{Q\theta}{2}\right)\left\{\sum_q e_q^2 \sum_{h_a} d_q^{h_a}(2,b,Q^2)\sum_{h_b} d_{\bar{q}}^{h_b}(2,b,Q^2) + (q \leftrightarrow \bar{q})\right\} \tag{3.9}$$

The evolution equations (3.5) are now required in impact parameter space, and so using the Fourier transform,

$$d(x,b,Q^2) \equiv \int d^2\vec{P}_T\, e^{-i\vec{P}_T.\vec{b}/x} D(x,\vec{P}_T,Q^2) \tag{3.10}$$

(where subscript and superscripts have now been dropped for convenience), equation (3.5) becomes,

$$\frac{\partial\, d(x,b,Q^2)}{\partial \ln Q^2} = \int_x^1 \frac{dz}{z}\left[\frac{\alpha_s(Q^2)}{2\pi} P_{qq}(z)\right]_+ \frac{1}{2\pi}\int d\theta \int d^2\vec{P}_T \cdot e^{-i\vec{b}.\vec{P}_T/x} D\left(\frac{x}{z}, \vec{P}_T - \frac{xQ\sqrt{z(1-z)}}{z}\frac{\vec{k}_T}{|\vec{k}_T|}, Q^2\right), \tag{3.11}$$

where the δ function in eq (3.5) was used to do the k_T^2 integration, leaving the angular integration Θ . The r.h.s. of eq (3.11) is now written,

$$\int_x^1 dz \left[\frac{\alpha_s(Q^2)}{2\pi} P_{qq}(z)\right]_+ \int \frac{d\varphi}{2\pi} \int d^2\vec{k}_T \, e^{-i\vec{b}\cdot\vec{R}_T/x} D(Q^2, \vec{R}_T, x/z) \cdot$$
$$\cdot e^{-i\frac{\vec{b}}{x}\cdot\left[xQ\sqrt{\frac{1-z}{z}}\cdot \vec{k}_T/|\vec{k}_T|\right]}$$

where
$$\vec{R}_T = \vec{P}_T - xQ\sqrt{\frac{1-z}{z}}\,\vec{k}_T/|\vec{k}_T|$$

and performing the angular integration yields,

$$\frac{\partial d(x,b,Q^2)}{\partial \ln Q^2} = \int_x^1 \frac{dz}{z}\left[\frac{\alpha_s(Q^2)}{2\pi} P_{qq}(z)\right]_+ J_0\left(bQ\sqrt{\frac{1-z}{z}}\right) d(Q^2, b, x/z) \tag{3.12}$$

One now just needs to cast eq (3.12) into an energy weighted form, using the Mellin transform,

$$d(b,Q^2) = \int_0^1 dx\, x\, d(Q^2, b, x) \tag{3.13}$$

where all moments from now on will be for $n=2$, (so this argument will be dropped). Eq (3.12) therefore becomes,

$$\frac{\partial d_{NS}(b,Q^2)}{\partial \ln Q^2} = \int_0^1 dz\, z\left[\frac{\alpha_s(Q^2)}{2\pi} P_{qq}(z)\right]_+ J_0\left[Qb\sqrt{\frac{1-z}{z}}\right] d_{NS}(Q^2, b/z) \tag{3.14}$$

for the non-singlet moment.

Eq (3.14) must now be solved in order to use eq (3.9) to find the acollinearity distribution. The approximate solution proposed by Bassetto et al [40], and used by Baier and Fey [42] and Cleymans and Kuroda [43], consists of splitting up the r.h.s of eq (3.14) into two parts as follows,

$$\int_0^1 dz\, z\, P_{qq}(z) d_{NS}(b,Q^2) + \int_0^1 dz\, z\, P_{qq}(z) \cdot$$
$$\cdot \left\{ d_{NS}\left(\frac{b}{z}, Q^2\right) J_0\left[Qb\sqrt{\frac{1-z}{z}}\right] - d_{NS}(b,Q^2)\right\}.$$

and then the leading log approximation is hopefully picked up by letting $z=1$ in all slowly varying functions of z in the second term above, to give,

$$\frac{\partial d_{NS}(b,Q^2)}{\partial \ln Q^2} = \frac{\alpha_s(Q^2)}{2\pi} d_{NS}(b,Q^2)\left[A_2^{NS} + \int_0^1 dz \frac{2C_F}{(1-z)}\left[J_0(Qb\sqrt{1-z})-1\right]\right] \tag{3.15}$$

where A_2^{NS} is the zeroth order n=2 anomalous dimension,

$$A_2^{NS} = \int_0^1 dz\, z P_{qq}(z) = -\frac{4}{3}C_F$$

The solution to eq (3.15) can therefore now be written,

$$d_{NS}(b,Q^2) = d_{NS}(b,Q_0^2)\, Exp\left[\int_{Q_0^2}^{Q^2}\frac{dk^2}{k^2}\frac{\alpha_s(k^2)}{2\pi}A_2^{NS}\right]\cdot$$

$$\cdot\, Exp\left[\int_{Q_0^2}^{Q^2}\frac{dk^2}{k^2}\frac{\alpha_s(k^2)}{2\pi}\int_0^1 dz\frac{2C_F}{(1-z)}\left[J_0(Qb\sqrt{1-z})-1\right]\right]$$

which gives the solution [40],

$$d_{NS}(b,Q^2) = d_{NS}(b,Q_0^2)\left[\frac{\alpha_s(Q^2)}{\alpha_s(Q_0^2)}\right]^{\left(\frac{-2A_2^{NS}}{\beta_0}\right)}\cdot F_{NS}(Q^2,Q_0^2,b) \tag{3.16}$$

where the non-singlet form factor F_{NS} is given by,

$$F_{NS}(Q^2,Q_0^2,b) = Exp\left[\frac{2C_F}{\pi}\int_{Q_0^2}^{Q^2}\frac{dk^2}{k^2}\alpha_s(k^2)\int_0^{bk}\frac{dy}{y}\left(J_0(y)-1\right)\right] \tag{3.17}$$

Swapping the order of the integration round in eq (3.17) and doing the k^2 integration yields,

$$F_{NS}(Q^2,0,b) = Exp\left[\frac{4C_F\alpha_s}{\pi}\int_0^{bQ}\frac{dy}{y}\ln\left(\frac{Qb}{y}\right)\left(J_0(y)-1\right)\right] \tag{3.18}$$

if $Q_0=0$ and α_s is assumed fixed for simplicity. And writing eq(3.18) in terms of transverse phase space gives,

$$F_{NS}(Q^2,0,b) = Exp\left[\frac{C_F}{\pi}\int_0^{Q^2}\frac{dk_T^2}{k_T^2}\alpha_s\ln\left(\frac{Q^2}{k_T^2}\right)\left[J_0(bk_T)-1\right]\right] \tag{3.19}$$

which is the form factor of Parisi and Petronzio [24], eq (2.28). So the $\geq \to 1$ approximation yields the leading double log result discussed in chapter 2.

Only one thing remains before the acollinearity can be calculated; a form for $d_{NS}(b,Q_0^2)$ must be obtained. The discussion can be simplified by assuming the input functions are independent of the type of constituents, i.e.

$$\sum_h d_q^h(b,Q_0^2) = \sum_h d_{\bar{q}}^h(b,Q_0^2) \equiv d_{NS}(b,Q_0^2) \tag{3.20}$$

Taking Q_0=9.0Gev (as in ref [42]), one can use the convenient parametrization for the fragmentation functions,

$$\sum_h D_q^h(x,k_T) = 3\frac{(1-x)^2}{x}\cdot\frac{2\,Exp(-2k_T/\langle k_T\rangle)}{\pi\langle k_T\rangle^2} \tag{3.21}$$

where $\langle k_T\rangle$ is the average intrinsic transverse momentum of the partons, since at Q=9.0Gev the dominant contribution to the hadron spectra comes from sharp two jet events, which the above parametrization describes well with $\langle k_T\rangle \leq$ 0.5Gev. The form used in eq (3.21) must satisfy energy-momentum conservation,

$$\sum_h \int_0^1 dx \int_{all\ \vec{k}_T} d^2\vec{k}_T \times D_q^h(x,\vec{k}_T) = 1$$

which it obviously does. [Little difference is made to the results by using a Gaussian form in eq (3.21) instead of an exponential].

$d_{NS}(b,Q_0^2)$ can now be obtained by performing the Fourier-Mellin transform of eq (3.8) to give,

$$d_{NS}(b,Q_0^2) = \frac{6}{\langle k_T\rangle^2}\int_0^1 dx\,(1-x)^2 \int_0^\infty dk_T^2\, e^{\frac{-2k_T}{\langle k_T\rangle}} J_0(k_T b/x) \tag{3.22}$$

and using the fact that [29],

$$\int_0^\infty e^{-sk} \cdot k \cdot J_0(ak)dk = \frac{s}{(a^2+s^2)^{3/2}} \qquad (s>0)$$

gives,

$$d_{NS}(b,Q_0^2) = \frac{24}{b^3\langle k_T\rangle^3}\int_0^1 dx \frac{(1-x)^2}{\left(\frac{1}{x^2}+\frac{4}{b^2\langle k_T\rangle^2}\right)^{3/2}}$$

which can be integrated to give,

$$d_{NS}(b,Q_0^2) = 9\bar{b}^2 \ln\left[\frac{1+\sqrt{1+\bar{b}^2}}{\bar{b}}\right] - 6\bar{b} + 8\bar{b}^3 + (1-8\bar{b}^2)\sqrt{1+\bar{b}^2} \qquad (3.23)$$

where $\bar{b} = \frac{b\langle k_T\rangle}{2}$. Eq (3.23) gives $d_{NS}(0,Q_0^2) = 1$, and for large b, $d_{NS}(b,Q_0^2) \sim 1/b^3$.

All the ingredients are now available to enable the acollinearity to be evaluated and compared with the data. However, before proceeding it will be worthwhile examining the approximations used above in more detail.

3.3 Erroneous Leading Logarithms

From the limits on the integration in eq (3.8), it can be seen that $0 \leq k_T \leq \infty$, which is clearly incorrect at finite Q, particularly $Q=Q_0$. Eq (3.8) leads to a very sharp form for $d_{NS}(b,Q_0^2)$, arising from the $x \sim 0$ region of the double integration, and this can be seen in fig (3.3); this then gives a very appreciable effect on the cross section $dA/d\Theta$ as shown in reference [42], over a noticeable range in angle $0 \lesssim \Theta \lesssim 20^\circ$, leading to an order of magnitude effect at $\Theta \simeq 0^\circ$. The correct range of phase space should be $0 \leq k_T \leq \frac{xQ_0}{2}$, which also now makes the δ function in eq (3.6) make sense. So the upper limit in eq (3.8) must be changed, and this modifies eq (3.22) to read,

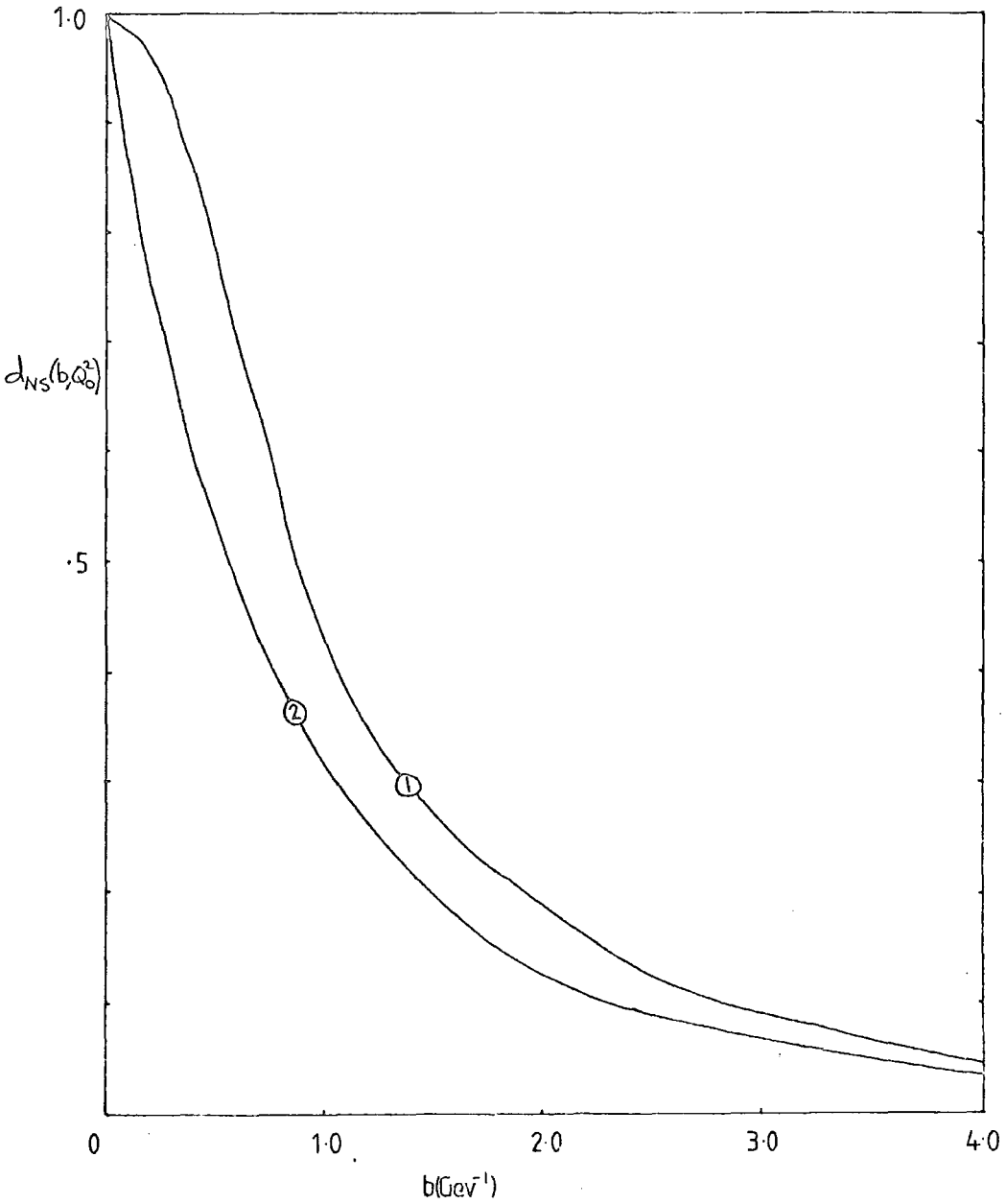

Fig.(3.3) The starting function $d_{NS}(b,Q_o^2)$ for Q_o=9.0 Gev. Curve 1 is that of eq(3.24) and curve 2 is that of eq(3.22).

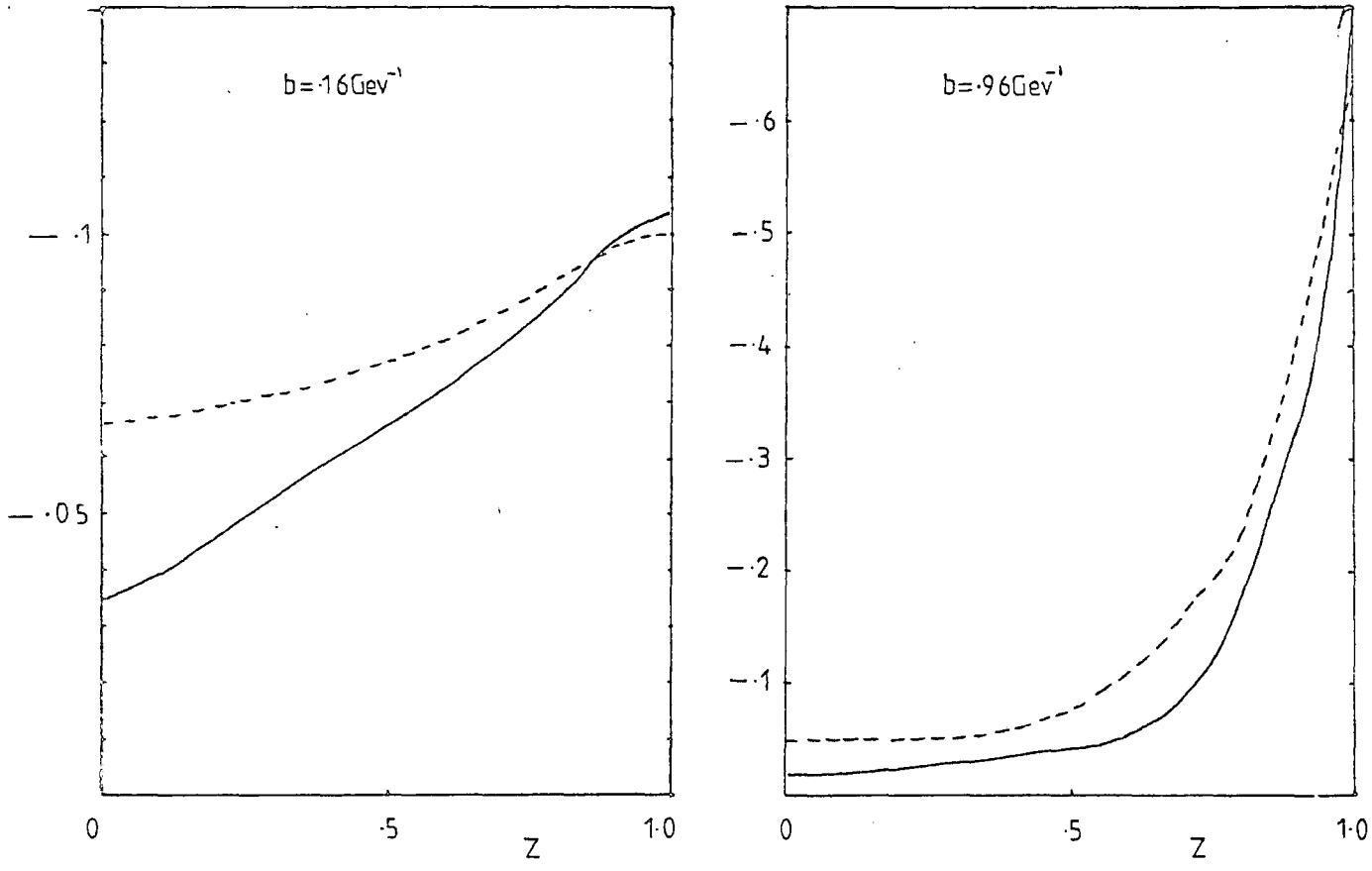

Fig(3.4). Integrands in eq(3.14) for $Q = Q_0 = 9.0$ Gev. The solid curve is the exact result, whereas the dotted curve is the approximate form of eq (3.15). Both curves use $d_{NS}(b, Q_0^2)$ from eq(3.24).

$$d_{NS}(b,Q_0^2) = \frac{b}{\langle k_T\rangle^2}\int_0^1 dx(1-x)^2 \int_0^{x^2Q_0^2/4} dk_T^2\, e^{-\frac{2k_T}{\langle k_T\rangle}} J_0(k_T b/x) \qquad (3.24)$$

Eq (3.24) can be integrated numerically quite simply and the result for $\langle k_T\rangle = 0.5$ is shown in fig (3.3), where the normalization is fixed by $d_{NS}(0,Q_0^2)=1$. Again it is the region of small b which dominates the cross section, and this is particularly where the curves in fig (3.3) are more largely different. (Also recall that these functions occur squared in the cross section).

Furthermore, the $z\to 1$ approximation used to solve the evolution equation (3.14) analytically is too harsh at finite values of Q^2; it does correctly produce the leading double log result which is a good approximation asymptotically. As already pointed out, it is the region of small b which is important in inverting the Fourier-Bessel transform (eqs (2.29), (3.9)) to obtain the cross section, and it is in this region of finite Qb where the leading double log approximation, (generated by the approximation of Bassetto et al. [40] and used by Baier and Fey [42] and Cleymans and Kuroda [43]), does not dominate and can therefore lead to erroneous results. This is exemplified in fig (3.4) where the exact integrand in eq (3.14) is plotted out for two values of b, along with the approximate form eq (3.15); both curves used the function $d(b,Q_0^2)$ evaluated using eq (3.24). This again shows an appreciable difference between the two curves at small b, the crucial region, and shows that the approximate integrand is not as peaked at $z=1$.

Moreover, putting b=0 in the exact evolution equation (3.14) yields,

$$Q^2\frac{\partial}{\partial Q^2} d_{NS}(Q^2,0) = -\frac{2}{3} C_F \frac{\alpha_s(Q^2)}{\pi} d_{NS}(Q^2,0)$$

and using $\alpha_s(Q^2) = 4\pi/\beta_0 \ln \frac{Q^2}{\Lambda^2}$ simply gives,

$$d_{NS}(Q^2,0) = d_{NS}(Q_0^2,0)\left[\frac{\alpha_s(Q^2)}{\alpha_s(Q_0^2)}\right]^{\gamma_2^{NS}} \tag{3.25}$$

where $\gamma_2^{NS} = -2A_2/\beta_0$. Eq (3.25) is also simply obtained for the approximate result of eqns (3.16), (3.17). However, the approximate result (eq (3.16)), gives,

$$\frac{\partial}{\partial b} d_{NS}(Q^2,0) = \frac{\partial}{\partial b} d_{NS}(Q_0^2,0)\left[\frac{\alpha_s(Q^2)}{\alpha_s(Q_0^2)}\right]^{\gamma_2^{NS}} \tag{3.26}$$

since $$\frac{\partial}{\partial b} F_{NS}(Q^2,Q_0^2,b)\Big|_{b=0} = 0$$

whereas the exact result of eq (3.14) yields,

$$\frac{\partial^2 d_{NS}(Q^2,b)}{\partial \ln Q^2 \, \partial b}\Big|_{b=0} = 0$$

so that,

$$\frac{\partial}{\partial b} d_{NS}(Q^2,0) = \frac{\partial}{\partial b} d_{NS}(Q_0^2,0) \tag{3.27}$$

which shows that the approximation of Bassetto et al does not predict the correct behaviour for the derivative at small b , which means it is not going to evolve correctly unless $\partial d_{NS}(Q_0^2,0)/\partial b = 0$.
Of course if Qb is large enough then the approximation becomes a reasonable one. However, this is not the case, since it is necessary to evolve the fragmentation function from some relatively low value of Q=Qo 9.0Gev or less, where two jet events dominate; if Q_0 is too large all the QCD evolution will be put into the starting function $d_{NS}(Q_0^2,b)$, and so that would not say anything about QCD behaviour.

So a way to proceed is now to evolve eq (3.14) numerically using the correctly integrated input function of eq (3.24) and fig (3.4).

3.4 The Acollinearity Distribution (Continued)

The numerical evolution of eq (3.14) is fairly straightforward, starting from a value Q_0=9.0 Gev , at which the input function $d_{NS}(b, Q_0^2)$ from eq (3.24) was used with values at the arguments (b/z) interpolated at each stage in the evolution for each z . The input function $d_{NS}(b,Q_0^2)$ was calculated exactly for $0 \leq b \leq 4.0\ \text{Gev}^{-1}$, after which a simple form was used out to infinity; the region $b > 4.0\ \text{Gev}^{-1}$ has a negligible effect on the final result, and it was irrelevant whether the parametrization was $\sim b^{-3}$, an exponential $\sim e^{-cb^2}$ or a straight line.

Thus the acollinearity can be written (from eq (3.9) in the small angle regime $P_T \simeq \frac{Q\Theta}{2}$),

$$\frac{dA}{dP_T^2} = \frac{1}{2}\int db\, d_q^{h_a}(b,Q^2)\, d_{\bar{q}}^{h_b}(b,Q^2)\, b\, J_0(bP_T) \tag{3.28}$$

in which the configurations where the particular hadron comes from a quark and an anti-quark have been summed over (i.e. a factor of 2). If again one assumes that the quark and antiquark fragment in the same way, this leads to an acollinearity,

$$\frac{dA}{d\cos\Theta} = \frac{Q^2}{4}\int db \left[d_{NS}(b,Q^2)\right]^2 b\, J_0\left(b\frac{Q\Theta}{2}\right) \tag{3.29}$$

which is to be compared with data for $\cos\Theta \gtrsim 0.97$.

The larger Q^2, the more independent $d_{NS}(b,Q^2)$ becomes on the input distribution. For instance, a good approximation of $d_{NS}(b,Q_0^2)$ is $e^{-b^2/2\cdot 5}$ for $0 \leq b \leq 2\text{Gev}^{-1}$, but for $b > 2$ it falls off much faster than the exact value, so was not used in practice. Yet the resulting

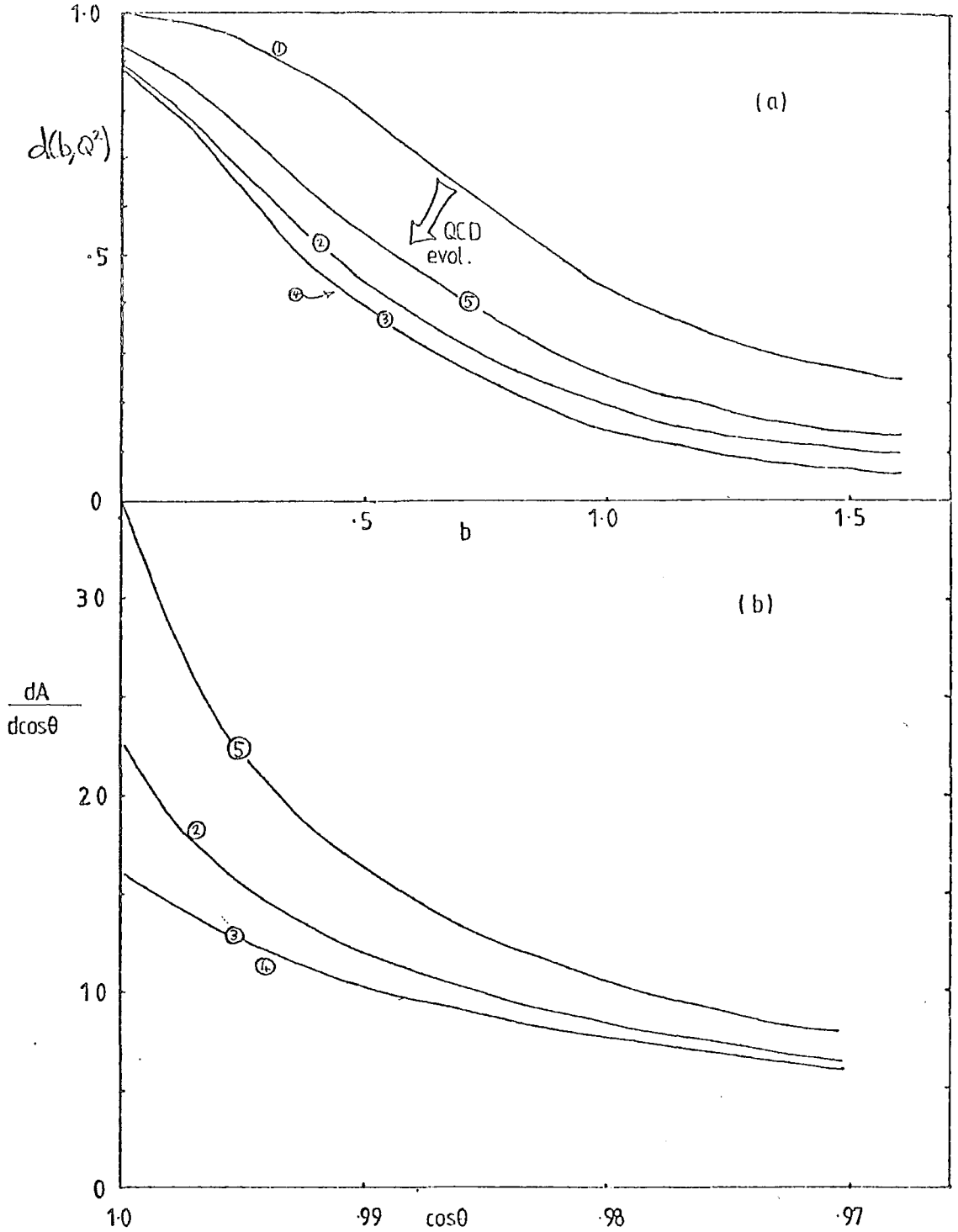

Fig.(3.5) (a) The b-space fragmentation functions in the non-singlet sector for Q_0 = 9.0 Gev, Q=30 Gev, Λ = 0.2 Gev. Curve 1 is the starting function $d_{NS}(b,Q_0^2)$ of eq.(3.24). Curves 2-5 are the $d_{NS}(b,Q^2)$ obtained by numerically evolving eq.(3.14) from Q_0 to Q. Curve 2 uses $\alpha_s(Q^2)$. Curve 3 uses $\alpha_s(Q^2(1-Z))$. Curve 4 uses $\alpha_S(Q^2(1-Z))$ and the two loop Altarelli-Parisi densities from ref[44] with $\Lambda_{\overline{MS}}$=0.2 Gev. Curve 5 is as curve 4 with $P^{(1)}_{qq}(z)$ of ref[45] and Λ_{MS}=0.2.

(b) The resulting energy weighted acollinearity obtained from the $d_{NS}(b,Q^2)$ functions of (a).

$d_{NS}(b,Q^2)$ evolved functions in the two cases were closer together than their respective input functions. So even at modest $Q \lesssim 30$Gev this effect can be observed.

The resulting fragmentation function and acollinearity can be seen in fig (3.5) with $\alpha_s(Q^2)$ and an arbitrary $\Lambda=0.2$. This can however be improved upon, as we will now demonstrate.

Consider the second order Altarelli-Parisi splitting function in the non-singlet sector. This can be written,

$$P^{(1)}_{qq}(z) = C P^{(0)}_{qq}(z)\ln(1-z) + \overline{P^{(1)}_{qq}}(z) \tag{3.30}$$

where $P^{(0)}_{qq}$ is the first order result of eq (3.2) (previously simply referred to as Pqq (z)). The first term in eq (3.30) is the leading term and gauge independent with $C=-\frac{11}{6}C_A+\frac{2}{3}n_f T_R=-\frac{1}{2}\beta_0$, (see for example the results of the calculations performed in references [44], [45], [46]). And the term $\overline{P^{(1)}_{qq}}(z)$ contains no terms like $P^{(0)}_{qq}(z)\ln(1-z)$. To this order the evolution eq (3.14) will be,

$$\frac{\partial}{\partial \ln Q^2} d_{NS}(b,Q^2) = \int_0^1 dz\, z\left[\frac{\alpha_s(Q^2)}{2\pi} P^{(0)}_{qq}(z) + \left(\frac{\alpha_s(Q^2)}{2\pi}\right)^2 P^{(1)}_{qq}(z) + \ldots\right] \cdot J_0\left[Qb\sqrt{\frac{1-z}{z}}\right] d_{NS}(Q^2, b/z) \tag{3.31}$$

α_s was shown to run with Q^2[2] using the renormalization group equation; but an explicit evaluation of the graphs which produce this running can be done in an axial gauge in leading logarithms, which shows that the argument of α_s is the maximum value of P_T^2 which is $Q^2(1-z)$ [49]. One can then write,

$$\alpha_s(Q^2(1-z)) \equiv 4\pi/\beta_0 \ln\left[\frac{Q^2(1-z)}{\Lambda^2}\right]$$

$$\simeq \left[1 - \frac{\alpha_s(Q^2)}{4\pi}\beta_0 \ln(1-z) - \ldots\right]\alpha_s(Q^2)$$

asymptotically. So clearly using this definition of α_s sums the term in $P_{qq}^{(1)}(z)$ of the form $-\frac{1}{2}\beta_0 P_{qq}^{(0)}(z)\ln(1-z)$, which is the leading term of next to lowest order $P_{qq}^{(1)}(z)$. Furthermore, Amati et al. showed that this argument of α_s will correctly sum all the leading double log terms of $P_{qq}(z)$ to all orders, into the first term too [47]. So that eq (3.31) can now be written.

$$\frac{\partial d_{NS}(Q^2,b)}{\partial \ln Q^2} = \int_0^1 dz\, z\left[\frac{\alpha_s(Q^2(1-z))}{2\pi} P_{qq}^{(0)}(z) + \left(\frac{\alpha_s(Q^2(1-z))}{2\pi}\right)^2 \overline{P}_{qq}^{(1)}(z) + \text{higher terms} \sim \sum_{n=3}^{\infty}\left(\frac{\alpha_s(Q^2(1-z))}{2\pi}\right)^n \overline{P}_{qq}^{(n-1)}\right]_+ J_0\left(Qb\sqrt{\tfrac{1-z}{z}}\right) d_{NS}\left(\tfrac{b}{z},Q^2\right) \tag{3.32}$$

where all terms $\overline{P}_{qq}^{(m)}$ do not contain the leading double logarithm parts, which are themselves a gauge invariant subset of the whole result. So using just the lowest order result in eq (3.32) will include the gauge independent leading terms to all orders. This was the form used, where again $|\alpha_s(Q^2(1-z))|$ was taken (see chapter 2),

$$|\alpha_s(Q^2(1-z))| = \frac{4\pi}{\beta_0\left[\ln^2\left(\frac{Q^2(1-z)+C}{\Lambda^2}\right)+\pi^2\right]^{1/2}} \tag{3.33}$$

where the parameter C was used to regularize α_s as $z \to 1$; C=1.0 Gev [48]. Four flavours of quarks were used.

The terms of a less leading form in $\ln(1-z)$, at each order, are gauge dependent and cannot be summed into $P_{qq}^{(0)}(z)$. And it must be remembered that large logarithms are still present, even though the perturbative expansion using $\alpha_s(Q^2(1-z))$ is an improved one.

The results of the evolution using $\alpha_s(Q^2(1-z))$ are again displayed in fig (3.5), where it can be seen that modifying the argument of the strong coupling constant does have an appreciable affect, particularly at small angles where the acollinearity is quite larger when using $\alpha_s(Q^2)$.

In view of recent results [50] and discussion ([30], [51]), it is a worthwhile exercise to go one stage further in the evaluation of the acollinearity, viz. to examine the effect of adding in the term $\overline{P_{qq}^{(1)}}(z)$ in its leading form.

3.5 Including Two-Loop Altarelli-Parisi Probabilities And Gauge Dependence

Kodaira and Trentadue [50] have attempted to go beyond the leading results discussed above, (i.e. soft Altarelli-Parisi (AP) splitting function at lowest non-trivial order and summation of leading higher order terms), by including the $O(\alpha_s^2)$ AP density and also some terms beyond the leading log result, which to $O(\alpha_s)$ is given by eq(2.24). The motivation for the $O(\alpha_s^2)$ part can be seen from looking at eq (2.41), where the next to leading terms are given in $\Delta_2(b)$. However, contributions of this type can also originate in $\alpha_s.\Delta_1(b)$ and this is therefore included by using the AP probability to next order, shown in eq (3.32). The analytic results of reference [50] again rely heavily on the harsh $z \to 1$ approximation of Bassetto et al.

After performing the above calculation, Kodaira and Trentadue conclude that there is no agreement with experiment [50]. This erroneous conclusion comes mainly from the form they use to generalize eq.(2.24) to include the dominant non-logarithmic pieces; so for the moment consider just the $O(\alpha_s)$ input. (This is equivalent to the discussion in chapter 2, concerning the form of the cross section to put in eq (2.47)). The form they use is,

$$\frac{4\alpha_s}{3\pi Q_T^2}\left[\ln\frac{Q^2}{Q_T^2} - \frac{3}{2}\right] \qquad (3.34)$$

and this is hoped to be a good approximation to the full $O(\alpha_s)$ result, (i.e. that obtained by integrating eq (1.5)). This is then transformed into impact parameter space and the evolution equations then

provide the form factor which is analogous to that of Baier and Fey (eq (3.17)) with the logarithm modified by the constant term -3/2. One might therefore expect the form factor to look something like $\left[d_{NS}(b,Q^2)\right]^2$ of fig (3.5), which is monotonically decreasing in b. However, the form factor of Kodaira and Trentadue has a hump at small b before decreasing away, and it is this which gives their conclusion that the theory is not consistent with the data.

The reason for this enhancement [51] comes from their approximation of the full $O(\alpha_s)$ result by just including the single term '$-\frac{3}{2}$'. The full distribution to $O(\alpha_s)$ is positive definite and so the log of the b space form factor ($\Delta(b)$ of eq (2.47)) or the argument of the exponential in eq (3.17)) will be negative definite since $J_0(x) \leq 1$ for all real $x \geq 1$. To get a hump in the b space form factor (i.e. $\exp[\Delta(b)] > 1$) would require $\Delta(b)$ to be positive over that particular range in b, and this is what happens if only the term '$-\frac{3}{2}$' is added in. It is the behaviour of the $O(\alpha_s)$ cross section at large k_T which determines that of the b- space transform at small b (finite Q), and it is precisely this region which Kodaira and Trentadue have not incorporated correctly. The full $O(\alpha_s)$ result (integral of eq (1.5)) can be written analytically as [27,51],

$$\frac{1}{\sigma_0}\frac{d\sigma'}{dx_T^2} = \frac{2\alpha_s C_F}{\pi x_T^2}\left\{\left[1-\frac{x_T^2}{4}+\frac{x_T^4}{4}\right]\ln\left[\frac{1+\sqrt{1-x_T^2}}{x_T}\right]-\frac{1}{4}\sqrt{1-x_T^2}\,(3-x_T^2)\right\} \tag{3.35}$$

on integrating eq (A2) from 0 to $1-x_T^2$, where $x_T = \frac{2k_T}{Q}$. '$-\frac{3}{2}$' is the next term in the expansion of eq (3.35) for $k_T^2 \ll Q^2$ but the terms which are small for small k_T make sure the cross section remains positive at large k_T and it is these next terms which Kodaira and Trentadue leave out, and so their $O(\alpha_s)$ result of eq (3.34) is not positive definite. Hence their results cannot be expected to be accurate. The simplest way to ensure that the $O(\alpha_s)$ cross section

remains positive definite is to use the full $O(\alpha_s)$ result as in chapter 2, or using eq (3.35).

There are other problems in extending the lowest order results of eq (3.32) and section (3.4) to incorporate higher order AP probabilities. The double leading log terms are summed to all orders using $\alpha_s(Q^2(1-z))$ as described above, which is fine since they are gauge independent. One can then think about putting in the next to leading $O(\alpha_s^2)$ parts (as done in ref [50]), i.e. those like $\sim P_{qq}^{(0)}(z) \sim (1+z^2)/(1-z)$, but these are now gauge dependent and also renormalization scheme dependent. For instance consider the calculations of refs [44], [45], [46], which calculate $P_{qq}^{(1)}(z)$ in various gauges. The leading term is

$$-\frac{1}{2}\beta_0 \frac{(1+z^2)}{(1-z)} \ln(1-z) \tag{3.36}$$

in all three calculations, as expected. The next to leading term derived by Kalinowski et al. [44] is,

$$\left\{C_F C_A\left(\frac{67}{18}-\frac{\pi^2}{6}\right)+C_F N_F T_R\left(-\frac{10}{9}\right)\right\}\frac{(1+z^2)}{(1-z)} \tag{3.37}$$

where the authors used a light - like axial gauge and the $\overline{MS}$ renormalization scheme. Whereas for comparison, Floratos et al [45] find this term to be,

$$\left\{C_F T_R\left(\frac{22}{9}\right)-C_F C_A\left(\frac{145}{18}-\frac{\pi^2}{3}\right)\right\}\frac{(1+z^2)}{(1-z)} \tag{3.38}$$

for four flavours of quarks, and where they use the Feynman gauge and the MS renormalization scheme. (Curci et al.[46] find a next to leading term identical with that of Kalinowski et al, using a light - like axial gauge and the MS scheme, so care must be taken to redefine

Λ in each scheme). So as can be seen from the two examples quoted above, they are quite different and so this means it's difficult to get an unambiguous $O(\alpha_s^2)$ next to leading result to compare with experiment.

It is straightforward to incoporate these extra higher order terms into the evolution equations, simply by writing eq (3.14) as,

$$\frac{\partial d_{NS}(b,Q^2)}{\partial \ln Q^2} = \int_0^1 dz\, z \left\{ \left[\frac{\alpha_s(Q^2(1-z))}{2\pi} + K\left(\frac{\alpha_s(Q^2(1-z))}{2\pi}\right)^2 \right] P_{qq}^{(0)}(z) \right\}_+ \cdot J_0\left(Qb\sqrt{\frac{1-z}{z}}\right) d_{NS}\left(\frac{b}{z}, Q^2\right) \tag{3.39}$$

where K is given by either of the expressions (3.37) or (3.38) divided by C_F, (depending upon which gauge one uses).

And so using eq (3.39), an estimate of the effect of gauge and scheme dependence can be made, to this level of approximation. Eq(3.39) makes the assumption that the rescaled coupling $\alpha_s(Q^2(1-z))$ is the correct choice also at second order, which has not yet been proven. Fig (3.5) also shows the results of doing the above calculation in the two different gauges and schemes, and shows a sizeable effect between the two. It is interesting to note that for $\Lambda = 0.2$, when using the $O(\alpha_s^2)$ result of ref [44], a negligible change occurs from the $O(\alpha_s)$ result with $\alpha_s(Q^2(1-z))$, as shown in fig (3.5). In this gauge the parameter $K \simeq 1.6$, and the effect of this together with that of taking α_s to 2 loops almost exactly cancel out. A more sizeable (though not large) difference between the two occurs for $\Lambda = 0.5$.

As mentioned above, the coupling constant must be put in at the two loop level also, and as a function of Q^2 this can be written,

$$\frac{\alpha_s(Q^2)}{4\pi} = \frac{1}{\beta_0 \ln \frac{Q^2}{\Lambda^2}} - \frac{\beta_1 \ln\left(\ln \frac{Q^2}{\Lambda^2}\right)}{\beta_0^3 \ln^2 \frac{Q^2}{\Lambda^2}}$$

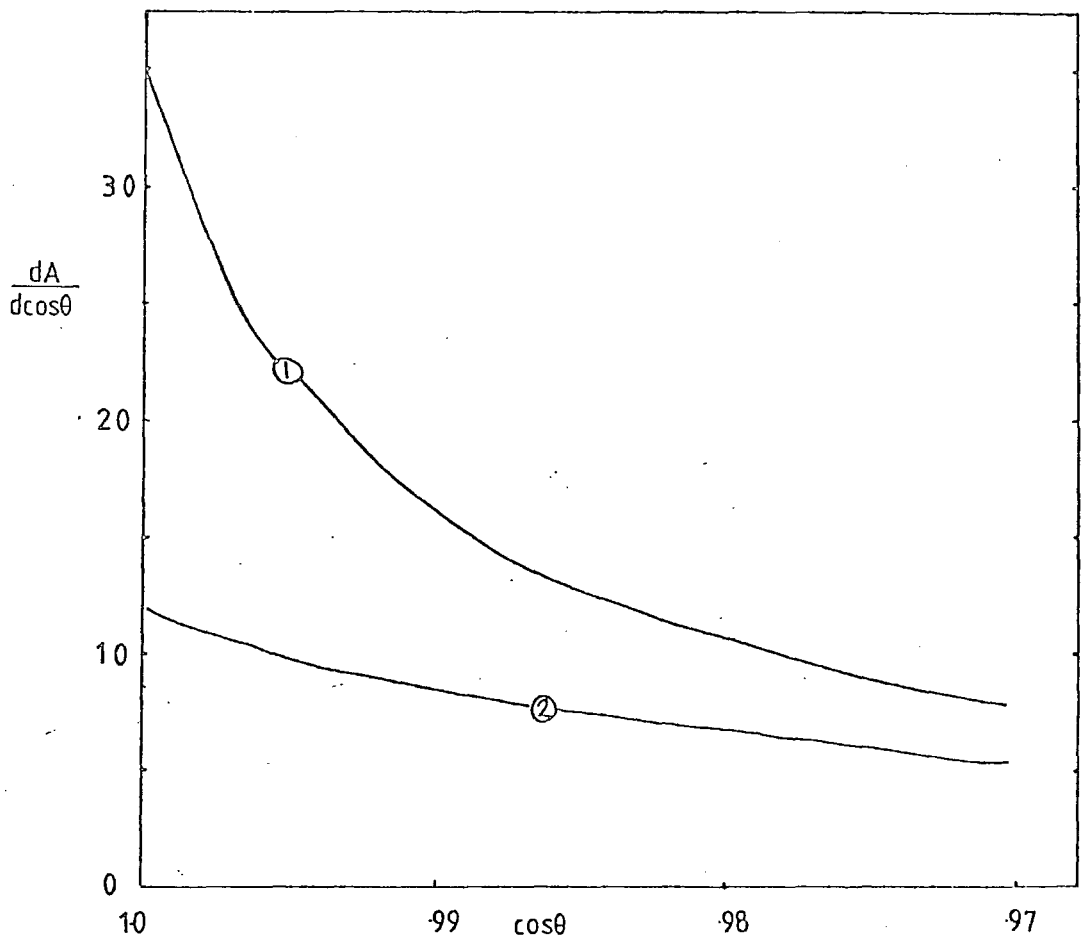

Fig (3.6). Comparison of the effect of gauge dependence at the two loop level in the acollinearity, with $\Lambda_{\overline{ms}} : \Lambda_{ms} = 5:2$, and $\alpha_s(Q^2(1-z))$ Curve 1 uses $P^{(1)}_{qq}(z)$ of ref[45], with $\Lambda_{ms} = 0.2$. Curve 2 uses $P^{(1)}_{qq}(z)$ of ref [44] with $\Lambda_{\overline{ms}} = 0.5$.

When α_s runs with $Q^2(1-z)$ and the modulus is taken (as in eq(3.33)), one obtains,

$$\left|\frac{\alpha_s(Q^2(1-z))}{4\pi}\right| \longrightarrow$$

$$\frac{1}{\beta_0 r} - \frac{\beta_1}{\beta_0}\left(\frac{1}{\beta_0 r}\right)^2\left[\frac{\ln(Q^2(1-z)+c)}{r}\ln r + \frac{\pi}{r}\sin^{-1}\frac{\pi}{r}\right] \qquad (3.40)$$

where,

$$\beta_0 = 11 - \frac{2}{3}n_f$$

$$\beta_1 = 102 - \frac{38}{3}n_f$$

and

$$r^2 = \ln^2\left(\frac{Q^2(1-z)+c}{\Lambda^2}\right) + \pi^2$$

Furthermore, since $\Lambda_{\overline{MS}} : \Lambda_{MS} = 2.66 : 1$ [2], the calculation was repeated using the results of [45] with $\Lambda_{MS} = 0.2$ and those of [44] with $\Lambda_{\overline{MS}} = 0.5$ (i.e. $2\frac{1}{2}:1$), in order to try to equalize the effect of the scheme dependence. This leads to an even greater difference between the two results, as shown in fig (3.6). So to attach any significance to the comparison of a two loop calculation, as performed above or in ref [50], with experiment would seem very optimistic in view of the theoretical ambiguities.

It must not be forgotten that only the next to leading $O(\alpha_s^2)$ parts were added in, which makes the extension from using lowest order particularly simple. The rest of the many terms present at $O(\alpha_s^2)$ might also be expected to play a part, even though these will be down from the next to leading ones by powers of logarithms. In principle it might be thought possible to just "gauge" or "scheme" these higher non-leading terms away, just leaving the gauge independent leading term, which was summed to all orders using $\alpha_s(Q^2(1-z))$ and lowest order. Similarly, no significance can be attached to the possibly large effect this sort of $O(\alpha_s^2)$ modification has (see fig (3.5)) on the lowest order result, since for the reasons discussed above the $O(\alpha_s^2)$ modification has not been reliably incorporated. Only an

exact $O(\alpha_s^2)$ calculation is reliably gauge independent and this is obviously far more difficult to include in the calculations. It is for these reasons that two-loop calculations will no longer be considered, and only one-loop gauge independent calculations will be compared with data.

To compare with data, one must also consider the singlet sector, and so extend the evolution equations to incorporate it. This will also check whether the non-singlet does provide the dominant contribution or not [42], [50].

3.6 The Singlet Sector

To find the fragmentation functions $d_q^h(b,Q^2)$ for a quark or a gluon $d_g^h(b,Q^2)$ one must solve the following coupled evolution equations,

$$\frac{\partial d_q^h(b,Q^2)}{\partial \ln Q^2} = \int_0^1 dz\, z \frac{\alpha_s}{2\pi}\left[P_{qq}(z) d_q^h\left(\frac{b}{z},Q^2\right) + P_{gq}(z) d_g^h\left(\frac{b}{z},Q^2\right)\right] J_0\left(Qb\sqrt{\frac{1-z}{z}}\right) \tag{3.41a}$$

$$\frac{\partial d_g^h(b,Q^2)}{\partial \ln Q^2} = \int_0^1 dz\, z \frac{\alpha_s}{2\pi}\left[P_{qg}(z).2n_f d_q^h\left(\frac{b}{z},Q^2\right) + P_{gg}(z) d_g^h\left(\frac{b}{z},Q^2\right)\right] J_0\left(Qb\sqrt{\frac{1-z}{z}}\right) \tag{3.41b}$$

where the extra splitting functions needed are:

$$P_{gq}(z) = \frac{4}{3}\left[\frac{1+(1-z)^2}{z}\right]$$

$$P_{qg}(z) = \frac{1}{2}\left[z^2 + (1-z)^2\right]$$

$$P_{gg}(z) = 6\left[\frac{z}{(1-z)_+} + \frac{1-z}{z} + z(1-z) + \eta\,\delta(1-z)\right]$$

where $\eta = \left(\frac{11}{12} - \frac{n_f}{18}\right)$. These describe the probabilities for the

splittings shown in fig (3.7) to occur in addition to that of fig (3.1).

Fig (3.7)

Decay processes described by the AP probabilities in Eqns (3.41).

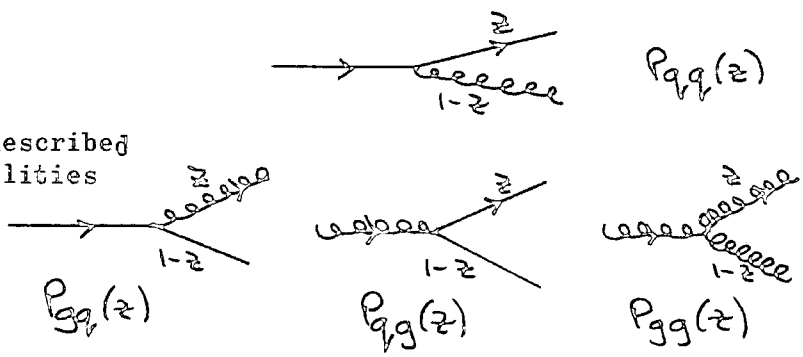

And so now we allow a quark to decay to a gluon (and vise versa) before hadronization.

The regularization used in eq (3.14) is implicit in eqs (3.41).

Using the above form for $P_{gg}(z)$ the r.h.s. of eq (3.41b) can be written,

$$\int_0^1 dz\, z \frac{\alpha_s}{2\pi}\left[P_{qg}(z) 2n_f d_q^h\left(\frac{b}{z}, Q^2\right) + \overline{P}_{gg}(z) d_g^h\left(\frac{b}{z}, Q^2\right)\right] J_0\left(Qb\sqrt{\frac{1-z}{z}}\right)$$

$$+ 6\frac{\alpha_s}{2\pi} \eta\, d_g^h(b, Q^2) \qquad (3.41c)$$

where $\overline{P_{gg}}(z)$ does not contain the term involving the δ function. For simplicity the argument of α_s remains unspecified for the moment.

Eqns (3.41) can be solved numerically in a coupled way, in a similar fashion to eq (3.14). The same starting function at $Q=Q_0=$ 9.0 Gev was chosen for both $d_q^h(b,Q^2)$ and $d_g^h(b,Q^2)$, viz. that of eq (3.24). It is again interesting to look at the b=0 results.

Setting b=0 in eqns (3.41) gives, with $Q=Q_0$,

$$\frac{\partial\, d_q(0,Q_0^2)}{\partial \ln Q^2} =$$

$$\frac{\alpha_s}{2\pi}\int_0^1 dz\, z\left[P_{qq}(z) d_q(0,Q_0^2) + P_{gq}(z) d_g(0,Q_0^2)\right] \qquad (3.42a)$$

$$\frac{\partial d_g(0,Q_0^2)}{\partial \ln Q^2} =$$

$$\frac{\alpha_s}{2\pi}\int_0^1 dz\, z\left[2n_f P_{qg}(z) d_q(0,Q_0^2) + P_{gg}(z) d_g(0,Q_0^2)\right] \qquad (3.42b)$$

where the argument of α_s is assumed to be z independent. Now the starting functions $d_q(b,Q_0^2)$ and $d_g(b,Q_0^2)$ are both identical and so call them $d(b,Q_0^2)$, so eqns (3.42) can simply be written,

$$\frac{\partial d_q(0,Q_0^2)}{\partial \ln Q^2} = \frac{\alpha_s}{2\pi} d(0,Q_0^2)\left[A_2(qq) + A_2(gq)\right] \qquad (3.43a)$$

$$\frac{\partial d_g(0,Q_0^2)}{\partial \ln Q^2} = \frac{\alpha_s}{2\pi} d(0,Q_0^2)\left[2n_f A_2(qg) + A_2(gg)\right] \qquad (3.43b)$$

where the anomalous dimensions $An(ij)$, $i,j \equiv q,g$ are defined in terms of the moments of $P_{ij}(z)$,

$$An(ij) = \int_0^1 dz\, z^{n-1} P_{ij}(z)$$

It is easy to see that momentum conservation,

$$\int_0^1 dz\, z\left[P_{qq}(z) + P_{gq}(z)\right] = 0$$

$$\int_0^1 dz\, z\left[2n_f P_{qg}(z) + P_{gg}(z)\right] = 0$$

gives,

$$A_2(qq) + A_2(gq) = 0$$

$$2n_f A_2(qg) + A_2(gg) = 0$$

so that eqns (3.43) give,

$$\frac{\partial}{\partial \ln Q^2} d_q(0,Q_0^2) = 0 \qquad (3.44a)$$

$$\frac{\partial}{\partial \ln Q^2} d_g(0,Q_0^2) = 0 \qquad (3.44b)$$

This means that the value of the fragmentation functions remains unchanged throughout the evolution at b=0, and so remains fixed at 1.0 for both. This can be compared with the result for the non-singlet sector eq (3.25), which can be viewed as a measure of momentum non-conservation by excluding gluonic decays, (and which provides a decrease of about 15%). The non-singlet sector only allows an evolution such as that of fig (3.8a), whereas the singlet sector also allows the quark line to decay along the way into a gluon as for instance in fig (3.8b). And so the non-singlet evolution does not account for momentum lost to gluons.

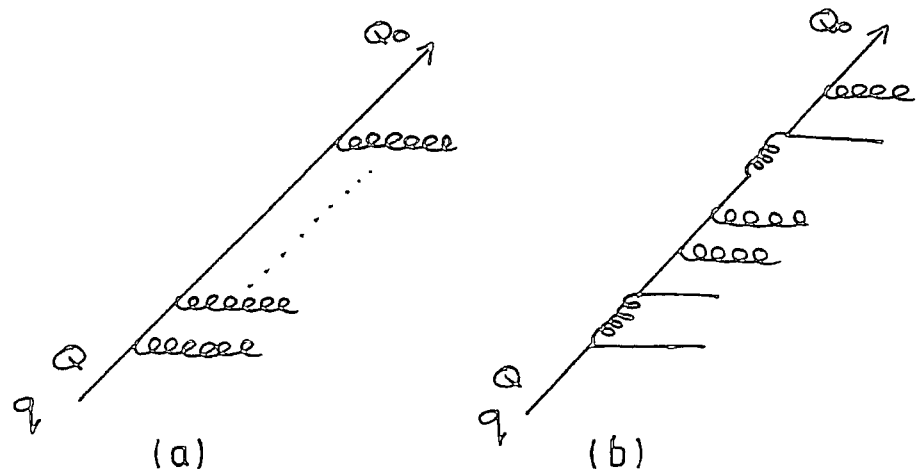

Fig (3.8): Examples of evolution (a) in non-singlet (b) in singlet case.

However, if α_s is chosen to have a z dependent argument, as in $\alpha_s(Q^2(1-z))$, then clearly the simple result obtained above (eqs (3.44)) will not obtain and momentum conservation will be violated to some degree. This is borne out in fig (3.9a) where the evolved functions $d_q(b,Q^2)$ and $d_g(b,Q^2)$ are plotted, and which shows $d_g(0,Q^2) = 1.25$ for an $\alpha_s(Q^2(1-z))$; whereas for an $\alpha_s(Q^2)$ the correct behaviour $d_q(0,Q^2) = d_g(0,Q^2) = 1.0$ is obtained. The resulting acollinearity is shown in fig (3.9b) using,

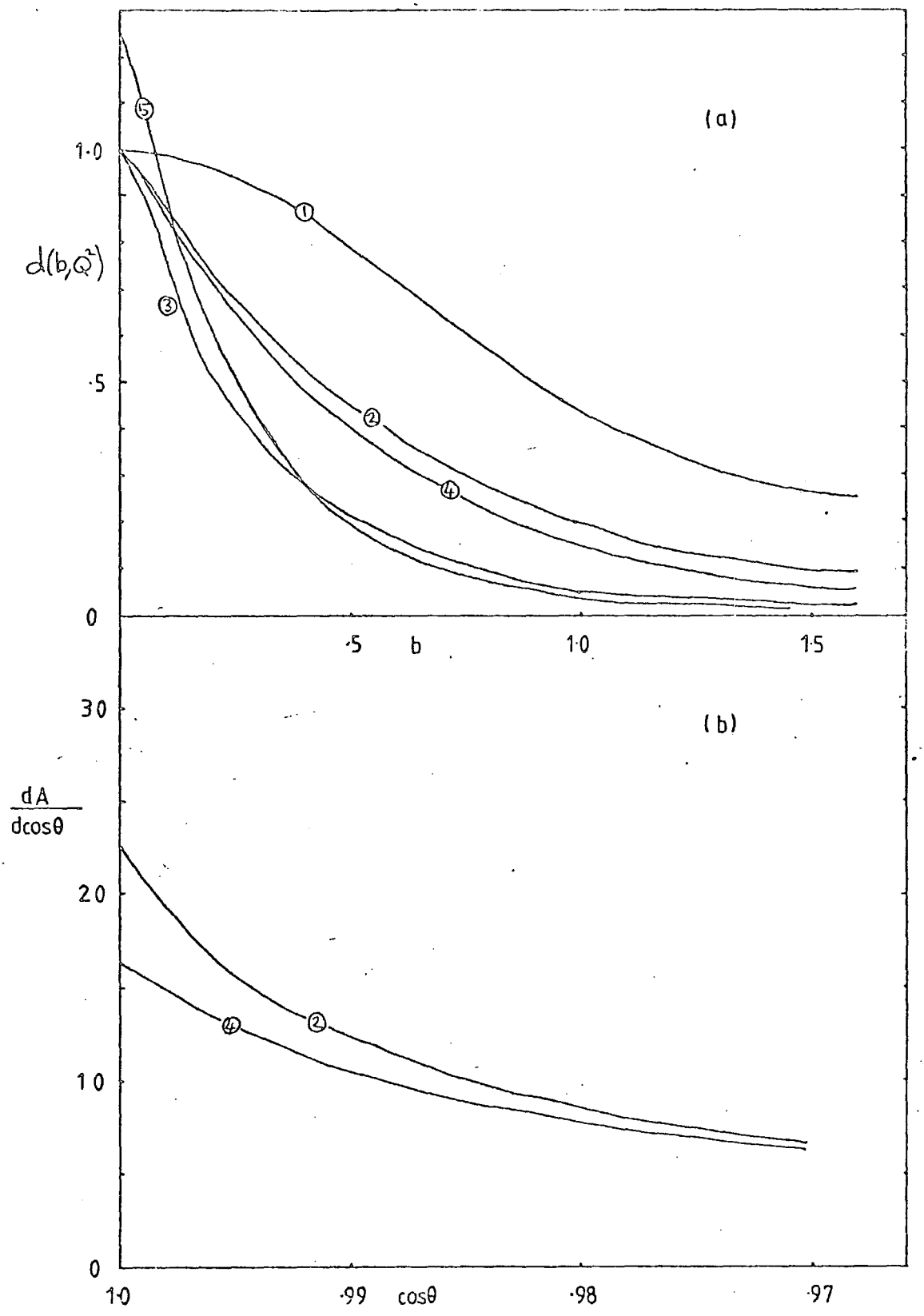

Fig. (3.9.) (a) The b space fragmentation functions in the singlet sector $d(b_0,Q^2)$ for $Q_0=9.0$ Gev, $Q=30.0$ Gev and $\Lambda = 0.2$ Gev. Curve 1 is the starting function $d(b_0,Q_0^2)$ of eq.(3.24). Curves 2-5 are obtained by numerical evaluation of eqs.(3.41). Curves 2 and 3 use $\alpha_s(Q^2)$ and are $dq(b_0,Q^2)$ and $dg(b_0,Q^2)$ respectively. Curves 4 and 5 use $\alpha_s(Q^2(1-Z))$ and are $dq(b_0,Q^2)$ and $dg(b_0,Q^2)$ respectively. (b) The energy weighted acollinearity obtained using the appropriate $dq(b_0,Q^2)$ of (a).

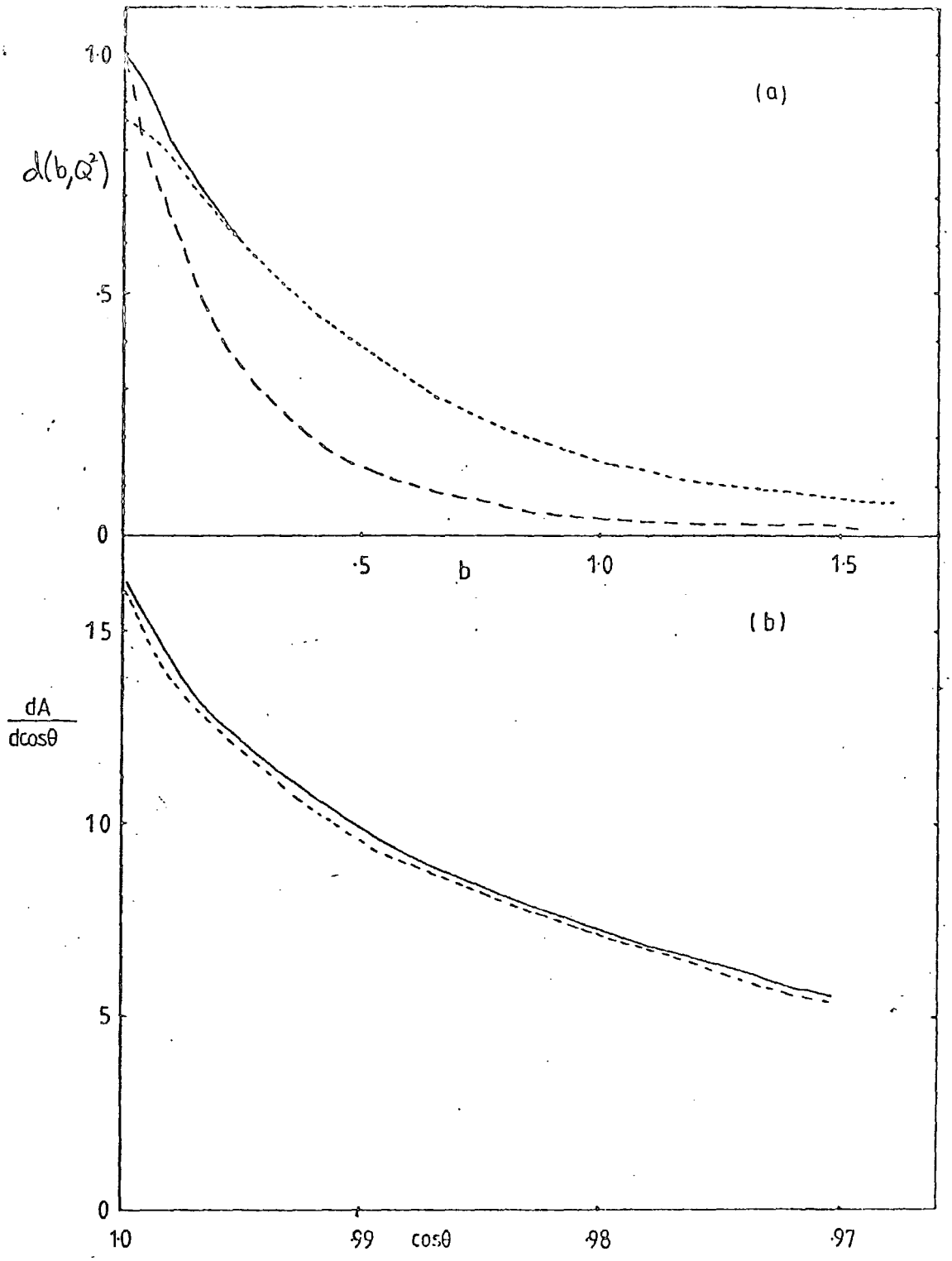

Fig.(3.10) (a) Comparison of singlet (Full curve $d_q(b,Q^2)$, long dashed curve $d_g(b,Q^2)$) and non-singlet (short dashed curve) b-space fragmentation functions, and (b) energy weighted accollinearities for Q_0=9.0 Gev, Q=30 Gev, Λ =0.5 Gev and $\alpha_s(Q^2)$.

$$\frac{dA}{d\cos\Theta} = \frac{Q^2}{4}\int db \left[d_q(b,Q^2)\right]^2 b\, J_0\left(b\frac{Q\Theta}{2}\right) \qquad (3.45)$$

for small angles.

The reason for the unsatisfactory behaviour when using $\alpha_s(Q^2(1-z))$ can be traced back to the higher orders summation. This argument sums the leading $\ln(1-z)$ terms in the non-singlet sector to all orders. However, in the singlet sector the diagonal splitting functions $Pgq(z)$ and $Pqg(z)$ do not contain these $\ln(1-z)$ terms (as can be seen for example to $O(\alpha_s^2)$ in refs [44,45]), and so $\alpha_s(Q^2(1-z))$ is summing terms which are not there, hence leading to momentum non-conservation. $Pgg(z)$ does contain the $\ln(1-z)$ terms at higher orders, but it must also obviously be symmetric in z and $(1-z)$, which it is not if α_s runs with $Q^2(1-z)$.

A reasonable assumption is to use $\alpha_s(Q^2(1-z))$ in the $Pqq(z)$ term of eq (3.41a), and $\alpha_s(zQ^2)$ in the $Pgq(z)$ term (in line with momentum conservation), with $\alpha_s(Q^2)$ in eq (3.41c). This produces a $d_q(b,Q^2)$ almost identical with that when using $\alpha_s(Q^2)$ throughout, but in this case now both $d_q(0,Q^2)$ and $d_g(0,Q^2)$ remain at 1.0. So the resulting acollinearity is identical with that obtained using $\alpha_s(Q^2)$. This suggests the coupling in eqns (3.41) is only weak as far as $d_q(b,Q^2)$ is concerned.

The results obtained with non-singlet and singlet fragmentation and $\alpha_s(Q^2)$ are compared in fig (3.10), with Λ=0.5, Q=30 GeV. This suggests that the non-singlet does indeed provide the dominant contribution to the cross section, so that soft gluon emission from quarks dominates $dA/d\cos\Theta$ at these modest values of Q. However, when the non-singlet is used with $\alpha_s(Q^2(1-z))$, the difference between the two is more appreciable, which can be seen from fig (3.11), where

at very small angles the non-singlet is approximately 67% of the singlet cross section.

3.7 Comparison with Data

Before beginning this section it is worthwhile to point out that changing the regularizing parameter C of eq (3.33) from 1.0 to 2.0 increases $d\sigma/d\cos\theta$ by about 2% for $\Lambda = 0.2$, and clearly less for $\Lambda = 0.5$; so the results obtained may be regarded as accurate to within this figure.

Fig (3.11) also compares singlet ($\alpha_s(Q^2)$) and non-singlet ($\alpha_s(Q^2(1-z))$) with PLUTO data for $d\sigma/d\cos\theta$ at Q=30.0 GeV. The data as a function of $\cos\theta$ are actually for a centre of mass energy Q=27.6-31.6 GeV, and as a function of θ for Q=30.0 - 31.6 GeV. It is the normalization of this particular set of data which corresponds most closely to that of the predictions, which are normalized to unity over just half of the angular range $(0 \leq \theta \leq \frac{\pi}{2})$ in θ, the data being normalized to 2.0 for $0 \leq \theta \leq \pi$. Agreement with data is satisfactory in both cases with $\Lambda = 0.2$. However, as $\cos\theta \to 1.0$ the singlet cross section can be seen to rise more sharply and so fits the data in the first three bins, whereas the non-singlet does not, and requires a smaller value of Λ.

The Q^2 evolution of the cross section $d\sigma/d\theta$ is shown in fig (3.12) for Q=21 and 30 GeV, for non-singlet and singlet predictions, which can both be seen to fit the data much better than the parton model result which just uses the input function $d(b,Q_0^2)$ of eq (3.24) with no QCD evolution. The peak of $d\sigma/d\theta$ predicted by the parton model is much too large. The peak of the QCD evolved cross-section gets higher and sharper as Q^2 increases, which indicates that QCD behaviour does in fact predict that hadronic jets become more acollinear at small angles θ as Q^2 increases, while at the same time becoming narrower, i.e.

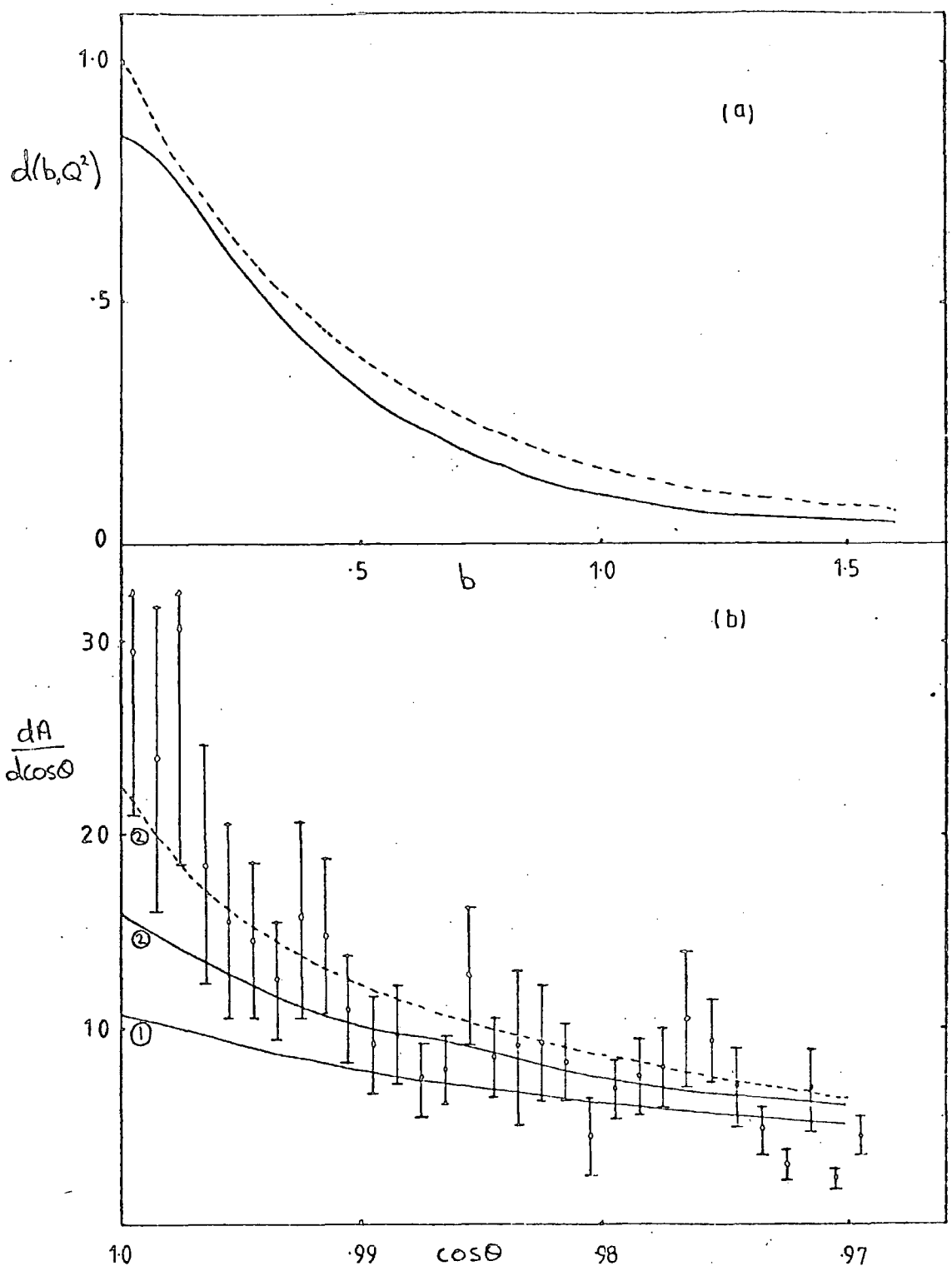

Fig. (3.11) Comparison of singlet (dashed curve) and non-singlet (full curve) predictions. (a) The singlet functions $dq(b,Q^2)$ are obtained with $\alpha_s(Q^2)$ (or equivalently the mixed form described in the text) and non-singlet functions $d_{NS}(b,Q^2)$ with $\alpha s(Q^2(1-z))$. Q=30.0 Gev and curve 1 uses Λ=0.5 Gev with curve 2 using Λ =0.2 Gev. (b) The acollinearity compared with PLUTO data [18].

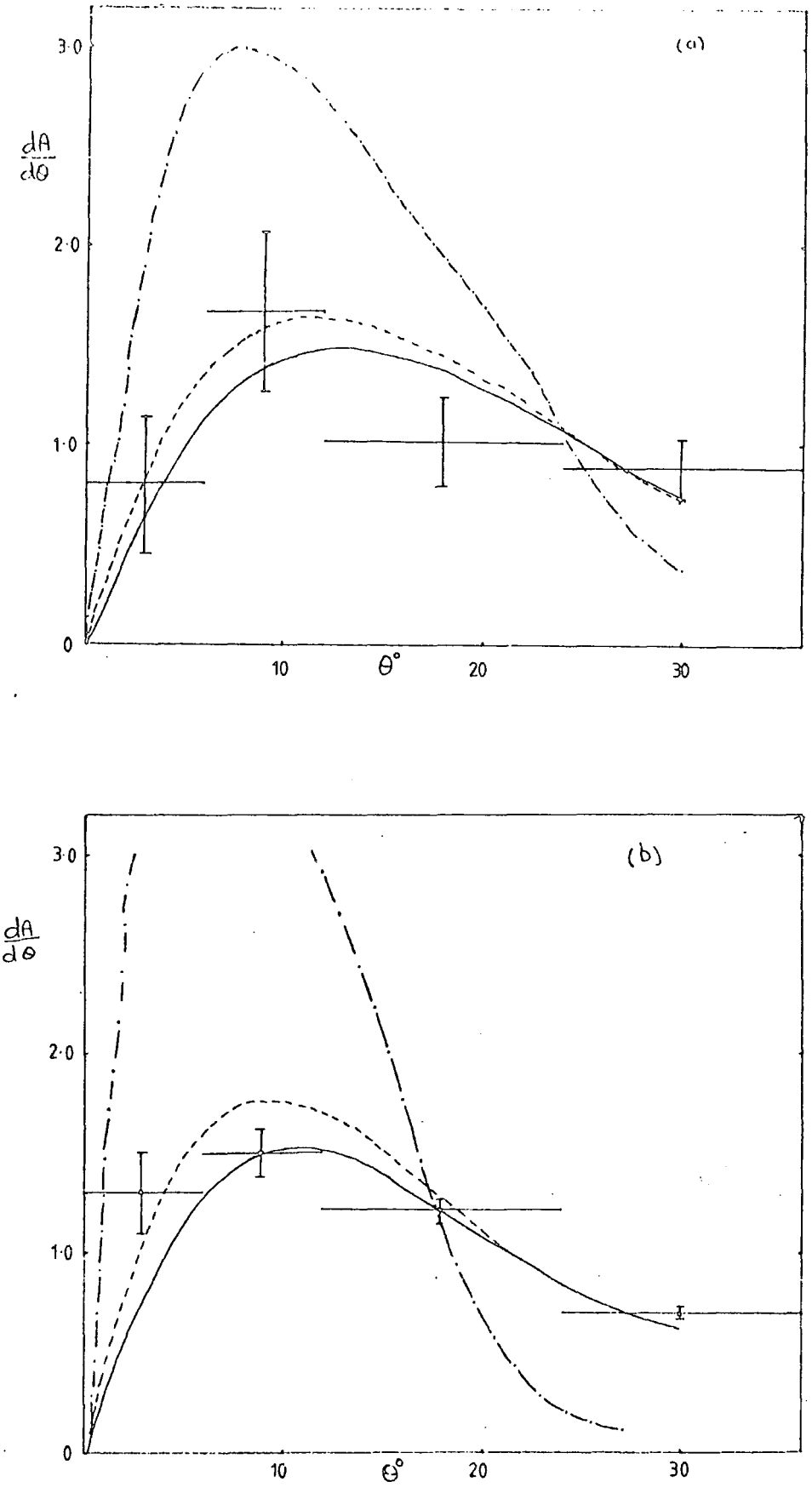

Fig. (3.12) The Q^2 evolution of singlet (dashed curve) and non-singlet (full curve) acollinearity $dA/d\theta$ is compared with the parton model result (dashed-dotted curve) and the data [18]. (a) at Q=21 Gev and (b) at Q= 30 Gev. Singlet predictions use $\alpha_s(Q^2)$, non-singlet $\alpha_s(Q^2(1-z))$, with Λ =0.2 Gev.

Fig (3.13).
The effect of the $\langle k_T \rangle$ dependence on the singlet ($\alpha_s(Q^2)$) predictions for acollinearity $dA/d\cos\theta$; $\Lambda = 0.2$ Gev, $Q = 30$ Gev. Curves, 1, 2, 3 correspond to $\langle k_T \rangle = 0.3$, 0.5 0.7 Gev respectively.

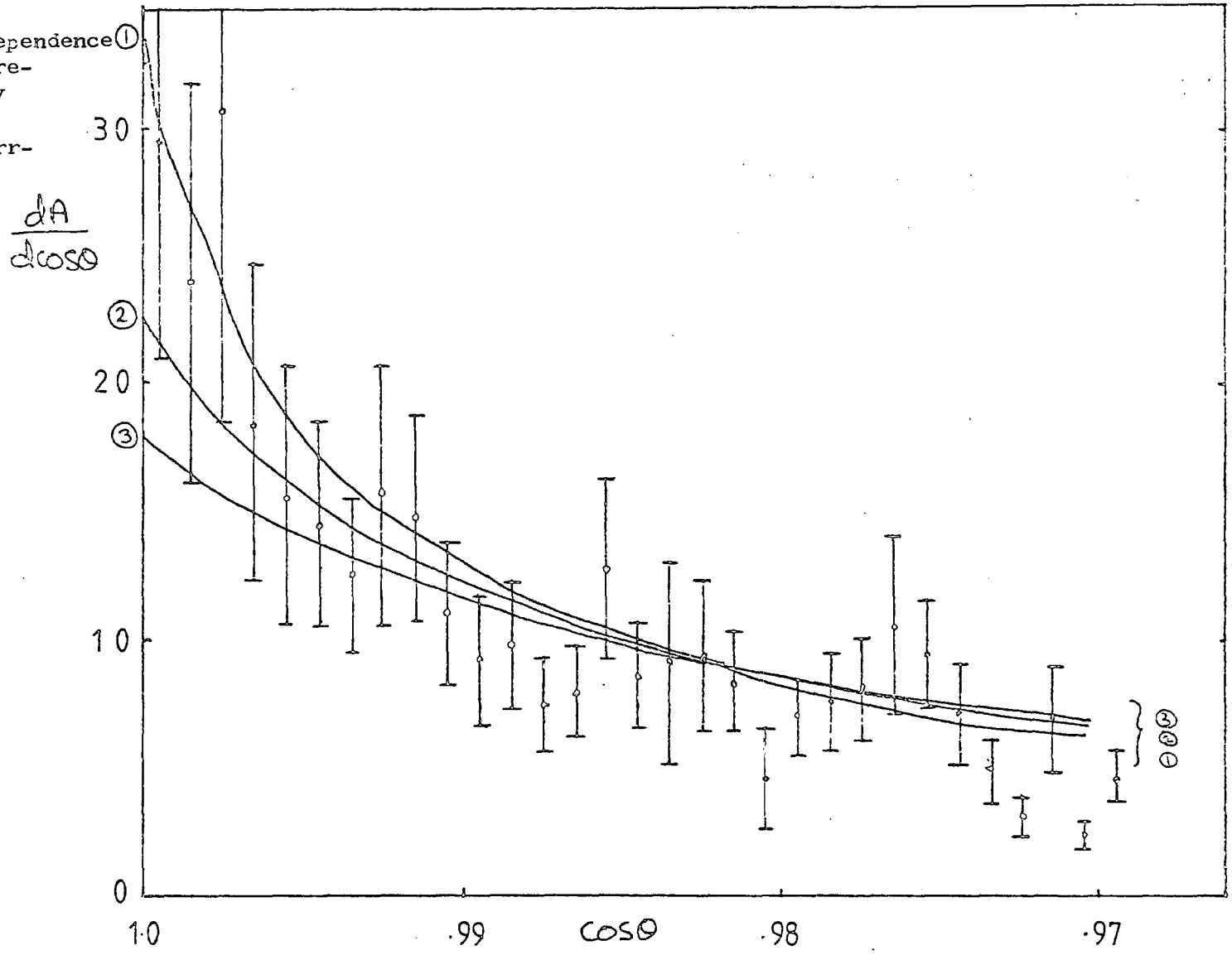

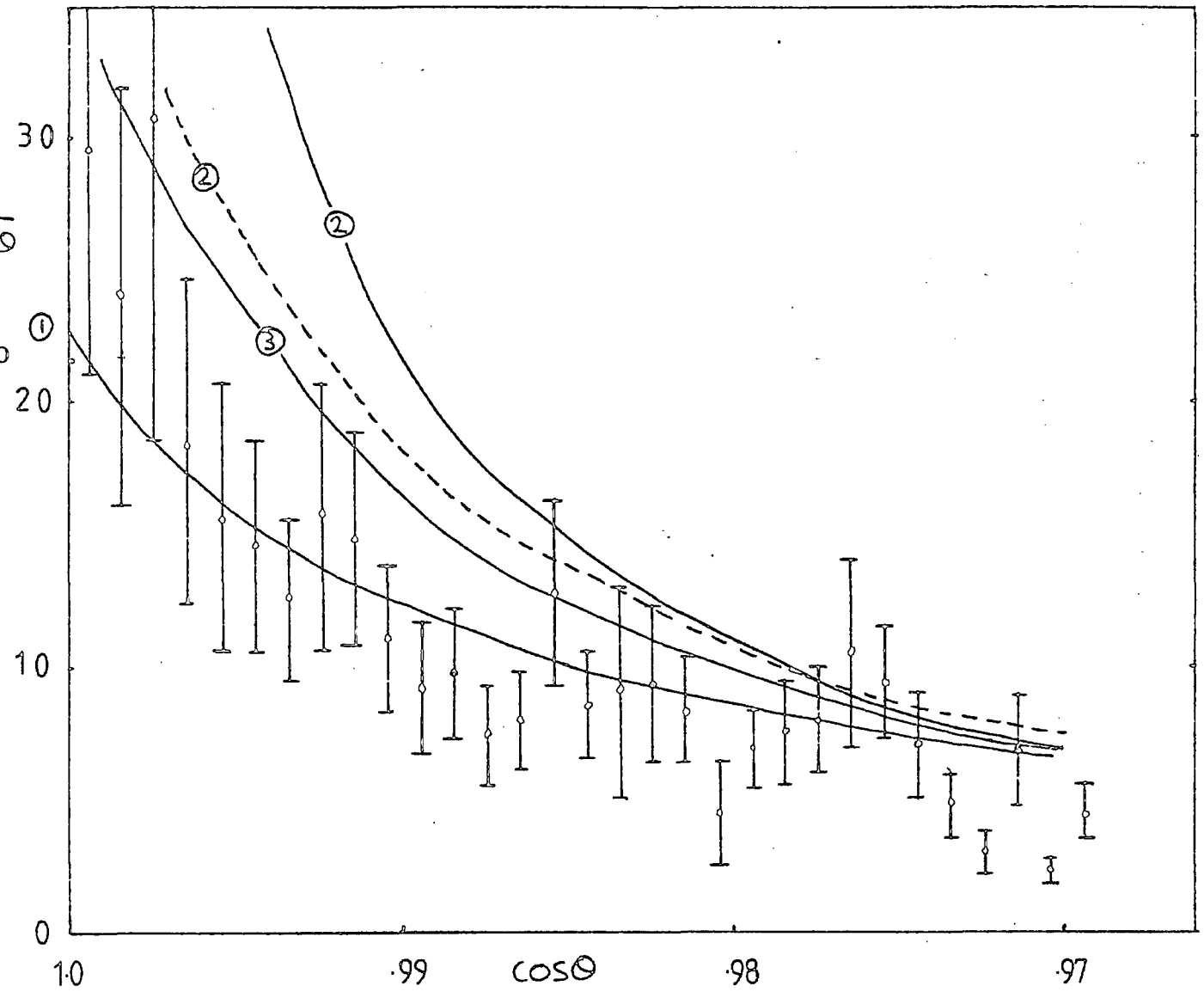

Fig.(3.14). Comparison of the PPP and evolution equation predictions for dA/dcosΘ at Q=30 Gev. Curve 1 is the singlet prediction from the evolution equations with Λ=0.2. Curve 2 (solid) is that of the PPP with Λ=0.2 and full O(α_s) input. Curve 2 (dashed) is the same as curve 2 (solid) with Λ=0.8 Gev. Curve 3 is the PPP with LLA as input. All use $\langle k_T \rangle$ =0.5 Gev.

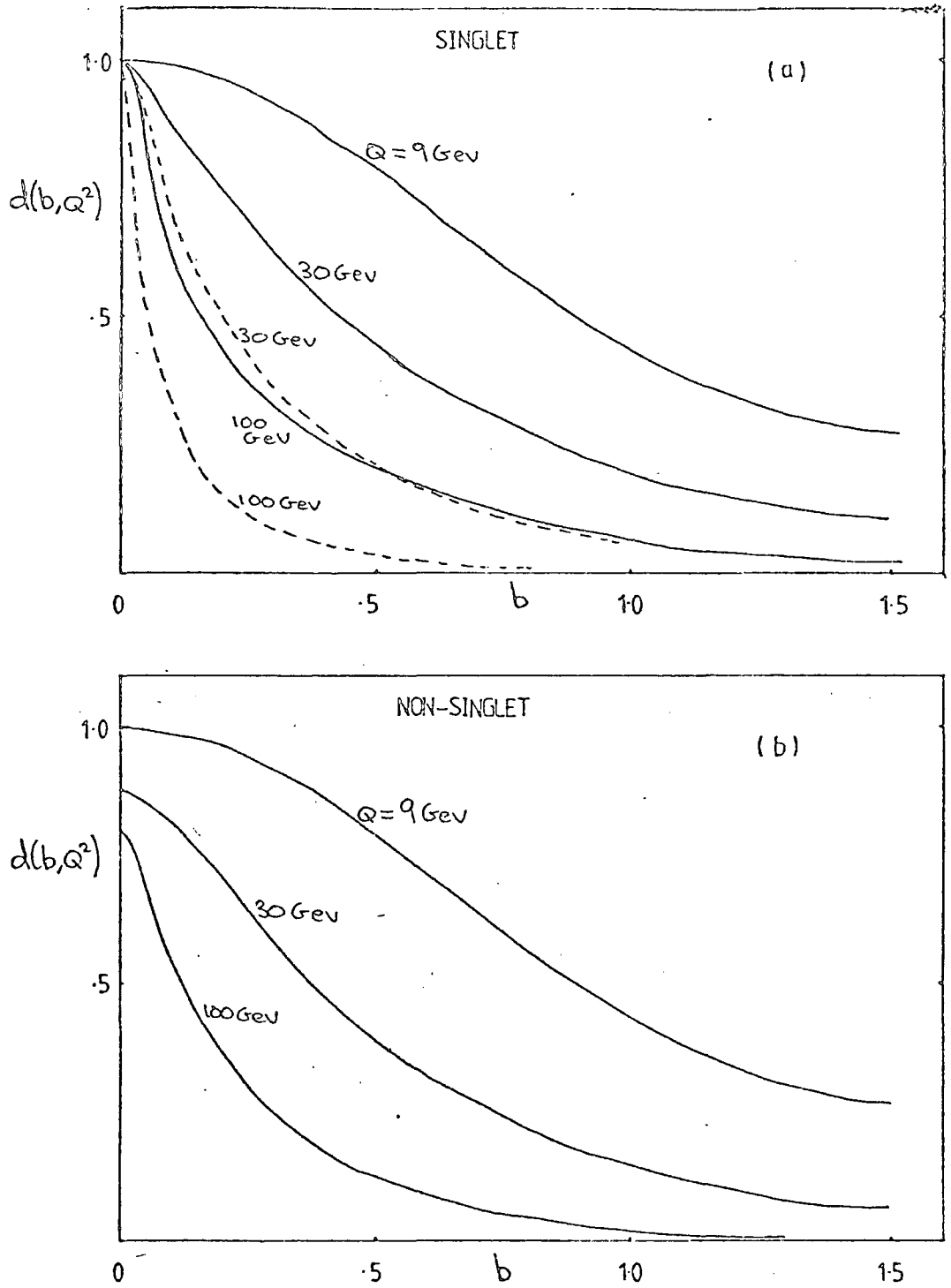

Fig. (3.15). Singlet, $(\alpha s(Q^2))$ and non-singlet, $(\alpha s(Q^2(1-z)))$ (b) predictions for the functions $d(b,Q^2)$ at Q=100 Gev. Solid lines are $dq(b,Q^2)$, dashed $dg(b,Q^2)$. Λ =0.2 Gev, Q_0= 9.0 Gev, $\langle k_T \rangle$ =0.5 Gev.

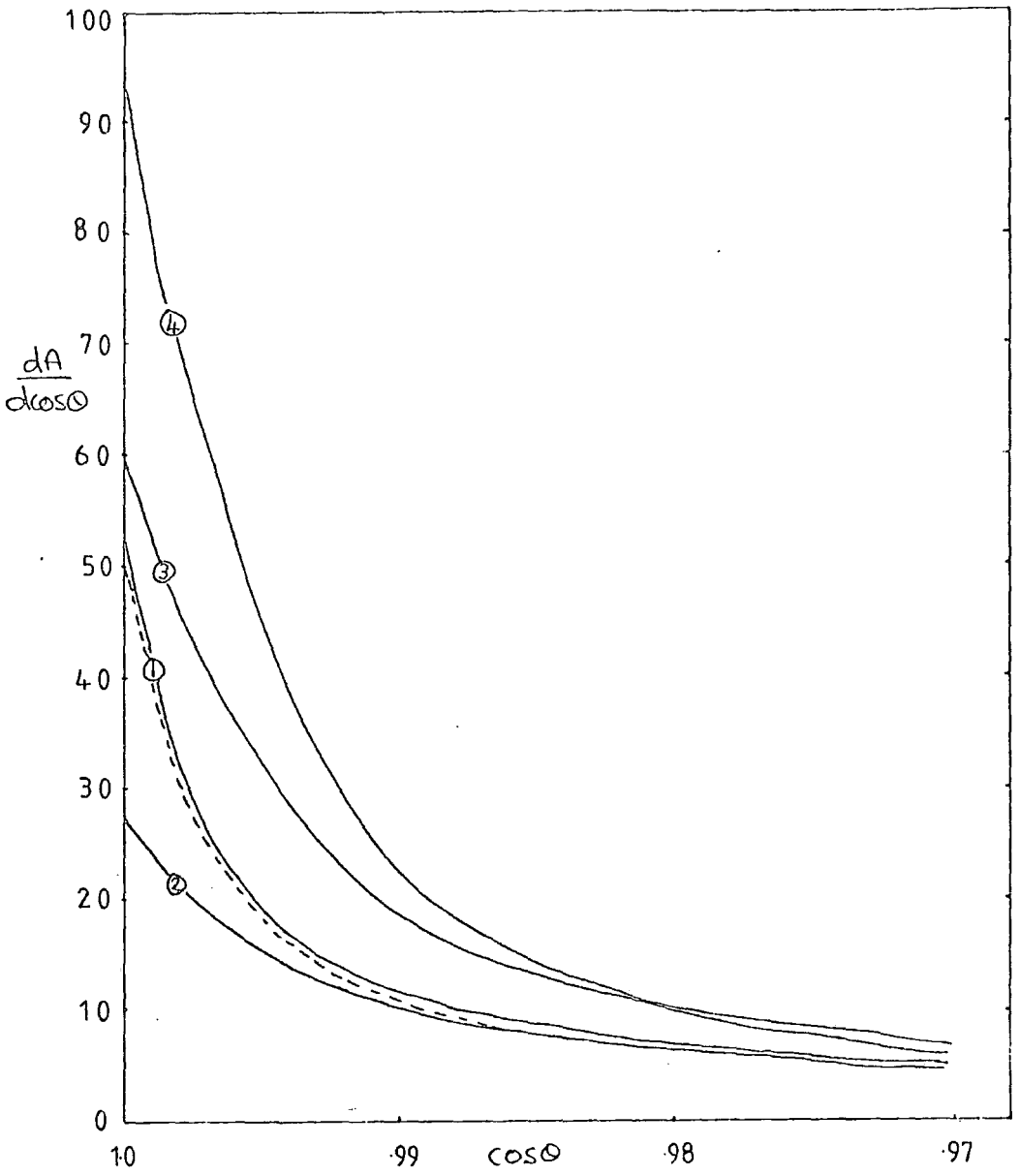

Fig.(3.16) Predictions for the acollinearity at Q= 100 Gev, Λ =0.2 Gev, $\langle k_T \rangle$ =0.5 Gev. Curves 1 (full line) and 2 are the singlet and non-singlet results respectively obtained from Fig.(3.15). Curve 1 (dashed) is the non-singlet prediction with $\alpha_s(Q^2)$. Curve 3 is the PPP with LLA input. Curve 4 is the PPP with full $O(\alpha_s)$ input.

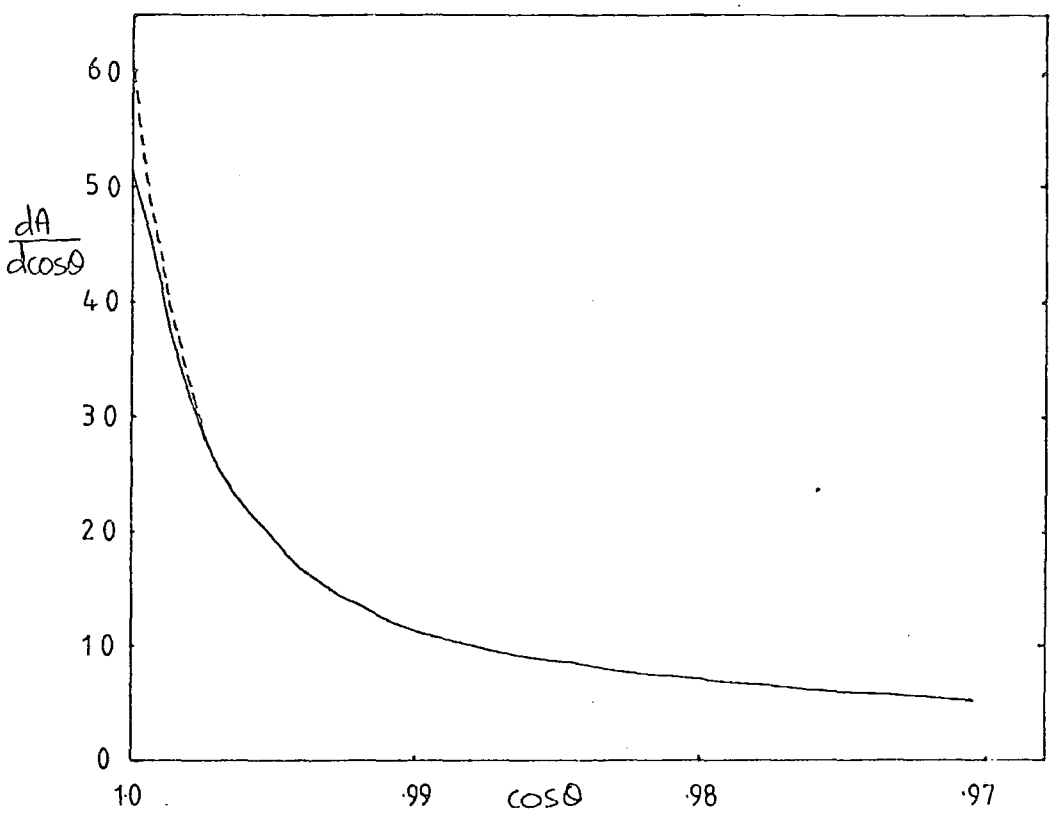

Fig. (3.17). The effect of the $\langle k_T \rangle$ dependence at Q=100 Gev, using singlet ($\alpha_s(Q^2)$) results with Λ =0.2 Gev. Full curve has $\langle k_T \rangle$ =0.5 Gev, dashed $\langle k_T \rangle$ =0.3 Gev.

$\langle P_T \rangle$ increases but $\langle P_T \rangle / Q$ decreases due to multiple emission of soft gluons, in agreement with data.

Fig (3.13) shows the effect of intrinsic transverse momentum dependence in the QCD evolved result. The curves shown correspond to $\langle k_T \rangle$ = 0.3,0.5 and 0.7 GeV respectively and show a sizeable dependence of the cross section on $\langle k_T \rangle$ at small angles, in contrast to the PPP (c.f. fig (2.5)), which is only affected by $\langle k_T \rangle$ dependence for $P_T \lesssim .75$ GeV or 3^0 ($\cos\Theta \gtrsim .998$), for Q=30.0 GeV. Clearly this difference between the two approaches stems from the more realistic way the k_T dependence is embodied in the function $d(b,Q_0^2)$, and so it plays a more significant role in the subsequent evolution of multiple soft gluon emission.

The leading log approach of the evolution equations (singlet) is compared in fig (3.14) with the acollinearity obtained using the PPP, from which it can be seen that the PPP can be made to fit the data, but with a much larger value of Λ. Comparing the leading log curves (1) and (3) shows that the results of the two approaches only differ numerically by a factor which can be corrected by altering Λ and $\langle k_T \rangle$ (c.f. fig (3.13)).

In view of the fact that LEP will hopefully be providing data in 1988, results for Q=100 Gev are shown in figs (3.15)-(3.17) for both singlet and non-singlet. Fig (3.15) shows the evolution of the decay functions $d(b,Q^2)$, and shows a much sharper rise in both cases at small b, as expected asymptotically, and so a much smaller range in b gives the dominant contribution to the acollinearity at Q=100 GeV. than at Q=30 GeV. Fig (3.16) shows the resulting acollinearity and again shows that the non-singlet appears to give the dominant contribution. Also included are results using the PPP, and again all predictions merge together as Θ increases (c.f. fig (3.14)). The

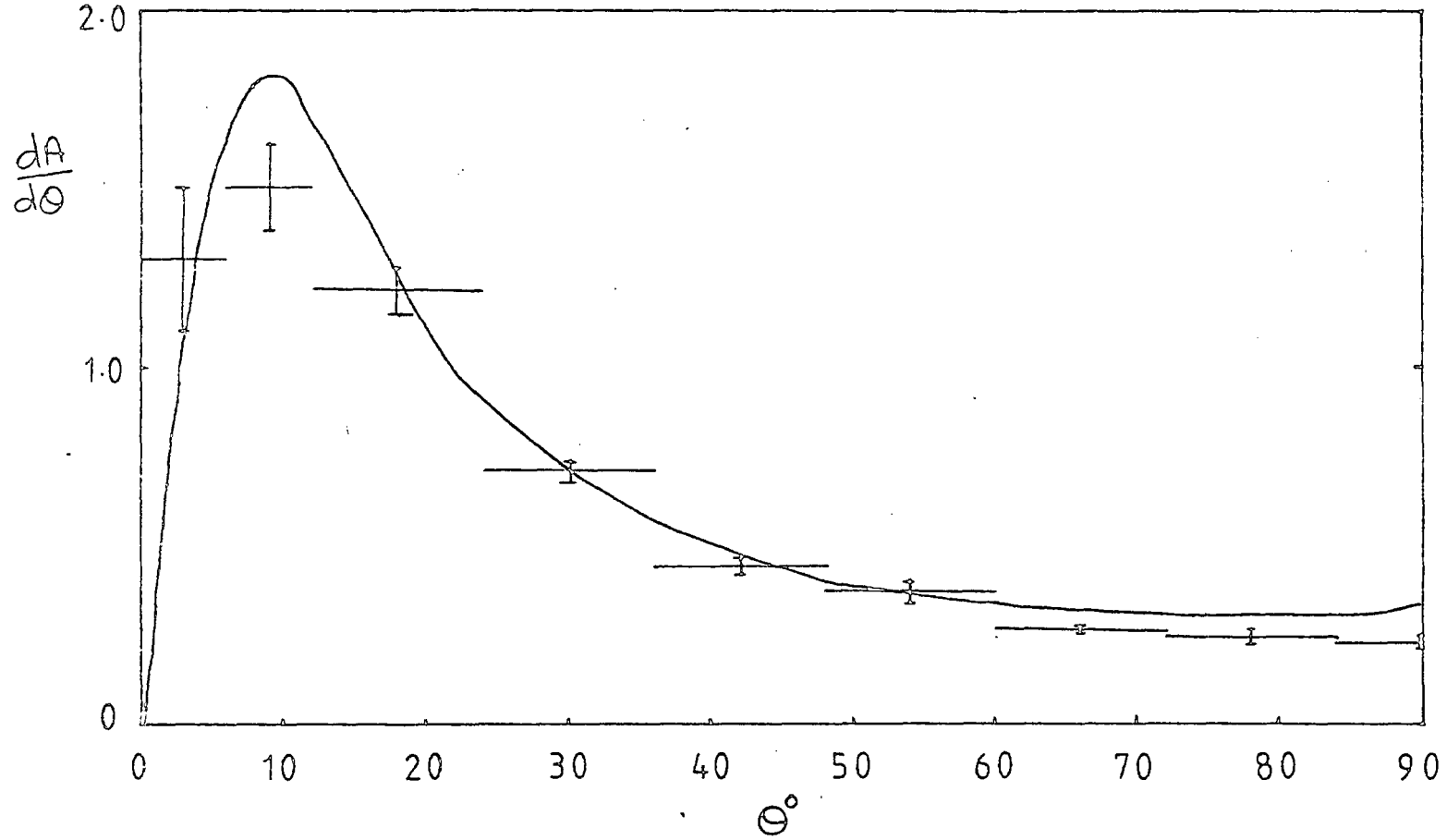

Fig. (3.18) The acollinearity $dA/d\Theta$ for $0 \leq \Theta \leq 90^{\circ}$ compared with data of ref [18]. Curve shown is obtained from the singlet prediction ($\alpha_s(Q^2)$) with Q=30 Gev, Λ =0.2 Gev and $\langle k_T \rangle$ = 0.5 Gev.

effect of the intrinsic transverse momentum dependence is greatly reduced by the time the decay functions have evolved to 100 GeV (see fig (3.17)), and can be compared with that of 30 GeV (fig (3.13)). This again shows that as the evolution occurs, the evolved decay functions become less dependent on the initial form as Q increases.

For the sake of completeness, the above calculation was extended to cover $0 \leq \Theta \leq 90^{\circ}$ using the method of Collins and Soper [39], alluded to earlier. This splits up the acollinearity into two parts,

$$\frac{dA}{d\cos\Theta} = W(Q,\Theta) + Y(Q,\Theta),$$

where the leading log parts of the $O(\alpha_s)$ result are contained in $W(Q,\Theta)$, in which the multigluon evolution or sum is performed. And $Y(Q,\Theta)$ contains the rest of the first order expression [12], i.e. the terms which do not behave like $1/Q^2$ as $\Theta \to 0$. So $W(Q,\Theta)$ corresponds to the calculations performed above, onto which the term $Y(Q,\Theta)$ was added [39],

$$Y(Q,\Theta) = \frac{4\alpha_s(Q^2)}{3\pi}\left[\frac{1}{4x}\left(\left(\frac{3}{y^5} - \frac{4}{y^4}\right)\ln x + \frac{3}{y^4} - \frac{5}{2y^3} - \frac{1}{y^2}\right) - \frac{1-2x}{8x}\left(\left(\frac{12}{y^5} - \frac{16}{y^4} + \frac{4}{y^3}\right)\ln x + \frac{12}{y^4} - \frac{10}{y^3}\right)\right] + \frac{4\alpha_s(Q^2)}{3\pi}\,\frac{1}{4x}\left(\ln x + \frac{3}{2}\right)$$

where $x = \sin^2\frac{\Theta}{2}$ and $y = 1-x$.

The results are shown in fig (3.18) as a function of Θ, which shows reasonable agreement with data.

3.8 Summary and Conclusions

Within limitations the above results may be viewed as encour-

aging, in that the predictions of perturbative QCD are seen not to conflict with the data, and in fact give the correct shape and normalization. The PPP is limited by the fact that it only considers independent emissions (as discussed in chapter 2), and does not allow a quark to decay into a gluon before it fragments into the observed hadrons; the latter is a point which can be included using the coupled evalution equations in the singlet sector. The leading log approximations used will become more justifiable as the beam energy is increased with the running of LEP.

It is a pity that the 2 loop calculation cannot be compared meaningfully with data, in view of the uncertainties stemming from gauge and renormalization scheme dependence. It is also disappointing that the summation of leading higher order terms in the splitting function $P_{qq}(z)$, by using $\alpha_s(Q^2(1-z))$, have not been extended to the singlet sector.

However, problems encountered in chapter 2 concerning fragmentation (i.e. the naive incorporation of intrinsic k_T in the function $\rho(b)$) and transverse momentum distributions are overcome by using the more physically meaningful approach of the evolution equations, with energy weighted distributions, which are everywhere finite.

The simple factorized form of $Dq(x,k_T)$ of eq (3.21) may be viewed as too naive, and there remains scope for investigation into a more realistic form. However, ultimately the initial form of $d(b,Q_0^2)$ will not be so crucial as larger beam energies and more high statistics data become available at say Q=100 GeV. The data at the moment does not seem to have a preference for a fixed or running coupling constant α_s.

The calculations using evolution equations can be extended to structure functions and then applied to lepton pair production in Drell-Yan and leptoproduction for instance, although e^+e^- annihilation

does have the virtue of providing cleaner results due to it being a more simpler process. There has also been a significant amount of investigation recently in applying the transverse momentum distributions derived from gluon bremsstrahling in W, Z production [53], and the first experimental results are eagerly awaited.

The good agreement of perturbative QCD with data in e^+e^- annihilation must support the view that QCD is the theory of strong interactions, although there is still much to be done to show this beyond any doubt, particularly a solution to the confinement problem would put an end to speculation about fragmentation problems.

Appendix A

Parton Cross Section $\frac{1}{\sigma_0}\frac{d\sigma}{dQ_T^2}$ to 0 (α_s)

It is the purpose of this appendix to obtain the $0(\alpha_s)$ parton cross section in transverse momentum Q_T^2, from eq (1.5), then it can be used in eq (1.19) directly or eqns (2.28),(2.29) first then eq (1.19), to obtain the hadron distribution in transverse momentum.

The parton variables are shown in fig (1.5). Eq (1.5) is in the two independent variables (X_1,X_2). Depending upon the situation under consideration eq (1.5) must be transformed to the variables (X_1,Θ) or (X_1,Q_T^2). We require the latter here. Defining $X_T=2QT/Q$, eq (1.16) can be written,

$$X_T^2 X_1 = (1-X_1)(1-X_2)(X_1+X_2-1)$$

using energy conservation and assuming for the moment that X_1 defines the thrust axis. Solving for X_2 yields,

$$\begin{aligned} X_2 &= 1-\tfrac{1}{2}X_1 \pm \tfrac{1}{2}X_1\left(1-\frac{X_T^2}{(1-X_1)}\right)^{1/2} \\ &\equiv 1-\tfrac{1}{2}X_1 \pm R \end{aligned} \tag{A1}$$

where,

$$R = \tfrac{1}{2}X_1\left(1-\frac{X_T^2}{(1-X_1)}\right)^{1/2}$$

Also from eq (1.6)

$$\frac{\partial Q_T^2}{\partial X_2} = \frac{Q_T^2}{(1-X_2)(1-X_1)}(2-2X_1-X_1)$$

So for the case when X_1 defines the thrust axis eqn (1.5) gives [10],

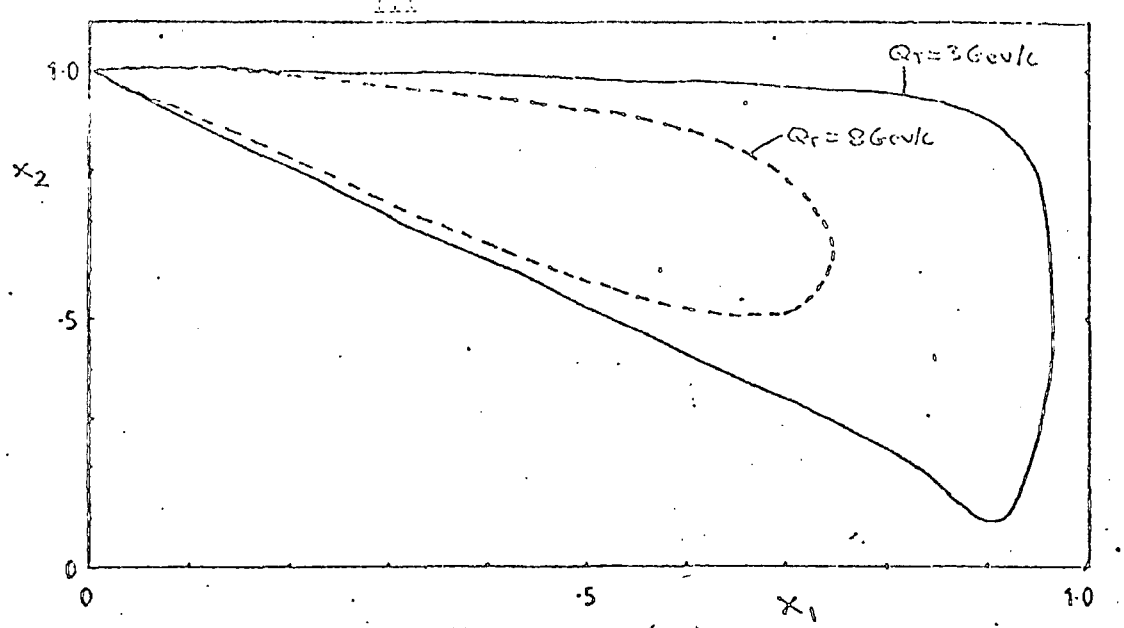

Fig. (A1). (X_2, X_1) plane for fixed X_T, from eq.(A1).

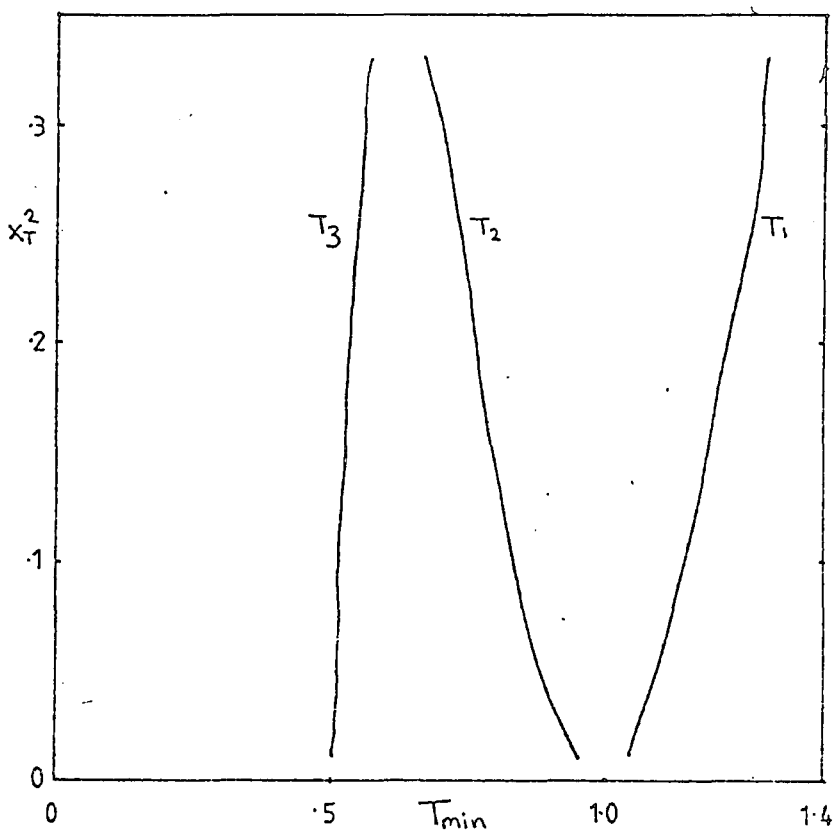

Fig. (A2). Solutions of eq.(A4) to find Tmin. Solution chosen is clearly T_2.

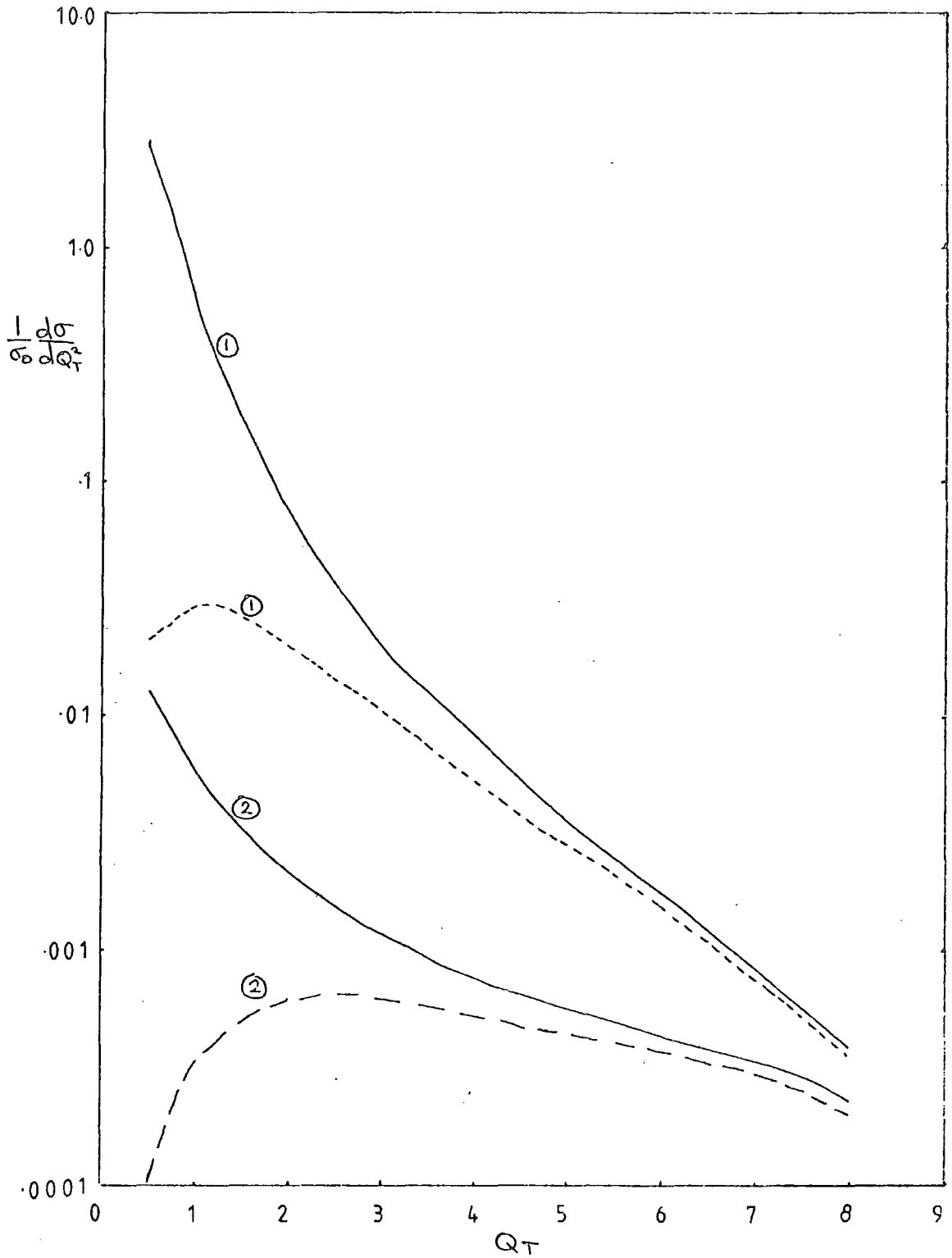

Fig. (A3). The cross section $\frac{1}{\sigma_0} d\sigma/dQ_T^2$ to $O(\alpha_s)$. Curves 1 are obtained from eq.(A2), curves 2 from eq.(A3). The dashed curves are the results of putting on the Sudakov-type form factor. $Q=30$ Gev, $\Lambda=0.5$ Gev.

$$\frac{1}{\sigma_0}\frac{d\sigma^q}{dx_1 dQ_T^2} = \frac{2\alpha_s}{3\pi}\frac{1}{Q_T^2}\left\{\frac{(\frac{1}{2}x_1+R)\left[x_1^2+(1-\frac{1}{2}x_1+R)^2\right]}{2(1-x_1)R} + \frac{(\frac{1}{2}x_1-R)\left[x_1^2+(1-\frac{1}{2}x_1-R)^2\right]}{2(1-x_1)R}\right\} \qquad (A2)$$

taking both solutions for X_2.

Since there is complete symmetry under the interchange of quark anti-quark variables, the above result also applies when the antiquark is the thrust axis.

Similarly, when the gluon defines the thrust axis,

$$\frac{1}{\sigma_0}\frac{d\sigma^g}{dx_3 dQ_T^2} = \frac{4\alpha_s}{3\pi}\frac{1}{Q_T^2}\frac{(1-\frac{1}{2}x_3)^2+R^2}{R} \qquad (A3)$$

Equations (A2),(A3) must be integrated over the thrust variable $T \equiv x_1 \text{ or } x_3$ before inserting into eq (1.19) or (1.28).

The maximum value of T is that permitted by eq (A1) for real X_2 and so,

$$T_{max} = 1 - x_T^2$$

A plot of the phase space region can be seen in fig (A1), showing the double valued nature of eq (A1).

The minimum value Tmin is the minimum value at which T is still the largest of the three variables. This is therefore given by eq (1.16) with the two independent variables set equal. So Tmin is the solution of

$$x_T^2 = 4(1-T_{min})^2(2T_{min}-1)/T_{min}^2$$

This yields the cubic,

$$8T_{min}^3 - T_{min}^2(20+x_T^2) + 16T_{min} - 4 = 0 \qquad (A4)$$

For small X_T it is straightforward to solve (A1) to give,

$$T_{min} \simeq 1 - \frac{1}{2}x_T.$$

However, in general eq (A4) must be solved, which can be done either iteratively or analytically by noting that one can write eq.(A4) in the form $y^3 - qy - r = 0$ with $27r^2 < 4q^3$, so that the cubic has three real roots (displayed in fig (A2)). It is solved analytically by defining an angle Φ such that $\cos\Phi = \left(\frac{3}{q}\right)^{3/2} r/2$, then

$$y_1 = \frac{2}{\sqrt{3}} q^{1/2} \cos\Phi/3$$

$$y_2 = -\frac{2}{\sqrt{3}} q^{1/2} \cos\left(\frac{\pi - \Phi}{3}\right)$$

$$y_3 = -\frac{2}{\sqrt{3}} q^{1/2} \cos\left(\frac{\pi + \Phi}{3}\right)$$

As can be seen from fig (A2), only two of the roots lie in the physical range $\frac{2}{3} < T_{min} < 1$, so the largest of these is chosen.

In order to integrate eqns (A2), (A3) numerically, it was necessary to change variables to remove the square root singularity caused by the factor R in the denominator, which causes the integrand to blow up at the end point. A suitable choice was $Y = (1 - T - x_T^2)^{1/2}$ so that,

$$\int_{T_{min}}^{T_{max}} \frac{dT}{R} \ldots \rightarrow \int_{Y_{min}}^{Y_{max}} dY \, \frac{4\sqrt{1-T}}{T} \ldots .$$

where,

$$Y_{min} = 0 \quad , \quad Y_{max} = \sqrt{1 - T_{min} - x_T^2}$$

The resultant parton cross sections are shown in fig (A3), along with modifications produced by the Sudakov-type form factor, producing the dip at small Q_T, as mentioned earlier and very little alteration at larger Q_T as expected. Notice that $d\sigma^q$ is by far the dominant cross section over $d\sigma^g$. Putting these $O(\alpha_s)$ results into eq (1.19) gives the hadron distribution shown in fig (1.6).

The leading log result (LLA) can be obtained by integrating eq (A2). From the form of eq (A3) and shown in fig (A3), the term with the gluon as thrust axis does not have the soft singularity evident in eq (A2).

As $Q_T^2 \to 0, x_1 \to 1$ and R tends to $\frac{1}{2}\left(1-\frac{x_T^2}{(1-x_1)}\right)^{1/2} \equiv \frac{Y}{2\sqrt{1-x_1}}$.

So the integrand in eqn (A2) goes to,

$$\left[3R^2+5/4\right]/2(1-x_1)R$$

leaving the integral in Y as,

$$\int_0^{\left(\frac{x_T}{2}-x_T^2\right)^{1/2}} \frac{dY}{2\sqrt{1-x_1}}\left[\frac{3Y^2}{(1-x_1)}+5\right] \equiv \frac{5}{2}I_1+\frac{3}{2}I_2$$

where,

$$I_1 = \tfrac{1}{2}\ln\left[x_T/2\right]$$

$$I_2 = \tfrac{1}{2}\ln\left[x_T/2\right]+1$$

for small X_T. This gives the result of the integral as

$$2\ln\left[x_T/2\right]+3/2$$

but the 3/2 can be neglected in the LLA, leaving

$$\frac{1}{\sigma_0}\frac{d\sigma}{dQ_T^2}\bigg|_{LA} = \frac{2\alpha_s}{3\pi Q_T^2}\ln\left[\frac{4}{x_T^2}\right] \qquad (A.5)$$

where X_1=T. Summing over configurations where q and $\bar{q}$ define the thrust axis introduces a factor of 2, giving eq (2.24).

Putting the factor of 4 into the denominator of the argument of the logarithm causes the LLA to mimic more closely the full $O(\alpha_s)$ result towards the edge of phase space.

The top limit in the Q_T^2 integration in eq (1.19), i.e. $Q^2/12$ can be obtained from eq (A1) by inserting the absolute minimum value

of thrust variable $X_1=2/3$ and keeping X_2 real. This corresponds to the situation of maximal symmetry in the three jets, where each is separated from its neighbour by 120^0, with each variable $Xi=2/3$.

The two values of X_2 must be used (corresponding to $\pm R$), in order to cover both situations of small and large X_2 corresponding to the same Q_T, as shown in fig (A4).

Fig A4

Two configurations corresponding to the same X_1.

Although X_2 is a double valued function of X_1, this just corresponds to a single point in the (X_1, Q_T^2) plane, since a plot such as fig (A1) is for fixed Q_T. The integral over the thrust variable T from Tmin to $1-X_1^2$ obviously only includes the one pole (in X_1 say) as can be seen from fig (A5). To include both poles, one must obviously add in the configurations where the $\bar{q}$ and g are the thrust variables.

Fig (A5)

(X_1, X_2) plane for fixed X_T

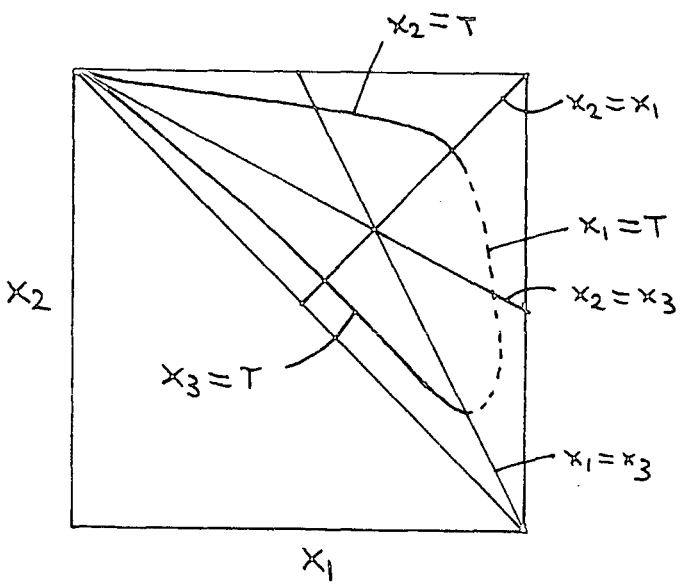

Setting the lower limit Tmin to zero will obviously include both poles from the q and the $\bar{q}$, and corresponds to the situation where no preferential thrust direction is chosen. In the LLA,

the two situations come together as:

$$2\int_{T_{min}}^{1-x_T^2} dT \ldots\ldots \simeq \int_{0}^{1-x_T^2} dT \ldots\ldots \quad \text{for} \quad x_T \ll 1$$

which clearly must be true, and can be seen from fig (2.6) for small X_T. So one must add the contributions where the $q,\bar{q}$ and g define the thrust axis, and in the limit of small X_T, they give contributions of eq (A.5), eq (A.5) and zero respectively. The smallness of $d\sigma^g$ is due to the fact that the q or $\bar{q}$ are much more likely to carry a large thrust than the gluon is [31], which can be deduced by transforming eq (1.5) to $\frac{1}{\sigma_0}\frac{d\sigma^{q,\bar{q}}}{dT}$.

Appendix B

Sudakov-type Form Factor with A Running Coupling

When α_s is allowed to run with k_T^2 then eq (2.19) can be written,

$$\frac{1}{\sigma_0}\frac{d\sigma^2}{dQ_T^2} = \left[\frac{C_F}{\pi}\right]^2 \frac{1}{2\pi}\int_{\lambda^2}^{Q_T^2} \frac{d^2\vec{k}_{T1}}{k_{T1}^2}\frac{d^2\vec{k}_{T2}}{k_{T2}^2}\,\alpha_s(k_{T1}^2)\ln\frac{Q^2}{k_{T1}^2}\,.$$

$$.\,\alpha_s(k_{T2}^2)\ln\frac{Q^2}{k_{T2}^2}\,S^{(2)}(\vec{k}_{T1}+\vec{k}_{T2}+\vec{Q}_T) \qquad (B1)$$

and so after strong ordering, one obtains,

$$\frac{1}{\sigma_0}\frac{d\sigma^2}{dQ_T^2} = \left[\frac{C_F}{\pi}\right]\frac{\alpha_s(Q_T^2)}{Q_T^2}\ln\frac{Q^2}{Q_T^2}\int_{\lambda^2}^{Q_T^2}\alpha_s(k_T^2)\ln\frac{Q^2}{k_T^2}\frac{dk_T^2}{k_T^2} \qquad (B2)$$

As before the virtual graphs take care of the divergent λ dependent terms, so that in effect only the top limit of integration contributes. So one now obtains for two gluon emission,

$$\frac{1}{\sigma_0}\frac{d\sigma^2}{dQ_T^2} = \left[\frac{1}{\sigma_0}\frac{d\sigma^1}{dQ_T^2}\right]\frac{4C_F}{\beta_0}\left\{\ln\ln\frac{Q_T^2}{\lambda^2}\ln\frac{Q^2}{\lambda^2} + \ln\frac{Q_T^2}{\lambda^2}\right\} \qquad (B3)$$

using,

$$\alpha_s(k_T^2) = \frac{4\pi}{\beta_0 \ln k_T^2/\lambda^2}$$

Again, this can simply be extended for any number of gluons and summation results in exponentiation, for multigluon emission,

$$\frac{1}{\sigma_0}\frac{d\sigma}{dQ_T^2} = \frac{1}{\sigma_0}\frac{d\sigma^1}{dQ_T^2}\,Exp\left[\frac{4C_F}{\beta_0}\left\{\ln\ln\frac{Q_T^2}{\lambda^2}\ln\frac{Q^2}{\lambda^2} + \ln\frac{Q_T^2}{\lambda^2}\right\}\right] \qquad (B4)$$

Eq (B4) again predicts a sizeable suppression in the cross section for small Q_T. The presence of a running coupling merely

softens the singularity in the argument of the exponential.

In the region where $Q_T \to 0$, Q_T^2/Λ^2 will become less than 1 and so $\ln \ln Q_T^2/\Lambda^2$ must be written as $\ln|\ln Q_T^2/\Lambda^2| - i\pi$, so that one can write the argument of the exponential in eq (B4) as,

$$\frac{4C_F}{\beta_0}\left\{\ln\left|\ln\frac{Q_T^2}{\Lambda^2}\right|\ln\frac{Q^2}{\Lambda^2} - i\pi\ln\frac{Q^2}{\Lambda^2} + \ln\frac{Q_T^2}{\Lambda^2}\right\} \tag{B5}$$

so that as $Q_T \to 0$, the $\ln Q_T^2/\Lambda^2$ term diverges faster than the other and one again gets the dip as $Q_T \to 0$, but in this case it is not as precipitous as in the fixed coupling case.

REFERENCES

PART I

1. See for example:

(a) I.J.R. Aitchison and A.J.G. Hey, "Gauge Theories in Particle Physics", Adam Hilger (1982).

(b) L.D. Fadeev and A.A. Slavnov, "Gauge Fields: Introduction to Quantum Theory", Benjamin (1982).

(c) E.S. Abers and B.W. Lee, Phys. Rep. 9C (1973), 1.

(d) L. Maiani, CERN 76-20 (1976), 23.

(e) J. Iliopoulos, CERN 77-18 (1977), 36.

(f) J.C. Taylor, "Gauge Theories of Weak Interactions", C.U.P. (1979).

2. For a review of QCD see for instance:

(a) W. Marciano and H. Pagels, Phys. Rep. 36C (1978), 137.

(b) E. de Rafael in "Quantum Chromodynamics", Proc. of the X.G.I.F.T. Int. Seminar on Theoretical Physics, Ed. J.L. Alonso and R. Tarrach (1980).

(c) J.D. Bjorken, SLAC-PUB-2372 (Dec. 1979).

For a review with particular interest in Perturbative QCD see:

(d) H.D. Politzer, Phys. Rep. 14C (1974), 129.

(e) E. Reya, Phys. Rep. 69 (1981), 195.

(f) M.R. Pennington, Durham Univ. Preprint DTP-82/2 (July 1982).

(g) G.G. Ross, Proc. 21st Scottish Univ. Summer School in Physics, St. Andrews, 1980, ed. by K.G. Bowler and D.G. Sutherland, 1-100.

(h) J. Ellis and C.T. Sachrajda, 1979 Proc. Cargese Summer Institute on "Quarks and Leptons".

(i) F. Close, Rutherford Laboratory Preprint RL-80-063. Also in Physica Scripta, Vol. 25 (1982).

3. F. Close, "An Introduction to Quarksand Partons", Academic Press (1979).

4. Section 3 of Ref. 2(b) above.

5. Claude Itzykson and Jean-Bernard Zuber, "Quantum Field Theory", McGraw Hill (1980).

6. For a review of jet phenomenology see for example: B.R. Webber, Physica Scripta Vol. 25 (1982), 198; T.F. Walsh in XIX Internationale Universitäts - Wochen für Kernphysik, DESY 80/45 (May 1980); see also refs. 2(e)-(h) above.

7. See for example: P. Soding DESY 81-070, Oct. 1981 and references therein.

8. J. Ellis, M.K. Gaillard and G.G. Ross, NPB III (1976), 253; A. de Rujula, J. Ellis, E.G. Floratos and M.K. Gaillard NPB 138 (1978), 387.

9. J.B. Kogut, L. Susskind, PRD9 (1974), 697, 3391.

10. F. Halzen, D.M. Scott, Ann. Phys. 135 # 1 (1981), 1.

11. J. Cleymans, M. Dechantsreiter, F. Halzen and D.M. Scott, PL89B, 403.

12. C. Louis Basham, Lowell S. Brown, Stephen D. Ellis and Sherwin T. Love, PRD17 (1978), 2298; PRL41 (1978), 1585; PRD19 (1979), 2018; Lowell S. Brown and Stephen D. Ellis, PRD24 (1981), 2383.

13. G. Sterman and S. Weinberg, PRL39 (1977), 1436.

14. T. Kinoshita, J. Math, Phys. 3 (1962), 650; T.D. Lee and M. Nauenberg PRB133 (1964), 1549.

15. F. Halzen and D.M. Scott, PL94B (1980), 405.

16. Stephen M. Barr and Lowell S. Brown, PRD25 (1982), 1229.

17. R. Brandelik et al. PL86B (1979, 243.

18. Ch. Berger et al. PL90B (1980), 312; PL99B (1981), 292.

19. Y.I. Dokshitzer, D.I. D'Yakonov and S.I. Troyan, PL76B (1978), 269; SLAC TRANS-183 from 13th Winter School of the Leningrad B.P. Konstantinov Institute of Nuclear Physics, Leningrad (1978); Phys. Rep. 58 (1980), 269.

20. S.D. Ellis and W.J. Stirling, PRD23 (1981), 214.

21. Geoffrey C. Fox and Stephen Wolfram, "A Gallimaufry of e^+e^- Annihilation Event Shapes", CALT-68-723 (unpublished).

22. S.D. Ellis, N. Fleishon and W.J. Stirling, PRD24 (1981), 1386.

23. C.Y. Lo and S.D. Sullivan, PL86B (1979), 327.

24. G. Parisi and R. Petronzio, NPB154 (1979), 427.

25. P.E.L. Rakow and B.R. Webber, NPB187 (1981), 1254.

26. H.F. Jones and J. Wyndham, J. Phys. A14 (1981), 1457.

27. M.R. Pennington, Durham Univ. Preprint (Jan. 1982).

28. M.R. Pennington and G.G. Ross, PL102B (1981), 167.

29. "Handbook of Mathematical Functions", edited by M. Abramowitz and I. Stegun (DOVER, New York, 1970).

30. Stephen D. Ellis, Univ. of Washington preprint, DOE/ER/40048-20 P2.

31. E.G. Floratos, F. Hayot and A. Morel, PL90B (1980), 297.

32. G. Altarelli, G. Parisi and R. Petronzio, PLB76 (1978), 356.

33. J.C. Collins, Phys. Rev. D22 (1980), 1478; J.C. Collins and D.E. Soper, NPB193 (1981), 381 and Oregon preprints OITS-153 (1981), 155 (1981).

34. G. Curci, M. Greco and Y. Srivastava, PRL43 (1978), 834; NPB159 (1979), 451. G. Curci and M. Greco, PL79B (1979), 406.

35. D. Schlatter et al. SLAC-PUB-2846 LBL 13599 (Nov. 1981).

36. H.J. Behrend et al. CELLO Collaboration DESY82-022 (April 1982).

37. D.G. Richards, N.J. Stirling, S.D. Ellis, DAMPT-82/18 (1982).

38. A. Ali and F. Barreiro DESY 82-033 (June 1982).

39. J.C. Collins and D.E. Soper, PRL48 (1982), 655.

40. A. Bassetto, M. Ciafaloni, G. Marchesini, PL86B (1979), 366; NPB 163 (1980), 477.

41. G. Altarelli and G. Parisi, NPB126 (1977), 298.

42. R. Baier and K. Fey, NPB179 (1981), 49.

43. J. Cleymans and M. Kuroda, NPB189 (1981), 483.

44. J. Kalinowski, K. Konishi, P.N. Scharback and T.R. Taylor, NPB181 (1981), 253.

45. E.G. Floratos, R. Lacaze and C. Kounnas, PL98B (1981), 89.

46. G. Curci, W. Furmanski and R. Petronzio, NPB (1980), 27.

47. D. Amati, A. Bassetto, M. Ciafaloni, G. Marchesini and G. Veneziano, NPB173 (1980), 429; M. Ciafaloni, PL95B (1980), 113.

48. M.R. Pennington, G.G. Ross and R.G. Roberts, Rutherford Laboratory preprint, RL-82-033 T304.

49. S.J. Brodsky and G.P. Lepage, SLAC Summer Institute 1979, SLAC report no. 224.

50. Juro Kodaira and Luca Trentadue, SLAC-pub-2867 (Sept. 1981) and SLAC-pub-2862 (Dec. 1981).

51. M.R. Pennington, Durham Univ. preprint.

52. E.G. Floratos, R. Lacaze and C. Kounnas, PL98B (1981), 285.

53. F. Halzen and D.M. Scott, PRD21 (1980), 131; Bruges Multiparticle Dynamics Conf. Prof. (1980), 593.

P. Aurenche and J. Lindfors, PL96B (1980), 171; NPB185 (1981), 301.

F. Halzen, A.D. Martin, D.M. Scott and M. Dechantsreiter, PL106B (1981), 147.

F. Halzen, A.D. Martin and D.M. Scott, PRD25 (1982), 745.

KEY:

PRD	:	Physical Revue D
PRL	:	Physical Revue Letters
NPB	:	Nuclear Physics B
Z. Phys. C.	:	Zeitschrift fur Physik C
Annals of Phys.	:	Annals of Physics
Phy. Rep.	:	Physics Reports
J. Math. Phys.	:	Journal of Mathematical Physics
J. Phys.	:	Journal of Physics

PART II

ANALYSES INVOLVING THE S^{*} AND RELATED SCALAR MESONS.

CHAPTER 1

THE SCALAR MESONS.

In this chapter we introduce the scalar mesons, and in order to motivate the need for work in this area, we review briefly their crucial place in meson spectroscopy. This will then lead us to discuss $\pi\pi$ and $K\bar{K}$ production, and the formalism used to do partial wave analysis and to extract resonance parameters. We can then outline the experimental signatures of the scalar mesons, particularly the S^*, before going on in chapter 2 to discuss a coupled channel analysis of $\pi\pi$ and $K\bar{K}$. In chapter 3 we attempt a double moment analysis of $K^-p \rightarrow K^-K^+\Lambda$, and study S wave production via S-P interference effects in the ϕ mass region.

1.1. Scalar Meson Spectroscopy.

Mesons are described in the L-excitation quark model [1] as quark-antiquark bound states. Since quarks and anti-quarks belong to the 3 and $\bar{3}$ representations of SU(3) respectively, mesons occur in $3 \otimes \bar{3}$ representations, i.e. $1 \oplus 8$ and so are predicted to group themselves in nonets. Including the spin $\frac{1}{2}$ nature of the quarks and their orbital excitations leads to the full symmetry group structure,

$$SU(6) \otimes O(3)$$

The fermion-antifermion system with angular momentum L is an eigenstate of parity with,

$$P = (-1)^{L+1} \tag{1.1}$$

and the total angular momentum $\vec{J}$ is given by,

$$\vec{J} = \vec{L} + \vec{S}$$

where $\vec{S}$ is the total spin of the quarks and equals 0 or 1. The charge conjugation applied to the neutral systems is,

$$C = (-1)^{L+S} \tag{1.2}$$

so that one has a series of states with CP= + for S=1 and CP = - for S=0. One can define natural and unnatural parity for mesons such that

$$P = (-1)^J \qquad \text{natural parity} \qquad (1.3)$$

$$P = (-1)^{J+1} \qquad \text{unnatural parity} \qquad (1.4)$$

and so natural parity mesons must have S=1, since $J = L \pm 1$.

Using eqns. (1.1) and(1.2), one finds for S=0, $J \equiv L$ so that C = -P giving the sequence of states $J^{PC}=0^{-+}$, 1^{+-}, 2^{-+}..... However one cannot form states with $J^{PC}=0^{+-}$, 1^{-+}, 2^{+-}....and these are known as "exotics". The resulting allowed values of J^{PC} for $q\bar{q}$ mesons composed of uds and $\bar{u}\bar{d}\bar{s}$ flavoured quarks are listed in table (1.1).

Table (1.1):

J^{PC} for mesons

	S=0	S=1
L=0	0^{-+}	1^{--}
L=1	1^{+-}	0^{++}
		1^{++}
		2^{++}
L=2	2^{-+}	1^{--}
°		2^{--}
°		3^{--}
°		°
°		°
		°
		°

Only the $J^{PC} = 0^{-+}$, 1^{--} and 2^{++} nonets are completely filled with well-established mesons. The other nonets have members which are missing or which have properties which are not well known. Apart from these well-established nonets, only the 0^{++} nonet has candidates for all its members, and these are listed in table (1.2), along with some important parameters[2]. Their role in meson spectroscopy is therefore a very important one, although it is not as clear cut as the above discussion might lead one to believe. This is because there is no reason to believe that the low-lying mesons have to be $q\bar{q}$ states

TABLE (1.2) Scalar Mesons (PDG April 1982)

Meson	I^G	MASS (mev)	FULL WIDTH (mev)	DECAY MODES	Fraction
S^*	0^+	975 ± 4	33 ± 6	$\pi\pi$	78
				$K\bar{K}$	22
δ	1^-	983 ± 2	54 ± 7	$\eta\pi$	
				$K\bar{K}$	
ε	0^+	1300 approx.	200-600	$\pi\pi$	90
				$K\bar{K}$	10
				$\eta\eta$	
κ	$\frac{1}{2}$	1350 approx.	250 approx.	$K\pi$	

alone, since four quark states $qq\bar{q}\bar{q}$ can also form colour singlets and therefore are expected to be observed. Moreover, as a consequence of QCD, mesons are also expected to exist which are composed completely of gluons - glueballs. The situation does not rest there, since obviously there can also occur hybrid mesons, made partly of constituent glue, partly of quarks. In particular, the $J^{PC}=0^{++}$ mesons have been classified as $qq\bar{q}\bar{q}$ states or even glueballs [3,4,5]. This provides the most important reason for studying the scalar mesons, to clarify whether or not such "cryptoexotic" states exist in addition to the more usual $q\bar{q}$ SU(3) nonets. We briefly discuss the compatibility of the scalar mesons with multiquark/gluon states.

Assuming a constituent mass for u,d quarks of 350 Mev and 500 Mev for strange quarks, then $qq\bar{q}\bar{q}$ S-wave masses will be about 1400 ($uu\bar{u}\bar{u}$) to 2000 Mev ($ss\bar{s}\bar{s}$), before spin-dependent mass splittings are considered. The same $J^P=0^+,1^+,2^+$ states can be obtained by a P-wave $q\bar{q}$ (c.f. table 1.1), where one might expect masses of order 1000 Mev before mass splittings. By considering spin-spin splittings, Jaffe [4,5] showed that the 0^+ $qq\bar{q}\bar{q}$ state is pushed lower down in mass than the 0^+ state of $q\bar{q}$. And so both $q\bar{q}$ and $qq\bar{q}\bar{q}$ may be of the same order

of mass. In fact Jaffe predicts that the $qq\bar{q}\bar{q}$ states are lower in mass than the $q\bar{q}$.

The OZI rule is familiar from discussions of $q\bar{q}$ decays, whereby decays requiring several gluons to enable the decay to occur are forbidden (see fig.1.1). When one considers $qq\bar{q}\bar{q}$ decays, it is clear that

Fig (1.1) Decay diagrams in OZI rule.

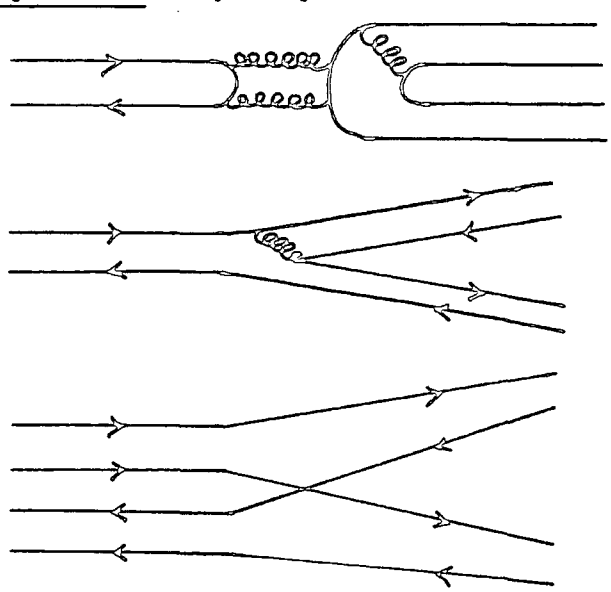

(a) 1st. forbidden

(b) allowed.

(c) super allowed

$qq\bar{q}\bar{q}$ can "fall apart" into $q\bar{q}$ + $q\bar{q}$ as in fig.(1.1c) if phase space allows it, thus providing a class of OZI superallowed decays. These will then give rise to very broad states, which might be hard to identify. However, if the $qq\bar{q}\bar{q}$ state is low enough in mass, then its decays to $q\bar{q}$ + $q\bar{q}$ might be kinematically suppressed, leaving it with a much less broad width.

The weight diagram for a nonet of $qq\bar{q}\bar{q}$ is shown in fig.(1.2) along with that for a conventional $q\bar{q}$ nonet. It was originally thought [1] that one might assign the following four quark states to the scalar mesons : $u\bar{u}d\bar{d} \equiv \epsilon$; $s\bar{s}\,(u\bar{u}+d\bar{d}) \equiv S^*$; $s\bar{s}\,(u\bar{u}-d\bar{d}) \equiv \delta$; and $u\bar{s}d\bar{d} \equiv \kappa$. The ϵ could then easily fall apart into $\pi\pi$, which would give it a very broad width as observed. The S* would be able to fall apart into $K\bar{K}$ as shown in fig. (1.3a) whereas a decay to $\pi\pi$ would require the strange quarks first to annihilate, as shown in fig. (1.3b).

Fig. (1.2). Weight diagrams for $q\bar{q}q\bar{q}$(a) and $q\bar{q}$ (b).

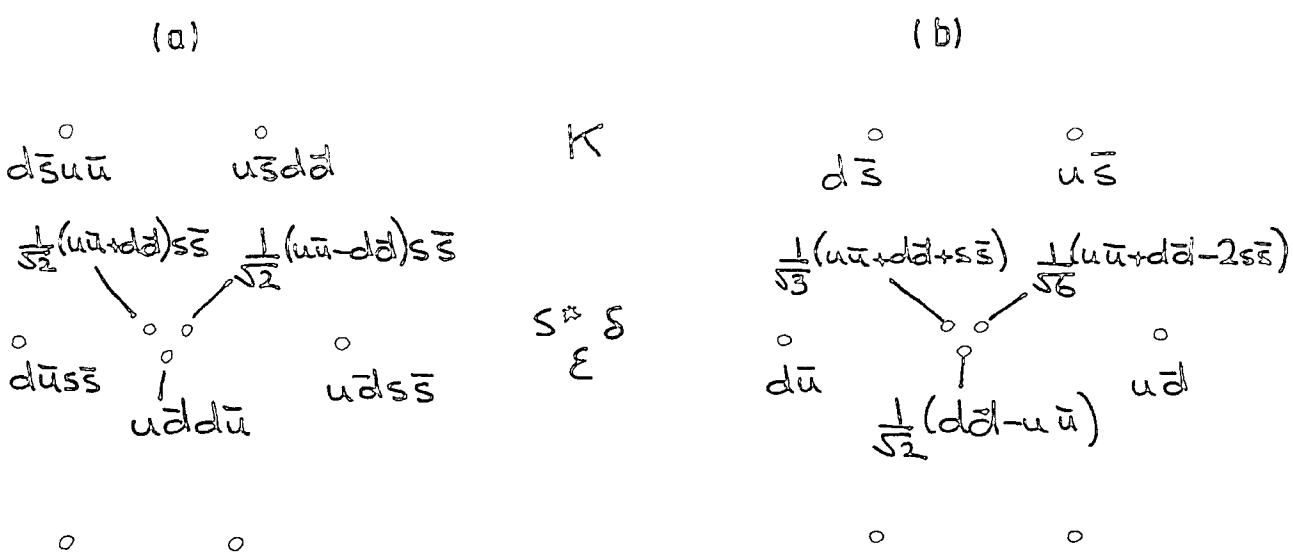

Fig. (1.3) Four quark decays of the S*

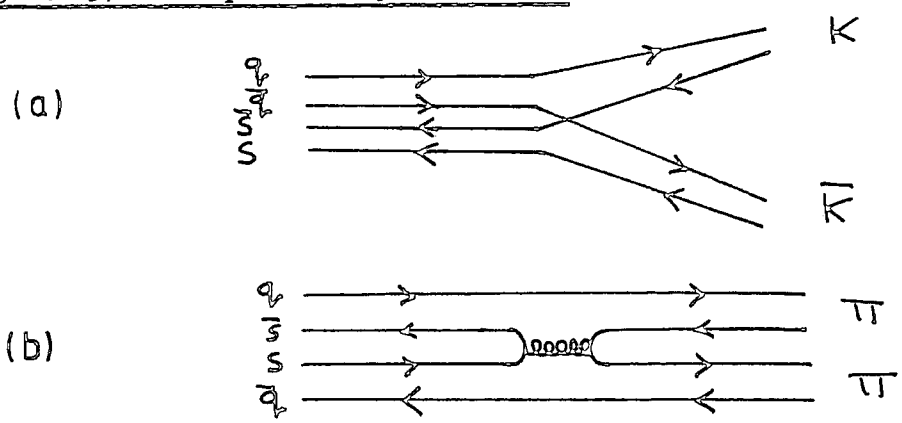

So the dominant decay mode of the S* would be to $K\bar{K}$, but since the S* is just below $K\bar{K}$ threshold, the width is consequently narrow. Furthermore, under this model the S* and δ would be mass degenerate with ϵ lying at a lower mass, which might be expected to be due to the extra $s\bar{s}$ pair, which the S* and δ contain.

Comparing this situation with the $q\bar{q}$ nonet, in which if the isoscalar singlet and octet states mix magically, then the ϵ and δ will be degenerate in mass, with the S* (pure $s\bar{s}$) at a higher mass. In fact the S* and δ are approximately degenerate and this seems to

lend support to the claim that the 0^{++} nonet is composed of $q\bar{q}q\bar{q}$ states. A problem with this classification is that the δ would be expected to be much broader, since $\delta \to \pi\eta$ is a superallowed decay. Also, the above situation is very naive, since magic mixing will not necessarily be dominant in practice and members of the two nonets can intermix by gluon exchange. Furthermore, the mass of the ε is now measured to be about 1300 Mev, which puts it well above the S* and δ.

The observed $K\bar{K}$ S- wave enhancement at 1.3 Gev [6] might lend support to the idea that two complete 0^{++} nonets exist [4,5]. If in fact this bump is an I=1 resonance [6,7,8], then it might be identified as the member of the $q\bar{q}$ nonet, analogous to the δ (983) I=1 member of the $q\bar{q}q\bar{q}$ nonet. It would then, however, be necessary to observe the other three members. Clearly the real situation is a complex one, which encourages further work in this area.

The idea that glueballs exist is an interesting one, particularly in our present case, since all QCD based models predict that the lightest glueballs will be in the energy range 1-2 Gev, with spin-parities $J^{PC}=0^{++},0^{-+},2^{++}$ [1,3,9]. ψ meson decays might be expected to be a copious source of glueballs, for instance the decay of fig.(1.4). Indeed, QCD predicts that the dominant spin parity of the 2 gluons is

Fig.(1.4) $\psi \to \gamma$ hadrons.

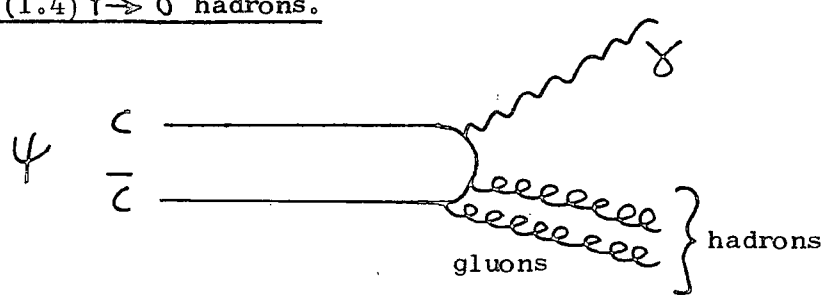

that stated above, which may be looked upon as optimistic for the observation of the production of glueballs in ψ decays. If these two gluons resonate, then one has a glueball particle. However, the two gluons might perturbatively decay into two $q\bar{q}$ pairs, and if these

resonate then one has a multiquark state $q\bar{q}q\bar{q}$ as discussed above. One might also imagine the situation where just one gluon perturbatively decays into a $q\bar{q}$ pair, which itself then resonates with the remaining gluon to form a hybrid state. These possible enhancements and connections are shown in fig. (1.5) [3]. Although it is not possible to tell

Fig. 1.5. Possible enhancements from two gluons. A—glueball, B—hybrid, C—multiquark, D—two $q\bar{q}$ mesons.

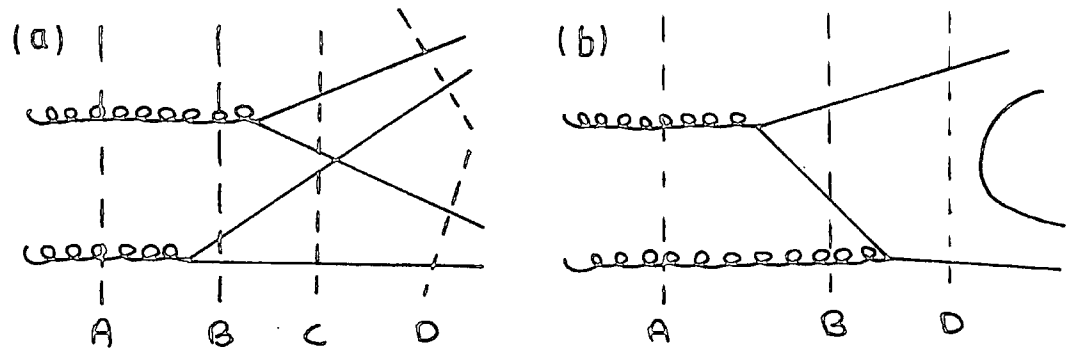

from QCD which is the favoured enhancement, it is certainly true that it can wait until stage D is reached, since $q\bar{q}$ mesons such as the η are seen in $\psi \rightarrow \gamma X$. Even if fig.(1.5b) is found to dominate, that still does not forbid copious production of hybrid $q\bar{q}g$ resonant states, even though $q\bar{q}q\bar{q}$ states can be avoided. Clearly the glueballs and hybrids must be flavour and colour singlets, and if they are found to actually exist, they might be expected to be rather narrow since their decay to hadrons violates the OZI rule. The existence of scalar glueballs is highly speculative at the moment, and it is another factor which points to the necessity for detailed data and analysis in the 0^{++} sector.

Although there occur problems with the decay modes of the scalar mesons (which will be discussed in sec.(1.3), they are experimentally reasonably accessible, particular in the $\pi\pi$ and $K\bar{K}$ channels which we will now briefly discuss.

1.2 $\pi\pi$ and $K\bar{K}$ Production.

Much information on $\pi\pi$ scattering, particularly the I=0 S wave,

can be gleaned from the production processes

$$\pi N \longrightarrow \pi\pi N \qquad (1.5)$$

$$\pi N \longrightarrow K\bar{K}N \qquad (1.6)$$

especially since high statistics studies have now been performed [10, 11]. The produced di-meson state is a CP eigenstate with eigenvalues $P = (-1)^L$, $C=(-1)^L$ [12], where L is the orbital angular momentum of the state ($\cong J$ in this case of spinless particles). So the allowed quantum numbers of the dimeson state are $J^{PC}=0^{++}, 1^{--}, 2^{++}, \ldots$. The $\pi\pi$ system has G-parity eigenvalue $G=(+)$, and since G parity for the di-meson state is $(-1)^{I+L}$, where I is the total isospin, this means that I+L is even. Isospin of the $\pi\pi$ system can have values $I=0, 1, 2$, and so the isospin values are separated out, in particular the S wave J=L=0 will have components in I=0 and I=2, but no I=1. This limitation does not apply to the $K\bar{K}$ system, which has total isospin $I=0, 1$, but whose G-parity is not unique as in the π case. This leads to difficulties in assigning isospin to new resonances in the $K\bar{K}$ system, and is the origin of the debate about the isospin of the $K\bar{K}$ enhancement at 1.3 Gev [6,7,8] referred to in section (1.1).

The $K^0\bar{K}^0$ system may decay through the $K^0_S K^0_S$ state, which Bose statistics forces to have only odd values of angular momentum. If one restricts oneself to this particular decay mode (since there is a reasonable body of data here), then this allows the $K^0\bar{K}^0$ state to have the following quantum numbers $J^{PC}=0^{++}, 2^{++}, 4^{++}, \ldots$. So altogether, the $\pi\pi$ and $K\bar{K}$ channels are a valueable source of scalar mesons.

One pion exchange (OPE) dominates the processes of eq.(1.5), (1.6) in the forward scattering region, and this allows a study of $\pi\pi \rightarrow \pi\pi(K\bar{K})$ amplitudes, provided the OPE contribution can be isolated, (see refs.[13,14] for a detailed discussion). This might seem a reasonable

assumption in view of the close proximity of the pion pole to the physical region. The situation is again more complicated in the $K\bar{K}$ production, since in $\pi\pi$ production G parity severely restricts the number of possible exchanges. This is exemplified in table (1.3) where possible exchanges are listed for the processes of (1.5) and (1.6).

Table (1.3) Possible natural (NPE) and unnatural (UPE) parity exchanges in $\pi N \rightarrow \pi\pi(K\bar{K})N$

Reaction	Exchanges		I^G	J^P
	UPE	NPE		
$\pi^- p \quad \pi^+\pi^- n$	π		1^-	0^-
			1^-	1^+
	A_1		1^-	2^+
		A_2		
$\pi^- p \quad K^0_S K^0_S n$	π		1^-	0^-
	A_1		1^-	1^+
		A_2	1^-	2^+
	B		1^+	1^+
	Z		1^+	2^-
		ϱ	1^+	1^-

We will now go on to discuss the kinematic formalism of OPE, which is described by fig. (1.6.) The resonance contribution (R) which we will wish to isolate will be that of the scalar mesons,

Fig. (1.6) OPE for $\pi N \rightarrow \pi\pi(K\bar{K})\ N$

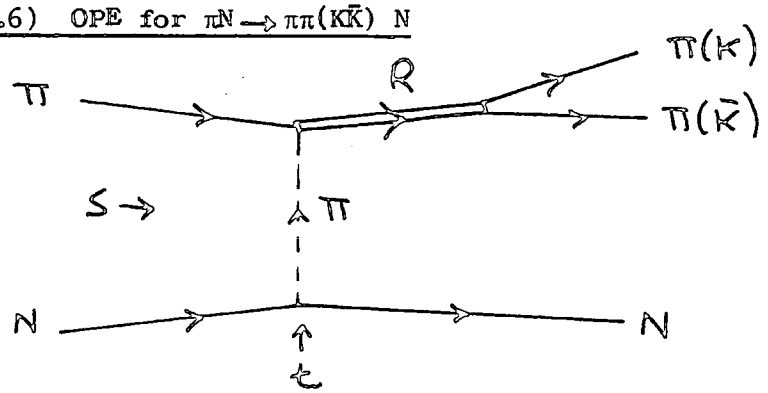

particularly the S* and $\mathcal{E}$.

1.2.1 Cross Sections and Amplitudes.

To discuss the amplitude for the process of eqns. (1.5), (1.6), we can define the particle 4-momenta as in fig. (1.7), and the following

Fig. (1.7) Diagram of kinematic variables used to describe $\pi N \to \pi\pi(K\bar{K})N$. Mesons M_1, M_2 are either both π or both K.

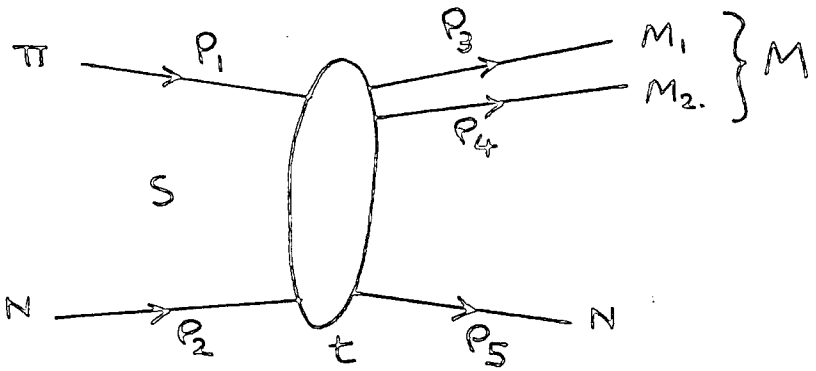

Mandelstam invariants, $S=(P_1+P_2)^2$, $t=(P_2-P_5)^2$, $M^2=(P_3+P_4)^2$ - (1.7)

The amplitude will then be a function of the kinematic variables in eq.(1.7) and the di-meson decay angles Θ, Φ in the M_1 M_2 rest system (see fig. (1.8)). For a given incident momentum one can describe the experimentally observed intensity distribution in terms of the four variables t, m, Θ, Φ, where the angles Θ and Φ can be measured in the t or S frames, which are shown in Fig. (1.8). The intensity distribution

Fig. (1.8) The S and t channel axis used to describe the angular distribution of the produced $M_1 M_2$ system in its rest frame.

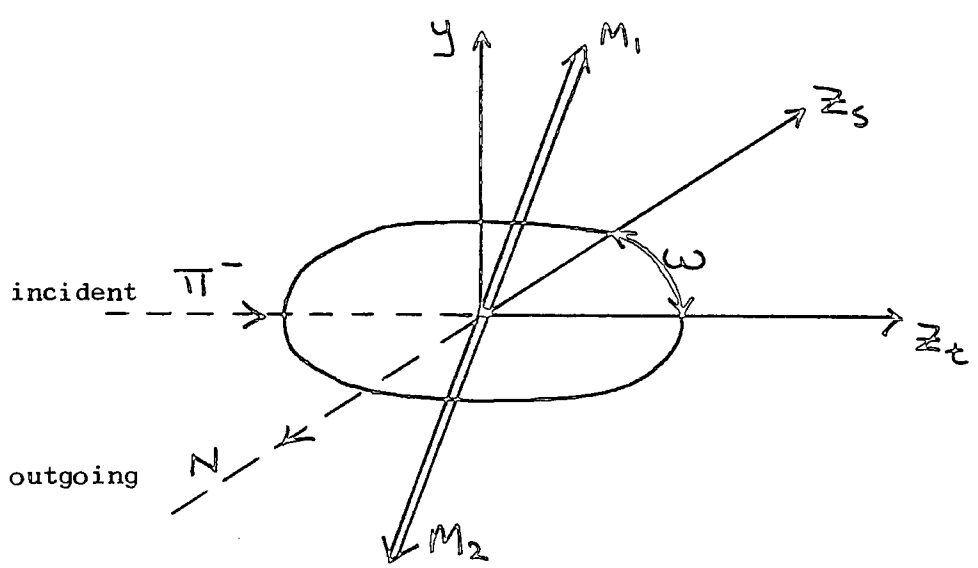

can be written,

$$I(s,t,M,\theta,\phi) \equiv \frac{\partial^4\sigma}{\partial t\,\partial M\,\partial(\cos\theta)\,\partial\phi} = \frac{\partial^2\sigma}{\partial M\,\partial t}\,W(\theta,\phi) \qquad (1.7)$$

and is usually written in terms of the integrated intensity,

$$N \equiv 4\pi \langle I \rangle \equiv \frac{\partial^2 \sigma}{\partial M \partial t} \quad . \tag{1.8}$$

$W(\Theta,\Phi)$ describes the M_1, M_2 angular distribution, and can be expanded in terms of spherical harmonics,

$$W(\Theta,\Phi) = \sum_{J=0}^{\infty} \sum_{M=0}^{\infty} \langle Y_M^J \rangle \, \mathrm{Re}\, Y_M^J(\Theta,\Phi) \tag{1.9}$$

where the $\langle Y_M^J \rangle$ are the Legendre moments, which contain the normalization factor N, which is simply the number of events in the element dtdm [15], and which will be described below.

The intensity distribution may be expressed in terms of helicity amplitudes, $H^{s,(t)}_{\lambda'\lambda}(s,t,M,\Theta,\Phi)$, in the S or t channel. λ' and λ refer to the initial and final nucleon helicities. These amplitudes are normalized according to,

$$\frac{\partial^4 \sigma}{\partial t \, \partial M \, \partial(\cos\Theta) \, \partial\Phi} = \frac{1}{2} \sum_{\lambda,\lambda'} \left| H^{s,(t)}_{\lambda',\lambda} \right|^2 \tag{1.20}$$

In most of the subsequent discussion we shall use the t-channel axes and so for the sake of convenience we shall suppress the channel label on the helicity amplitudes. The full helicity amplitude $H_{\lambda'\lambda}(t,M,\Theta,\Phi)$ may be decomposed into a sum of contributions corresponding to intermediate di-meson states of spin L and helicity $\nu \equiv |\lambda' - \lambda|$. This gives

$$H_{\lambda'\lambda}(t,M,\Theta,\Phi) = \sum_{L=0}^{\infty} \sum_{\nu=-L}^{L} (2L+1)^{1/2} H^L_{\lambda'\lambda\nu}(t,M) \, d^L_{\nu 0}(\Theta,\Phi) \, e^{i m \Phi} \tag{1.21}$$

Substituting this result into the intensity formula, eq. (1.20), one obtains,

$$\frac{d^4\sigma}{dt\,dM\,d(\cos\theta)\,d\Phi} = \frac{1}{2}\sum_{\lambda'\lambda}\sum_{L_1\nu_1}\sum_{L_2\nu_2}(2L_1+1)^{\frac{1}{2}}(2L_2+1)^{\frac{1}{2}}e^{i(m_1-m_2)\Phi}$$

$$\cdot H^{L_1 *}_{\lambda'\nu_1} H^{L_2}_{\lambda'\nu_2} d^{L_1}_{\nu_1 0}(\theta,\Phi)\, d^{L_2}_{\nu_2 0}(\theta,\Phi) \tag{1.22}$$

So the observables $\langle Y^J_M \rangle$ can be expressed in terms of sums of bilnear products of individual helicity amplitudes. Since the experimental moments $\langle Y^J_M \rangle$ contain an overall normalization factor N, we now need to calculate this to normalize our partial wave helicity amplitudes correctly.

Consider again purely π exchange of fig. (1.6). To isolate the $\pi\pi \to \pi\pi(K\bar{K})$ amplitude, one can write the amplitude for the process of fig. (1.6) in the form [12],

$$T = V(N\pi N)\cdot\frac{F(t)}{(t-\mu^2)}\cdot A(\pi\pi \to \pi\pi(K\bar{K})) \tag{1.23}$$

where $V(N\pi N)$ describes the lower vertex in fig. (1.6). Using the Feynman rules at this vertex, and averaging over initial and summing over final nucleon helicity states, gives [13],

$$\frac{1}{2}\sum_{\lambda'\lambda}\left|V(N\pi N)_{\lambda'\lambda}\right|^2 = -G^2 t \tag{1.24}$$

where $G^2/4\pi \simeq 14.6$. $1/(t-\mu^2)$ is the pion propagator, with μ the pion mass. $F(t)$ is a form factor, which satisfies $F(\mu^2)=1$ and is determined by fitting the overall amplitude T to the t dependence of the data; this is usually parametrized as $e^{b(t-\mu^2)}$ [15].

This method of determining the $\pi\pi \rightarrow \pi\pi(K\bar{K})$ amplitudes was first proposed by Chew and Low , and by Goebel [12-16], and can be expected to work very well provided the OPE contribution (which has a characteristic t-dependence (see below)) shows up clearly in the data. Deviations from this t-dependence might be partly described by form factors, but this cannot be the whole story as we mention below.

The amplitude of eq(1.23) then leads to the following expression for the intensity distribution [13,14,15],

$$\frac{d^4\sigma}{dt\,dM\,d\Omega} = \frac{2}{M_N^2 P_L^2}\left(\frac{\sigma}{4\pi}\right)^2 \frac{-t}{(t-\mu^2)^2}|F(t)|^2 q M^2 \frac{d\sigma_{\pi\pi}}{d\Omega} \tag{1.25}$$

where $d\Omega \equiv d(\cos\theta)\,d\Phi$, and M_N is the nucleon mass, P_L the pion laboratory momentum and q the di-meson centre of mass momentum $(\frac{1}{4}M^2-\mu^2)^{1/2}$. $d\sigma_{\pi\pi}/d\Omega$ represents the OPE contribution to the cross-section. The factor $4M_N^2P_L^2$ is a flux factor and the factor qM^2 comes from the phase space. Thus we have the normalization factor N from eq.(1.25), which is contained in the partial wave helicity amplitudes $H^L_{\lambda'\lambda\nu}$ as $\sqrt{N}$.

It is convenient to use the following combinations of helicity amplitudes,

$$L_{\nu\pm} = \frac{1}{\sqrt{2}}\left(H^L_\nu \mp (-1)^\nu H^L_{-\nu}\right) \tag{1.26}$$

At high energies the amplitudes $L_{\nu+}$ and $L_{\nu-}$ describe the production of a di-meson system of spin L, helicity ν , by natural and unnatural parity exchange respectively. We see that $L_{0+}=0$, so that a zero helicity di-meson system cannot be produced at high energies by natural parity exchange. In that case, we have an unnatural parity exchange amplitude, simply defined as L_0.

As can be seen in eq. (1.26), we have temporarily omitted the nucleon helicity labels. Each amplitude is in fact two independent amplitudes, a nucleon helicity flip $H^{L}_{\upsilon+-}$ and non-flip $H^{L}_{\upsilon++}$. Eq. (1.26) is to apply to both flip and non-flip amplitudes. For an experiment involving unpolarized nucleons, we sum over the nucleon helicities as follows,

$$|L|^2 \equiv |L_{++}|^2 + |L_{+-}|^2$$

$$Re(L'L^*) \equiv Re(L'_{++}L^*_{++} + L'_{+-}L^*_{+-}) \tag{1.27}$$

where we have suppressed all indices except the nucleon helicity components.

We can now express the observable moments $\langle Y^J_M \rangle$ of eq.(1.9) in terms of the amplitudes $L_{\upsilon\pm}$ ($S_0, P_0, P_{1\pm}$, etc..)of eqn.(1.26). Each moment is a sum over terms of the form $Re\,(L'_{\upsilon'}\, L^*_{\upsilon})$, and will only contain terms with $L'+L \geq J$ and $|\upsilon'-\upsilon| = M$. Also $L'+L$ must be even when J is even and vice versa. Assuming only S and P wave di-meson production is significant we obtain the following relations,

$$\sqrt{4\pi}\langle Y^0_0\rangle = |S|^2 + |P_0|^2 + |P_+|^2 + |P_-|^2$$

$$\sqrt{4\pi}\langle Y^1_0\rangle = 2\,Re(SP^*_0)$$

$$\sqrt{4\pi}\langle Y^1_1\rangle = \sqrt{2}\,Re(SP^*_-)$$

$$\sqrt{4\pi}\langle Y^2_0\rangle = \frac{1}{\sqrt{5}}(2|P_0|^2 - |P_+|^2 - |P_-|^2)$$

$$\sqrt{4\pi}\langle Y^2_1\rangle = \sqrt{\frac{6}{5}}\,Re(P_0P^*_-)$$

$$\sqrt{4\pi}\langle Y^2_2\rangle = -\sqrt{\frac{3}{10}}(|P_+|^2 - |P_-|^2) \tag{1.28}$$

Notice that there are no interference terms between L_{v+} and L_{v-} amplitudes; we would need nucleon polarization measurements to do this.

Thus we have written the observable moments $\langle Y_M^J \rangle$ in terms of the helicity amplitudes $L_{v\pm}$ for the whole reaction of eqn. (1.5) or (1.6) (or figs. (1.6) and (1.7)). We can write $L_{v\pm}$ in terms of a partial wave amplitude f_L, for the subprocess $\pi\pi \to \pi\pi(K\bar{K})$ (i.e. upper vertex of fig. (1.6) or (1.7)) as,

$$L = \sqrt{N}\sqrt{2L+1}\, f_L \tag{1.29}$$

where all indices have been suppressed for simplicity. This will allow us to describe the OPE contribution to reactions (1.5) and (1.6) in terms of the partial wave amplitude f_L for the subprocess $(\pi\pi \to \pi\pi(K\bar{K}))$. In particular, we will be interested in the I=0 S wave amplitude $f_o^{I=0}$ to describe the S* effect. We will consider the poles and analytic structure of f_L in the next section. To make the formalism of this section easily compatible with that of the next, it is convenient to take a factor $1/q$ out of f_L, which modifies N to read,

$$N = \frac{2}{M_N^2 P_L^2}\left(\frac{G}{4\pi}\right)^2 \frac{-t}{(t-\mu)^2}\,|F(t)|^2\,\frac{M^2}{q} \tag{1.30}$$

with eq.(1.29) left as it stands.

The isospin decomposition of the amplitudes f_L in terms of components f_L^I is given for $\pi\pi \to \pi\pi$ by,

$$f_L = \frac{2}{3} f_L^0 + \frac{1}{3} f_L^2 \qquad \text{for L even}$$

$$f_L = f_L^1 \qquad \text{for L odd} \tag{1.31}$$

and for $\pi\pi \to K\bar{K}$ by,

$$f_L = \frac{1}{\sqrt{3}} f_L^0 \qquad \text{for L even}$$

$$f_L = \frac{1}{\sqrt{2}} f_L^1 \qquad \text{for L odd}$$

(1.32)

We now turn again to the OPE cross section of eq. (1.25), and discuss some important factors concerning it. Clearly it vanishes as -t at $t \neq 0$, and has the pole factor $(t-\mu^2)^{-2}$. Both these factors give it a dramatic and characteristic t dependence [13,14,15]. Deviations from this t dependence could be partly explained by form factors. However, π exchange produces only helicity zero di-meson systems, which gives a pure helicity non-flip structure in the t channel frame. This implies the absence of any Φ dependence, which means $\langle Y_M^J \rangle = 0$ for $M \neq 0$. In this simplified situation then both P_+ and P_- would be zero. (Note it is observed in the $\pi\pi$ channel (1.5) that $\langle Y_{M>1}^J \rangle = 0$, which means $|L_+| = |L_-|$ from eqs. (1.28)). But the $\langle Y_1' \rangle$ moments are sizeable in both channels (1.5) and (1.6) (see chapter 2), which suggests other exchange mechanisms are present, and so $|L_+| = |L_-| \neq 0$, and also the existence of absorptive corrections 13,14,15]. A simple phenomenological way to include absorptive corrections [see ref[13] for a detailed discussion] is the Ochs-Wagner method [17] of adding on a constant piece C to the L=1, s channel helicity flip amplitudes. This leads to the assumption that the t channel amplitudes $L_{\nu\pm}$ of eq.(1.26) satisfy [18].

(i) $|L_{1+}| = |L_{1-}|$

(ii) $L_{\nu\pm} = 0$ for $\nu > 1$

(iii) $L_{1-} = \sqrt{L(L+1)}\, L_0 / C$

where C is real and can be parametrized as a quadratic function of the di-meson mass M. One can then express the moments in terms of L_o and C(M).

Absorptive corrections are assumed to be the main corrections to OPE [13]. Contributions in the $\pi\pi$ channel (1.5) from A_1 and A_2 exchanges (c.f. table (1.3)) are assumed to have a negligible effect in the small t region [13,15,22]. In the $K\bar{K}$ channel, since the non-OPE contributions are more complicated it is usual to extrapolate the data to the π- exchange pole (see chapter 2).

In chapter 2 we shall wish to study the properties of the I=0 S-wave in the $\pi\pi$ and $K\bar{K}$ channels. Resonances are associated with poles in the two-channel S matrix and so we will briefly describe the analytic structure of the S matrix, which will be used to describe the behaviour of the I=0 partial wave amplitudes $f_{L=0}$ in the region of interest around the $K\bar{K}$ threshold.

1.3 The S Matrix.

The two channel problem can be described by the channel phase shifts $\delta_1(\pi\pi)$ and $\delta_2(K\bar{K})$ and the inelasticity η. The S matrix is then written,

$$S_{ii} = \eta e^{2i\delta_{ii}}$$

$$S_{12} = i\sqrt{1-\eta^2}\, e^{i(\delta_1+\delta_2)} \qquad (1.33)$$

where,

$$S_{11} \equiv S(\pi\pi \to \pi\pi)$$

$$S_{22} \equiv S(K\bar{K} \to K\bar{K})$$

$$S_{12} \equiv S(\pi\pi \to K\bar{K}) \qquad (1.34)$$

Unitarity is imposed by the condition,

$$\underset{\sim}{S}^{\dagger}\underset{\sim}{S} = \underset{\sim}{S}\underset{\sim}{S}^{\dagger} = \underset{\sim}{I} \tag{1.35}$$

One can write the S matrix in terms of the T matrix by,

$$\underset{\sim}{S} = \underset{\sim}{I} + 2i\underset{\sim}{\rho}^{1/2}\underset{\sim}{T}\underset{\sim}{\rho}^{1/2} \tag{1.36}$$

where $\underset{\sim}{\rho}$ is the diagonal matrix of the C.M. channel momenta k_i,

$$\rho_{ij} = k_i \delta_{ij}/\sqrt{s} \tag{1.37}$$

with,

$$k_i = \frac{1}{2}(s - 4M_i^2) \tag{1.38}$$

S is the total C.M. energy squared and M_i the $\pi(1)$ and K(2) mass respectively. The elements of the S-matrix will have right hand cuts in the S plane starting at each threshold $4M_i^2$, and therefore a four-sheeted structure in the complex S plane, as shown in Fig. (1.9) [18]. We shall refer to the physical sheet as sheet I; the physical amplitudes are evaluated on the upper side of the right-hand cuts on this

Fig. (1.9) The Riemann sheets for the two channel problem. The cuts are displaced below the real axis for clarity.

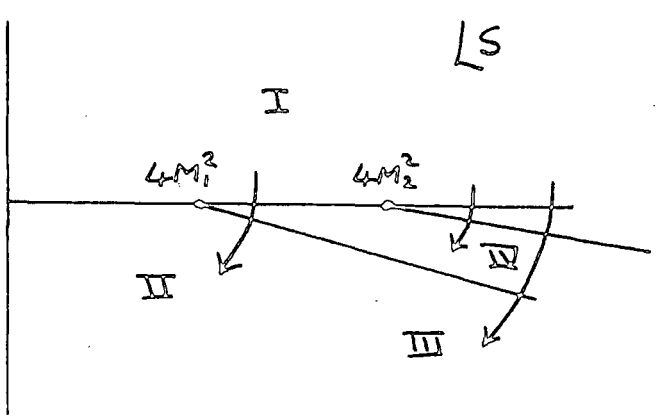

sheet. We can analytically continue through the cuts from the physical sheet to sheets II, III and IV as defined such that sheets I - IV correspond to $(\mathrm{Im}\rho_1, \mathrm{Im}\rho_2) = (++), (-+), (--), (+-)$ respectively.

The Argand amplitudes can be written as,

$$\underset{\sim}{A} = \underset{\sim}{\rho}^{1/2}\,\underset{\sim}{T}\,\underset{\sim}{\rho}^{1/2} \tag{1.39}$$

so that unitarity becomes,

$$\mathrm{Im}\,\underset{\sim}{A} = |\underset{\sim}{A}|^2 \tag{1.40}$$

and the A matrix can be written in terms of the phases and inelasticity,

$$A_{11} = \frac{\eta e^{2i\delta_1} - 1}{2i}$$

$$A_{12} = \frac{\sqrt{1-\eta^2}\, e^{i(\delta_1+\delta_2)}}{2} \tag{1.41}$$

Eqns. (1.41) correspond to the partial wave amplitudes f_L defined in eqns. (1.29), (1.30), but since we are only interested in the $I=0$ S wave here, the subscript L has been dropped.

One can incorporate the unitarity properties and threshold singularities of the S matrix by defining a real, symmetric K matrix, such that,

$$\underset{\sim}{T}^{-1} = \underset{\sim}{K}^{-1} - i\,\underset{\sim}{\rho} \tag{1.42}$$

The imaginary part of T is given by unitarity as,

$$\mathrm{Im}\,\underset{\sim}{T} = \underset{\sim}{\rho}^{1/2}\,|\underset{\sim}{T}|^2\,\underset{\sim}{\rho}^{1/2} \tag{1.43}$$

or equivalently,

$$\mathrm{Im}\, \underset{\sim}{T}^{-1} = -\underset{\sim}{\rho} \tag{1.44}$$

This latter result may be taken to define the analytic continuation of T from (say) sheet I to sheet II [27,28],

$$\underset{\sim}{T}^{-1\,II} = \underset{\sim}{T}^{-1\,I} + 2i\,\underset{\sim}{\rho} \tag{1.45}$$

Alternatively these S matrix properties can be conveniently described in terms of a real analytic function $d \equiv d(\rho_1, \rho_2)$, the determinant of the Jost function matrix [13,28], with square root branch points at $k_1 = 0$ and $k_2 = 0$. Then the S matrix is written in the form,

$$\begin{aligned} S_{11} &= d(-\rho_1, \rho_2)/d(\rho_1, \rho_2) \\ S_{22} &= d(\rho_1, -\rho_2)/d(\rho_1, \rho_2) \\ S_{11}S_{22} - S_{12}^2 &= d(-\rho_1, -\rho_2)/d(\rho_1, \rho_2) \\ &\equiv \Delta_{12} \end{aligned} \tag{1.46}$$

Analytic continuation of S into various sheets is given by $\rho_i \to -\rho_i$ and so for example [28],

$$S_{11}^{II} = \frac{1}{S_{11}^{I}} \; ; \quad S_{22}^{II} = \frac{\Delta_{12}^{I}}{S_{11}^{I}} \; ; \quad \Delta^{II} = \frac{S_{22}^{I}}{S_{11}^{I}} \tag{1.47}$$

The poles in the S-matrix are caused by the zeros of $d(\rho_1, \rho_2)$. A pole on sheet II will correspond to a zero on sheet I and vice versa.

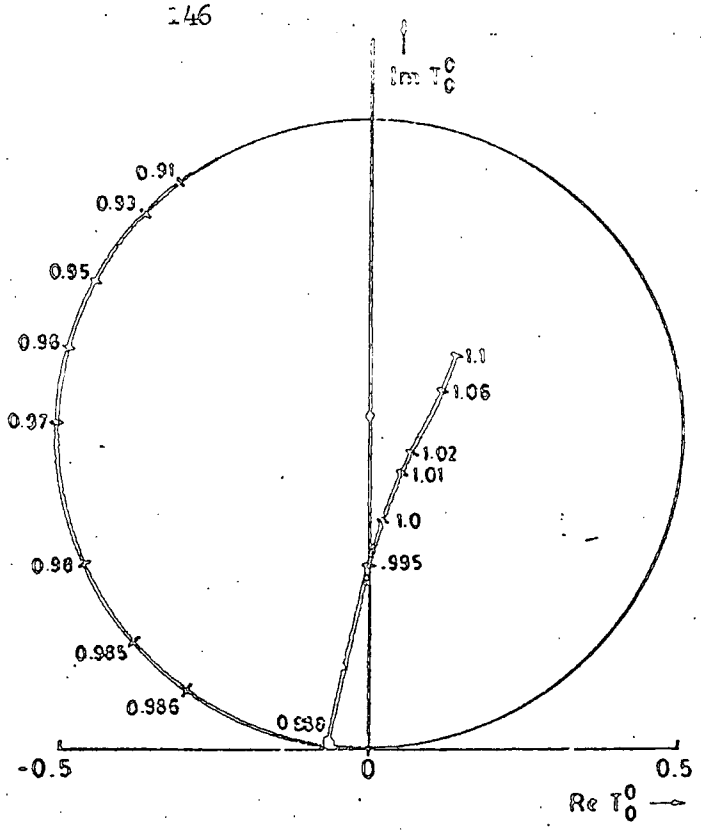

Fig. (1.10). Argard diagram for the I=0 S wave obtained from the coupled channel $\pi\pi \to \pi\pi$ and $\pi\pi \to K\bar{K}$ analysis of ref[34].

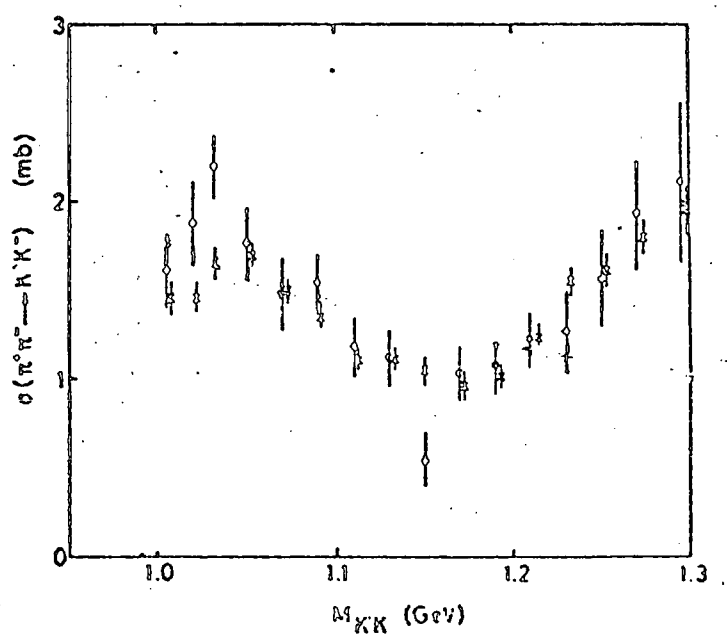

Fig. (1.11). The inferred cross section $\sigma(\pi\pi \to K\bar{K})$ between threshold and 1.3 Gev from ref[34], which rises sharply to the unitarity limit for the S wave cross section.

So the dynamics in the physical sheet is dependent upon the behaviour on the other sheets.

Since the S* pole is located very near to the $K\bar{K}$ threshold, we must take into account the opening of the new channelby making the correct analytic continuation across the threshold. This is done by taking $k_2 = +i|k_2| = +i(4M_K^2 - s)^{1/2}/2$ below $K\bar{K}$ threshold.

Having now set up all the formalism we will need, we can now describe the experimental evidence for the 0^{++} mesons, particularly the S*, before going on in chapter 2 to describe a coupled channel analysis of $\pi\pi$ and $K\bar{K}$ data.

1.4 Evidence For the Scalar Mesons.

The most striking effect around 1 Gev in the reactions of (1.5) and (1.6) is the strong opening of the $K\bar{K}$ channel. The sudden rise of $K\bar{K}$ production, which can be seen from the inferred cross section $\sigma(\pi^+\pi^- \to K^+K^-)$, is shown in fig. (1.10). This shows a peak at about 1.03 Gev followed by a fall. Evidence for this sharp onset of inelasticity can then also be clearly seen in the $\pi\pi \to \pi\pi$ channel, as in for instance the Argand plot of fig(1.11) (from an early coupled channel analysis) of the I=0 S wave. Further evidence for this significant effect is seen in the interference moment $\langle Y_0^1 \rangle$ in the $\pi\pi$ channel (see fig. (2.1)) which has a shoulder between 910 and 950 Mev, followed by a sharp drop between 950 and 980 Mev, with a flat region after that. Since $\langle Y_0^1 \rangle \sim \mathrm{Re}(SP^*)$ (c.f. eqns(1.28), this drop suggests a significant change in either the S or P wave over that small range of mass. As implied already, (c.f.fig. (1.11)) this effect is most easily understood in terms of a rapid variation of the I=0 S wave amplitude, associated with $K\bar{K}$ threshold.

This interpretation was originally suggested by an LBL group [19],

who assumed that the I=0 $\pi\pi \rightarrow \pi\pi$ S wave amplitude could be parametrized as a coupled channel resonance [20], and who analysed $\pi\pi \rightarrow \pi\pi$ data and the (K^+K^-) mass spectrum accordingly. They found that the I=0 S wave amplitude started around 900 Mev with phase 90°, which reached 180° at about 990 Mev (c.f. fig (1.11)). This structure indicated that the amplitude was being observed on a large background with phase about 90° at 900 Mev. Morgan subsequently found a slowly rising elastic background phase, which reaches 90° around a $(\pi\pi)$ mass of 1100-1300 Mev[21]. The original S wave effect is attributable to the S* resonance, with the background being interpreted as largely due to the ε resonance.

The I=1 member of the scalar nonet (δ) is seen as a peak in the $\pi\eta$ mass spectrum just below $K\bar{K}$ threshold and as a threshold enhancement in the K^-K^0 spectrum. The broad κ resonance is seen as a rise through 90° of the I=$\frac{1}{2}$ $K\pi$ S wave around 1200 Mev. We will subsequently however, be concerned in analyses which predominantly involve the I=0 S wave and the problem of pinning down the S* and ε resonances. It is convenient, therefore, at this stage to summarize the data which we will use in the $\pi\pi \rightarrow \pi\pi(K\bar{K})$ S wave.

There is a rapid variation in the phase δ_1 across the $K\bar{K}$ threshold, between .85 and 1.2 Gev, where it rises from 90° to 270°, accompanied by a dip in the elasticity η just above threshold (c.f.figs.(1.11), (2.3)). The S* is responsible for this behaviour. δ_1 increases again at about 1.4 Gev and this is attributable to the ε resonance. The non-diagonal phase $\delta(\pi\pi \rightarrow K\bar{K}) \equiv \delta_1 + \delta_2 \equiv \delta_{\pi K}$ is fairly stationary from threshold up to about 1.3 Gev (see fig.(2.2)), after which it rises rapidly, with η approaching unity. The flat behaviour of $\delta_{\pi K}$ below 1.3 Gev suggests that the S* cannot be parametrized as a Breit-Wigner resonance.

Early analyses of the I=0 S wave were restricted by the available

data to concentrate almost entirely on $\pi^+\pi^-$ data (e.g. $\pi^-p \rightarrow \pi^+\pi^-n$) (see for example [13-15, 19-22]). Clearly this is not sufficient to establish whether the S* is a Breit-Wigner resonance or some other more complicated effect associated with the close proximity of the $K\bar{K}$ threshold. One would also like to understand at the same time the nature of the background to the S*, which in the $\pi\pi$ channel is predominantly the broad ϵ effect. Only when high statistics data was obtained in the $K\bar{K}$ channel did this become possible [6, 11, 23, 8, 18]. Most information can clearly be gained from a coupled channel analysis, such as that described in Chapter 2, to which we now turn.

CHAPTER 2

COUPLED CHANNEL ANALYSIS OF $\pi\pi$ AND $K\bar{K}$

2.1. Introduction.

In this chapter we analyse data on $\pi\pi$ and $K\bar{K}$ production in order to try to understand the isospin zero S wave scattering near the $K\bar{K}$ threshold. We study various coupled channel parametrizations in order to assertain the properties of the S* and ε enhancements [26].

A system with the quantum numbers of the scalar mesons, $J^{PC}=0^{++}$, and isospin zero can in principle decay to other channels besides $\pi\pi$ and $K\bar{K}$, such as $\eta\eta$. However, only $\pi\pi$ and $K\bar{K}$ have been measured, but seem to provide by far the dominant modes, as can be seen in table (1.2), or reference [2]. The other channels may be restricted by insufficient phase space below about 1.5 Gev; there is no evidence for any dramatic effects with the opening of the $\eta\eta$ threshold, in stark contrast to the case for the $K\bar{K}$ threshold. The data also provides negligible 4π inelastic effects in the mass region around $K\bar{K}$ threshold. We therefore feel justified in continuing with a two channel analysis. We try to use all the available information below and above $K\bar{K}$ threshold in both channels in contrast to the work done by the ANL group for instance, who use mainly $K\bar{K}$ data [23].

We consider data obtained from high statistics experiments using reactions (1.5) and (1.6). The $\pi^+\pi^-$ moments $\langle Y_M^J \rangle$ used are obtained in reaction (1.5) at 17.2 Gev/c in reference [10], and displayed in fig (2.1). We use information in the mass range .85-1.55 Gev, and fit to the $\pi\pi$ moments (eqs.(1.28)) in the region of 0.9-1.06 Gev. In the range 1.25-1.55 Gev the $\pi\pi$ amplitude is constrained to be consistent with the β phase shift solution of reference [24]. Refinements of solutions from reference [22] were obtained in reference [24] by Pennington and Martin, by imposing analyticity on the $\pi\pi$ phase shift analysis. We choose the β solution since that contains the $\rho'(1600)$ [2]

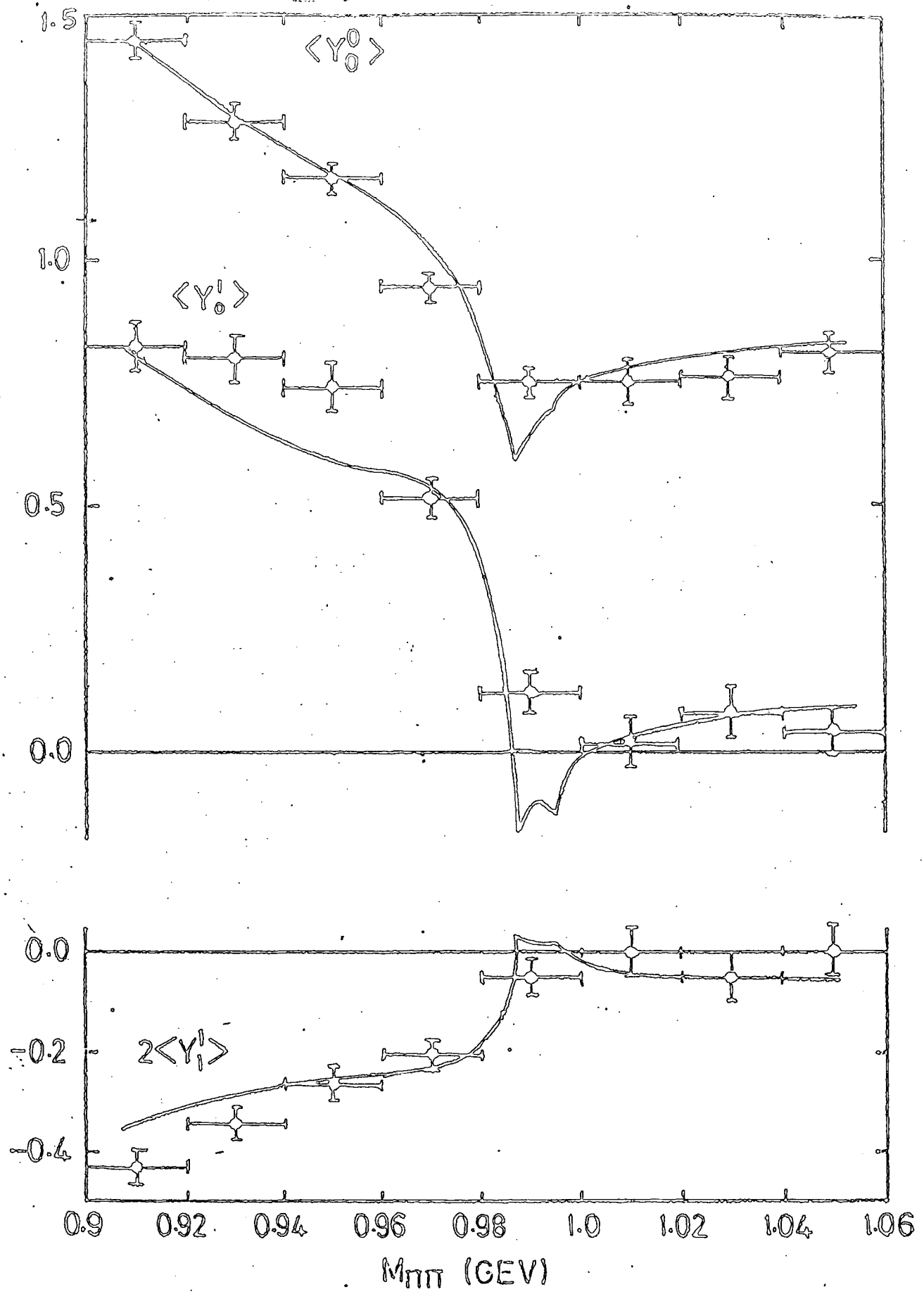

Fig. (2.1) The mass spectra of the unnormalized $\pi\pi$ moments in the region of the K^+K^- and $K^0\bar{K}^0$ thresholds. The data are from the 17.2 Gev/c $\pi^- p \to \pi^- \pi^+ n$ experiment [10] and correspond to $-t < 0.15$ Gev^2. The curve is the fit using parametrization I of sec (2.21)

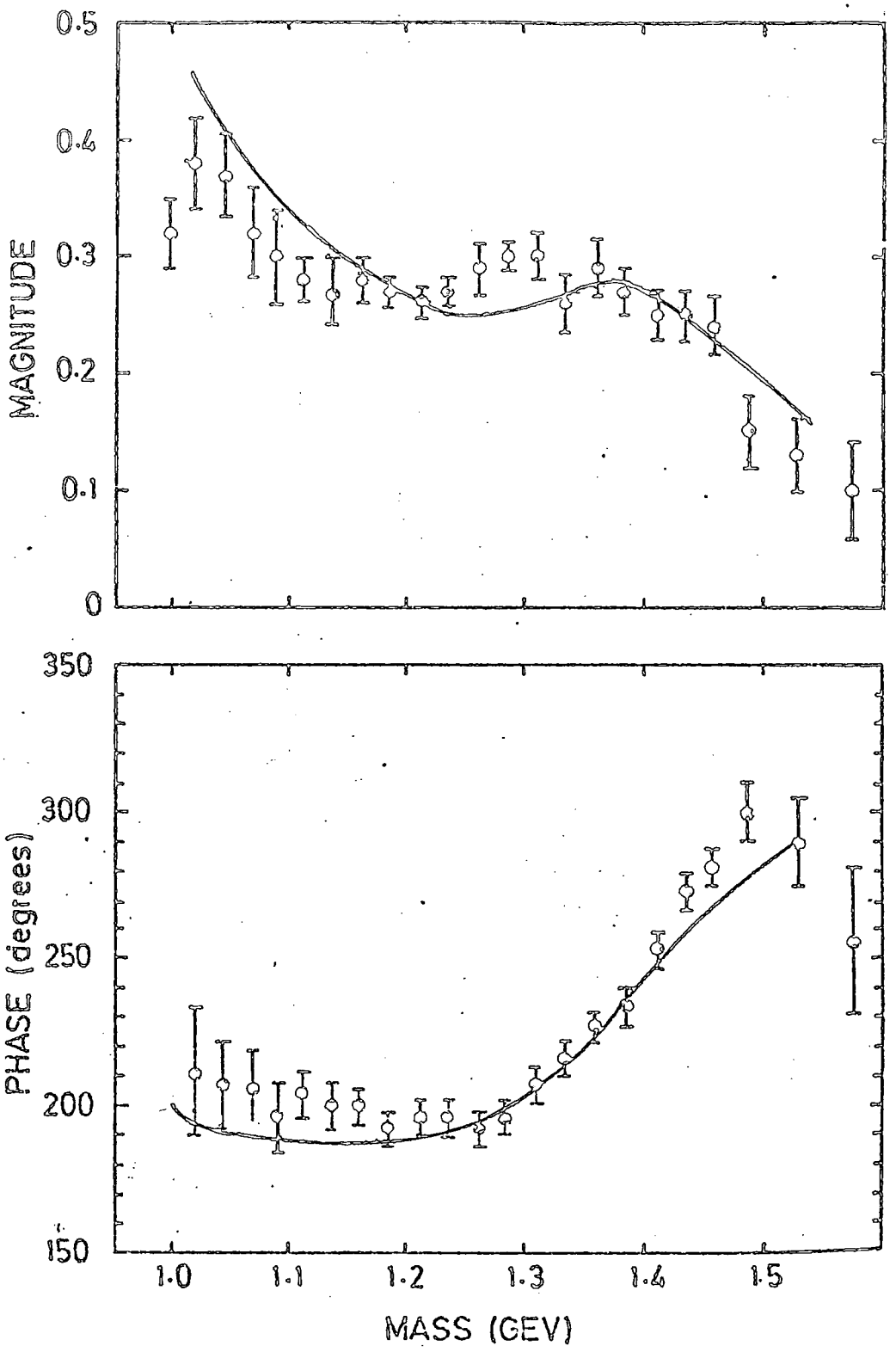

Fig. (2.2). The modulus and phase of the S wave $\pi\pi \to K\bar{K}$ amplitude. The points correspond to the points favoured by the ANL partial wave analysis [6,7,11,23] of their spectrometer data for K^+K^- production. The modulus is normalized to a unitarity circle of radius 0.5. The curve is the fit using parametrization I of sec(2.2.1).

and it also gives a satisfactory description of polarized target data [23,25].

The $K\bar{K}$ data used is the modulus and phase of the I=0 S wave amplitude found in the ANL $\pi N \to K\bar{K}N$ single channel analysis of reference [23]. The exchange mechanisms are more complicated in this reaction (c.f. table (1.3)), and so to obtain the $K\bar{K}$ mass dependence and resolve the partial wave uncertainties one can extrapolate the data to the π exchange pole. This was done by the ANL group, who used the t-dependence extracted from the data and the extrapolation of eqs. (1.25), (1.29) and (1.30). The data are shown in fig. (2.2).

To use the $\pi\pi$ moments to extract the I=0 S wave behaviour, we specified the P wave to be the ρ tail which we describe by the Breit-Wigner,

$$f_\rho \equiv f_\rho = \frac{M_\rho \Gamma_\rho(q)}{M_\rho^2 - M^2 - i M_\rho \Gamma_\rho(q)} \qquad (2.1)$$

where

$$\Gamma_\rho(q) = \left(\frac{q}{q_\rho}\right)^3 \Gamma_0 \frac{M_\rho}{M} \frac{1 + R^2 q_\rho^2}{1 + R^2 q^2} \qquad (2.2)$$

with, $M_\rho = 0.773$ gev, $\Gamma_\rho = 0.15$ gev, R = 3.5 gev^{-1}. q is the π momentum in the π centre of mass, with q_ρ that at the ρ mass M_ρ.

For the I=2 S wave, we simply use,

$$f_S^{I=2} = \sin\delta_2 \, e^{i\delta_2} \qquad (2.3)$$

with values of δ_2 used from reference[22] for(example $\delta_2 = -22.4^\circ$ at M=1 Gev).

We now wish to study the possible parametrizations of the I=0 two channel S matrix in order to extract the parameters of the S wave

resonances, the S* and ϵ . Since the S* occurs on a large background, which could be largely interpreted as the ϵ resonance in the $\pi\pi$ channel (c.f. sec.(1.4)), the I=0 S wave $\pi\pi$ amplitude must be parametrized by two overlapping structures. To do this we use the $d(\rho_1, \rho_2)$ function (of sec(1.3)), and we now decide which is the most appropriate parametrization.

2.2 Coupled Channel Parametrizations.

Consider the following examples of parametrizations of $d(\rho_1, \rho_2)$.

(a) Breit-Wigner resonance:

$$d_R(\rho_1,\rho_2) = m_R^2 - s - i(\rho_1\gamma_1^2 + \rho_2\gamma_2^2) \tag{2.4}$$

where, $m_R \Gamma_R^i = \rho_i \gamma_i^2$

This leads to poles in the S matrix on sheet III and sheet II (see for example [27]). When the resonance occurs far above threshold, only the sheet III pole is important.

(b) K matrix parametrization:

$$d_K = \det(\underset{\sim}{K}^{-1} - i\underset{\sim}{\rho}) \tag{2.5}$$

The Breit-Wigner form is equivalent to a pole in the K matrix. Yet a resonant effect can still occur even if the K matrix elements are slowly varying as a function of energy. To see this, consider the K^{-1} matrix to be parametrized as,

$$\underset{\sim}{K}^{-1} = \begin{pmatrix} \alpha & \gamma \\ \gamma & \beta \end{pmatrix} \tag{2.6}$$

so that,

$$d_K = (\alpha - i\rho_1)(\beta - i\rho_2) - \gamma^2 \tag{2.7}$$

For β small and negative one obtains a sheet II ($\mathrm{Im}\,\rho_2$ positive) pole just below the $K\bar{K}$ threshold ($\rho_2 = +i|\rho_2|$) at

$$|\rho_2| = -\beta + \gamma^2/(\alpha - i\rho_1) \tag{2.8}$$

The effects of this pole are observed as a resonance in the $\pi\pi$ channel and so we shall refer to it as a $K\bar{K}$ bound state resonance. There is no nearby sheet III pole. If α, β, γ are chosen to be (real) constants we have a simple 3-parameter description of a resonance and its background. For example, one can write the $\pi\pi \to \pi\pi$ S matrix element as,

$$S_{11} = \left(\frac{\alpha + i\rho_1}{\alpha - i\rho_1}\right)\left(\frac{i\rho_2 + \rho_R^*}{i\rho_2 + \rho_R}\right) \tag{2.9}$$

where ρ_R is the value of $|\rho_2|$ given by eq.(2.8). Thus S_{11} is written in the form of a resonance (second factor, which gives the sheet II pole), multiplied by a background, which has a large phase ($\sim 90^\circ$) provided $|\alpha| \ll k_1$. Therefore the resonance is described by two parameters, the background one.

(c) Two Breit-Wigner poles:

$$d_{RR'} = d_R d_{R'} + (\rho_1 \gamma_1 \gamma_1' + \rho_2 \gamma_2 \gamma_2')^2 \tag{2.10}$$

(d) A Breit-Wigner resonance and background in the $\pi\pi$ channel:

$$d_{R\beta} = d_R d_\beta \tag{2.11}$$

with,

$$d_\beta = \exp(-i k_1 \phi_\beta) \tag{2.12}$$

(e) Factorizing Breit-Wigner and smooth K matrix,

$$d_{RK} = d_R d_K \tag{2.13}$$

We wish to use one of the above parametrizations to describe the I=0 S wave in the range $0.85 < M < 1.55$ Gev, where it must incorporate both the S* and ε effects. This might suggest we should simply use (c), but since the phase $\delta_{\pi K}$ is very flat below 1.3 Gev, this would imply a very large width for the S*. We therfore turn to the $K\bar{K}$ bound state picture of the S*, and so consider parametrizations (e) or (b), which we shall call I and II respectively.

Since the S* occurs very close to the $K\bar{K}$ threshold, where we fit to data, we must take into account isospin violation which manifests itself in the K^+K^- and $K^o_o\bar{K}^o_o$ mass difference. This is disucssed in the Appendix A, where it is shown that to a good approximation the main modification to the above description is the replacement of k_2 by $\frac{1}{2}(k_c+k_o)$, where k_c and k_o are the magnitudes of the K^+K^- and $K^o\bar{K}^o$ c.m. momenta respectively. As can be seen in fig. (2.1), the mass bin centred on .99 Gev contains both thresholds and the fit to the $\pi\pi$ moments leads to the structure displayed. We now turn to the results of the fits to the data described in sec. (1.4.), using parametrizations I and II.

2.2.1 Factorizing Jost Function Parametrization I

The data were fitted using

$$d_{RK} = d_R(\varepsilon) d_K^{(S^*+\text{ background})} \tag{2.14}$$

where d_K was parametrized in terms of a slowly varying inverse K matrix,

$$\underset{\sim}{M} \equiv \underset{\sim}{K}^{-1} = \underset{\sim}{M}^{(0)} + 4k_2^2 \underset{\sim}{M}^{(1)} \tag{2.15}$$

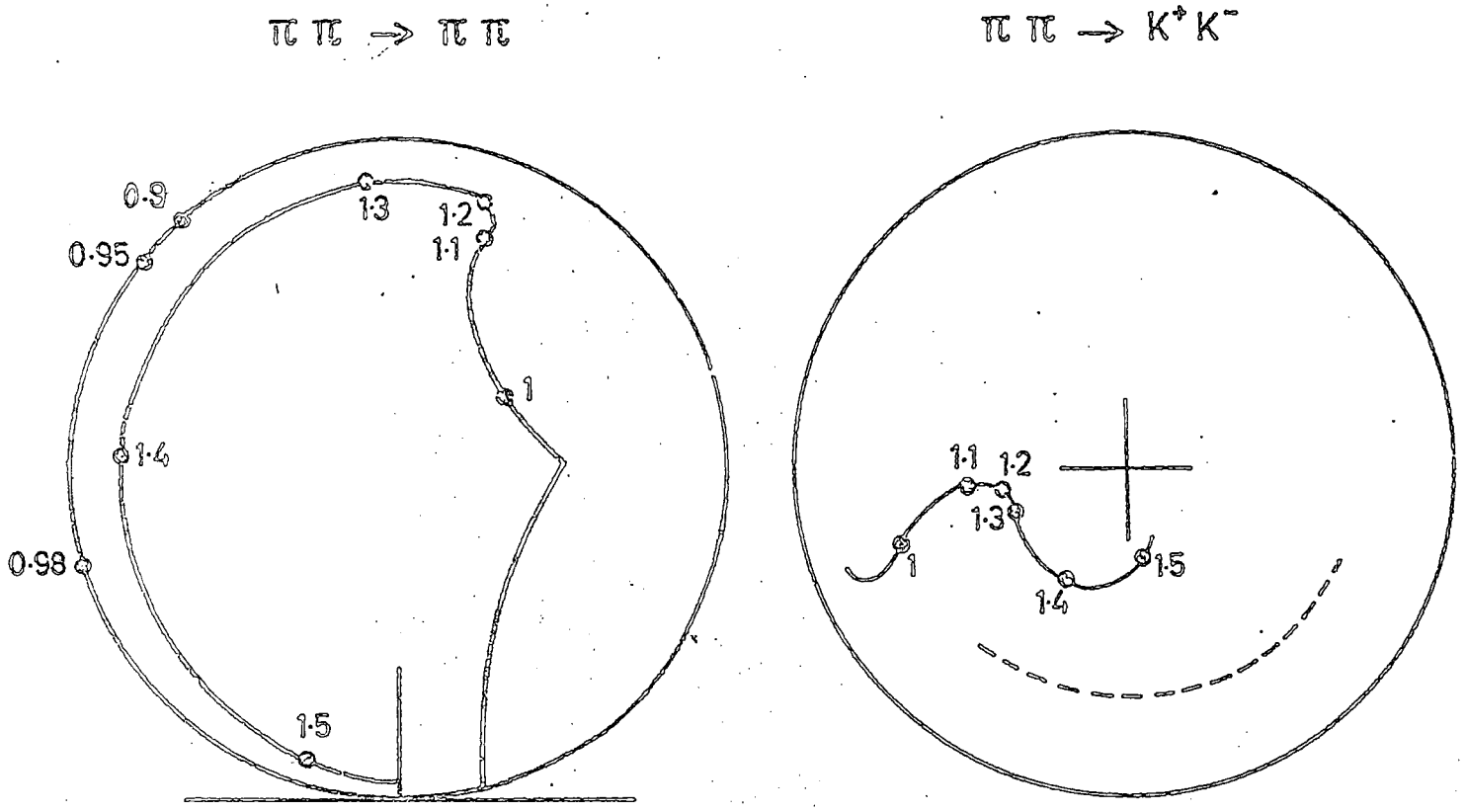

Fig. (2.3). The I=0 $\pi\pi \rightarrow \pi\pi$ and $\pi\pi \rightarrow K^+K^-$ amplitudes. The curves correspond to parametrization I of sec(2.2.1). In the absence of K^+-K^0 mass difference the $\pi\pi \rightarrow K^+K^-$ amplitude should be in a unitarity circle of radius $1/\sqrt{2}$ (shown by the dashed curve). The violation below about 1 Gev is due to this mass difference.

The results of the fit are shown by the continuous cruves on figs. (2.1), (2.2), with the amplitudes shown in fig. (2.3). The parameter values are (in units of Gev),

$$d_R: M_R = 1.391, \gamma_1 = 0.76, \gamma_2 = -0.25$$

$$d_K: M_{11}^{(0)} = 0.16, M_{22}^{(0)} = -0.03, M_{12}^{(0)} = 0.16$$

$$M_{11}^{(1)} = 0.46, M_{22}^{(1)} = -0.09, M_{12}^{(1)} = -0.08$$

(2.16)

The most significant M matrix element is $M_{11}^{(1)}$.

The pole positions of the T matrix nearby the physical region are,

S* pole on sheet II at $\sqrt{s}$ = 988- 8i Mev

ε pole on sheet III at $\sqrt{s}$= 1394-110i Mev

(2.17)

The ratio of the residues at the ε pole determines the ratio of its coupling to $\pi\pi$ and $K\bar{K}$. We get,

$$\left| \frac{T_{22}}{T_{11}} \right|^{1/2} = 0.32$$

(2.18)

2.2.2 K Matrix Parametrization.

Under this description we include the ε effect as a pole term and take into account the S* and background using a slowly varying K matrix, viz.

$$\underset{\sim}{K} = \underset{\sim}{K}(\varepsilon) + \underset{\sim}{K}^{(0)} + 4k_2^2 \underset{\sim}{K}^{(1)}$$

(2.19)

with,

$$\left(\underset{\sim}{K}(\varepsilon)\right)_{ij} = \gamma_i \gamma_j / (m_R^2 - s) \tag{2.20}$$

The parameter values (in units of Gev) obtained from the fit are,

$$M_R = 1.397, \quad \gamma_1 = 1.0, \quad \gamma_2 = 3.2$$
$$K_{11}^{(0)} = 1.5, \quad K_{22}^{(0)} = -10.3, \quad K_{12}^{(0)} = 4.2$$
$$K_{11}^{(1)} = -0.2, \quad K_{22}^{(1)} = -24.3, \quad K_{12}^{(1)} = -4.6 \tag{2.21}$$

The poles in the T matrix are,

S* pole on sheet II at $\sqrt{s}$ = 986-7i Mev

ε pole on sheet III at $\sqrt{s}$ =1394-118i Mev. (2.22)

with the ratio of the residues at the ε pole,

$$\left| \frac{T_{22}}{T_{11}} \right|^{1/2} = 0.25 \tag{2.23}$$

The two different parametrizations are therefore seen to produce very similar T matrix elements, with both the S* and ε turning out much narrower than in earlier determinations [2]. This is a result of requiring a desirable fit to the $\pi\pi$ moments, especially in the region 0.96-1.0 Gev (c.f.[18]). The difference in the values of eqs.(2.17) and (2.21) may be taken as a measure of the uncertainty in the pole positions. The ε parameters are not critically dependent on the fit to the $\pi\pi$ moments, as those of the S* wave are particularly around the $K\bar{K}$ threshold.

The properties of the ε resonance found in our analysis are quite similar to those found in the ANL analysis, even though their parametrization is completely different [23]. They parametrize the T matrix directly and include the S* as a background to the ε . Their main interest is in $K\bar{K}$ data and they do not attempt to describe the $\pi\pi$ moments close to the $K\bar{K}$ threshold, which is a crucial feature of our analysis. In view of such differences between our respective approaches,

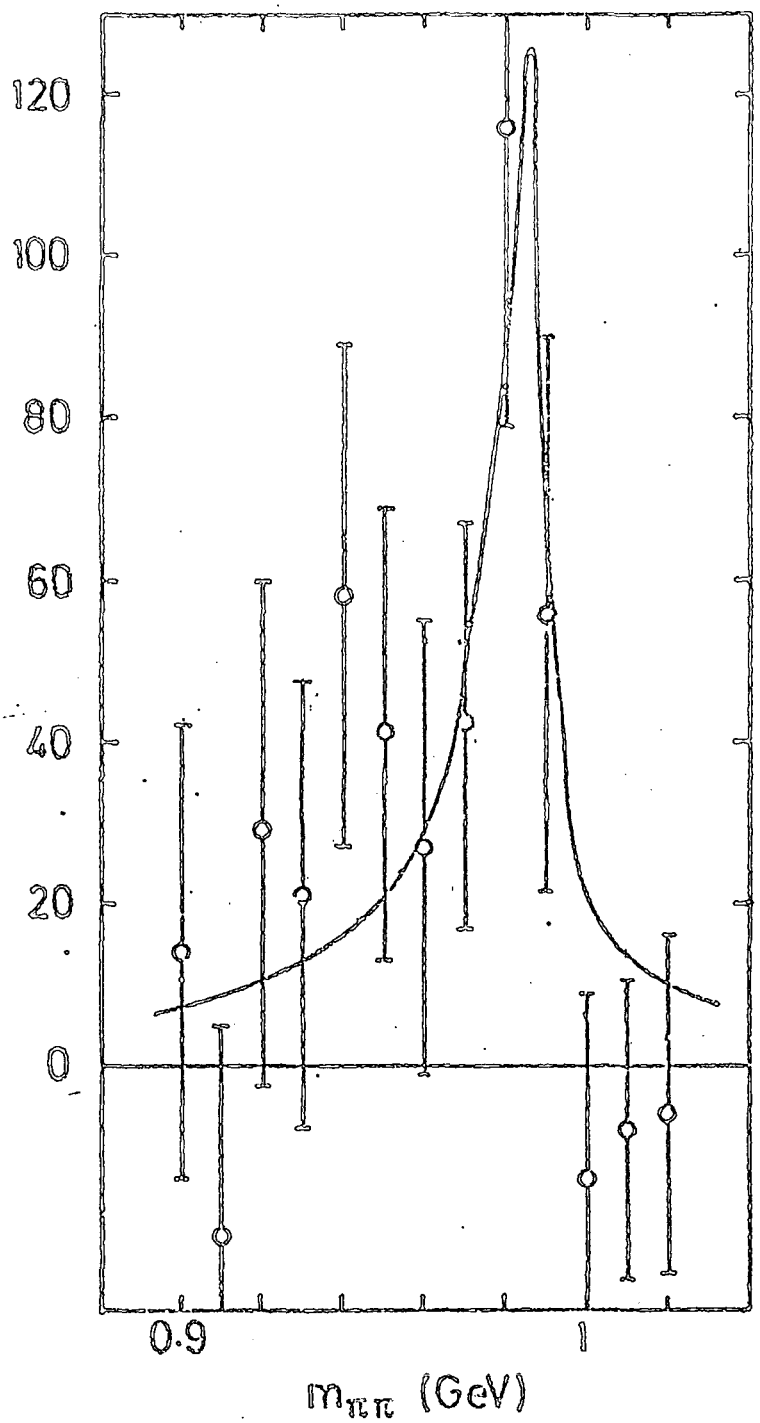

Fig. (2.4). The $\pi^+\pi^-$ mass distribution observed in $K^-p \to \pi^-\pi^+\Lambda$ at 13 Gev/C [29], with the background and ρ resonance events subtracted. The curve is proportional to $k_1 m |T_{12}|^2$ and corresponds to the prediction of parametrization I of sec (2.2.1).

it is encouraging that their $\xi(1425)$ has quite similar properties to our $\xi(1394)$ [26].

2.3 Discussion.

Before summarising the main results of this chapter, there are a few more salient points which should be mentioned.

One could try to examine K exchange by looking at reactions of the type,

$$K^- p \rightarrow \pi\pi(K\bar{K})\Lambda \qquad (2.24)$$

Assuming that K exchange is the dominant mechanism leads to cross section estimates which are much larger than the data [26], so that there must be sizeable contributions from non-K exchanges. It is therefore not possible to perform an analysis of $K\bar{K} \Rightarrow \pi\pi$, $K\bar{K}$ in the same spirit as that of a $\pi\pi \Rightarrow \pi\pi, K\bar{K}$ analysis. The S* enhancement is however also observed in the $\pi\pi$ mass spectrum from reaction (2.24). The $\pi\pi$ mass distribution is shown in fig. (2.4), with the background and ρ tail subtracted, at 13 Gev/c[29] in arbitrary units. This data is fitted with a curve proportional to $R_1 M |T_{12}|^2$, calculated using parametrization I of sec.(2.3)[26]. Although there is reasonable agreement, the data does suggest that the S* is narrower and occurs slightly lower in mass than that predicted from the analysis.

One can, however, predict that S wave K^+K^- production will be much larger than $K_S^0 K_S^0$ [26]. The process $K^- p \longrightarrow K^+K^-\Lambda$ is dominated by Φ production around the threshold, and this opens up the possibility of studying S wave production by examining S-P interference effects in the Φ mass region. This is the subject of chapter 3, where we perform a double moment analysis of the data [30].

One can now also look to the decay $\Psi \rightarrow \Phi\pi^+\pi^-$ to

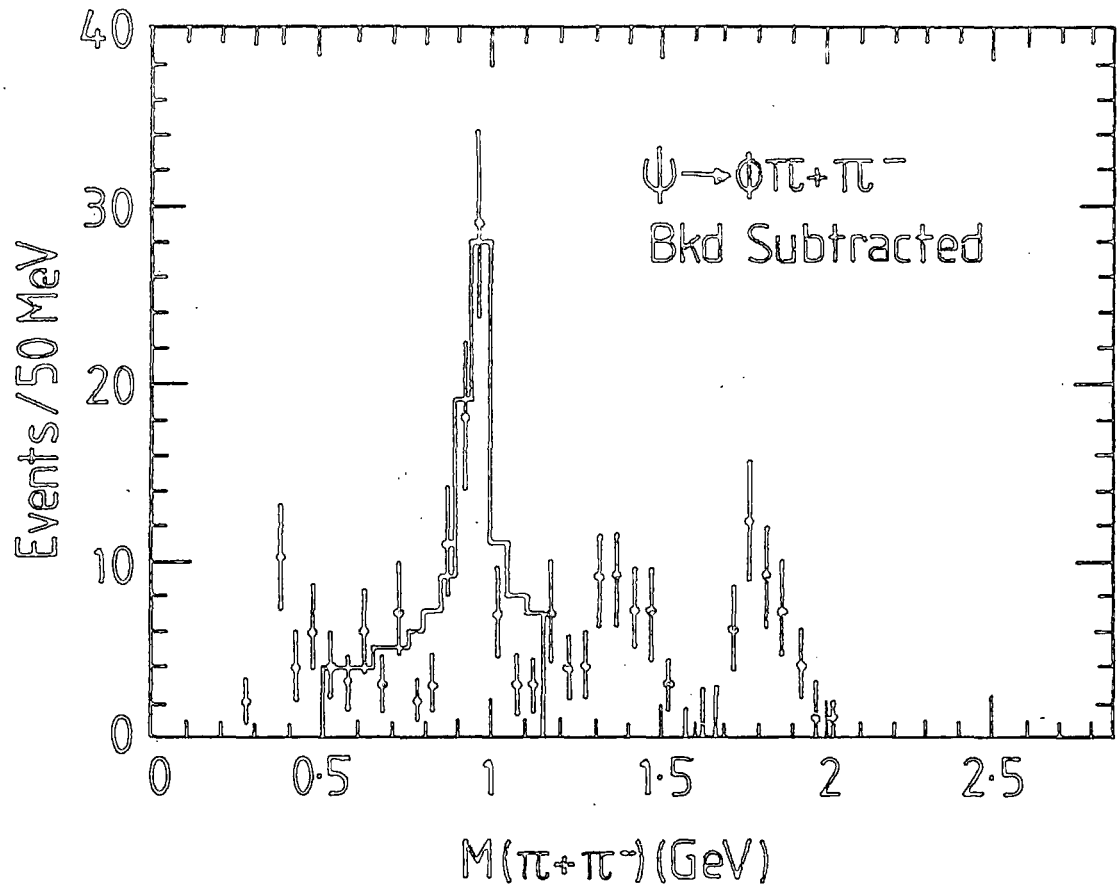

Fig. (2.5). Background subtracted invariant mass of $\pi^+\pi^-$ pairs for events in $\psi \longrightarrow K^+K^-\pi^+\pi^-$ which have a K^+K^- invariant mass in the ϕ region.

give us information about the S* resonance. Data in the $\pi^+\pi^-$ mass distribution [25] clearly show a peak near 970 Mev (see fig. (2.5)). The production mechanism is shown in fig(2.6).

Fig. (2.6) Production mechanism for the S* in $\psi \to \phi\pi^+\pi^-$

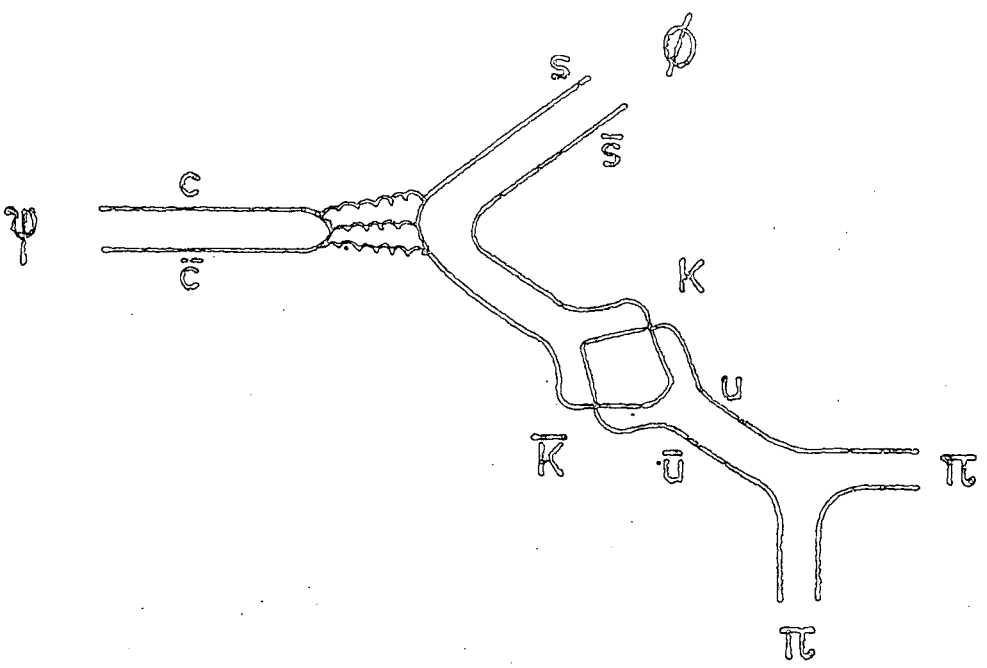

It is assumed that the coupling is to the $s\bar{s}$ component of ϕ, which belongs to an almost ideally mixed SU (3) nonet. Allowing for a small admixture of non-strange $q\bar{q}$ would provide a lesser Zweig-suppressed mechanism than that of fig. (2.6), but the admixture is so small that this is neglected. Moreover, the final $\pi\pi$ state ($u\bar{d}d\bar{u}$) is reached by passing through an intermediate state composed of $u\bar{s}s\bar{u}$, which could form a $K\bar{K}$ bound state, since the $\pi^+\pi^-$ mass is close to $K\bar{K}$ threshold. This picture is consistent with the view that the S* is a $K\bar{K}$ bound state resonance, which we used in our K matrix parametrization of the completely different production mechanism in $\pi^- N \to \pi\pi(K\bar{K})N$. One might then also expect an S* threshold enhancement in $\psi \to \phi K\bar{K}$ in the $K\bar{K}$ mass spectrum. It would be interesting to see the results of a coupled channel analysis of these ψ decay modes, from which much could be deduced.

Isospin violation was touched upon in sec (2.3), and its effects are shown in fig. (2.2) around $K\bar{K}$ threshold. Achasov et al.[31] have discussed the effects of I=0,1 mixing near the $K\bar{K}$ threshold, which causes S^*-δ interference via $K\bar{K}$ loops. The four channel($\pi\pi, \pi\eta, K^+K^-, K^0\bar{K}^0$) formalism is discussed in Appendix A. Achasov et al. examine the influence of S^*-δ mixing in the reaction $\pi N \to \pi^0 \eta N$, in which π exchange is forbidden by isospin symmetry, and predict significant effects. However, reliable data on such a process does not exist at present. We now summarize the main results of this chapter.

It was found that the $\pi\pi \Rightarrow \pi\pi, K\bar{K}$ data suggested the existence of two I=0 S wave resonances in the mass range 0.86-1.55 Gev. Due to the lack of phase variation in $\pi\pi \Rightarrow K\bar{K}$ over the $K\bar{K}$ threshold, it was not possible to parametrize the S^* resonance as a Breit-Wigner, which would have required poles in the T matrix on sheet III and sheet II. The K matrix was found to be a successful parametrization of the S^* resonance, and in both alternative forms (I and II) requires just a sheet II pole, which ensures that the $\pi\pi \Rightarrow K\bar{K}$ phase is slowly varying over and above the $K\bar{K}$ threshold. The K matrix formalism is a convenient tool to use to expose the distinction between a Breit-Wigner (sheet III) pole and a $K\bar{K}$ bound state (sheet II) pole. The former corresponds to a pole in the K matrix, the latter a slowly varying one.

The same data also require the existence of a Breit-Wigner ε resonance, which couples predominantly to the $\pi\pi$ channel, and which has a mass of about 1.4 Gev. The parameters of the ε were found to be stable against changes of parametrization. The pole position ($\sqrt{s} \simeq 1400-110i$ Mev) and ratio of couplings to $\pi\pi$ and $K\bar{K}$ channels ($\simeq 4:1$) compare favourably with the results of the ANL analysis [23], which predicts a mass of 1425 ± 15 Mev and half-width 80 ± 15 Mev for the ε .

We now turn to a study of the interference effects between the ϕ meson and K^-K^+ S wave in the reaction $K\bar{p} \longrightarrow K^-K^+\Lambda$ at 4.2 Gev/c.

CHAPTER 3

INTERFERENCE EFFECTS IN $K^-p \to K^-K^+\Lambda$ AT 4.2 Gev/c AND THE THRESHOLD $K\bar{K}$ S WAVE AMPLITUDE

3.1 Introduction.

As was mentioned in chapter two, it is much more difficult to obtain information on the $K\bar{K} \to K\bar{K}$ channel than $\pi\pi \to K\bar{K}, \pi\pi$, since it's more difficult to isolate K exchange. We make an attempt to do this by examining the reaction $K^-p \to K^+K^-\Lambda$, where the Λ acts as a polarization analyser, allowing one to assess the importance of the contribution of unnatural parity, non-K exhange amplitudes. Furthermore the data around the $K\bar{K}$ threshold are dominated by the Φ resonance and so by examining S-P wave interference in this region we can study the behaviour of the $K\bar{K}$ S wave amplitudes, which we assume to be due to the S* and δ resonances.

Our results are obtained [30] from an analysis of the reaction $K^-p \to K^-K^+\Lambda$ at 4.2 Gev/c. The data show interference effects in the relevant moments of the decay distributions of the and (K^-K^+) systems. The data are described briefly in sec.(3.2). In sec. (3.3) we describe the amplitude analysis, with discussion of results in sec(3.4).

3.2 Data.

The dominance of the Φ resonance in the data at low values of K^-K^+ mass is shown by the data in fig. (3.1), with fig. (3.2) showing that the Φ is preferentially produced in the forward direction. The following analysis is restricted to the region $\cos\Theta_{p\Lambda} > 0.5$, which contains the main body of data.

The data is presented in terms of the joint moments, H , of the Λ and K^+K^- decay angular distributions and can be written as,

$$H(LMlm) = \sum_i D^L_{M0}(\Omega_i) D^l_{m0}(\Omega'_i) \qquad (3.1)$$

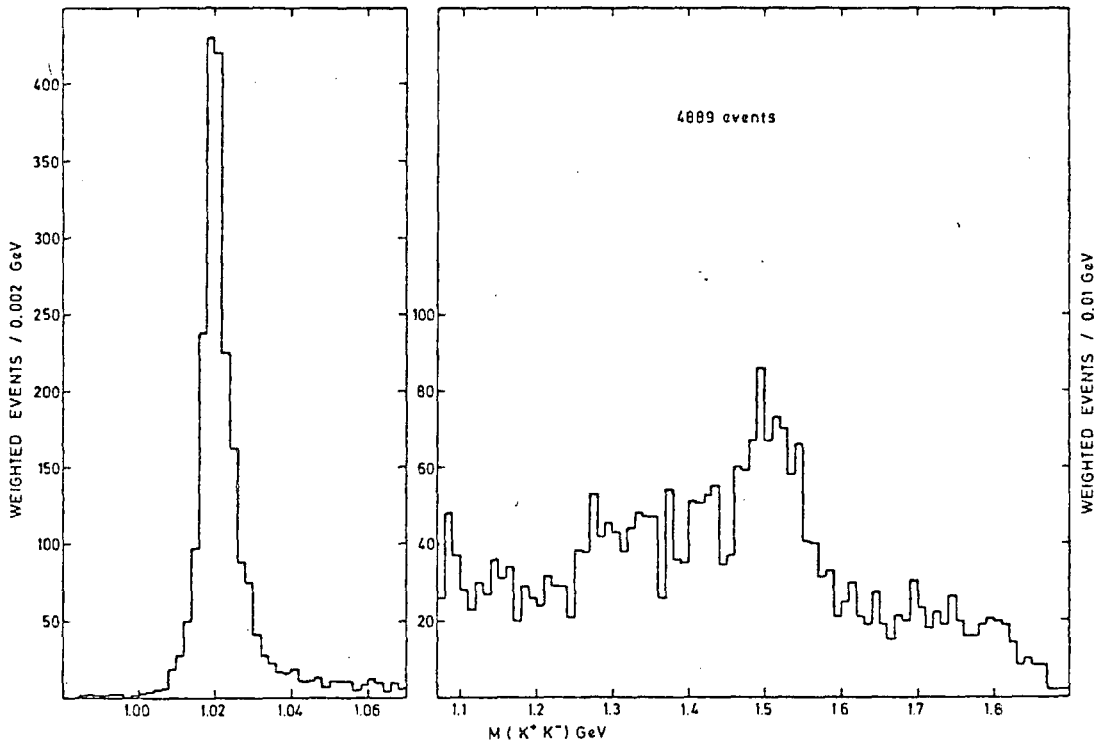

Fig. (3.1). The K^-K^+ effective mass distribution observed in the reaction $K^-p \rightarrow K^-K^+\Lambda$.

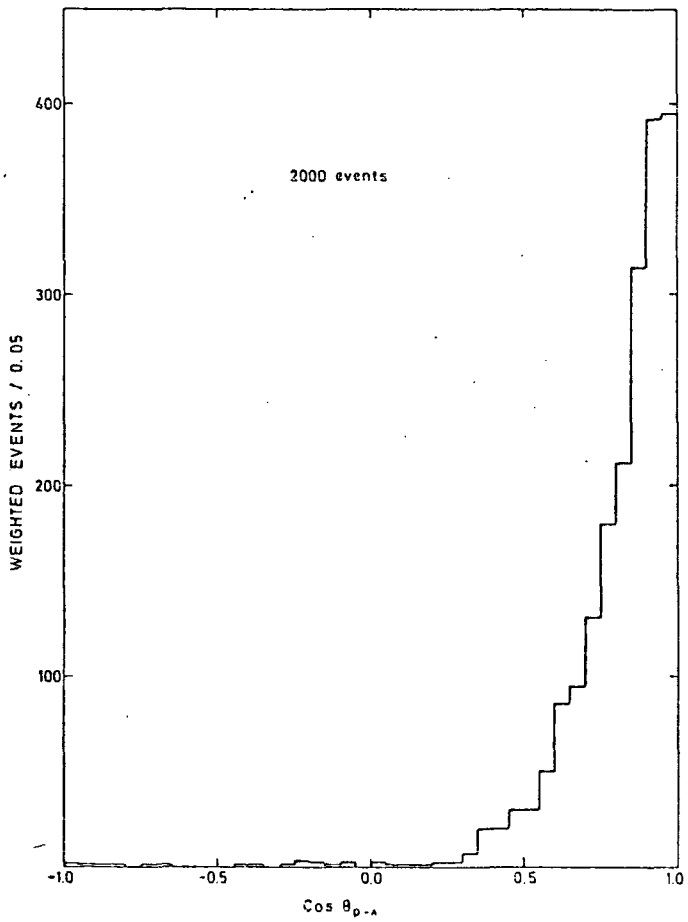

Fig. (3.2). The $dN/d\cos\Theta_{p\Lambda}$ distribution for events with $0.998 \leq m(K^+K^-) \leq 1.042$ Gev. $\Theta_{p\Lambda}$ is the angle between the incoming proton and the outgoing Λ in the overall centre of mass.

where the sum is over all events in the mass interval under consideration. The solid angles Ω and Ω' correspond to the directions of the K^- and decay proton in the K^-K^+ and Λ rest frames respectively, and Wi is the weight of the i^{th} event.

Fig. (3.3) shows the eighteen independent observable double moments ($L \leq 2$), in 4 Mev mass bins with $\cos\theta_{p\Lambda} > 0.5$. In particular, the six moments with L=1 contain interference terms between S and P wave $K\bar{K}$ amplitudes (see table (3.1)) and the data on these moments show small but important evidence for this. Also the twelve moments with $\ell = 1$ exist because of the parity violating decay of the Λ, and are purely imaginary, whereas those for $\ell = 0$ are purely real.

3.3 Amplitude Analysis.

The observed moments discussed above allow a model-independent S and P wave analysis to be done. The moments are derived in Appendix B in terms of the eight independent S and P wave (S channel) helicity amplitudes and displayed in table (1.1). The amplitudes are $S^0_{+\pm}$, $P^0_{+\pm}$, $P^{\pm}_{+\pm}$, where the subscripts represent the Λ and incident proton helicities, $\pm\frac{1}{2}$, and the superscripts the (K^-K^+) helicity. A helicity zero (K^+K^-) system (S^0 or P^0 wave) can only be produced by unnatural parity exchange. The amplitudes $P^{\pm}$ are defined as follows, in terms of helicity $\lambda = \pm 1$ amplitudes,

$$\rho^{\pm} = \frac{1}{\sqrt{2}}\left(\rho^{\lambda=1} \pm \rho^{\lambda=-1}\right) \qquad (3.2)$$

and represent unit helicity $K\bar{K}$ systems produced by natural and unnatural parity exchange respectively.

There are clearly 16 amplitude variables which are their magnitudes

$$H(0000) = |S^0_{++}|^2 + |S^0_{+-}|^2 + |P^0_{++}|^2 + |P^0_{+-}|^2 + |P^-_{++}|^2 + |P^-_{+-}|^2 + |P^+_{++}|^2 + |P^+_{+-}|^2$$

$$H(2000) = \frac{2}{5}\left(|P^0_{++}|^2 + |P^0_{+-}|^2\right) - \frac{1}{5}\left(|P^-_{++}|^2 + |P^-_{+-}|^2 + |P^+_{++}|^2 + |P^+_{+-}|^2\right)$$

$$H(2100) = \frac{\sqrt{6}}{5}\,\mathrm{Re}\left(P^0_{++}P^{-*}_{++} + P^0_{+-}P^{-*}_{+-}\right)$$

$$H(2200) = \frac{1}{5}\sqrt{\frac{3}{2}}\left(|P^-_{++}|^2 + |P^-_{+-}|^2 - |P^+_{++}|^2 - |P^+_{+-}|^2\right)$$

$$H(2110) = \frac{\alpha_\Lambda}{5}\sqrt{\frac{2}{3}}\,\mathrm{Im}\left(P^+_{++}P^{0*}_{++} + P^+_{+-}P^{0*}_{+-}\right)$$

$$H(2210) = \frac{\alpha_\Lambda}{5}\sqrt{\frac{2}{3}}\,\mathrm{Im}\left(P^+_{++}P^{-*}_{++} + P^+_{+-}P^{-*}_{+-}\right)$$

$$H(0011) = \frac{\alpha_\Lambda}{3}\sqrt{2}\,\mathrm{Im}\left(S^0_{+-}S^{0*}_{++} + P^0_{+-}P^{0*}_{++} + P^-_{+-}P^{-*}_{++} - P^+_{+-}P^{+*}_{++}\right)$$

$$H(2011) = \frac{\alpha_\Lambda}{15}\sqrt{2}\,\mathrm{Im}\left(2\,P^0_{+-}P^{0*}_{++} + P^+_{+-}P^{+*}_{++} - P^-_{+-}P^{-*}_{++}\right)$$

$$H(211\pm1) = \frac{\alpha_\Lambda}{5\sqrt{3}}\,\mathrm{Im}\left(P^0_{+-}P^{-*}_{++} - P^0_{++}P^{-*}_{+-} \mp P^0_{++}P^{+*}_{+-} \pm P^0_{+-}P^{+*}_{++}\right)$$

$$H(221\pm1) = \frac{\alpha_\Lambda}{5\sqrt{3}}\,\mathrm{Im}\left(P^+_{+-}P^{+*}_{++} + P^-_{+-}P^{-*}_{++} \pm P^+_{+-}P^{-*}_{++} \pm P^-_{+-}P^{+*}_{++}\right)$$

$$H(1000) = \frac{2}{\sqrt{3}}\,\mathrm{Re}\left(S^0_{++}P^{0*}_{++} + S^0_{+-}P^{0*}_{+-}\right)$$

$$H(1100) = \sqrt{\frac{2}{3}}\,\mathrm{Re}\left(S^0_{++}P^{-*}_{++} + S^0_{+-}P^{-*}_{+-}\right)$$

$$H(1110) = \frac{\alpha_\Lambda}{3}\sqrt{\frac{2}{3}}\,\mathrm{Im}\left(P^+_{++}S^{0*}_{++} + P^+_{+-}S^{0*}_{+-}\right)$$

$$H(1011) = \frac{\alpha_\Lambda}{3}\sqrt{\frac{2}{3}}\,\mathrm{Im}\left(S^0_{+-}P^{0*}_{++} - S^0_{++}P^{0*}_{+-}\right)$$

$$H(111\pm1) = \frac{\alpha_\Lambda}{3\sqrt{3}}\,\mathrm{Im}\left(S^0_{+-}P^{-*}_{++} - S^0_{++}P^{-*}_{+-} \mp S^0_{++}P^{+*}_{+-} \pm S^0_{+-}P^{+*}_{++}\right)$$

Table (3.1) Relations between $K^-p \to (K^-K^+)\Lambda$ double moments and helicity amplitudes. The moments $H(LM\ell m)$ are defined by eq. (3.1); (LM) and (ℓm) refer to the (K^-K^+) and Λ decays respectively. The decay asymmetry is taken to be $\alpha_\Lambda = 0.647$ in the $\ell = 1$ moments. For $\ell = 0$ and $\ell = 1$ H is used to denote Re H and Im H respectively.

Table (3.2) The $K^- p \to (K^- K^+)\Lambda$ production amplitudes at m=1.02 Gev. The overall phase is specified by $\phi(P^0_{+-}) = 90^\circ$ and the table lists the one-parameter (taken to be $\phi(S^0_{+-})$) family of solutions to the $(K^-K^+)\Lambda$ double moment data. The errors, shown in brackets for the solution with $\phi(S^0_{+-}) = 130^\circ$, are the average of the MINOS errors obtained using the CERN Minuit program. $|L^\lambda|^2$ and $P_{ol}(L^\lambda)$ are defined in eq. (3.5), and are the same for all solutions.

$\lvert S^0_{++}\rvert$	ϕ	$\lvert S^0_{+-}\rvert$	ϕ	$\lvert P^0_{++}\rvert$	ϕ	$\lvert P^0_{+-}\rvert$	ϕ	$\lvert P^-_{++}\rvert$	ϕ	$\lvert P^-_{+-}\rvert$	ϕ	$\lvert P^+_{++}\rvert$	ϕ	$\lvert P^+_{+-}\rvert$	ϕ
3.5	- 98	2.9	- 150	3.4	- 47	5.8	90	5.2	- 101	6.0	1	7.5	138	7.7	- 145
2.6	- 65	3.7	- 120	5.1	- 53	4.4	90	5.7	- 114	5.5	- 9	7.0	123	8.2	- 154
2.1	- 16	4.1	- 90	6.0	- 40	3.1	90	6.1	- 108	5.1	- 9	6.7	122	8.4	- 148
1.9	33	4.1	- 60	6.3	- 22	2.3	90	6.2	- 96	4.9	- 1	6.8	129	8.3	- 135
2.1	76	4.0	- 30	6.4	1	2.2	90	6.2	- 77	4.9	13	7.0	145	8.2	- 117
2.3	118	3.9	0	6.3	24	2.4	90	6.2	- 58	4.9	27	7.2	159	8.0	- 99
2.6	158	3.6	30	6.1	47	2.9	90	6.2	- 40	4.9	39	7.5	175	7.7	- 83
3.3	- 171	3.0	60	5.1	53	4.4	90	5.7	- 42	5.4	34	8.0	172	7.1	- 87
3.8	- 148	2.2	90	3.8	54	5.6	90	5.2	- 49	6.0	27	8.4	168	6.7	- 98
4.1	- 137	2.0	120	2.8	38	6.1	90	5.0	- 61	6.1	20	8.3	161	6.7	- 111
(±1.0)	(±23)	(±1.3)		(±1.9)	(±46)	(±1.3)		(±1.7)	(±28)	(±1.6)	(±20)	(±1.5)	(±24)	(±1.7)	(±28)
4.1	- 128	1.9	150	2.1	12	6.3	90	4.7	- 73	6.3	14	8.3	154	6.8	- 123
3.9	- 115	2.2	180	2.2	- 18	6.3	90	4.9	- 84	6.2	10	8.1	149	7.0	- 131
$\lvert S^2\rvert$ = 20 ± 16				$\lvert P^0\rvert^2$ = 45 ± 21				$\lvert P^-\rvert^2$ = 63 ± 32				$\lvert P^+\rvert^2$ = 115 ± 10			
Pol(S) = 0.75 ± 0.25				Pol(P^0) = -0.55 ± 0.3				Pol(P^-) = -0.96 ± 0.4				Pol(P^+) = -0.97 ± 0.3			

and phases, and obviously the overall phase cannot be obtained.

The moments were analysed in three mass bins centred on 1.016, 1.020 and 1.024 Gev, using a constant S wave and a ϕ Breit-Wigner form. The $K\bar{K}$ mass (m) dependence of the P wave was taken to be,

$$\rho^{\lambda} = \rho^{\lambda}(m_R)\, \frac{m_R \sqrt{\Gamma(m_R)\Gamma(m)}}{m^2 - m_R^2 - i m_R \Gamma(m_R)} \qquad (3.3)$$

where,

$$\Gamma(m) = \Gamma(m_R)\left(\frac{q}{q_R}\right)^3 \left(\frac{1 + q_R^2 R^2}{1 + q^2 R^2}\right) \qquad (3.4)$$

where $\rho^{\lambda}(m_R)$ is the magnitude of ρ^{λ} at the resonance mass (to be fitted to the data), and where q is the kaon c.m. momentum, $q^2 = m^2/4 - m_K^2$. The results given in table (3.2) correspond to the following resonance parameters,

m_R = 1.020 Gev, $\Gamma(m_R)$ = 4.8 Mev, R = 3.5 Gev^{-1}

The forms obtained for the moments were averaged over each mass bin before fitting.

The results of the fit in the three mass bins are shown in table (3.2), which shows the one-parameter family of solutions (since the target proton is unpolarized) in terms of the 14 amplitude components. The phases are all relative to the phase of $\rho^0_{+-}(m_R)$ which was set at 90^0. The solutions are shown as a function of the phase of S^0_{+-}, each of which gives an identical fit to the data and is shown in fig. (3.3). We also calculated the invariant quantities,

$$|L^{\lambda}|^2 \equiv |L^{\lambda}_{++}|^2 + |L^{\lambda}_{+-}|^2$$

$$Pol(L^{\lambda}) \equiv 2\, Im(L^{\lambda}_{++} . L^{\lambda *}_{+-}) / |L^{\lambda}|^2 \qquad (3.5)$$

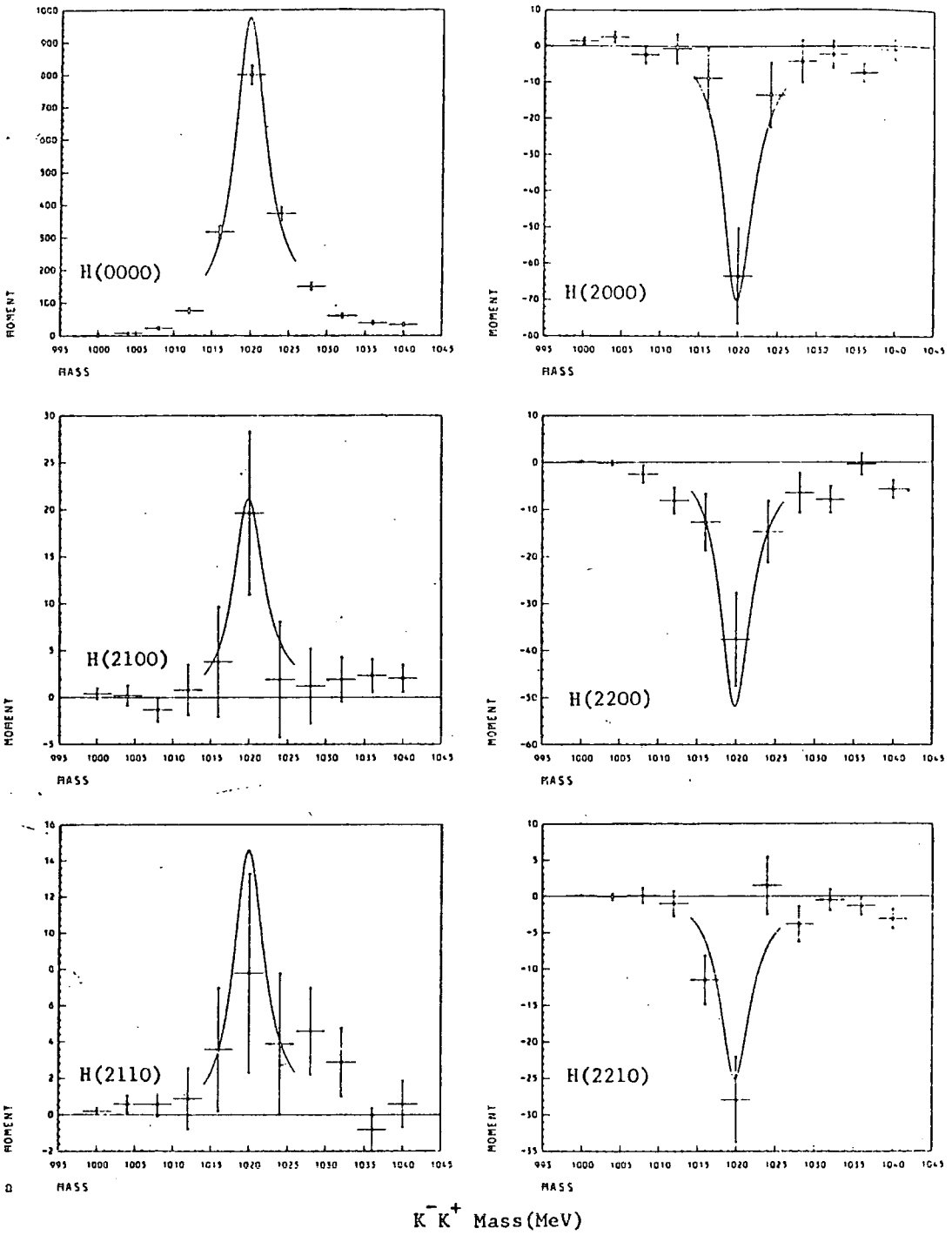

Fig.(3.3) The eighteen observable moments, H(LMℓm), as a function of m(K^-K^+) over the ϕ mass region for $0.5 \leq \cos\Theta_{GA} \leq 1.0$. The curves are the result of the amplitude analysis of the data in the three mass bins $1.014 \leq m(K^-K^+) \leq 1.026$ Gev of sec (3.3). The $\ell = 0$ and $\ell = 1$ moments are $Re\,H(LM\ell m)$ and $Im\,H(LM\ell m)$ respectively.

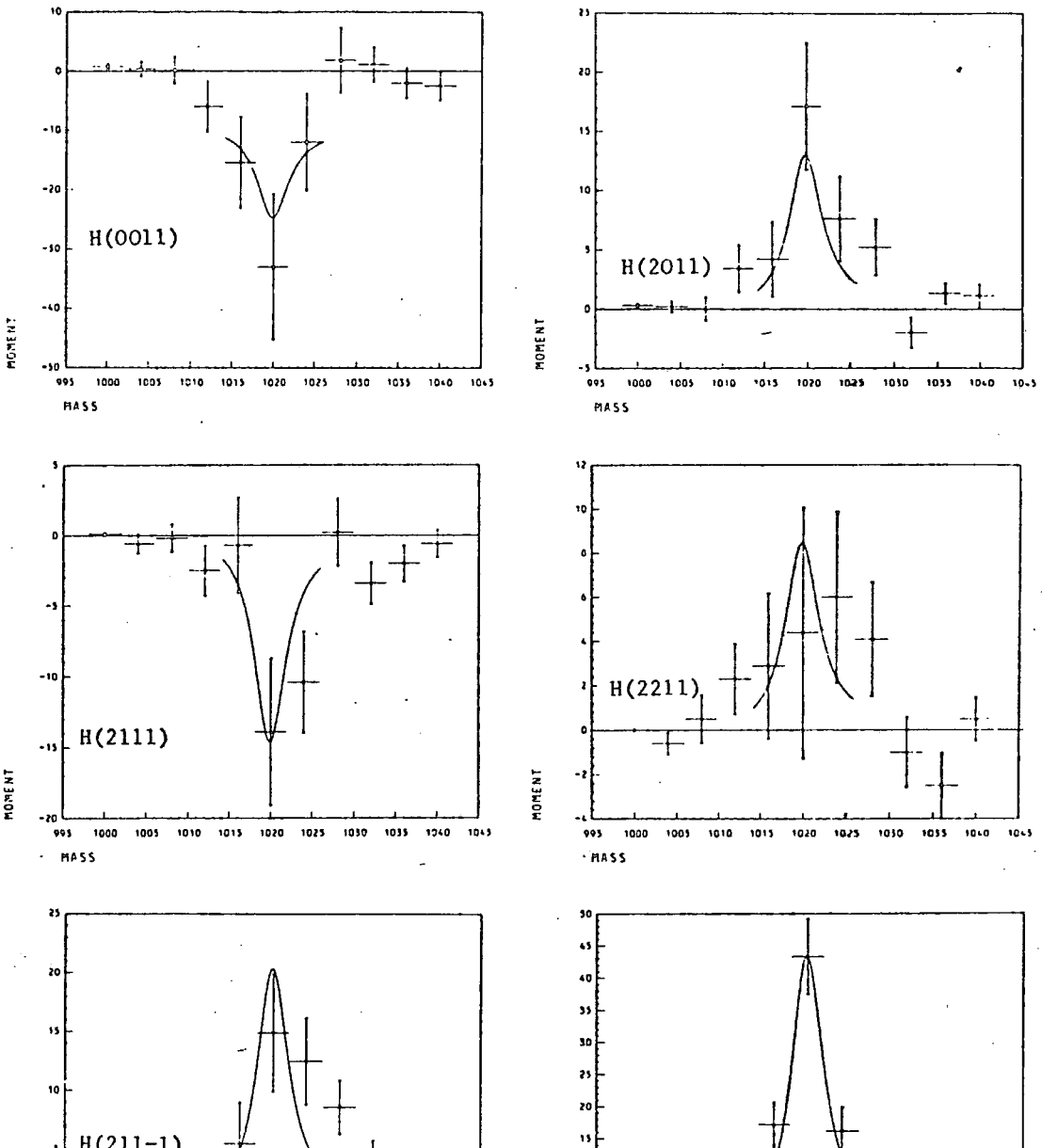
H(0011)
H(2011)
H(2111)
H(2211)
H(211-1)
H(221-1)
MOMENT
MASS
b
K⁻K⁺ Mass(MeV)

Fig. (3.3)

B

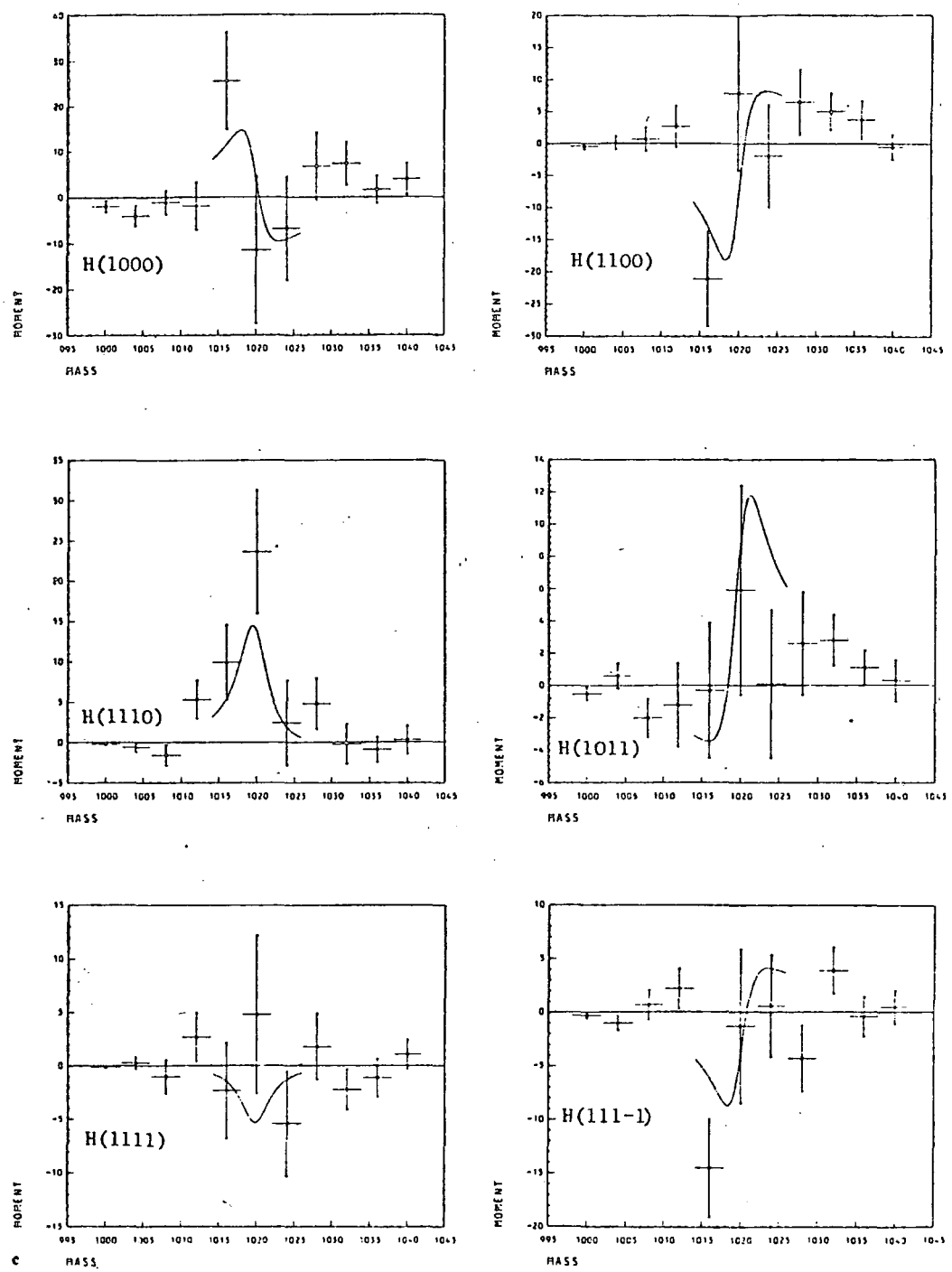

Fig. (3.3)

C

which can be taken as a measure of the cross section and baryon polarization in the production of meson states of spin L and helicity λ .

The fit was extrapolated beyond the fitted mass range, and was found to describe the data reasonably, except for the moments H(0000) and H(0011) where the prediction away from the ϕ mass region has too large a magnitude. These moments (c.f. Table (3.1)), are the only ones which contain products of S wave amplitudes (of the form SS*). If the mass bins beyond the ϕ mass are also included in the analysis, this just leads to a suppression of the S wave, which then causes a much less adequate description of the interference moments.

3.4. Discussion.

We would like to isolate K exchange in our reaction under study $K^-p \to K^+K^-\Lambda$, and to therefore obtain information on $K\bar{K}$ scattering. As described in Appendix C, K exchange much more favours baryon flip than non-flip , except in the very forward direction $\cos\Theta_{p\Lambda} > 0.95$. So we might hope to see evidence of this in the helicity zero amplitudes S^0_{+-} and P^0_{+-}. If K exchange is the dominant mechanism, then the solution we require has the S wave $K^-K^+ \to K^-K^+$ amplitude in terms of the known ϕ resonance P wave amplitude.

We can then write the relative phase and magnitude of the flip S and P wave amplitudes as,

$$\frac{S^0_{+-}}{P^0_{+-}} = \frac{1}{\sqrt{3}} \frac{(S^* + \delta)}{\phi} \qquad (3.6)$$

where S* and δ are the isoscalar and isovector S wave $K\bar{K}$ amplitudes, with ϕ the I=0 P wave. $\sqrt{3}$ is the $\sqrt{2L+1}$ factor for the P wave.

Using the S* prediction from the coupled channel analysis of chapter 2 [26], and the parameters of the δ deduced in reference [32], one can write eq. (3.6) at M_R = 1.02 Gev, as

$$\frac{S^0_{+-}}{P^0_{+-}}(m_R) \simeq 0.6 \exp(i25^\circ) \qquad (3.7)$$

(The relation between the δ, S* and Φ amplitudes used here is shown in fig. (3.4), where the Φ amplitude essentially fills the unitarity circle at the resonant mass). Thus for K- exchange we expect the phase of S^0_{+-} to be about 115°. It can be seen from table (3.2) that a solution not inconsistent with this prediction exists, within the large errors. However, it can also be seen that the non-flip amplitudes (e.g. S^0_{++}) are also quite large in this region, giving appreciable non-K exchange contributions. This was already obvious from the large polarizations in the S^0 and P^0 amplitudes (c.f. table (3.2)). Clearly the large t bin used makes the analysis only approximate, but with better statistics one could isoloate the K exchange amplitudes by studying the t-dependence, which would lead to much more accurate predictions about the $K\bar{K} \to K\bar{K}$ S wave.

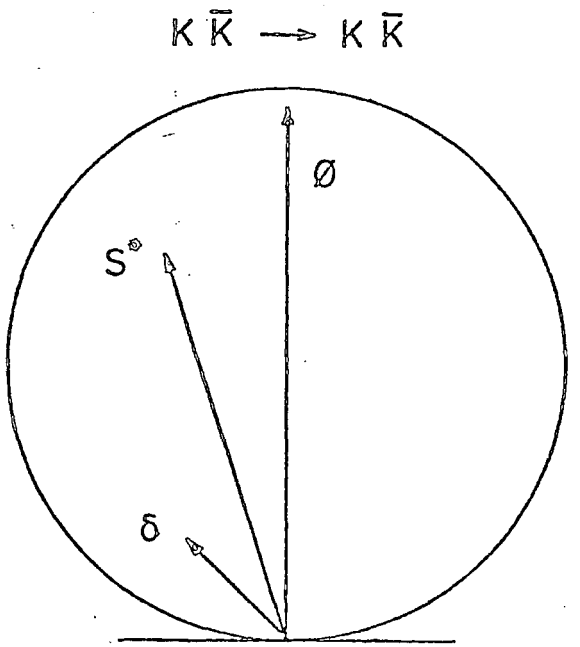

Fig.(3.4). S* and δ denote, respectively, the I=0 and I=1 $K\bar{K}$ S-wave amplitudes at the Φ mass, normalized to their respective unitarity circles. Ø is the I=0 P wave amplitude at M=MR

3.5 Summary, Conclusions and Epilogue.

We have observed S-P interference effects in the data from the reaction. $K^-p \to K^-K^+\Lambda$. We have performed a model independent amplitude analysis of the double moments of the decay distributions, resulting in a one-parameter series of solutions. The predicted amplitudes S^0_{+-} and P^0_{+-} can be used to give valuable information on the S wave $K^-K^+ \to K^-K^+$ amplitude on the ϕ resonance, which will help determine the parameters of the S* and ε resonances. However, there exists a large non-K exchange contribution to the unnatural parity exchange amplitudes (S^0 and P^0), and this leads to unreliable predictions about K-exchange. Hopefully studying the t dependence of high statistics data will improve this situation.

In chapter 2, we examined the two I=0 S wave states, the scalars the S* and ε. The S*(990) was consistent with a $K\bar{K}$ bound state picture and the ε(1400) as a coupled channel Breit-Wigner, with a strong preference for the $\pi\pi$ channel. The S* was found to be rather narrower than previous analysès would lead one to expect. With the possible exception of the ε, then clearly the other scalars do not fit easily into a quark model nonet; nor is it clear that they are whol'ly $q\bar{q}q\bar{q}$ states, although the $K\bar{K}$ bound state is a subset of the latter.

Since these analyses have been performed, there has been continued work in the area of scalar meson spectroscopy. In a recent analysis of Tornqvist [33], significant progress seems to have been made by making a coupled channel analysis which also includes the $\eta\eta$ channel, and simultaneously includes couplings to all $J^P=0^-$ meson pairs which can couple to the scalars. The resultant picture coming out of this analysis seems to be that the scalars are dominantly $q\bar{q}$ systems with a large $q\bar{q}q\bar{q}$ component in the form of a meson-

meson (mainly $K\bar{K}$) bound state. The physical masses are then found to be strongly influenced by the number of nearby di-meson thresholds (hence the need to include all channels). This clears up the problem of mass differences mentioned in chapter 1. However, the mass and width of the ε are still difficult to pin down. The mixing angle between SU (3) singlet and octet is found to be a strong function of energy, almost ideal below $K\bar{K}$ threshold, then tending towards the S^* being octet, ε singlet at about 1400 Mev. The scalar nonet might then appear to be gradually unveiling itself.

APPENDIX A
The Effect of the K^+ and K^o Mass Difference.

We discuss here the effect of isospin violation based simply on a non-zero difference between the u and d quark masses, effectively retaining isospin symmetry in the couplings. The K^+ and K^o mass difference then induces mixing effects near the $K\bar{K}$ threshold. To do this one can generalize the K or M matrix parametrization of sec (2.3) to four channels, which we shall call basis I, $\{|\pi\eta; I=1\rangle, |\pi\pi; I=0\rangle, |K^+K^-\rangle, |K^oK^o\rangle\}$. We then obtain mixing when we consider the K^+, K^o mass difference and take isospin 0, 1 components of the $K\bar{K}$ system,

$$|K\bar{K}\rangle_{1,0} = \frac{1}{\sqrt{2}}\left(|K^o\bar{K}^o\rangle \pm |K^+K^-\rangle\right) \tag{A1}$$

This leads us to define an isospin basis II, $\{|\pi\eta\rangle, |K\bar{K}\rangle_1, |\pi\pi\rangle, |K\bar{K}\rangle_0\}$. So the physical basis I now contains mixtures of I=0, 1 components in each charged or neutral kaon system. All we now require is the four channel M or K matrix in basis I. Consider the M matrix, and define the four channel matrix of particle momenta $\underset{\sim}{\rho}$ as,

$$\underset{\sim}{\rho}_I = \begin{pmatrix} \rho_\eta & 0 & 0 & 0 \\ 0 & \rho_\pi & 0 & 0 \\ 0 & 0 & \rho_c & 0 \\ 0 & 0 & 0 & \rho_o \end{pmatrix} \equiv \underset{\sim}{k}/\sqrt{s} \tag{A2}$$

where ρ_c and ρ_o correspond to charged and neutral scaled kaon momenta respectively. In the isospin basis II, the M matrix must be block diagonal in order to respect isospin conservation. One can write it as,

$$\underset{\sim}{M}_{II} = \begin{pmatrix} m_{11}^{(1)} & m_{12}^{(1)} & 0 & 0 \\ m_{12}^{(1)} & m_{22}^{(1)} & 0 & 0 \\ 0 & 0 & m_{11}^{(0)} & m_{12}^{(0)} \\ 0 & 0 & m_{12}^{(0)} & m_{22}^{(0)} \end{pmatrix} \tag{A3}$$

where the superscript (I) refers to that particular isospin sector I. So for example $M_{11}^{(0)}$ describes $\pi\pi \to \pi\pi$, $M_{12}^{(0)}$ the process $\pi\pi \to KK(I=0)$. To determine the physical amplitudes, one must transform M_{II} to basis I. The relevant operator is simply,

$$\underset{\sim}{U} = \begin{pmatrix} 1 & 0 & 0 & 0 \\ 0 & 0 & 1 & 0 \\ 0 & 1/\sqrt{2} & 0 & -1/\sqrt{2} \\ 0 & 1/\sqrt{2} & 0 & 1/\sqrt{2} \end{pmatrix} \tag{A4}$$

so that,

$$\{\text{basis I}\} = \underset{\sim}{U}\{\text{basis II}\} \tag{A5}$$

Then $\underset{\sim}{M}_I$ is given by,

$$\underset{\sim}{M}_I = \underset{\sim}{U}\,\underset{\sim}{M}_{II}\,\underset{\sim}{U}^{-1} \tag{A6}$$

So eqs. (A2), (A3), (A4) and (A6) result in

$$\det(\underset{\sim}{M}_I - i\underset{\sim}{\rho}_I) = \left[(m_{11}^{(1)} - i\rho_\eta)(m_{22}^{(1)} - i\bar{\rho}) - m_{12}^{(1)2}\right] \cdot \left[(m_{11}^{(0)} - i\rho_\pi)(m_{22}^{(0)} - i\bar{\rho}) - m_{12}^{(0)2}\right] + \frac{1}{4}(\rho_c - \rho_0)^2 (m_{11}^{(1)} - i\rho_\eta)(m_{11}^{(0)} - i\rho_\pi) \tag{A7}$$

where,

$$\bar{\rho} = \frac{1}{2}(\rho_c + \rho_0) \tag{A8}$$

Equivalently, working directly with the K matrix, one can write the determinant of the Jost function matrix as (c.f. eq. (2.20).

$$d = \det\left(\underset{\sim}{I} - i\underset{\sim}{\rho}\,\underset{\sim}{K}\right) \tag{A9}$$

With the same notation as above, this can then be written [26],

$$d = \det\left(\underset{\sim}{I} - i\underset{\sim}{\rho}^{(0)}\underset{\sim}{K}^{(0)}\right)\det\left(\underset{\sim}{I} - i\underset{\sim}{\rho}^{(1)}\underset{\sim}{K}^{(1)}\right) + \frac{1}{4}(\rho_c - \rho_0)^2\left(K_{22}^{(0)} - i\rho_{11}^{(0)}\det\underset{\sim}{K}^{(0)}\right)\left(K_{22}^{(1)} - i\rho_{11}^{(1)}\det\underset{\sim}{K}^{(1)}\right) \tag{A10}$$

where, $\rho_{22}^{(I)} = \frac{1}{2}(k_c + k_0)/\sqrt{s} \equiv \bar{\rho}$

In the I=0 $\pi\pi$, $K\bar{K}$ analysis described in the text, the effect of the $(k_c - k_0)^2$ term in eq. (A7) or (A10) is much smaller than the effect of putting $\frac{1}{2}(k_c + k_0)$ instead of k_2, and so the incorporation of isospin violation at this level is simple.

APPENDIX B

Double Moment Analysis of $K\bar{p} \rightarrow K^+K^-\Lambda$.

Consider the reaction $K\bar{p} \longrightarrow (K^+K^-)\Lambda$, shown in Fig. (B1), The production process is represented by the amplitude $T^{J\lambda}_{\mu\lambda\rho}$.

Fig. (B1) Definition of helicities in the production of resonance R (S^*, δ, Φ) of spin J, helicity λ . $\lambda\rho$ is the incident proton helicity, υ the final and μ the helicity of the Λ . Ω and Ω_1 are the appropriate centre of mass decay solid angles.

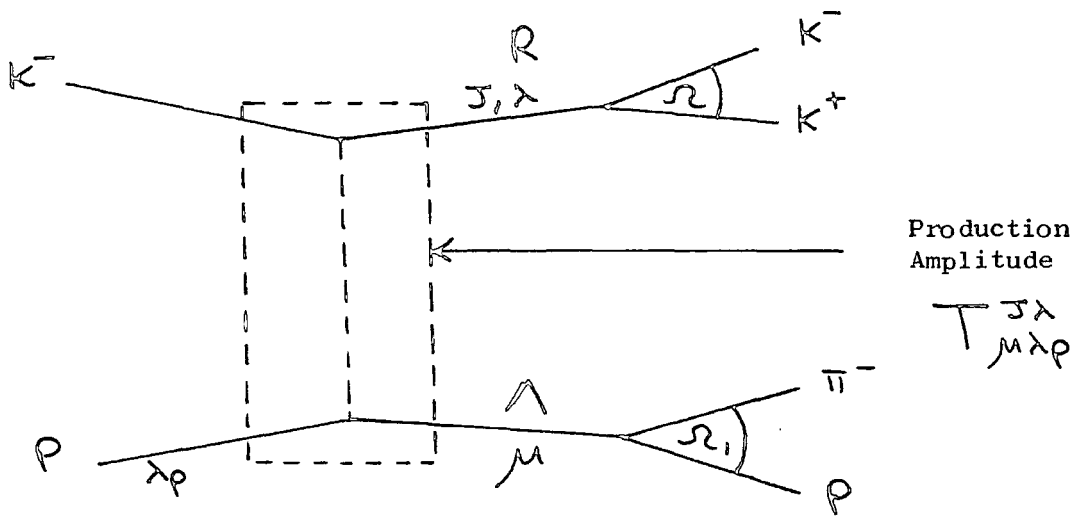

Using the following expansion for the helicity υ products of the $\Lambda \rightarrow p\pi$ decay,

$$|\Omega_1, \nu\rangle = \sum_{JM} \sqrt{\frac{2J+1}{4\pi}}\, D^J_{M\nu}(\Omega_1)\,|JM;\nu\rangle \qquad \text{(B1)}$$

one can write the amplitude for the decay as,

$$\langle \Omega_1, \nu | \mathcal{M} | \mu \rangle = \sqrt{\frac{1}{2\pi}}\, D^{\frac{1}{2}*}_{\mu\nu}(\Omega_1)\, t_\nu \qquad \text{(B2)}$$

where t_ν is defined in,

$$\langle JM;\nu | \mathcal{M} | J=\tfrac{1}{2}, \mu \rangle = \delta_{J\frac{1}{2}}\delta_{M\mu}\, t^J_\nu \qquad \text{(B3)}$$

where the superscript J will be dropped, since $J=\frac{1}{2}$. Similarly in the decay of resonance R,

$$\langle \Omega,0|\mathcal{M}|J,\lambda\rangle = \sqrt{\frac{2J+1}{4\pi}}\, D^{J\,*}_{\lambda 0}(\Omega)\, F^{J}_{\lambda} \tag{B4}$$

The complete amplitude is then given by,

$$A^{J}_{\lambda\rho;\mu\lambda\nu} = \langle \Omega,0|\mathcal{M}|J,\lambda\rangle \langle \Omega_1,\nu|\mathcal{M}|\mu\rangle T^{J\lambda}_{\mu\lambda\rho}$$

$$\equiv A \tag{B5}$$

The double angular distribution can then be written as,

$$W(\Omega,\Omega_1) = \frac{1}{2}\sum_{\nu,\lambda\rho}\left(\sum_{J\lambda\mu} A\right)\left(\sum_{J'\lambda'\mu'} A^{*}\right) \tag{B6}$$

where the factor $\frac{1}{2}$ is an average over initial proton helicity states. Substituting from (B2), (B4) and (B5) gives,

$$W(\Omega,\Omega_1) = \frac{1}{2}\sum_{\nu\lambda\rho}\sum_{\substack{JJ'\\ \lambda\lambda'\\ \mu\mu'}} \rceil^{J\lambda}_{\mu\lambda\rho}\, \rceil^{J'\lambda'}_{\mu'\lambda\rho} \sqrt{\frac{(2J+1)(2J'+1)}{(4\pi)^2}} \cdot$$

$$\cdot\, D^{J\,*}_{\lambda 0}(\Omega)\, D^{J'}_{\lambda' 0}(\Omega)\, \frac{1}{2\pi}\, D^{\frac{1}{2}\,*}_{\mu\nu}(\Omega_1)\, D^{\frac{1}{2}}_{\mu'\nu}(\Omega_1)\, |t_\nu|^2 \tag{B7}$$

where $\rceil \equiv T\,F$.

The products of D functions above can be decomposed into the Clebsh-Gordon series,

$$D^{J\,*}_{\lambda 0}(\Omega)\, D^{J'}_{\lambda' 0}(\Omega) = \sum_{L}(-1)\langle J0J'0|L0\rangle \langle J-\lambda J'\lambda'|LM\rangle D^{L}_{M0}(\Omega)$$

$$D^{\frac{1}{2}*}_{\mu\nu}(\Omega_1)\, D^{\frac{1}{2}}_{\mu'\nu}(\Omega_1) = \sum_{\ell} (-1)^{\mu-\nu} \langle \tfrac{1}{2}-\mu\, \tfrac{1}{2}\mu' | \ell m\rangle \langle \tfrac{1}{2}-\nu\, \tfrac{1}{2}\nu | \ell 0\rangle D^{\ell}_{m0}(\Omega_1)$$

(B8)

Consider now the resulting υ summation, which is,

$$S_\ell \equiv \sum_{\nu} |t_\nu|^2 (-1)^{-\nu-\frac{1}{2}} \langle \tfrac{1}{2}-\nu\, \tfrac{1}{2}\nu | \ell 0\rangle$$

$$= \frac{1}{\sqrt{2}}\left(|t_+|^2 + |t_-|^2\right) \equiv \frac{1}{\sqrt{2}} \quad \text{for } \ell = 0$$

$$= \frac{1}{\sqrt{2}}\left(|t_+|^2 - |t_-|^2\right) \equiv -\frac{\alpha_\Lambda}{\sqrt{2}} \quad \text{for } \ell = 1$$

(B9)

where α_Λ is the Λ polarization (=0.647), which selects out the odd ℓ components. The factor $(-1)^{\frac{1}{2}}$ was added on to give real coefficients and will be compensated for below. Thus the angular distribution becomes,

$$W(\Omega,\Omega_1) = \sum_{\lambda\rho} \sum_{\substack{JJ' \\ \lambda\lambda' \\ \mu\mu'}} \frac{\sqrt{(2J+1)(2J'+1)}}{16\pi^2} \Big]^{J\lambda}_{\mu\lambda\rho} \Big]^{J'\lambda'*}_{\mu'\lambda\rho} \cdot$$

$$\cdot \sum_{L} (-1)^{\lambda} \langle J0J'0|L0\rangle \langle J-\lambda J'\lambda|LM\rangle \sum_{\ell} (-1)^{\mu+\frac{1}{2}} \langle \tfrac{1}{2}-\mu\, \tfrac{1}{2}\mu'|\ell m\rangle \cdot$$

$$\cdot\, D^{L}_{M0}(\Omega)\, D^{\ell}_{m0}(\Omega_1)\, S_\ell$$

(B10)

The moments $H(LM\ell m)$ can now be wirtten in terms of the angular distribution as,

$$H(LM\ell m)^* = \int W(\Omega,\Omega_1)\, D^{L*}_{M0}(\Omega)\, D^{\ell}_{m0}(\Omega_1)\, d\Omega\, d\Omega_1$$

(B11)

and performing the angular integrations yields,

$$H(LM\ell m)^{\alpha} = \sum_{\lambda\rho} \sum_{\substack{JJ' \\ \lambda\lambda' \\ \mu\mu'}} \frac{\sqrt{(2J+1)(2J'+1)}}{(2L+1)(2\ell+1)} \Gamma^{J\lambda}_{\mu\lambda\rho} \Gamma^{J'\lambda'}_{\mu'\lambda\rho} (-1)^{\lambda} \cdot$$

$$\cdot \langle J0J'0|L0\rangle \langle J-\lambda J'\lambda'|LM\rangle (-1)^{\mu+\frac{1}{2}} \langle \tfrac{1}{2}-\mu\tfrac{1}{2}\mu'|\ell m\rangle S_{\ell}. \qquad \text{(B12)}$$

Defining the following combinations of amplitudes (where just the λ index is retained for simplicity).

$$\left.\begin{aligned} N^{\lambda} &= \frac{1}{\sqrt{2}}\left[\Gamma^{\lambda} - (-1)^{\lambda}\Gamma^{-\lambda}\right] \\ U^{\lambda} &= \frac{1}{\sqrt{2}}\left[\Gamma^{\lambda} + (-1)^{\lambda}\Gamma^{-\lambda}\right] \end{aligned}\right\} \quad \text{for} \quad \lambda \neq 0$$

$$U^{0} = \Gamma^{0} \qquad \text{for} \quad \lambda = 0 \qquad \text{(B13)}$$

and using the property of parity invariance,

$$\Gamma^{\lambda J}_{++} = (-1)^{\lambda+1}\Gamma^{-\lambda J}_{--}$$

$$\Gamma^{\lambda J}_{+-} = (-1)^{\lambda}\Gamma^{-\lambda J}_{-+} \qquad \text{(B14)}$$

gives,

$$N^{\lambda}_{++} = N^{\lambda}_{--} \; ; \; U^{\lambda}_{++} = -U^{\lambda}_{--}$$

$$N^{\lambda}_{+-} = -N^{\lambda}_{-+} \; ; \; U^{\lambda}_{+-} = U^{\lambda}_{-+} \qquad \text{(B15)}$$

The lower vertex summation over λ_ρ and μ can now be written,

$$X_{\ell m} \equiv \sum_{\lambda\rho} \sum_{\mu} (-1)^{\mu+\frac{1}{2}} \langle \tfrac{1}{2}-\mu\tfrac{1}{2}\mu|\ell m\rangle \Gamma^{J\lambda}_{\mu\lambda\rho} \Gamma^{J'\lambda'}_{\mu'\lambda\rho} \qquad \text{(B16)}$$

and this reduces to an expansion of four terms, each of which is of the form NJ^* or NN^* etc.....

Finally, the observed moments can be written

$$H(LM\ell m) = (-1)^{\ell} H(LM\ell m) \tag{B17}$$

which gives,

$$H(LM\ell m) = \frac{(-1)^{\ell} S_{\ell}}{(2L+1)(2\ell+1)} \sum_{J,J';\lambda} \sqrt{(2J+1)(2J'+1)} \cdot (-1)^{\lambda} \langle J0J'0|L0\rangle \langle J-\lambda J'\lambda|LM\rangle X_{\ell m} \tag{B18}$$

and the resulting summation gives the expressions of table (3.1) of the text.

APPENDIC C

To Flip or Not to Flip

We describe the contributions of flip and non-flip amplitudes to the cross section, assuming K exchange. Consider the K^-p centre of mass, as in fig. (C1), where Θ is the angle between the incident proton

Fig. (C1) The $k\bar{p}$ c.m.

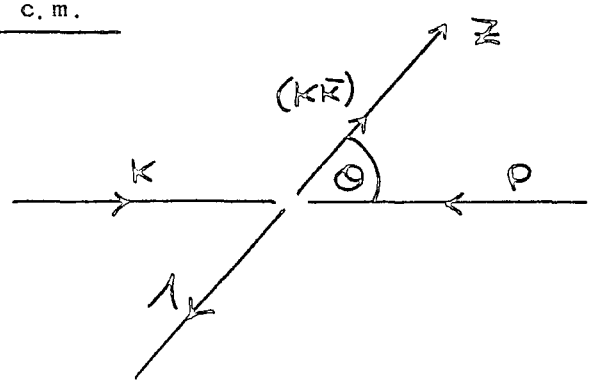

and emergent $(K\bar{K})$ system. The kaon-nucleon vertex of fig. (C2) is

Fig. (C2) The $P\Lambda$ vertex, with helicities λ_p and λ_Λ respectively.

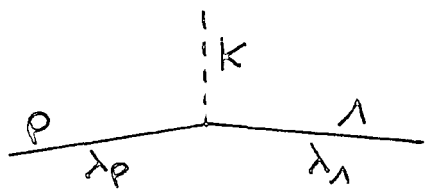

described by the amplitude,

$$V_{\lambda_p\lambda_\Lambda} = -ig_\Lambda \bar{U}_{\lambda_\Lambda}\gamma_5 U_{\lambda_p} \qquad (C1)$$

Substituting in the appropriate spinors, U, gives the result,

$$V_{+-} = -ig_\Lambda \sin\frac{\Theta}{2}\left[\sqrt{(E_\Lambda+m_\Lambda)(E_p-m_p)}+\sqrt{(E_p+m_p)(E_\Lambda-m_\Lambda)}\right]$$

$$V_{++} = ig_\Lambda \cos\frac{\Theta}{2}\left[\sqrt{(E_\Lambda+m_\Lambda)(E_p-m_p)}-\sqrt{(E_p+m_p)(E_\Lambda-m_\Lambda)}\right] \qquad (C2)$$

with a contribution to the cross section ,

$$|V_{+-}|^2+|V_{++}|^2 = g_\Lambda^2\left[(m_\Lambda-m_p)^2-t\right] \qquad (C3)$$

The results for a laboratory momentum P_L = 4.2 Gew/c are shown in table (C1), from which it can be seen that the flip amplitude dominates right up to the very forward direction $-t < 0.196$.

Table (C1) Values of flip and non-flip squared amplitudes for various values of CosΘ.

CosΘ	-t	$\lvert V_{+-}\rvert^2$	$\lvert V_{++}\rvert^2$
1	0.057	0	0.088
.95	0.196	0.15	0.086
.9	0.335	0.28	0.084
.75	0.750	0.70	0.077
.5	1.440	1.41	0.066

REFERENCES
PART II

1. F. Close, "An Introduction to Quarks and Partons", A.P. (1979), and references therein.

2. "Review of Particle Properties" - Particle Data Group, PL111B (April 1982).

3. F.E. Close, "QCD and the Search for Glueballs", rapporteur talk at "Unified Theories and their Experimental Tests", Venice, March 1982, RL-82-041, and references therein.

4. R.L. Jaffe, PRD15 (1977), 267.

5. R.L. Jaffe, PRD15 (1977), 281.

6. N.M. Cason et al., PRL36 (1976), 1485.

7. A.J. Pawlicki et al., PRL37 (1976), 1666.

8. A.D. Martin and E.N. Ozmutlu, NPB158 (1979), 520.

9. R.L. Jaffe and K. Johnson, PL60B (1976), 201.

10. G. Grayer et al., NPB75 (1974), 189.

11. A.J. Pawlicki et al., PRD15 (1977), 3196.

12. M. Pilkuhn, "The Interactions of Hadrons", North Holland (1967).

13. B.R. Martin, D. Morgan, G. Shaw, "Pion-Pion Interactions in Particle Physics", A.P. 1976 and references therein.

14. J.L. Petersen, "The $\pi\pi$ Interaction", Cern Yellow Report, CERN 77-04.

15. A.D. Martin and P. Estabrooks, in Proc. of the Daresbury Meeting on Pion Exchange (1973).

16. G.F. Chew and F.E. Low, PR113 (1959), 1640; C. Goebel, PRL1 (1958), 337.

17. W. Ochs and F. Wagner, PL44B (1973), 271.

18. A.D. Martin, E.N. Ozmultu and E.J. Squires, NPB121 (1977), 514.

19. M. Alston-Garnjost et al., PL36B (1971), 152.

20. S.M. Flatté et al., PL38B (1972), 232.

21. D. Morgan, PL51B (1974), 71.

22. P. Estabrooks and A.D. Martin, NPB79 (1974), 301; NPB95 (1975), 322.

23. D. Cohen et al., PRD22 (1980), 2595.

24. A.D. Martin and M.R. Pennington, Annals of Phys. 114 (1978), 1.

25. G. Gidal et al., PL107B (1981), 153.

26. A.C. Irving, A.D. Martin and P.J. Done, Z Phys. C 10 (1981), 45.

27. Roland Omnes, "Introduction to Particle Physics", Wiley (1971), Chapter 8.

28. M. Kato, Annals of Physics 31 (1965), 130.

29. G.W. Brandenburg et al., NPB104 (1976), 413.

30. M. Aguilar-Benitez, P.J. Done, A.D. Martin, Z. Phys. C. 10 (1981), 299.

31. N.N. Achasov, S.A. Devyanin, G.N. Shestakov, PL88B (1979), 89.

32. A.C. Irving, PL70B (1977), 217.

33. Nils A. Tornquist, PRL49 (1982), 624.

34. G. Grayer et al., Internat. Conf. on $\pi\pi$ Scattering and Associated Topics, Tallahassee, 1973, AIP Conf. Proc. 13, New York (1973), p. 117.

KEY:

PRD	:	Physical Revue D
PRL	:	Physical Revue Letters
NPB	:	Nuclear Physics B
Z. Phys. C.	:	Zeitschrift fur Physik C
Annals of Phys.	:	Annals of Physics
Phy. Rep.	:	Physics Reports
J. Math. Phys.	:	Journal of Mathematical Physics
J. Phys.	:	Journal of Physics